DOCTOR OF PHILOSOPHY

Differential expression of the tight junction proteins occludin, ZO1 and ZO2 with respects to the progression of liver diseases

Barson, Eliot

Award date:
2019

Awarding institution:
Coventry University

Differential expression of the tight junction proteins occludin, ZO1 and ZO2 with respects to the progression of liver diseases.

By

Eliot Barson

September 2017

A thesis submitted in partial fulfilment of the University's requirements for the Degree of Doctor of Philosophy

Acknowledgments

With the completion of this thesis I have accomplished a major milestone in my life and there are many people that I would like to acknowledge. Firstly, my supervisor Dr Christopher Mee for his invaluable and continued support throughout the PhD. He supervised during my final year undergraduate project and still had the bravery to accept me to be his PhD student. Although you did appear to be a lot happier when your office was moved away from the front of the lab!

I would also like to thank the other members of my supervisory team Dr Aftab Hussain and Dr Elaine Green, although I did not get to meet you often you were always keen to listen when to talk about my work whenever we met.

The technical staff that helped me through the PhD were the best set of people I could have hoped to work alongside. Susan Tompsett, without your laboratory guidance and your ability to turn a blind eye when I was raiding through your chemicals and reagent I would not have been able to finish my PhD.

I want to acknowledge all the PhD students and lab staff I have worked alongside Sarah Siverns, Gurpreet Sandu, Dr Dorota Dobrzanska, Pavneet Singh, Henry Nden, Danielle Meyer, Chloe Jagpal, Natasha Browne-Marke, Refik Kuburas and Charlie Gamage. You have all become good friends and I wish you all the best with your future careers!

More significantly I want to thanks James Dayus, we started the PhD as good friends and now we have become best friends and I know we will be friends for life. The amount of hours we have spent together over the last four years “working hard” has been enjoyable with you at my side.

To my family, Mum and Dad, you have given me so much support and freedom not only throughout my PhD but throughout my whole life and for this I can never thank you enough.

Finally, to the most important person in my life, Aimee Green, you are the best thing to come out of my time doing my PhD. You always supported and believed in me whenever I was down and never complained (much) about me working late. With every late night library session frantically trying to finish the thesis you cooked me food and bought it in to me. Well you know what they say, a way to a man’s heart is through his stomach and that is certainly true for me! We can now truly begin our adventure and I am so happy that you are the one I will be journeying with.

Abstract

Hepatocellular carcinoma (HCC) is the most common type of liver cancer globally but ranks third in mortality. Occludin expression analysis shows a low occludin expression in 83.5 % of HCCs and this is associated with increased metastasis and a low prognosis.

In a high proportion of hepatocellular carcinomas, there is a low expression of occludin and ZO1. The ZO2 expression has not been investigated in detail in hepatocellular carcinoma. Screening studies have shown there is reduced ZO2 expression in chronic liver disease and liver cancer. The loss of these proteins are seldom investigated together in respects to HCC.

Using a 2D cell migration and 3D invasion assay it was observed that ZO1 and ZO2 expression knockdown in HepG2 cells increased migration and invasion. This was shown to be associated with reduced occludin phosphorylation reducing its function. Silencing of HepG2 cells with combined occludin and ZO1 knockdown resulted in a further increase of migration and invasion rates. Occludin overexpression in HepG2 cells is partially protective and reduces migration and invasion rates with ZO1 and ZO2 knockdown and partially maintained it phosphorylation state.

The increased migration in occludin knockdown is due to the HepG2 cells losing their contact inhibition and show greater signs of proliferation and migration. Occludin silencing with ZO1 and ZO2 knockdown increases the migration and invasion rates due to ZO1 and ZO2 having anti-proliferative functions through YBX3 sequestration and ZO2 oncogenic transcription inhibition. Occludin overexpression reduces the migration and invasion rates as intracellular aggregates of occludin sensitise cells to apoptosis and maintain tight junction function.

Abbreviations

aa	-	Amino acids
ABCB11	-	ATP Binding Cassette Subfamily B Member 11
AKT	-	Protein kinase B
aPKC		atypical protein kinase C
APS	-	Ammonium persulfate
ATP	-	Adenosine triphosphate
BC	-	Bile canaliculi
BCLC	-	Barcelona clinic liver cancer
BSA	-	Bovine serum albumin
BSEP	-	bile acids export pump
CCAT1	-	Colon Cancer Associated Transcript 1
CCNE1	-	Cyclin E1
CD4+	-	Cluster of differentiation 4+
CD81	-	Cluster of differentiation 81
CDC42	-	Cell division cycle 42
CDH1	-	E-cadherin
CDH2	-	N-cadherin
CDK4	-	Cyclin-dependent kinase 4
cDNA	-	complementary DNA
CLDN	-	Claudin
CRISPR	-	Class 2 Clustered Regularly Interspaced Short Palindromic Repeat
CT	-	Cycle threshold

DAPI	-	4',6-diamidino-2-phenylindole, dihydrochloride
DEPC	-	Diethyl pyrocarbonate
DISC	-	Death-inducing signalling complex
Dlg	-	Drosophila Disc large protein
DMEM	-	Dulbecco's Modified Eagle's medium
DNA	-	Deoxyribonucleic acid
dNTP	-	Deoxynucleotide triphosphate
DTTP	-	Deoxythymidine triphosphate
ECM	-	Extra cellular matrix
EDTA	-	Ethylenediaminetetraacetic acid
EGF	-	Epidermal growth factor
EGTA	-	Ethylene-bis(oxyethylenenitrilo)tetraacetic acid
EL	-	Extracellular loop
EMT	-	Epithelial to meshenchymal transition
ERK	-	Extracellular signal–regulated kinases
FADD	-	Fas-associated protein with death domain
FN1	-	Fibronectin 1
FOX01	-	Forkhead box O1
FOXM1	-	Forkhead Box M1
G418	-	Geneticin
GAPDH	-	Glyceraldehyde 3-phosphate dehydrogenase
GEF	-	Guanine nucleotide exchange factor
GJA1	-	Gap junction alpha-1 protein
Guk	-	Guanylate kinases

HBV	-	Hepatitis B virus
HBx	-	Hepatitis B viral protein x
HCC	-	Hepatocellular carcinoma
HCl	-	Hydrochloric acid
HCV	-	Hepatitis C virus
HFE	-	Human hemochromatosis protein
iPS	-	Induced pluripotent stem cells
IgG	-	Immunoglobulin G
IMS	-	Industrial Methylated Spirit
JAM	-	Junctional adhesion molecule
kDa	-	kilo Daltons
LB	-	Lysogeny broth
LEF	-	Lymphoid enhancer factor
LHBs	-	large HBV surface proteins
MAGuK	-	Membrane-associated guanylate kinases
MAPK	-	Mitogen-activated protein kinases
Mcl-1	-	Myeloid cell leukaemia sequence
MDCK	-	Madin-Darby Canine Kidney cells
MDR	-	Multi-drug resistance protein
MLL4	-	Histone-lysine N-methyltransferase 2B
MHBs	-	Middle HBV surface proteins
miRNA	-	Micro RNA
MRP2	-	Multidrug resistance associated protein 2
NTCP	-	Na+-taurocholate cotransporting polypeptide

OCLN	-	Occludin
PALS1	-	Membrane palmitoylated protein 5
PAR3	-	Protease activated receptor 3
PATJ	-	PALS1-associated TJ protein
PBS	-	Phosphate buffered saline
PCR	-	Polymerase chain reaction
PDZ	-	Discs-large homologous regions
PFIC	-	progressive cholestatic liver disease
PIP2	-	Phosphatidylinositol 4,5-bisphosphate 2
PIP3	-	Phosphatidylinositol 4,5-bisphosphate 3
PKC	-	atypical protein kinase C
PLK1	-	Serine/threonine-protein kinase
PP1a	-	Protein phosphatase 1
PP2A	-	Protein phosphatase 2
PPP6C	-	Serine/threonine-protein phosphatase 6 catalytic subunit
RISC	-	RNA-induced silencing complex
RNA	-	Ribonucleic acid
ROCK1	-	Rho associated coiled-coil containing protein kinase 1
RT-PCR	-	Real-Time PCR
SDS	-	Sodium Dodecyl Sulphate
SENP5	-	SUMO specific peptidase 5
SEM	-	Standard error of the mean
Ser	-	Serine

SH3	-	SRC Homology 3 Domain
SHBs	-	Small HBV surface proteins
shRNA	-	Small hairpin RNA
siRNA	-	Small interfering RNA
S.O.C		Super Optimal broth with catabolite repression
SR-BI	-	Scavenger receptor class B type 1
TAE	-	Tris/Acetic/EDTA
TCF	-	T cell factor
TAMP	-	Tight junction-associated marvel proteins
TBE	-	Tris/Borate/EDTA
TBST	-	Tris-buffered saline with Tween-20
TERT	-	Telomerase reverse transcriptase
TGF-β1	-	Transforming growth factor beta 1
Thr	-	Threonine
TJ	-	Tight junction
TJP1	-	Tight junction protein 1
TJP2	-	Tight junction protein 2
TJP3	-	Tight junction protein 3
TLE1	-	Transducin like enhancer of split 1
TNF- α	-	Tumour necrosis factor alpha
Try	-	Tyrosine
VAP33	-	VAMP-associated protein of 33kDa ortholog A
VEGF	-	Vascular endothelial growth factor
YAP	-	Yes-associated protein 1

YBX3	-	Y-box binding protein
ZO1	-	Zona Occludens 1
ZO2	-	Zona Occludens 2
ZO-3	-	Zona Occludens 3
ZONAB	-	ZO1-Associated Nucleic Acid-Binding Protein
Zu5 Domain	-	ZO1 and uncoordinated protein 5 domain

Table of Contents Page

List of Figures Page

1. Introduction.

1.1 Liver anatomy and structure.

The human liver is situated in the right upper quadrant of the abdominal cavity and accounts for 2-3 % of total body weight (Abdel-Misih and Bloomston 2010). The correct position of the liver is mediated through peritoneal reflections, avascular ligament-like attachments encased in the capsule of Gilsson (Tirkes et al. 2012).

Some materials have been removed from this thesis due to Third Party Copyright. Pages where material has been removed are clearly marked in the electronic version. The unabridged version of the thesis can be viewed at the Lanchester Library, Coventry University.

(Sibulesky 2013)

Figure 1.1: The anatomy of the human liver. The live is divided into the left and right functional lobes. The left and right lobes are further divided into eight independent functional lobes numbered in a clockwise fashion beginning at segment II. The medial and left lateral segment are separated by a ligament. Blue: inferior vena cava; Purple: hepatic portal vein; Red: hepatic artery; Green: common bile duct.

The liver receives 20 % of its blood supply as oxygenated blood from the hepatic artery. The remaining 80 % of the blood supplied to the liver is by the hepatic portal

vein from blood that is drained from the spleen and intestines. The liver is divided into eight segments based on Couinaud classification, named after the anatomist that first divided the liver into the eight segments, see Figure 1.1 (Chen et al 2012). Segments II and III are divided from the other six segments by the falciform ligament, which attaches the liver to the abdominal wall. The segments are characterised by containing a portal pedicle, of which contains its own hepatic venous branch, arterial branch, portal branch and bile ducts (Shabbir et al. 2010).

Blood drains from the liver through the three portal veins, this separates the right and left lobes of the liver. The portal vein divides the liver into upper and lower segments and further divides the left and right lobes. The portal vein splits the right lobe into posterior and anterior segments while the left lobe is split into medial and left lateral segments (Sibulesky 2013).

The hepatic lobule is a hexagonal functional lobe of the liver formed by the arrangement between hepatocytes and liver sinusoids. Situated on the perimeter of the lobe is the portal triad comprised of the small branches of the portal vein, hepatic artery and bile duct located, as shown in Figure 1.2.

A)

Some materials have been removed from this thesis due to Third Party Copyright. Pages where material has been removed are clearly marked in the electronic version. The unabridged version of the thesis can be viewed at the Lanchester Library, Coventry University.

Figure 1.2: Schematic diagram of the hepatic portal vein, shown in blue, and its arrangement in the hepatic lobule. Adapted from (Duncan et al. 2009). A, the portal triad is comprised of the portal vein, arterial blood and bile duct. The portal triad forms a hexagonal arrangement around the central vein to form a lobule.

The portal veins transport venous blood from the intestines that contain nutrients that need to be absorbed, metabolised or filtered out and the hepatic artery supplies the liver with arterial oxygenated blood branching from the celiac artery (Jaeschke 2008). The blood from the hepatic artery and portal vein mix and travels through a sinusoid a layer of one-cell thick hepatocyte plates that extend from the portal tract to the central vein. The hepatocyte plates form the bile canalicular network within their apical domain; these facilitate hepatocyte bile secretion which drains in the opposite direction of the sinusoid toward the bile duct via the Canal of Hering. The hepatic lobe also contains non-parenchymal cells that aid hepatocyte function.

1.1.1 Hepatocyte physiology and unique functions.

Epithelial polarity is essential in maintaining efficient hepatocyte function. Cellular spatial asymmetry allows a hepatocyte to interact with both the sinusoid lumen through its apical domain and the flow of bile through its basal domain (Revenu and Gilmour 2009).

In healthy and frequent forms of epithelia, the apical membrane is oriented toward the inside space of a lumen and the basal and lateral membranes are oriented away from the lumen. Hepatocyte epithelia differ slightly as the apical domain forms a narrow lumen creating bile canaliculi and the basolateral domains face the sinusoids interacting with the extracellular matrix (ECM) creating a multipolar organisation, as shown in Figures 1.2 and 1.3 (Reshetnyak 2013; Tryer and Müsch 2013). Although 70-80 % of cells within the liver are hepatocytes, for correct function hepatocyte interaction with the non-parenchymal cells is essential such as liver sinusoidal endothelial cells aid in the absorption of bile.

Hepatocytes interact with the non-parenchymal cells outlined in Table 1-1 and Figure 1.3.

Hepatic Cell	Functions
Hepatocyte cell	Detoxification, protein synthesis and biliary secretion
Liver sinusoidal endothelial cell	Endocytosis, regulation of vascular tone, maintenance of stellate cell quiescence and liver regeneration.
Hepatic stellate cells	Hepatic development, regeneration, immunoregulation and intermediary metabolism.
Kuppfer cells	Phagocytosis, liver repair and anti-inflammation
Cholangiocytes	Modification of hepatocyte derived bile

Table 1.1: Hepatic cell types and their functions within the liver.

(Poisson et al. 2017; Friedman 2008; Dixon et al. 2013; Tabibian et al. 2013)

1.1.2 Hepatocellular biliary absorption and secretion through interactions with liver sinusoidal cells.

Bile acid and biliary precursors are initially absorbed from the sinusoidal blood by fenestrae a feature present on liver sinusoidal endothelial cells. Fenestrae are approx. 100 nm in diameter and act as a sieve between the space of Disse and the sinusoidal lumen, shown in Figure 1.3 (Adams and Eksteen 2006).

Figure 1.3: The relationship between the parenchymal and non-parenchymal cells in the liver. Hepatocytes form a single epithelial layer either side of the lumen. This aids the function of the hepatocyte to absorb bile acids from the space of Disse. Bile canaliculi form between neighbouring hepatocytes. Figure adapted from (Adams and Eksteen 2006).

Bile acid in the space of Disse is absorbed by hepatocytes via the Na^+ dependant bile acid transporter in the basolateral domain facing the sinusoid, Na+-taurocholate cotransporting polypeptide (NTCP) (Jungst et al. 2013). Hepatocytes are responsible for the excretion of bile acid via Adenosine Triphosphate (ATP)-binding cassettes located within the bile canaliculi. The ATP-binding cassette transport used depends if

they are mono or divalent bile acids. Monovalent bile acids are excreted through the bile acids export pump (BSEP) and divalent bile acids are excreted through multidrug resistance associated protein 2 (MRP2). The biliary system also aids in the clearance of drugs, another protein found at bile canaliculi multidrug export pump multi-drug resistance protein (MDR) once excreted the bile can drain via the canal of Hering to the intrahepatic bile ductile (Claudel et al. 2011).

1.1.3 Hepatocellular detoxification

Hepatocytes are responsible for the absorption, metabolism and detoxify compounds that can cause damage to the liver or body. The detoxification process can be split into two phases. 80 % of the blood supply to the liver is mediated by the portal veins, the blood drains directly from the gastrointestinal system and can contain xenobiotics and drugs. Phase I, lipophilic fat-soluble toxins are oxidised, reduced, hydrolysed and hydrated primarily by Cytochrome P450 enzymes. Phase II, the biomolecules are conjugated and become hydrophilic to increase solubility to be excreted (Crettol et al. 2010).

1.2 Hepatocellular carcinoma epidemiology and incidence

Hepatocellular carcinoma (HCC) is the most common type of liver cancer globally. Prognosis as with any cancer is dependent on multiple factors such as tumour size, stage and grade. Presently, there is no definitive cure for HCC, the only treatment that significantly increases the five-year survival rate of HCC is the physical removal of early identified tumours or transplantation of the liver (Diaz-Gonzalez et al. 2016).

HCC epidemiology differs with geographic location and gender. HCC is 2.4 times more common in males compared to females. This is due to men having higher rates of hepatitis B virus (HBV), hepatitis C virus (HCV) and higher alcohol consumption. Asia has the highest HCC rates compared with data from Africa, Europe and the Americas showing similar prevalence. The higher the rates of HCC in Asia is found in areas also have endemic HBV which explains the highest HCC rates found in North and South Korea (Mittal and El-Serag 2013). Globally primary liver cancer accounts for a fifth of male cancers and a seventh of female cancers, however, it is the third most common cause of cancer death per year with 9.2 % of all cancer deaths (Ferlay et al. 2010, Bosetti et al. 2014). However Western lifestyles have increased the rate of HCC incidence in Western countries with a +142 % increase in UK liver cancers since the early 1990s (Office for National Statistics 2017). From the UK incidence rates in 2014 liver cancer of which HCC accounts for 80 % is expected to increase by 38 % in 2035 and is among the largest increases in incidence in the UK along with thyroid, oral and kidney cancers (Smittenaar et al. 2016).

1.2.1 Aetiology of HCC development from non-viral causes

Non-viral factors leading to HCC can arise from genetic syndromes and lifestyle choices. Non-viral factors resulting in HCC development has increased recently and mirrors trends such as elevated obesity and alcohol rates (Major et al. 2014).

Iron plays an important role at the centre of enzymes, ATP and oxygen binding in haemoglobin. However, iron overload syndromes that result in excess iron absorption will, if left untreated, causes HCC through haemochromatosis. Typically, this is due to an autosomal recessive disorder hereditary haemochromatosis due to

a mutation in the human hemochromatosis (HFE) gene. HFE causes an excess of free iron, which converts oxygen to toxic free-radical species. The reactive oxygen species results in peroxidation of membrane lipids, proteins and DNA. (Blonski and David. Forde A 2010). Peroxidation of membrane lipids results in several by-products such as, malondialdehyde, which reacts with DNA bases. Iron overload syndromes result in a 200-fold increased risk of HCC as the tumour suppressor gene TP53 is often mutated (Hussain et al. 2007).

Aflatoxins can result in HCC, foods with a mould such as *Aspergillus fumigatus* produce the metabolite aflatoxin B1 that causes a nucleotide substitution in tumour suppressor p53 at codon 249. Half of HCC cases have the p53 mutation in areas with high aflatoxin B1 exposure (Kew 2013).

Cirrhosis is an independent risk factor that can lead to the development of HCC. The latter stages of non-alcoholic fatty liver disease stemming from obesity produce chronic inflammation and consequential hepatic fibrosis can ultimately lead to liver cirrhosis. When this occurs, alterations in cell signalling pathways occur such as increased TNF-α signalling, advances the disease state (Baffy et al. 2012).

Consumption of more than 80 g/d ethanol over the course of five years is shown to increase the likelihood of HCC fivefold. Meta-analysis shows a distinct correlation between the amount of alcohol consumed and the likelihood of HCC development (Blonski and David. Forde A 2010).

1.2.2 Aetiology of HCC development from viral causes

The primary causes of HCC are HBV and HCV. HBV (53 %) and HCV (25 %) account for 78 % of primary liver cancers globally (Perz et al. 2006). The aetiology of HCC displays variation globally. In some Asian countries such as Japan and Singapore, HBV and HCV account for 90 % of liver cancer deaths in comparison to Western countries such as America the percentage is much smaller with only 64 % (Perz et al. 2006). The aetiology of HCC is shifting towards HCV due to national immunisation programmes. In 1982 an effective HBV vaccine was produced, but the introduction of immunisation programmes was slow due to cost (2USD/vaccine), so uptake was mainly in developed countries. In 2006 164 countries routinely vaccinated infants with the HBV vaccine but it is too early to quantify the change in the aetiology of HCC from the hepatitis virus (Nordenstedt et al. 2010).

1.2.3 Pathways of hepatocellular carcinogenesis

Hepatocarcinogenesis is associated with chronic liver damage, it is not often seen in normal healthy livers with acute inflammation. The most common cause of hepatocarcinogenesis is cirrhosis, which develops after chronic liver disease. Chronic liver disease, disease of the liver lasting over six months, has a low risk factor for hepatocellular carcinoma development. The risk of developing HCC is high when cirrhosis of liver presents. Figure 1.4, shows the pathway of developing HCC from the aetiologies described in, 1.2.1 and 1.2.2.

Figure 1.4 Pathway from aetiology of HCC to the generation of hepatocellular carcinoma. The aetiology of HCC results in chronic liver injury, depending on the original cause will induce chronic hepatitis or cirrhosis. These will cause focal hepatic lesions which have the potential to develop into HCC. (Coleman 2003)

When chronic hepatitis or cirrhosis presents they can form focal hepatic lesions, Figure 1.4, benign growth of abnormal tissue. Here, one of two pathways can lead to the development of HCC from focal hepatic lesions. These Focal hepatic lesions may generate hyperplastic nodules, an increased aggregation of cells or dysplasia, cells that have generated mutations. These lead to the formation of dysplastic nodules, increased cell aggregates that have been mutated. However, these are only benign growths, HCC develops when the benign growth develops the ability to metastasise.

1.2.4 Molecular mechanisms that induce hepatocarcinogenesis.

The molecular mechanisms that induce hepatocarcinogenesis are multifactorial, the development of HCC may include a few or many of the mechanisms that will be discussed.

Chromosomal shortening of the telomere limits the proliferative potential of the hepatocytes ensuring that there is a finite number of cellular divisions. During chronic liver disease, the telomere shortening is accelerated, this leads to a build-up of senescent cells. When the telomere shortens to a critical length, chromosome uncapping occurs which induces DNA damage signals. This results in cell cycle arrest and eventually apoptosis through check point inhibition of p53. When this protective mechanism dysfunctions it allows for unlimited proliferative potential (Begus-Nahrmann et al. 2012).

Activation of the DNA repair pathway can result in chromosomal fusions, when these cells divide, chromosomal breakage leads to chromosomal translocations, gains and losses in the daughter cells resulting in aneuploidy (Carulli and Anzivino 2014). Cell cycle arrest during cirrhosis has been shown to enhance the development of HCC. Hepatocytes that have gained increased proliferation potential will expand their numbers in a liver that is not regenerating as normal. This is shown with increased expression of p21, a target of p53, and HCC risk (El–Serag et al. 2007).

Aberrant hepatocyte microenvironment aids the progression of liver disease and HCC. Liver mass is controlled by a balance of a variety of growth factors, during cellular senescence, there is a change to a growth stimulatory microenvironment. This is compounded by the effects of cirrhosis or chronic hepatitis, which activate stellate cells. These cells are responsible for producing cytokines, growth factors and components of the extracellular matrix (El–Serag et al. 2007).

When cell cycle progression inhibition is overcome due to modifications of the DNA damage check points, clonal expansion of the aberrant hepatocytes occurs. p53 is the major tumour suppressor pathway that is mutated in 20-50 % of cases in the development of HCC. p53 is responsible for limiting cellular proliferation after shortening of the telomeres, suppression of oncogene activation and protects chromosomal integrity. Mutations of p53 lead to inability to inhibit cell cycle arrest and increases resistance to apoptosis (Lujambio et al. 2013).

In 80 % of HCC cases there is d disruption of the p16 checkpoint tumour suppressor, typically through methylation of the promotor. Like p53, p16 is responsible for limiting

cell proliferation potential when there is critical shortening of the telomeres (El–Serag et al. 2007).

Disruptions in both p53 and p16 checkpoint pathways allow for expansion of premalignant hepatocytes. Inactivation of the checkpoint pathways increases the resistance to apoptosis, transforming growth factor β activation can induce apoptosis. However, the hepatocytes do not go through apoptosis, the molecular mechanisms are not fully understood but it is reasonable to assume the activation of oncogenic pathways play an important role in this process (Lujambio et al. 2013). Activation of oncogenic pathways is thought to occur later in hepatocarcinogenesis compared with other cancers. The two classically described oncogenic pathways are the Wnt/β-catenin and PI3K/Akt pathways.

The Wnt/β-catenin pathway shown in, Figure 1.5, becomes activated after transcriptional repression of negative regulators. Without Wnt signalling cytoplasmic β-catenin is ubiquitinated by a destruction complex and targeted for proteasomal degradation.

Figure 1.5: The canonical Wnt pathway with and without Wnt activation. Left shows, the inhibition of β-catenin nuclear translocation and resultant for proteasomal degradation of β-catenin. Right shows, activation of the pathway after Wnt ligand binding to frizzled. β-catenin translocates to the nucleus for form a complex with LEF/TCF promoting cell proliferation. (Dahmani et al. 2011)

Upon Wnt binding to frizzled on the cell membrane, resulting in the translocation of a constituent of the destruction complex, axin. Coupled with the loss E-cadherin, which sequesters β-catenin to sites of cellular adhesion, there is an increase in cytoplasmic β-catenin. β-catenin then is free to translocate to the nucleus to form a complex with T cell factor (TCF) and lymphoid enhancer factor (LEF). TCF is represses gene expression through interactions with transducin like enhancer of split 1 (TLE1) promoting histone deacetylation and chromatin compaction. LEF occupies the Wnt responsive element to increase expression of c-myc, responsible for increased cellular proliferation (Dahmani et al. 2011).

Activation of the prolactin induced protein 3 (PIP3)/protein kinase B (Akt) pathway, Figure 1.6, is activated when a growth factor, such as Epidermal growth factor (EGF), binds to the receptor tyrosine kinase. resulting in a conformational change resulting in the removal of the auto-inhibitory domain of PI3K. Activated PI3K catalyses the phosphorylation of prolactin induced protein 2 (PIP2) converting it to PIP3. PIP3 is responsible for the activation of intracellular signalling pathways including Akt.

Figure 1.6: The PI3K/Akt pathway and the resultant downstream signalling events. Downstream effect of Akt repress tumour suppressors and pro-apoptotic genes. (Toren and Zoubeidi 2014)

Downstream signalling of Akt, as shown in Figure 1.6, activates gene transcription. Transcription inhibition of pro-apoptotic genes, BCL2 associated agonist of cell death (BAD) and BCL2 associated x, apoptosis regulator BAX promote increased cell

survival. Akt is also responsible for the ubiquitination of forkhead box O1 (FOX01), which functions as a tumour suppressor (Toren and Zoubeidi 2014).

1.2.5 HBV endocytosis and induced hepatocarcinogenesis.

HBV hepatocyte entry is a multifactorial process, HBV initially binds to the surface heparan sulphate proteoglycans via large HBV (LHBs), middle HBV (MHBs) and small HBV (SHBs) viral surface proteins. The virus then binds to receptors of higher affinity, which facilitate the early entry step. These receptors are not fully alluded yet however sodium taurocholate co-transporting polypeptide has been suggested a possible candidate (Ni et al. 2014). The internalisation of the virus by endocytosis is reported to be mediated be caveolae, clathrin or macropinocytosis-dependent endocytosis. Different entry mechanisms have been highlighted due to the different cell types used in investigations (Gao et al. 2013; Huang et al. 2012; Macovei et al. 2010; Cooper and Shaul 2006).

Chronic HBV infections can cause HCC through direct or indirect mechanisms. Indirect methods of HBV induced HCC are due to HBV invoking a strong immune response resulting in chronic hepatitis cirrhosis a major risk factor for HCC (Yang et al. 2011). The molecular mechanisms behind cirrhosis leading to HCC has been described in 1.2.4.

Direct development of HCC due to HBV infection and can be independent of liver cirrhosis. HBV DNA integration has been localised to almost all chromosomes and can result in chromosomal rearrangements. There are two potential ways the host DNA becomes altered, the *cis* and *trans* effect.

The *cis* effect, occurs when, the integration of HBV DNA results in insertional mutagenesis. Large scale studies showed, that HBV integration into the host DNA is not random, it often targets genes involved in cell survival, proliferation and immortalisation (Neuveut et al. 2010).

The common integration sites include, telomerase reverse transcriptase (TERT), histone-lysine N-methyltransferase 2B (MLL4), cyclin E1 (CCNE1), fibronectin 1 (FN1), Rho associated coiled-coil containing protein kinase 1 (ROCK1) and SUMO specific peptidase 5 (SENP5).

These genes have a role in inhibiting or activating pathways driving tumourigenesis. For example, DNA integration of HBV into TERT and CCNE1, allows for the overriding of cellular senescence and progression of the cell cycle from G1 to S (Hai et al. 2014).

The *trans* effect, occurs through the production of mutated hepatitis B viral protein x (HBx) proteins. The C-terminal region of the HBx protein damages the mitochondria and increases the level of reactive oxygen species due to incomplete oxygen reduction in the electron transport chain. The DNA base guanine is prone oxidation by the reactive oxygen species converting it to 8-hydroxyguanine, over time this causes genetic alterations (Giampazolias and Tait 2016).

1.2.6 HCV endocytosis and induced hepatocarcinogenesis.

HCV does not enter the hepatocyte or induce carcinogenesis in the same mechanism as HVB. The primary attachment of the HCV virus occurs through cell surface attachment factors glycosaminoglycans and Low-Density Lipoproteins

Receptor. Currently it is believed that scavenger receptor class B type 1 (SR-BI) is the initial protein attachment to HCV, once this attachment occurs it forms a complex with cluster of differentiation 81 (CD81). CD81 then forms a complex with the tight junction proteins occludin or claudin-1. HCV is thought to activate the Rho GTPase proteins to facilitate in the lateral movement of the CD81 bound to HCV, this enables the interactions between CD81 and the tight junction proteins (Meredith et al. 2012). SR-BI, CD81 and claudin-1 essential for HCV entry however in non-permissive cells they are insufficient to allow HCV entry. Studies show that overexpression of occludin and endogenous expression of CD-81 and claudin allowed for efficient infection of HCV. As such hepatocytes downregulate the expression of claudin-1 and occludin to prevent HCV superinfection (Liu et al. 2009).

HCV endocytosis occurs at the tight junction, virus binding causes reorganisation of the actin cytoskeleton and redistribution of virus-receptor complexes to the tight junction. This results in pH independent, clathrin mediated endocytosis of the virus (Meredith et al. 2012).

Unlike HBV, HCV is a cytoplasmic-replicating virus as it is a single-stranded RNA virus that does not have reverse-transcriptase enzyme and therefore does not integrate into the host DNA. As with HBV, HCC invokes a large immune response resulting in chronic hepatitis cirrhosis.

The innate immune response to HCV initially facilitates the control and dissemination of HCV. During viral replication HCV structural proteins are release into the extracellular microenvironment. Immature dendritic cells recognise these viral antigens via their Toll-like receptors. Mature dendritic cells release several cytokines such as interleukin 12, tumour necrosis factor alpha and interferons alpha. These cytokines activate natural killer cells the initiate the apoptosis pathways in antigen

presenting cells. Activated natural killer cells induce inflammatory cluster of differentiation (CD4+) T-helper type cells. Insufficient cytokine production and the resultant lack of T-helper cell differentiation permits virus persistence and chronic disease (Castello et al. 2010).

1.2.7 Hepatocellular carcinoma grading

Barcelona clinic liver cancer (BCLC) has five classifications of HCC stage in order of severity; stages 0, A, B, C and D. Patients with HCC stage 0 and A have a single HCC tumour that can be treated by resection, transplantation and ablation of the liver. Patients with HCC at stages 0 and A have a five-year survival rate of ~60-80 %.

After stage, A surgery is no longer a viable option and chemotherapy agents are needed. The most commonly prescribed treatments for BCLC stages B, multiple liver tumours of HCC and C, distant metastasis of HCC are doxorubicin and sorafenib. These treatments aim to increase survival time by restricting HCC growth and angiogenesis. For stages B and C, the survival time is typically <2.5 years and <11 months respectively (Verslype et al. 2012; Raoul et al. 2012).

Patients with BCLC stage D have a loss of liver function and do not currently have any treatment options, instead any resulting complications are managed and supportive care is given (Dhir et al. 2016).

1.3 Cellular adhesion

In multicellular organisms, cells bind via protein interactions to allow the formation of complex tissue structures such as epithelia. Cells mediate attachment to each other

through membrane-spanning proteins creating adhesive junctions. These cellular junctions are not static complexes; besides their adhesive role they form selectively permeable membranes and are involved in cellular signalling. Cellular adhesion between eukaryotic cells occurs through tight, adherens, GAP and desmosome junctions (Balda and Matter 2016).

1.3.1 Tight junctions

Electron microscopy has shown that tight junctions (TJs) are located at the uppermost apical point of the lateral membrane in epithelial cells forming a succession of cellular “kissing points” between neighbouring cells (Farquhar and Palade 1963). Freeze-fracture experiments showed that the 2D “kissing points” were, in fact, a continuous 3D network of elevations along the extracellular face. As shown in Figure 1.7 (Staehelin 1973). The fence function of TJs maintains and delineates the apical and basolateral domains of the epithelial cells. The TJs, however, do not seal the apical intercellular space; they form a selectively permeable barrier to paracellular ions and solutes due to size and charge (Hartsock and Nelson 2008). Tight junctions are not static structures but instead regulated the epithelial phenotype through signalling, maintaining cell polarity, proliferation and trafficking of molecules (Lee and Luk 2010).

Figure 1.7: location of the tight junction in an epithelial sheet, the tight junctions form continues fibrils that seal the paracellular space between neighbouring cells. A: shows a transmission electron microscopic image of the kissing points formed by the tight junctions. B: shows the location of the tight junction in an epithelial cell, the tight junction is located at the upper most apical domain of the cell. Adapted from (Brander et al. 2008; Steed et al. 2010).

The extracellular domain of the TJ consists of four main proteins families occludin, claudins, marvel associated proteins and junction adhesion molecules (JAM) (Chiba et al. 2008). These proteins form complexes that create homophilic dimers with adjacent cells that link to the actin cytoskeleton. Due to their importance cancer progression is often associated with altered expression of these proteins, this is especially noted in epithelial to mesenchymal transition (EMT) (Martin 2014).

1.3.2 Occludin

The human OCLN gene located on 5q13.1 encodes for occludin a ~60 kDa tetraspanin membrane protein found in both epithelial and endothelial cells (Dörfel and Huber 2012). When occludin is phosphorylated (~65 kDa) it facilitates the maintenance of paracellular permeability and cell to cell adhesion. Occludin has a 64 aa (amino acids) N-terminal and a 259 aa C-terminal domain that projects

intracellularly into the cytoplasm (Cummins 2012). Occludin also has four transmembrane domains linked via two extracellular loops (EL), EL1 and EL2 of 46 and 48 aa respectively and a 10 aa intracellular loop (Liu, S. et al. 2009). The extracellular loops of occludin interact with their homotypic extracellular loops of occludin on neighbouring cells.

Figure 1.8: Visual representation of occludin when integrated into the phospholipid bilayer. The shows the NH_2 and COOH cytoplasmic domains of occludin, two extracellular loops and one cytoplasmic loop. (Dörfel and Huber 2012)

This is mediated by the amino acid content of the extracellular loops, EL1 and EL2, shown in Figure 1.8, are both enriched with tyrosine. EL1 is rich with both tyrosine and glycine accounting for nearly 60 % of the amino acids (Bewley et al. 2013). The cytoplasmic C-terminus of occludin has a coiled coil domain that binds to tight junction complex proteins VAP33, cingulin, ZO1, 2 and 3 via redox dependent dimerisation that anchor occludin to F-actin (Li et al. 2005).

Occludin knockout mice studies show occludin is not essential in embryonic development with the correct morphogenesis and maintenance of TJ. However, these mice displayed many abnormalities most importantly these were chronic inflammation, growth retardation and deafness suggesting occludin as alternative functions besides cellular adherence (Saitou et al. 2000).

The functional role as an adhesive and signalling molecule is not fully understood, the loss of occludin in (Madin-Darby Canine Kidney cells) MDCK cells did not affect transepithelial resistance, a measurement of electrical resistance across a monolayer of cells. This measurement is a method of confirming the integrity and permeability of a monolayer. Conversely, occludin overexpression in MDCK cells increases the transepithelial resistance up to 40 %. This shows similar results to the experiments conducted in the knockout mouse but it does show occludin has an adhesive function (Saitou et al. 2000).

A loss of occludin expression and disruption of occludin has different effects in TJ formation and function. In occludin delineated tight junction disruption of the extracellular loops of occludin increases paracellular permeability (Nusrat et al. 2005). This effect is mirrored in experiments in which truncated C-terminus of occludin was investigated. Occludin correctly localises to the TJ does not form correct cytoplasmic TJ complexes which increases paracellular permeability (Subramanian et al. 2007).

This evidence shows occludin is not necessary for the establishment of TJ but does have a regulatory role over TJ function, which is mediated by signalling pathways

(Murakami et al. 2009). One such signalling factor Tumour necrosis factor alpha (TNF- α) signalling results reduce in occludin redistribution from the tight junction to cytoplasmic vesicles (Raleigh et al. 2010). The inhibition of occludin endocytosis inhibits TNF- α induced and disruption of the tight junction, thus proving occludin has a role in regulating the tight junction (Van Itallie et al. 2010).

1.3.3 Protein phosphorylation in cancer

Protein phosphorylation in a post-translational modification of proteins. A specific amino acid residue becomes reversibly phosphorylated by a protein kinase, this covalently binds a phosphate group to a polar R group on an amino acid. This changes the conformational shape of the protein as the protein is less hydrophobic and becomes hydrophilic polar (Solaini et al. 2011).

Phosphorylation is important in cancer due to the regulatory capacity they have over the cell, any changes in the regulation can be oncogenic. Mutations or epigenetic changes that occur in cancer lead to the aberrant activation or dysregulation of cellular pathways. Protein kinases, the enzyme that facilitates phosphorylation is typically targeted in cancer. This is a molecular switch that activates of inhibits the cellular pathway (Ardito et al. 2017).

This does however, give a therapeutic target, as they are involved in all cancers. Sorafenib is a kinase inhibitor the inhibits Raf kinase in the Raf/MEK/ERK pathways (Pang et al. 2009)..

1.3.4 Occludin phosphorylation

Occludin is undergoes reversible phosphorylation of serine, threonine and tyrosine especially in the C-terminal region involved in tight junction complex binding (Elias et al. 2009). The phosphorylation of occludin is Ca^{2+} dependent, Ca^{2+} media switch assays show rapid dephosphorylation of occludin at serine and threonine residues and the rephosphorylation of these residues with the addition of Ca^{2+} containing media (Suzuki et al. 2009).

In quiescent epithelium, occludin displays high phosphorylation particularly at serine and threonine residues (Sundstrom et al. 2009). The correct function of occludin epithelial tight junctions is positively correlated with phosphorylated serine and threonine residues. The dissociation of tight junctions is correlated with the dephosphorylation of these residues and the phosphorylation of thymine residues, providing more evidence that occludin has a regulatory function in the tight junction (Murakami et al. 2009).

The atypical protein kinase C (aPKC) isoform PKCζ is located near the cellular tight junctions in MDCK cells. In experiments PKCζ incubated with the C-terminus of occludin resulted in phosphorylation of Ser/Thr residues, demonstrating PKCζ is a positive regulator of epithelial cell barrier function (Jain et al. 2011). Another PKC isoform PKCη is prevalent in epithelial cells specifically is involved in the phosphorylation of threonine at residues T403 and T404 essential for occludin tight junction assembly (Suzuki et al. 2009).

1.4 Zonula Occludens complexes.

The zonula occludens (ZO) family is made up of ZO1, ZO2 and ZO-3. These proteins are also known as tight junction proteins encoded by TJP1, TJP2 and TJP3 genes respectively. ZO1 was the first identified zonula occluden protein by Stevenson and Goodenough. A stable hybridoma cell line was isolated that produced an antibody that was specific to the kissing points seen in thin section slides. The antibody recognised a 220 kDa protein that was located at the tight junction in tight junction enriched liver fractions (Stevenson et al. 1986).

ZO2 and ZO-3 were later identified through coimmunoprecipitation with ZO1 complex (Gumbiner et al. 1991, Balda et al. 1993). MDCK cells were used to isolate ZO1, through coimmunoprecipitation investigations it was seen that the 160 kDa protein isolated was not degraded ZO1. Several antibody epitopes of ZO1 did not recognise the 160 kDa ZO2 band (Gumbiner et al. 1991). ZO3 was also discovered through coimmunoprecipitation with ZO1 from MDCK cells, however Haskins et al. identified there was a proline rich region between Discs-large homologous regions 2 (PDZ2) and Discs-large homologous regions 3 (PDZ3). Further investigations showed that it interacted with cytoplasmic domain of occludin but not ZO1 (Haskins et al. 1998).

These proteins are a member of the MAGuK superfamily identified by (PDZ), SRC Homology 3 Domain (SH3) and a noncatalytic guanylate kinase (GuK) interaction domains (Bauer et al. 2010). Zonula occldens proteins differ from the MAGuK family as they have an additional two PDZ domains before the conserved N-terminal PDZ/SH3/Guk domains (Bauer et al., 2010). MAGuKs are a family of scaffold proteins can form protein-protein interactions with cytoskeletal proteins. In epithelial

cells, MAGuKs are also involved in the development and maintenance of cell polarity.

The three zonula occludens proteins consist of a leucine zipper dimerisation motif, a basic domain, an acidic domain and a proline-rich region at the C-terminus, this allows the ZO complex to anchor the TJ to the actin cytoskeleton (Tsukita, Sachiko et al. 2009).

Figure 1.9: Tight junction and actin protein binding domains of ZO1, 2 and 3. The ZO proteins act as a tight junctional protein to F-actin converter through their binding domains. However, ZO1 binds to occludin through its GUK unlike ZO2 and 3 which bind to occludin through their PDZ domains. (Bazzoni and Dejana 2004).

The three ZO proteins have distinct roles in the tight junction complex; the PDZ/SH3/GuK and basic domains are different on each ZO protein allowing for different interactions to occur (Gao et al. 2016). ZO1 can directly bind to all the TJ proteins, ZO2, ZO-3 and actin as shown in Figure 1.9. ZO2 and ZO-3 cannot bind to as many of the TJ complex proteins, but ZO-3 has the unique ability to interact with

PALS1-associated TJ protein (PATJ), which is involved in the development of apical basal polarity (Gonzalez-Mariscal et al. 2016).

1.4.1 Zona Occludens 1

The human TJP1 gene located on 15q13.1 encodes for the zona occludens protein 1 (ZO1) a ~220 kDa scaffold protein located in the cytoplasmic membrane of tight junctions (Ciana et al. 2010). ZO1 differs from ZO2 and ZO-3 as it has a ZU5 domain at the N-terminus after the GuK domain. The function of the ZU5 domain is not well understood; Macromolecular flux experiments show that the ZU5 domain aids tight junction barrier formation by stabilising ZO1 at the tight junction (King et al. 2016). ZO1 also has an 80 aa domain, the α-motif that can be alternatively spliced resulting in a double band during Western blot analysis (Cummins 2012).

$ZO1^{-/-}$ deficient mice result in a lethal phenotype at E11.5, 11 days after the presence of a vaginal plug, showing the importance of ZO1 in the development of epithelia. $ZO1^{-/+}$ mice were not a lethal phenotype and epithelia could form but the mice presented vascular defects (Katsuno et al. 2008).

ZO1 as described above has a role in forming a complex at the apical tight junctions. Epithelial ZO1 localisation and function is Ca^{2+} dependent when cultured in low Ca^{2+} media ZO1 is associated with β-catenin at adherens junctions. The reintroduction of Ca^{2+} media dissociates ZO1 from β-catenin and ZO1 correctly localises to the tight junction (Van Itallie et al. 2013).

1.4.2 Zona Occludens 2

The human TJP2 gene located on 9q21.11 encodes for the zona occludens protein 2 (ZO2) a ~ 160 kDa scaffold protein located in the cytoplasmic membrane of tight junctions (Ciana et al. 2010). ZO2 also has two main spliced transcripts of which both have altered expression in cancers, such as the Alu-related transcript of ZO2 in colorectal cancers (Sambrotta et al. 2014; Kim et al. 2013).

$ZO2^{-/-}$ deficient mice was a lethal phenotype and embryos do not progress beyond E8.5, showing ZO2 is essential for development (Xu et al. 2008). However, it appears that the loss of ZO2 function is species specific, mutations in the TJP2 genes in humans is not a lethal phenotype, although it does result in progressive cholestatic liver disease and an increased chance of developing infant hepatocellular carcinoma (Sambrotta et al. 2014). This highlights ZO2 function within the liver, ZO2 appears to be important in the recruitment of export pumps to the bile canaliculi (Sambrotta and Thompson 2015).

1.4.3 Zona Occludens 3

The human TJP3 gene located on 19p13.3 encodes for the zona occludens protein 3 (ZO-3) a ~140 kDa scaffold protein located in the cytoplasmic membrane of tight junctions and is only expressed in epithelial cells (Ciana et al. 2010). The functional properties of ZO3 have not been investigated in detail in comparison with ZO1 and ZO2. $ZO3^{-/-}$ knockout mice experiments show no obvious change in phenotype and is not required for the formation or function of TJ. This is explained in part by the close structural similarity between the ZO proteins, in $ZO3^{-/-}$ mice ZO2 staining at was more concentrated at the junctions (Adachi et al. 2006).

1.4.4 Claudins

The occludin knockout mice investigation demonstrated occludin was not essential in the formation of tight junctions and showed there must be more TJ associated proteins that could compensate for occludin; this resulted in the discovery of claudin 1 and 2 (Furuse et al. 1998). Claudins are a family of tight junction proteins, they form tight junctions and cytoplasmic plaques like occludin (Singh et al. 2010).

Claudins (CLDN) in humans range from CLDN1-24 and are tight junction adhesion molecules that are much smaller than occludin, approximately 20-27 kDa (Singh et al. 2010). Humans have 23 different CLDN genes because they do not have CLDN-13 only present in rodents. The number of claudins in humans increases to more than 23 with the addition of CLDN isoforms (Lal-Nag and Morin 2009; Thompson et al. 2010). The evolution of the claudin family is likely due to the gene duplications that occurred in chordate development (Mukendi et al. 2016). Many of the claudin genes show high homology and are proximally located on the same chromosomes, CLDN-6 and 9 are only 200 bp apart on chromosome 16 (Lal-Nag and Morin 2009). The CLDN family is split into ‘classic’ claudins and ‘non-classic’ claudins based on their genetic sequence analysis (Krause et al. 2015). Like occludin, claudins are tetraspanin adhesion molecules with two extracellular loops with cytoplasmic N and C-terminals (Evans et al. 2007).

CLDNs are essential components of the tight junction and claudins have differences in expression and function in different tissues. CLDN-1 knockout mice die postnatally due to dehydration from transepidermal water loss and CLDN19 knockout mice

causes peripheral neuropathy and behavioural abnormalities due to the demyelination of axons (Furuse at al. 2002; Konrad et al. 2006).

The CLDN structure is closely related to occludin; they are both tetraspanin membrane proteins with four transmembrane domains. However, the EL2 domain of claudin is considerably smaller ranging between 16-35 aa and claudin has shorter N-terminal and C-terminal domains. Although occludin and claudin both colocalise at the tight junctions and have similar quaternary structure, they do not show any sequence likeness (Findley and Koval 2009).

1.4.5 Junctional adhesion molecule

Junctional adhesion molecules (JAM) were identified through confocal and immune electron microscopy (Martin-Paudura et al. 1998). They are another family of 4 tight junction proteins JAM A, B, C and D. Like occludin and claudin have two extracellular loops they are not tetraspanin, JAMs are instead IgG-like proteins that can bind as homo or heterophilic dimers. Unlike occludin and claudin, JAM is also expressed in cells that do not exhibit tight junctions such as leukocytes aiding in transendothelial migration. Like occludin and claudin however, JAM bind to the zona occludens through the PDZ domain. The JAMs can also directly bind to cytoplasmic protein PAR-3 through a PDZ domain and JAM-A can directly bind to the PDZ domains of cytoplasmic proteins AF-6 and MUPP1.

JAMs binding to PAR3 results in cellular polarity after the establishment of nectin junctions. Nectins can bind in both homotypic and heterotypic independently of Ca^{2+} this recruits PAR3 which binds via the first of three PDZ domains to the JAMs. This

correctly localises PAR3 and in turn, promotes the localisation E-cadherin and JAM to the basolateral plasma membrane (Harris and Tepas 2010). JAM binds to the second PDZ domain of phosphatidylinositide phosphates (PIP_2 and PIP_3) located in the plasma membrane and the third PDZ domain binds directly to Phosphatase and tensin homolog (PTEN) (Wu et al. 2007). PAR3 binding to PTEN converts PIP3 to PIP2 which attracts Anx-2, in turn attracting more PAR complexes. This occurs in two opposing cells allowing basolateral adherence facilitated through Rho-family GTPase activity (Iden and Collard 2008).

1.4.6 Tricellulin and marvelD3

Tricellulin (marvelD2) and mavelD3 along with occludin form a group of marvel proteins, more specifically a family of tight junction-associated marvel proteins (TAMP). These proteins meet at cellular junctions where more than two cells meet creating a tricellular tight junction tTJ (Mariano et al. 2011).

Although these three proteins share a similar function they have distinct roles. In siRNA knockdown experiments the other proteins do not compensate for the loss of the knocked down gene (Raleigh et al. 2010). Although mutations in tricellulin result in non-syndromic hearing loss a similar phenotype in the occludin knockout mice (Chishti et al. 2008).

1.4.7 Adherens junctions

Adherens junctions are also found in the upper apical domains on the lateral membrane of epithelial cells, however, adherens juncations are more basal than TJ.

However, unlike TJ they form rod-like homodimers that bind to their complementary junctional protein found on an opposing apical membrane. The two adherens junctions are mainly comprised of cadherin or nectin-afadin (Harris and Tepass 2010).

The nectin-afadin complex consists of nectin, a transmembrane protein bound to intercellular afadin that directly binds to the actin cytoskeleton. There are three IgG-like extracellular loops in the nectin protein that gives rise to its binding ability (Niessen and Gottardi 2008). Nectin-afadin junctions are critical as it is theorised they provide the scaffolding for the development of adherens junctions and tight junctions (Indra et al. 2013).

The Cadherin-catenin junctions form weak cell-to-cell adhesion that is Ca^{2+} dependent. They form cadherin-catenin clusters to give adhesion strength (Tian et al. 2011). The transmembrane cadherin binds to the actin cytoskeleton through intercellular α and β-catenin. Cadherin-catenin junctions are epithelial phenotypical cell markers of polarity and a loss of the epithelial cadherin (E-cadherin) occurs in metastatic progression (Tian et al. 2011).

1.4.8 GAP junctions

Gap junctions are present in almost all human cell types are formed by connexin, they allow for the sharing of small molecules and ions between neighbouring cells. There are over 20 connexins and their nomenclature is derived from their predicted molecular weights via cDNA sequencing (Bai and Wang 2014). Connexin expression is cell specific but structurally similar as all cadherins share 4 transmembrane

domains, 2 extracellular loops, 1 cytosolic loop and cytosolic C and N-terminal domains (Meşe et al. 2007). Six connexin molecules form a hexagonal connexon in the lateral domain of the cell. The gap junction is formed when a connexon from one cell becomes docked to another connexon in an opposing cell (Falk et al. 2016; Gong et al. 2013) Gap junctions account for 3 % of the total membrane surface of hepatocytes and have a rapid turnover. Cx32 the most common hepatic connexin has a half-life ~1-5 hours and is degraded via the lysosomal pathway (Vinken et al. 2010).

1.5 The Interactions between occludin and the zona occludens proteins.

The function of the tight junction complex is to provide an anchor for occludin to bind to F-actin. Occludin bound ZO proteins to allow binding to a vast array of proteins resulting in a cellular signalling network controlling cell fate. These proteins include afadin, cingulin, cortactin, α and β-catenin which predominantly act as F-actin conversion molecules for the ZO proteins (Gissen and Arias 2015; Herr et al. 2014; Konopka et al. 2007; Ooshio et al. 2007). When TJ complexes form there is inhibition of G1/s phase and the generation of cellular polarity (Matter et al. 2005).

Occludin can bind to cytoplasmic cingulin, VAP33, directly to F-actin or zona occludens. The binding of occludin to ZO proteins is facilitated through the C-terminal GuK domain present on the ZO proteins and the cytoplasmic C-terminal domain, E of occludin (Paris et al. 2008). Once occludin-ZO proteins bind, the cytoplasmic complex of the tight junction can form and acts as a cytoplasmic scaffold converter between occludin and F-actin.

The cytoplasmic tight junction complex is not a fixed protein arrangement and can display different conformational formations. For example, the ZO2 may directly bind to the c-terminal region of occludin or indirectly bind to occludin by binding to occludin bound ZO1. When the ZO proteins bind to each other via their PDZ2 domains, this functional similarity shows an overlapping function of the ZO proteins.

The correct occludin phosphorylation state is needed for ZO proteins to associate with occludin. As mentioned, phosphrylated tyrosine on occludin reduces barrier function, phosphorylation of occludin via c-Src activation at Tyr-398 and Tyr-402 residues attenuates occludin-ZO interactions resulting in mislocalistion of the proteins (Elias et al. 2009).

1.5.1 Occludin, ZO1 and ZO2 interactions in endothelial cell types

Occludin is present in epithelial and endothelial cells and forms complexes with ZO1 and ZO2 similarly to epithelial cells. In epithelial cells the junctional complexes are well organised unlike endothelial cells. Tight junctions in endothelial cells are located below the adherens junctions. Although the interactions between ZO proteins and occludin are similar in both epithelial cells, endothelial tight junctions have an additional role in vascular homeostasis in the endothelium (Luissint et al. 2012). Due to this occludin/ZO interactions are implicated in disease.

Occludin and claudin are responsible for the formation of the blood brain barrier along with the ZO proteins. ZO proteins have been shown to be associated with

oxidant-induced barrier disruption as they form the cytoplasmic scaffold with perijunctional actin and occludin (Balbuena et al. 2011).

It has been shown that experimental diabetes reduces the level of occludin and ZO1 interaction at the tight junction in the retinal arterioles and capillaries increasing vascular permeability in the same manner as the blood brain barrier (Gardener et al. 2002).

1.5.2 Interactions and distribution of occludin and zona occludens proteins in the liver

Through coimmunfluorescence investigations the distribution of occludin, ZO1 and ZO2 have been assessed in the liver. Occludin, ZO1 and ZO2 in hepatocytes outline the bile canaliculi, see Figure 3.10.

Some materials have been removed from this thesis due to Third Party Copyright. Pages where material has been removed are clearly marked in the electronic version. The unabridged version of the thesis can be viewed at the Lanchester Library, Coventry University.

Figure 3.10: Location of occludin, ZO1 and ZO2 in coimmunfluorescence studies in a normal rat liver. A. Occludin in green and ZO1 is red. Where expressed equally such as along the porto-central axis there is fluorescence overlap between green and red to make yellow. B. ZO1 is red and ZO2 is green. Unlike occludin/ZO1 staining ZO1/ZO2 had a stronger expression in periportal hepatocytes, yellow fluorescence overlap. (Maly and Landmann 2008).

Occludin, ZO1 and ZO2 show expression around the bile canaliculi forming uninterrupted rings, see Figure 3.10. Occludin and ZO1 was equally expressed in by all hepatocytes in the liver lobule, however, coimmunfluorescence studies show that occludin and ZO1 localise together in the porto-central axis. ZO2 however, shows strong expression in the tight junctions of periportal hepatocytes and there is a gradient decrease in expression level towards the perivenous hepatocytes (Maly and Landmann 2008).

1.5.3 Occludin and zona occludens proteins in liver disease

Liver hepatitis is predominantly caused by chronic infections of HBV and HCV. HBV/HCV invoke hepatic inflammation and a strong immune response resulting in chronic hepatitis cirrhosis a major risk factor for HCC (Yang et al. 2011). Occludin has been recognised as a co-receptor essential for late-post binding of HCV and has been linked to viral internalisation (Ploss et al. 2009). HCV internalisation is mediated by clathrin-mediated endocytosis via interactions between the second extracellular loop of occludin and HCV bound glycoproteins (Liu et al. 2009). As a result, occludin is downregulated during HCV infection to prevent superinfection (Liu et al. 2009)

Cholangiocarcinoma a rare biliary tract cancer accounting for 1 % of global cancers and is associated with a downregulation of occludin, ZO1 and E-cadherin with upregulated claudin-2 and -4 (Németh et al. 2009; Németh et al. 2009). Typically cholangiocarcinoma has metastasised before the onset of symptoms resulting in a

poor prognosis. The TJ disruption through downregulation of occludin and ZO1 allows for an aggressive tumour that metastasis throughout the liver (Malaguarnera et al. 2011).

Protein-truncating mutations in the TJP2 gene cause progressive cholestatic liver disease (PFIC). PFIC2 presents with persistent neonatal cholestasis with mutations in the biliary export pump gene ABCB11 (Van Mil et al. 2004). For patients who presented with these symptoms but who did not have mutations in biliary export pumps; next-generation sequencing identified a mutation in the TJP2 gene that can singularly be responsible for PFIC2 (Sambrotta et al. 2014). Western blot experiments show no positive staining for ZO2 in these patients suggesting degradation via non-sense mediated mRNA decay pathways (Sambrotta and Thompson 2015). A prerequisite of non-sense mediated mRNA decay is the presence of one retained exon junction complex downstream to the premature termination codon, typically the TJP2 mutations that present with PFIC fit the prerequisites (Dröge et al. 2016). Further evidence that alluded to TJP2-truncated non-sense mediated mRNA decay was a reduction of TJP2 mRNA (Sambrotta and Thompson 2015).

The loss of ZO2 from the canaliculi results in the mislocalisation of claudin 1 from the TJ. The resultant disruption of hepatobiliary function causes the cholestasis presented in the disease (Sambrotta and Thompson 2015). Mutations of TJP2 and the resultant PFIC2 disease increases the likelihood of the progression into hepatocellular carcinoma (Zhou et al. 2015). TJP2 deficiency alone may not cause

any other cellular abnormalities in other cells; this is because of the specialised role of hepatocytes to form bile canaliculi in the liver (Sambrotta et al. 2014).

Due to specialised functions of hepatocyte TJ to form bile canaliculi TJP2 deficiency alone may not cause any cellular abnormalities in other cells (Sambrotta et al. 2014). Currently, it is unknown whether occludin and ZO1 play a part in the development of PFIC.

The alterations in occludin, ZO1 and ZO2 mentioned above play essential roles in the progression of liver diseases that primarily result in primary liver cancer, namely hepatocellular carcinoma.

1.5.4 Occludin and zona occludens proteins in cancer

Tight junctions are associated with a vast array of cancers especially carcinomas, the loss of cellular polarity decreases cellular differentiation and specific cellular function (Tsukita et al. 2008).

Alterations in occludin expression and phosphorylation are seen in numerous cancers and are predominately downregulated and dephosphorylated in the four most common cancers in the UK breast, prostate, lung and colorectal (Mistry et al. 2011). In the specific cancers originating from these organs with downregulation of occludin and or altered phosphorylation were associated with a poorer prognosis and a more aggressive phenotype (Hahn-Strömberg et al. 2009; Martin et al. 2010; Morgan et al. 2013; Tobioka et al. 2004).

ZO1 shows a similar expression profile to occludin in these cancers, with low level of protein expression correlated to TJ disruption and a poor prognosis of disease (Aljameeli et al. 2017; Martin et al. 2004; Ni et al. 2013). In some forms of lung cancer such as non-small cell lung cancer ZO1 protein was upregulated in 66 % of patients, these patients presented with favourable clinical parameters and a higher five-year survival rate (Ni et al. 2013). ZO1 overexpression has also been linked to a better prognosis in prostate and colon, breast and prostate cancers (Martin et al. 2004; Paul et al. 2015).

ZO2 is also noted with altered expression in two of the four main cancers in the UK, breast and prostate cancers. ZO2 expression decreased >70 % in squamous cell and adenocarcinomas. In breast adenocarcinomas, the ZO2 expression is decreased and decreases with increased tumour grade (Paschoud et al. 2007).

ZO1 and ZO2 downregulation have shown to be a marker of poor prognosis in cancers, but the molecular mechanisms resulting in these phenotypes are different. ZO1 knockdown in MDCK cells increases paracellular permeability and rearranges actin and myosin filaments. The same experiment but with the silencing of ZO2 does not reproduce the increased paracellular permeability or filament rearrangement, suggesting ZO2 must have a signalling or regulatory function in the development and progression of cancer (Van Itallie et al. 2009).

Drosophila Disc large protein (Dlg) is homologous to the human PDZ, SH3 and GuK domains of ZO1. The SH3 domain of Dlg is a tumour suppressor, further investigations in cells showed the same function of the SH3 domain in ZO1 (Willott et

al. 1993; Qian and Prehoda 2006). Tumour suppression studies in MDCK cells found ZO1 associated with ZO1-Associated Nucleic Acid-Binding Protein (ZONAB), a DNA-binding protein. ZONAB interacted with ZO1 in a regulatory capacity increased levels of ZO1 suppressed ZONAB activity and vice versa (Ruan et al. 2014). The human homologue of ZONAB is Y-box binding protein 3 (YBX3) shows the same function of ZONAB in human cell lines.

ZO1 downregulation in cancer allows for increased YBX3 activity which promotes increased proliferation as the cell can now progress from G1 to S phase (Nie et al. 2012). YBX3 interacts with CDK4 a central regulator of cell proliferation and translocates to the nucleus, where it promotes transcription cell cycle progression genes. In the nucleus CDK4 binds to cyclin D1 transcription factor promoting transcription of G2 genes and activates the pro-oncogenic FOXM1 transcription factor, pushing the cell into a proliferative phenotype (Spadaro et al. 2014).

ZONAB has less of a regulatory role over ZO2 instead ZO2 can alter gene transcription directly. ZO2 achieves the alteration of gene transcription by translocating to the nucleus where it interacts with SAF-B, Fos, Jun and c-myc inhibiting their proto-oncogene transcription. ZO2 interacts with c-myc and an enhancer box (E-box) to inhibit cyclin D1 transcriptionally downregulating cyclin D1 (Gonzalez-Mariscal et al. 2012). ZO2 binds the PDZ domain of YAP via its 1 PDZ domain thus sequestering its function when translocating it to the nucleus where it ZO2 mediates positive regulating transcription. ZO2 in this regard can be classed as a tumour suppressor with a regulatory role in apoptosis (LaQuaglia et al. 2016).

The downregulation of occludin and ZO occludens has the same outcome in the progression of hepatocellular carcinoma. As the incidence of hepatocellular carcinoma is increasing rapidly in the UK, investigations need to look at the loss of function of occludin and the ZO proteins (Smittenaar et al. 2016).

1.5.5 Occludin, ZO1 and ZO2 expression in hepatocellular carcinoma

In HCC occludin expression is predominantly downregulated and dephosphorylated however there are a small proportion of HCC tumours that display an upregulation of occludin (Bouchagier et al. 2014).

A study of 67 hepatectomy specimens showed differences in tight junction expression in relation to tumour grade, size and frequency of tumour nodules. Occludin expression analysis shows a low occludin expression in 83.5 % of HCCs but an increase of occludin expression in 16.4 % of patients. Tumours with an up and downregulation of occludin in HCC showed no significant difference in gender, tumour size and frequency of tumour nodules. However, there was a difference in tumour grading between the low and high expression of occludin tumours. High expression of occludin accounted for 23.81 % of grade I tumours but only accounted for 12 % of the grade III tumours (Bouchagier et al. 2014).

More importantly, the same study of the 67 hepatectomy specimens, survival and disease-free rates of patients with hepatocellular carcinoma with high expression of occludin were 2-fold higher in patients that had a higher expression of occludin. Localisation of the increased occludin was not always junctional giving evidence to the theory occludin has unknown functions (Bouchagier et al. 2014).

Hepatocellular carcinoma associated with a loss of occludin shows different expression throughout the liver. An investigation of 57 cases, have shown HCC with downregulated occludin have an 8.2-fold decrease in expression and the surrounding tissue occludin decreased 3.7-fold. This shows the decrease of occludin expression is correlated to the HCC phenotype (Orbán et al. 2008).

In the same 57 cases described, ZO1 displayed a similar pattern to occludin in HCC downregulated occludin expression. ZO1 was downregulated 4.6-fold in HCC and in the surrounding tissues ZO1 was downregulated 3.5-fold. The phenotype of these cells was more motile and had increased oncogenic behaviour (Orbán et al. 2008). A diseased liver creates a field of carcinogenesis, known as the field effect, especially when liver fibrosis or inflammation occurs during HCC progression. This can lead to *de novo* tumours even when the primary cancer has been removed. This may explain why the tumour-adjacent tissue had reduced occludin and ZO1 expression (Hoshida et al. 2009).

The ZO2 expression has not been investigated in detail in hepatocellular carcinoma. Screening studies have shown there is reduced ZO2 expression in chronic liver disease and liver cancer (Kamarajah et al. 2016).

Mutations in the TJP2 gene cause PFIC2, children with PFIC2 and TJP2 mutations develop HCC. Yet, there has been no link between ZO2 and HCC tumourigenesis and HCC development could be secondary (Zhou et al. 2015). These cancers are poorly understood and little research has been completed into their phenotype.

1.5.6 Alterations in other adhesion molecules and their relationship to occludin, ZO1 and ZO2 in HCC.

The other TJ proteins show a different expression profile to occludin in hepatocellular carcinoma. Like occludin claudin-4 and -7 show downregulation in a majority of HCC tumours, however, claudin-1 and -5 present with an upregulation in a majority of HCC tumours (Bouchagier et al. 2014). An increase or decrease of claudin expression is associated with HCC progression. Decreased CLDN-1 expression and increased CLDN-1 expression in hepatocellular carcinoma is associated with reduced life expectance and high disease reoccurrence (Hagashi et al. 2007; Stebbing et al. 2013). An increase of CLDN-1 expression in HCC promotes EMT through c-Abl/Raf/Ras/ERK signaling pathway and downregulated claudin-1 through disruption of the TJ and loss of cell polarity (Stebbing et al. 2013)

1.6 Epithelial to mesenchymal transition with respects to occludin, ZO1 and ZO2 in hepatocellular carcinoma

Epithelial to mesenchymal transition is reversible process occurring in epithelial cells which results in a loss of cellular polarity and attachment, resulting in a migratory phenotype. There are three types of EMT based on the outcome of the transition. Types 1 and 2 are involved in embryogenesis and tissue repair respectively. Type 3 EMT is associated with metastasis of cancer a migratory and invasive cancer cell behaviour resulting in a poorer prognosis of disease (Kalluri and Weinburg 2009). HCC cells that undertake EMT lose expression of epithelial-related genes and gain expression of genes promoting a mesenchymal phenotype. E-cadherin is a marker

of EMT in HCC as its downregulation is noted in metastatic HCC. In non-metastatic HCC patients E-cadherin shows strong staining at adhesions junctions, this is not seen in metastatic HCC. E-cadherin, as mentioned, is frequently downregulated in hepatocellular carcinoma and is regarded as one of the first steps in the dedifferentiation process in carcinoma progression (Wells et al. 2008).

Activation of transcription factors in HCC promote EMT through the inhibition of epithelial gene transcription and an upregulation mesenchymal associated genes. Transcription factors SNAIL, TWIST and ZEB are commonly activated in HCC and are correlated to a more mesenchymal phenotype and are all regulatory of one another as shown in Figure 1.1. The repression of occludin, ZO1 and ZO2 are mediated via these transcription factors.

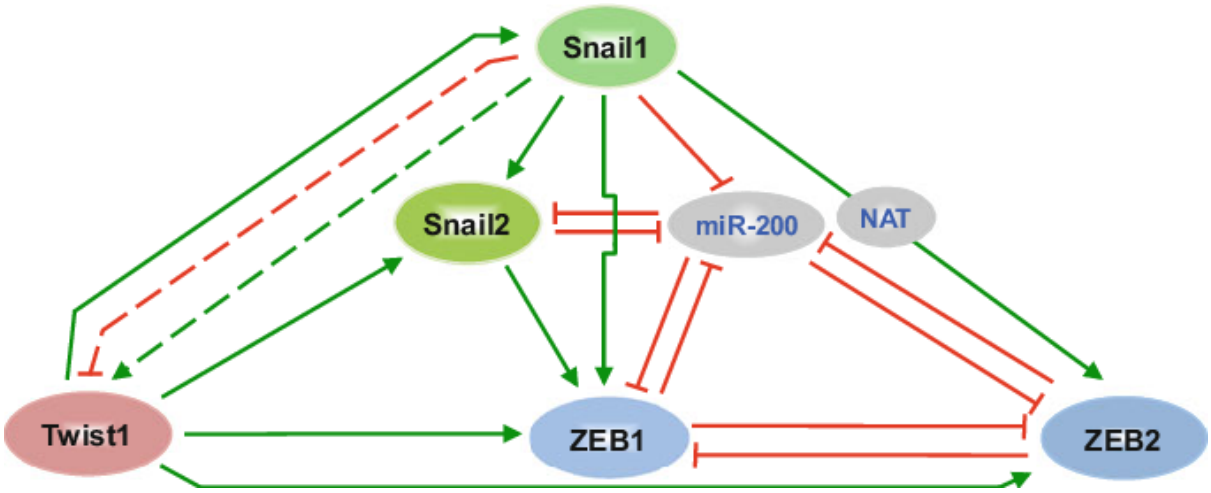

Figure 1.11: Regulatory relationship between the three classic EMT transcription factors TWIST, ZEB and SNAIL1 in the progression of cancer. These three transcription factors work together to increase cellular proliferation and loss of apical-basal polarity.

SNAIL activation in HCC correlates with a poorer prognosis and associated with recurrence of HCC. Overexpression of SNAIL in HCC presents with portal vein invasion, metastasis and poor cellular differentiation (Woo et al. 2011). SNAIL1 can

directly and completely inhibit expression of E-cadherin and occludin by binding to their E-box in the promotor sequences promoting a loss of cellular adhesion (Kedinger et al. 2009). SNAIL does not alter the expression of ZO1, as SNAIL decreases both occludin and claudin expression this causes ZO1 to become mislocalised to the cytoplasm (Ikenouchi et al. 2003).

TWIST is a basic helix-loop-helix and like SNAIL it binds to E-box promotor sequences of genes including occludin and ZO1/2 proteins (Vensuna et al. 2008; Salt et al. 2014). In HCC, the high TWIST1 expression is associated with low ZO1 expression and low TWIST1 expression is associated with high ZO1 expression. As alluded to before low ZO1 expression in HCC is correlated to a poorer prognosis and increased metastasis (Orbán et al. 2008). Furthermore, increased TWIST1 expression and decreased ZO1 expression are associated with a significantly increased probability of HCC recurrence (Nagai et al. 2012). This suggests ZO1 as an epithelial marker and has a regulatory role in tumour suppression in HCC (Nagai et al. 2016).

ZEB is a zinc finger transcription factor that can bind to a variety of DNA binding domains including the E-box domain to inhibit transcription. Like with SNAIL and TWIST increased activation of ZEB in HCC is associated with intrahepatic metastasis and a poorer prognosis. Knockdown ZEB1 experiments increase occludin expression restores of epithelial polarity. The knockdown of ZEB1 also restores the correct location of ZO1/2 to the TJ complex as occludin expression is corrected (Aigner et al. 2007). ZEB and TWIST have overlapping roles in HCC over the regulation of occludin and ZO1/2.

1.7.1 Aims of the study

The multifactorial process undertaken by a hepatocyte during cancer progression is still being fully elucidated. Disruption of the tight junction is one of the first steps undertaken by the hepatocyte in the loss of epithelial polarity and generation of a mesenchymal phenotype during HCC progression. The consequences pertaining whether the cell gain a motile and more invasive cancer cell behaviour directly by this step of by further cellular changes are still unknown.

Therefore the major aims of the investigation was to establish the regulatory relationship between occludin, ZO1 and ZO2. To assess the effect changes when there are changes in regulation between occludin, ZO1 and ZO2 have on cancer cell behaviour.

1.7.2 Study objectives

1. To silence and overexpress occludin to understand if occludin expression is required for the regulation of the epithelial phenotype in a HepG2 cell, using RT-PCR to assess changes in tight junction expression and cell motility assays.

2. To create a HepG2 cell model system with differential occludin expression to attain whether occludin is required for the maintenance of the epithelial phenotype, using RT-PCR and immunefluorescence to assess if there is a change in tight junction gene expression or protein localisation.

3. To determine if there is a regulatory between the occludin, ZO1 and ZO2 in HepG2 cells by using RT-PCR and Western blotting to assess where expression or activation changes had occurred.

4. To analyse if a change in the expression levels of occludin, ZO1 and ZO2 simultaneously increases cancer cell behaviour by investigating cell motility, polarity, markers of EMT and protein localisation.

5. To analyse the differential expression of occludin and ZO1 knockdown through miRNA analysis to gain an insight into how these proteins govern the epithelial phenotype in HepG2 cells.

2. Methodology

2.1 Standard solutions.

2.1.1 Solutions used for cell culture.

NaCl, KCl, $Na_2HPO_4.12H_2O$, KH_2PO_4, puromycin and geneticin were laboratory grade and acquired from Fisher Scientific Chemicals. Trypsin-EDTA was acquired from Biosera.

Phosphate buffered saline (10x) was prepared free from Ca^{++} and Mg^{++}. Dissolved in 800 ml of dH_2O was 8 g NaCl, 2 g KCl, 14.4 g $Na_2HPO_4.12H_2O$ and 2 g KH_2PO_4. The pH was adjusted to 7.4 with HCl and assessed using a Jenway 3505 pH probe before increasing the final volume 1 litre. When needed, PBS was diluted to a 1x working solution, autoclaved and stored at room temperature.

Trypsin-EDTA (10x) 0.5 % / 0.2 % in DPBS was diluted 1:5 to a working concentration of 2x with PBS. 20 ml of Trypsin was aliquot into sterilin 30 ml universal disposable containers and stored at -20ºC until use.

Puromycin antibiotic (1000x) was prepared in 5 ml PBS with 20 mg of puromycin powder. The 5 ml solution was filter sterilised through a 0.22 µm filter and aliquoted into 1 ml microcentrifuge tubes and stored at 4ºC for short term storage or -20ºC for long-term storage. When used 500 µl of the puromycin stock was pipetted into 500 ml media to give a working concentration of 4 µg/ml.

Geneticin antibiotic (1000x) was prepared in 25 ml PBS with 2.5 g of geneticin powder. The 5 ml solution was filter sterilised through a 0.22 µm filter, 5 ml was aliquot into bijou tubes and stored at 4^{o}C for short term storage or -20^{o}C for long-term storage. When used the 5 ml of the geneticin stock was pipetted into 500 ml media to give a working concentration of 1 mg/ml.

Freezing medium was produced by mixing 9 ml FBS with 1 ml DMSO. The freezing medium was stored at 4^{o}C until use.

2.1.2 Solutions used for microbiological procedures.

Ampicillin, chloramphenicol, kanamycin, yeast extract, glucose, NaCl and NaOH was acquired from Fisher Scientific Chemicals and the Tryptone and LB agar were purchased from Oxoid.

Ampicillin antibiotic (1000x) was prepared in 10 ml dH_2O with 1 g of ampicillin powder. The 10 ml solution was filter sterilised through a 0.22 µm filter and aliquot into 1 ml microcentrifuge tubes for storage at -20^{o}C. When used 100 µl of ampicillin was pipetted into 100 ml of LB broth or LB agar to give a working concentration of 100 µg/ml.

Chloramphenicol antibiotic (1000x) was prepared in 10 ml ethanol with 250 mg of chloramphenicol powder. The 10 ml solution was filter sterilised through a 0.22 µm filter and aliquot into 1 ml microcentrifuge tubes for storage at -20^{o}C. When used

100 µl of chloramphenicol was pipetted into 100 ml of LB-broth or LB-agar to give a working concentration of 250 µg/ml.

Kanamycin antibiotic (1000x) was prepared in 10 ml dH_2O with 500 mg of kanamycin powder. The 10 ml solution was filter sterilised through a 0.22 µm filter and aliquot into 1 ml microcentrifuge tubes for storage at -20^oC. When used 100 µl of kanamycin was pipetted into 100 ml of L-broth or LB-agar to give a working concentration of 250 µg/ml.

LB-broth was prepared with 800 ml of dH_2O, 10 g tryptone, 5 g yeast extract, 5 g NaCl and 1 g glucose. The pH was adjusted to 7.5 with NaOH and assessed with the Jenway 3505 pH probe before bringing the total volume to 1 litre. Once fully dissolved the LB- broth was autoclaved and stored at room temperature until needed.

LB-agar was prepared with 800 ml of dH_2O, 10 g tryptone, 5 g yeast extract, 5 g NaCl, 1 g glucose and 15 g technical agar. The pH was adjusted to 7.5 with NaOH before bringing the total volume to 1 litre. Once fully dissolved the LB-agar was autoclaved and stored at room temperature until needed. When required the LB-agar was melted in a microwave for 3 minutes and kept at 55^oC until used. Before use, antibiotics were added as needed and the LB-agar was poured into Petri dishes. Petri dishes stood in a laminar flow cabinet to dry for 4 hours before being stored at 4^oC long term.

Super optimal broth with catabolite repression S.O.C was prepared with 400 ml of dH_2O, 2.5 g yeast extract, 10 g tryptone, 0.292 g NaCl, 0.093 g KCl and 1.2 g $MgSO_4$. The pH was adjusted to 7.5 with NaOH before increasing the total volume to 490 ml. The medium was autoclaved to sterilise then stored at 4^oC. A 20 mM glucose solution was prepared by dissolving 4 g of glucose in 20 ml dH_2O, then filter sterilised through a 0.22 µm filter. Before use 10 ml of the 20 mM glucose solution was added to the 490 ml of medium.

2.1.3 Solutions used for RNA and DNA analysis.

Diethyl pyrocarbonate, ethidium bromide, Tris base, glacial acetic acid, boric acid, EDTA.Na_2.$2H_2O$, urea, 40 % acrylamide (acryl:bis acryl = 19:1), ammonium persulfate and TEMED was acquired from Fisher Scientific Chemicals. Electrophoresis grade agarose was acquired from Melford.

Diethyl pyrocarbonate (DEPC) treated water was made by adding 5 ml Diethyl pyrocarbonate to 95 ml of Milli-Q water. The DEPC treated water was autoclaved and stored at room temperature.

Ethidium bromide was dissolved in dH_2O at a concentration of 5 mg/ml; 2 µl was added to a molten but cool agarose gel. For denaturing acrylamide gels 10 µl ethidium bromide was added to 50 ml 1x TBE for a working concentration of 1 µg/ml.

Tris/Acetic/EDTA buffer [TAE] (10x). Into 800 ml of dH_2O was 48.4 g Tris base, 11.42 ml glacial acetic acid and 7.44 g EDTA**.**Na_2**.**$2H_2O$. The pH was adjusted to 8.5 before making the total volume to 1 litre. The T.A.E was autoclaved and stored at room temperature. When used the T.A.E was diluted to a 1x working concentration, 40 ml of T.A.E buffer was used per gel electrophoresis tank.

Tris/Borate/EDTA buffer [TBE] (10x). Into 800 ml of dH_2O was 108 g Tris Base, 55 g boric acid, 9.5 g EDTA**.**Na_2**.**$2H_2O$. The pH was adjusted to 8.0 before making the total volume to 1 litre. The T.B.E was autoclaved and stored at room temperature. When used the T.B.E was diluted to a 1x working concentration, 40 ml of T.B.E buffer was used per gel electrophoresis tank.

T.A.E/T.B.E agarose gels (2 %) was comprised of 40 ml of T.A.E or T.B.E (1x) buffer and 0.8 g of agarose then autoclaved and stored at room temperature. Before use, a gel was heated in a microwave for 1.5 minutes or until molten. Once cool but still molten 2 µl of ethidium bromide was added, and the mixture is poured onto into a gel electrophoresis tank.

Ammonium persulfate 10 % w/v, 100 mg ammonium persulfate was dissolved in 1 ml dH_2O. Ammonium persulfate was used immediately or stored for a maximum of two days at 4^oC.

Denaturing acrylamide gel, 7.2 g urea, 1.5 ml 10x TBE, 5.6 ml 40 % acrylamide (acryl:bis acryl = 19:1) was mixed and the total volume was increased to 15 ml with dH_2O. To this 75 µl 10 % ammonium persulfate and 15 µl TEMED was added. Once the last two ingredients were added the gel was immediately mixed and poured into a Bio-Rad gel casting cassette.

2.1.4 Solutions for protein isolation and Western blotting.

Tris base, SDS, HCl, Glycerol, β-Mercaptoethanol, Glycine, NaCl, APS, bromophenol blue, guanidine hydrochloride and Tween 20 was supplied by Fisher Scientific Chemicals. The mixed weight any kD precast gels were purchased from Bio-Rad.

Guanidine hydrochloride 0.3 M, 2.87 g guanidine hydrochloride was dissolved in 80 ml 95 % ethanol. The total volume was increased to 100 ml with 95 % ethanol.

SDS 10 % (w/v), 10 g SDS was dissolved in 90 ml dH_2O. Once dissolved with gentle stirring the total volume was increased to 100 ml.

Tris-HCl, pH 6.8 was made by adding 6 g Tris base to 60 ml dH_2O. The pH was adjusted to 6.8 with use of HCl. The total volume was increased to 100 ml with dH_2O and stored at 4^oC. Before use Tris-HCl was warmed to room temperature.

Sample buffer (SDS reducing buffer), 3.55 ml dH_2O was added to 1.25 ml 0.5 M Tris-HCl, pH 6.8, 2.5 ml glycerol, 10 % SDS (w/v) and 0.2 ml 0.5 % (w/v) bromophenol blue. The total volume was 10 ml after the addition of 500 µl β-Mercaptoethanol just before use.

Running/electrode buffer (10x), 30.3 g Tris base, 144.0 g glycine and 10 g SDS was dissolved in 900 ml dH_2O. The total volume was increased to 1000 ml with dH_2O after it was fully dissolved. The pH was assessed using a Jenway 3505 pH probe, a value of 8.3 was required. As the pH of this buffer should not be adjusted with an acid or base, any buffer with a value other than 8.3 was discarded. Electrode buffer (10x) was stored at 4^{o}C and was warmed to room temperature before use. To use this buffer, 100 ml buffer was diluted in 900 ml dH_2O to make a 1x working solution.

Tris-buffered saline with Tween-20 (TBST) (10x), 12.1 g Tris base, 58.4 g NaCl and 0.5 ml Tween 20 was dissolved in 900 ml dH_2O. The pH was altered with HCL to pH 7.5. The final volume was made to be 1000 ml with dH_2O. The buffer was stored at 4^{o}C and was warmed to room temperature before use. 50 ml of TBST was added to 450 ml of dH_2O to make a 1x working buffer.
For antibody blocking MARVEL was added to TBST at 5 % w/v. Antibody dilutions used 0.5 % w/v MARVEL/TBST.

2.1.5 Solutions for immunocytochemistry.

Tris base, NaCl, Tween 20, DAPI and 37 % formaldehyde was purchased from Fisher Scientific Chemicals. Bovine serum albumin was purchased from Oxoid.

Bovine serum albumin 5 % w/v, to block unspecific protein binding, was made by dissolving 2.5 g of BSA in 40 ml TBST. The final volume was increased to 50 ml and the BSA/TBST was stored at 4^{o}C. Antibody dilutions were carried out using 0.5 % w/v BSA in TBST by a 1:10 dilution with TBST of the 5 % stock.

4',6-diamidino-2-phenylindole, dihydrochloride (DAPI) nucleic acid stain, 10 mg DAPI of powder was diluted into 10 ml of dH_2O and filter sterilised through a 0.22 µm filter. The diluted DAPI was aliquot into 10 separate 1 ml microcentrifuge tubes that was wrapped in aluminium foil to protect from light. For long-term storage aliquots were stored at -20^{o}C and for use the aliquot was stored at 4^{o}C. For use, the DAPI was diluted to a concentration of 0.5 µg/ml in 5 % BSA/PBS.

Formaldehyde 3.7 % v/v, 37 % formaldehyde was diluted 1:10 with PBS. This was carried out immediately before fixing cells at room temperature. Remaining 3.7 % v/v formaldehyde was discarded.

2.2 Cell lines, cell culture and maintenance.

Cell culture was carried out in a Nuaire Labgard class II biological safety cabinet sterilised with 70 % IMS. Everything that entered the sterile environment was also sterilised with 70 % IMS. All investigations were carried out using aseptic techniques.

Cells were incubated at 37ºC with a 5 % CO_2 at 95 % relative humidity and the sterility was maintained by a 1 % w/v copper sulphate solution in a water tray at the base of the incubator.

Cell line	Species	Tissue	Morphology	Adherent	Origin	Features
HepG2	*Homo sapiens*	Liver	Epithelial	Yes	Male Caucasian Aged 15	Liver biopsy Polarised
HEK293T	*Homo sapiens*	Kidney, Embryo	Epithelial	Yes	Foetus	Lentiviral particle production

Table 2.1: Cell lines used in experiments with cell characteristics. Cell lines were purchased from American Type Culture Collection. HepG2 [HEPG2] (ATCC® HB-8065™) and HEK293T [HEK 293T/17] (ATCC® CRL-11268™).

The features of HepG2 cells are outlined in, Table 2.1, HepG2 [HEPG2] (ATCC® HB-8065™) was acquired from ATCC and were used throughout all investigations.

HepG2 cells are a secondary epithelial hepatocyte cell that generate distinct apical and basolateral domains (LeCluyse et al. 2012). HepG2 cells were isolated from a 15-year-old Caucasian male that had well differentiated HCC.

Well differentiated HCC shows the presence of malignant cells that resemble normal hepatocytes (Qiu et al. 2015). HepG2 cells are hepatitis B virus negative and are non-tumorigenic (Knasmuller et al. 1998). When polarised HepG2 cells produce less proteins involved in hepatic development and perform hepatic functions such as bile secretion and xenobiotic metabolism (Palakkan et al. 2015). HepG2 cells however, have 55 pairs of chromosomes this leads to genetic instability in which HepG2 cells use as a survival strategy.

Table 2.1 shows cells used during investigations; HEK293T cells were used only to produce lentiviral particles from transfected plasmids. HepG2 cells was the experimental cell line; the lentiviral particles were cultured with HepG2 cells to alter gene expression.

2.2.1 Cell growth media

Cell Growth media DMEM, L-glutamine, penicillin/streptomycin and Foetal bovine serum was purchased from Biosera.

All cells were cultured in high glucose 4.5 g/l DMEM growth media containing 10 % v/v FBS. In addition to this 5 ml of 200 mM L-glutamine and 5 ml of penicillin/streptomycin (100x) was added. When transfecting HEK293T cells, antibiotic-free DMEM was used with 3 % FBS to limit the progression of the cell cycle and therefore cell proliferation.

2.2.2 Cell maintenance

Cells were cultured in vented Nunc™ Cell Culture Treated EasYFlasks™ acquired from Fisher Scientific. The flask sizes were 75 cm^2 and 25 cm^2 depending on the quantity of cell required. Cells were left to incubate until a confluence of greater than 80 % was achieved before being used in investigations.

2.2.3 Cell Trypsinisation and cell culture.

Cells were subcultured every 48 hours; this was typically when the cells had reached >80 % confluence, this was gauged by eye using an inverted microscope. The spent Dulbecco's Modified Eagle Medium (DMEM) was removed from the flask and discarded. The cell flask was washed with 10 ml PBS (1x) to remove cell debris and dead cells. The PBS was removed and discarded into a disinfectant pot. To detach the cells from the flask wall, 3 ml of Trypsin-EDTA (2x) in PBS was added for 3 minutes and incubated at 37^{o}C. To dissociate the cells from the flask gentle agitation of the cells was needed. The trypsin cell suspension was transferred to the sterilin containing fresh DMEM to inhibit the trypsin enzyme. The cell suspension was centrifuged at 150 x g for 5 minutes to pellet the cells.

The spent media and trypsin was decanted into the disinfectant pot. The pellet of cells was resuspended in 6 ml fresh DMEM media. The cells were subcultured into new flasks, counted for use in investigations or lysed for analysis.

2.2.4 Cell counting

Quantification of cell numbers was achieved through counting cells on a haemocytometer under a light microscope under a 10x objective. Cells 50 µl were diluted 1:1 with trypan blue to stain the dead cells then 20 µl of the cell solution was loaded onto a haemocytometer. The clear colourless cells in the 4 outer corner squares of the haemocytometer grid that consisted of 16 squares were counted. The average count from the 4 corners was calculated by dividing cell count by 4. As the cells were diluted by 2-fold in trypan blue the average was multiplied by 2. The area

of each corner was $1mm^2$ so to calculate the number of cells per ml in suspension the count number multiplied by 10^4.

The formula was as follows:

$$\frac{\text{Total cell count of 4 corners}}{4} \times (1 \times 10^4) \times 2 = \text{Cell count/ml}$$

Cells were acquired from a frozen stock stored in liquid nitrogen at -196°C, upon receiving the cells they were immediately thawed at 37°C. Once thawed the cell stock was transferred into a Sterilin tube containing fresh DMEM media that had been preheated to 37°C to decrease the DMSO toxicity. The cells were centrifuged at 150 x g for 5 minutes. Once centrifuged the DMEM containing the cell debris and the freezing medium was decanted into a discard pot. The pellet was resuspended in 12 ml DMEM, transferred into a cell culture flask, and incubated as described in 2.2.2.

Cell storage was completed by dissociating cells from the cell culture flask as described in 2.2.3 cell trypsinisation and cell subculture. The cells were centrifuged at 350 x g for 5 minutes in a swinging bucket centrifuge. The supernatant was discarded and the cell pellet was resuspended in 2 ml of freezing medium. The cell suspension was transferred to a labelled 2 ml cryovial. The cryovial was cool at a rate of -1°C/min until cooled to -80°C or for long-term storage, stored in liquid nitrogen.

2.2.5 Cell migration assay

Cell motility was assessed using Ibidi 2 well cell culture inserts (Ibidi 2018). The culture inserts were sterilised in 100 % ethanol for 1 minute, washed with PBS and dried in a sterile petri dish at 37ºC. The inserts were transferred using sterile forceps to a 6 well plate, typically 3 inserts per well. HepG2 cells were seeded into each chamber at a concentration of $4x10^4$ cells/70 µl DMEM, following the cell counting protocol 2.2.4 and trypsinisation 2.2.5. After 24 hours, the cell culture inserts were removed with sterile forceps and 2 ml of fresh DMEM was added. An image was taken every 24 hours starting at time 0, immediately after the removal of the cell culture insert. The experiment was continued for 72 hours to monitor migration (Ibidi 2018).

2.2.6 Determining the rate of migration across a 2D surface with altered occludin *in vitro.*

HepG2 cells were cultured in a six-well plate containing Ibidi 2 well silicone inserts with a defined cell-free gap at a concentration of $4x10^5$ cells per well with a N=6. After an initial 24-hour incubation period in a humidified chamber at 37ºC with 5 % CO_2, the inserts were removed with sterile forceps, 2 ml fresh DMEM was added and time 0 images were taken (Ibidi 2018). For the following 72 hours, the cells were maintained at 37ºC with 5 % CO_2. Every 24 hours the cell migration across the cell-free gap was monitored using the Microtec MDC-C1.3F microscope camera with a Nikon inverted microscope using a 4X objective.

The images were processed through the image processing software, ImageJ 1.8.0 (URL imagej.nih.gov/ij/download.html) an image processing program. The MRI wound healing tool macro

(URL http://dev.mri.cnrs.fr/projects/imagej-macros/wiki/Wound_Healing_Tool) was installed to analyse how many pixels were in the cell-free gap. The software automatically determines any cell-free gap with a surface area over 10000 pixels and draws an outline. The change in pixel quantity was compared to the 0-hour control to quantify how much of the cell-free gap had migrating cells in. The migration images were opened in ImageJ, the find edges tool in the process tab was used to give contrast between the cell-free gap and the cells. Once the optimum contrast was achieved the MRI macro was run resulting in pixel count and image outlines of the cell free gap produced Figure 2.1.

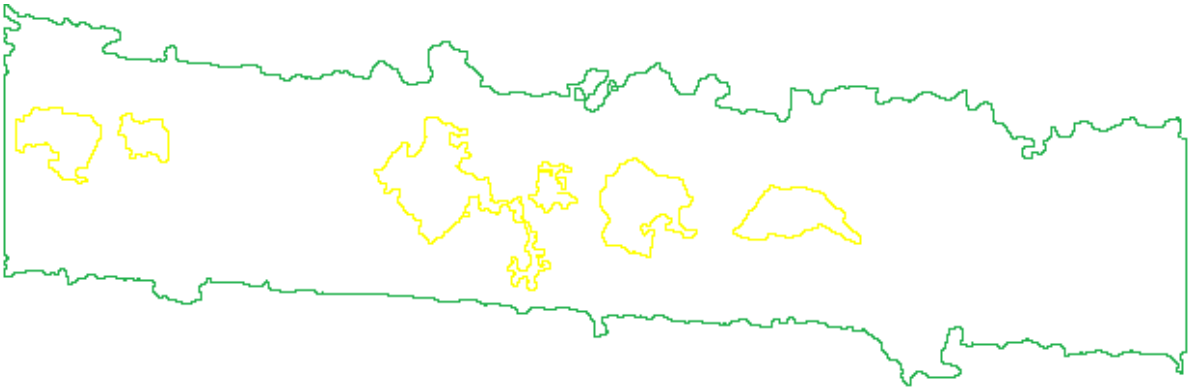

Figure 2.1: Conversion of an image showing cells growing either side of a cell free gap to a simple outline by the MRI wound healing tool in ImageJ. The software calculates the differences in pixels area within the cell free gap to give migration rates. Here the figure shows 2 representative images of the cell free gap of HepG2 cells with knocked down occludin expression at 0 hours (green) and 72 hours (yellow).

2.2.7 Statistical analysis for 2D migration

The spheroid invasion data was processed in Excel, the mean, standard deviation and standard error of the mean were calculated. The mean of the control was set to 1.000 and all test variables were normalised against the control. The mean, standard error of the mean and N number was imported into GraphPad Prism 7.0.2, the graphs and the one-way analysis of variance were produced using the software.

2.2.8 Cell invasion assay.

This protocol was adapted from Cultrex® 96-Well 3D Spheroid BME Cell Invasion Assay supplied by Sigma, 10X Spheroid Formation ECM (3500-096-01) and Invasion Matrix (3500-096-03) (Cultrex 2013).

The 10X Spheroid Formation ECM is a mix of ECM proteins purified from murine EHS sarcoma cells designed to prevent cell to basement adhesion while allowing cell-cell adhesion. The invasion matrix promotes the movement of cells from the spheroid into the ECM. The invasion matrix is a blend of basement membrane extract from murine EHS sarcoma cells. The invasion matrix also includes collagen I and bovine extensor tendons which forms the hydrogel, so cells can migrate into it.

To produce a spheroid, 96 well plates were coated with 50 µl molten 1.5 % agarose/PBS. The agarose/PBS produces a concave surface in the base of the well that is inert to cell attachment. The plates were left to set for 20 minutes at room temperature, this allowed the agarose to cool without being distorted with the addition of media. The outer wells contained 200 µl of 1X PBS to act as an evaporation barrier due to the low volume of media/well used. This procedure outlines amounts needed per one well; replicates were produced in the same tube by increasing the amounts stated appropriately. 24 hours before spheroid production, 10X spheroid formation ECM and invasion matrix was thawed at 4^{o}C and before the start of the experiment diluted to 2X spheroid formation matrix with complete DMEM at 4^{o}C.

Following, Ibidi, Cells were counted following section 2.2.4 and 500 HepG2 cells were added to a microcentrifuge tube to make a total volume of 50 µl. To this, 50 µl of the 2X spheroid formation ECM matrix was added to the same microcentrifuge tube and was mixed by gently tapping the tube. The 100 µl cell/ECM mix was transferred with a 200 µl pipette to a single well of the 96 well plate that had an agarose coating. To ensure the cells formed a single spheroid the plates were centrifuged at 200 x g for 3 minutes in a swinging bucket rotor. After 24 hours, 100 µl of the invasion matrix was added and again the plates were centrifuged at 200 x g for 3 minutes in a swinging bucket rotor (Ibidi 2015).

The cells were left to incubate for 72 hours without disruption to form spheroids in a 37^{o}C incubator at 95 % humidity with 5 % CO_2. After the incubation period, the spheroids were imaged under an inverted microscope at a magnification of x4.

The images taken were processed with ImageJ an image processing program. The number of pixels across the maximum diameter of the spheroid was measured and the four results were averaged and compared to the control to give an overall change in invasiveness as shown in Figure 2.2.

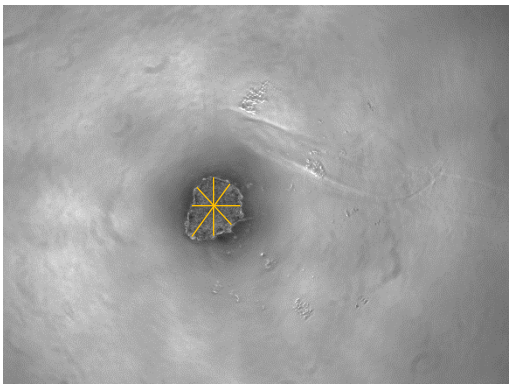

Figure 2.2: Methodology of determining the size of the spheroid. The spheroid was measured in pixels across 4 planes. The four diameter measurements were averaged to give a single diameter for the spheroid. This figure shows representative data to demonstrate the measuring of the spheroid. It is HepG2 spheroid after 72 hours incubation in an artificial ECM with the measuring marks on from ImageJ.

As shown in Figure 2.2, the spheroids were measured along 4 planes, this ensured an irregular shape was considered, the 4 diameter measurements were averaged. All spheroid the mean spheroid size for each test variable was calculated and the standard error was calculated (Ibidi 2015).

Statistical analysis for 3D invasion

The migration data was analysed in Excel; the percentage changes of the area in pixels for each cell line was imported into a table. The mean, standard deviation and standard error of the mean were calculated for each test variables migration over the 72-hour time course.

The mean, standard error of the mean and N number was imported into GraphPad Prism 7.0.2, the graphs and the one-way analysis of variance were produced using the software.

2.3 Amplification of plasmid DNA through the transformation of *E. coli* cells.

DNA was amplified in One Shot Stbl3 Chemically Competent *E. coli* (Invitrogen 2015)*;* they were chosen as the lentiviral plasmids have long direct repeating sequences that are typically unstable in other host bacteria. Stbl3 also has endA mutations; this eliminates non-specific endonuclease activity improving miniprep

plasmid quality. All plasmids used contained bacterial and mammalian resistance genes for antibiotic selection.

2.3.1 Plasmids used in experiments.

The lentiviral packaging vectors used were purchased via OriGene, TR30037. The packaging plasmids used were Lenti-vpak, a 3rd generation lentiviral packaging mix that contained 4 plasmids (OriGene 2015). Short hairpin RNA knockdown of RNA was achieved through a lentiviral shRNA occludin plasmid supplied by Santa Cruz Biotechnology, sc-36117-SH. The plasmid mix contained a pool of four shRNA plasmids encoding for 19-25 nt shRNA specific to occludin each with puromycin resistance for mammalian selection in HepG2 cells. Lenti-vpak and shRNA occludin plasmids are sequenced validated before shipping and the sequence is not shared in public domain, the plasmid maps for these plasmids are unknown. Both the Lenti-vpak and occludin shRNA plasmids are sold as a mixed pool of plasmids. As such, the plasmids were not transformed into *E. coli* due to the inability to ensure all plasmids could be produced at the correct concentrations. These plasmids were used directly from the purchased aliquot.

The overexpression and control plasmids were amplified for a continuous stock of occludin, TJP2, pUC19 and Control DNA. Each plasmid had a bacterial and a mammalian antibiotic resistance gene for antibiotic selection of positive *E. coli* colonies and positive HepG2 cells. Figures 2.3, 2.4, 2.5 and 2.6 are plasmid maps for pLenti-OCLN-C-Myc-DDK-IRES-Puro and pCMV6-TJP2-C-Myc-DDK-NeoR/KanR that are responsible for the overexpression of occludin and TJP2 respectively. pLenti-C-Myc-DDK-IRES-Puro is the same expression vector as

occludin but does not include a target insert, this was used as a control for the overexpression investigations. pUC19 plasmid was used to measure transformation efficiency as a positive control, positive pUC19 colonies suggested transformation was successful. All four of the plasmids were purchased from OriGene and the plasmid maps were generated and edited using the, analyse plasmid sequence tool provided by Addgene (URL https://www.addgene.org/analyze-sequence/), shown in, Figure 2.3, 2.4, 2.5 and 2.6.

pLenti-OCLN-C-Myc-DDK-IRES-Puro and pCMV6-TJP2-C-Myc-DDK-NeoR/KanR plasmids contain a myc tag, a polypeptide chain derived from the c-myc gene. This allows for the quantification of endogenous and induced expression of the protein. This feature of the plasmid was not used in experiments.

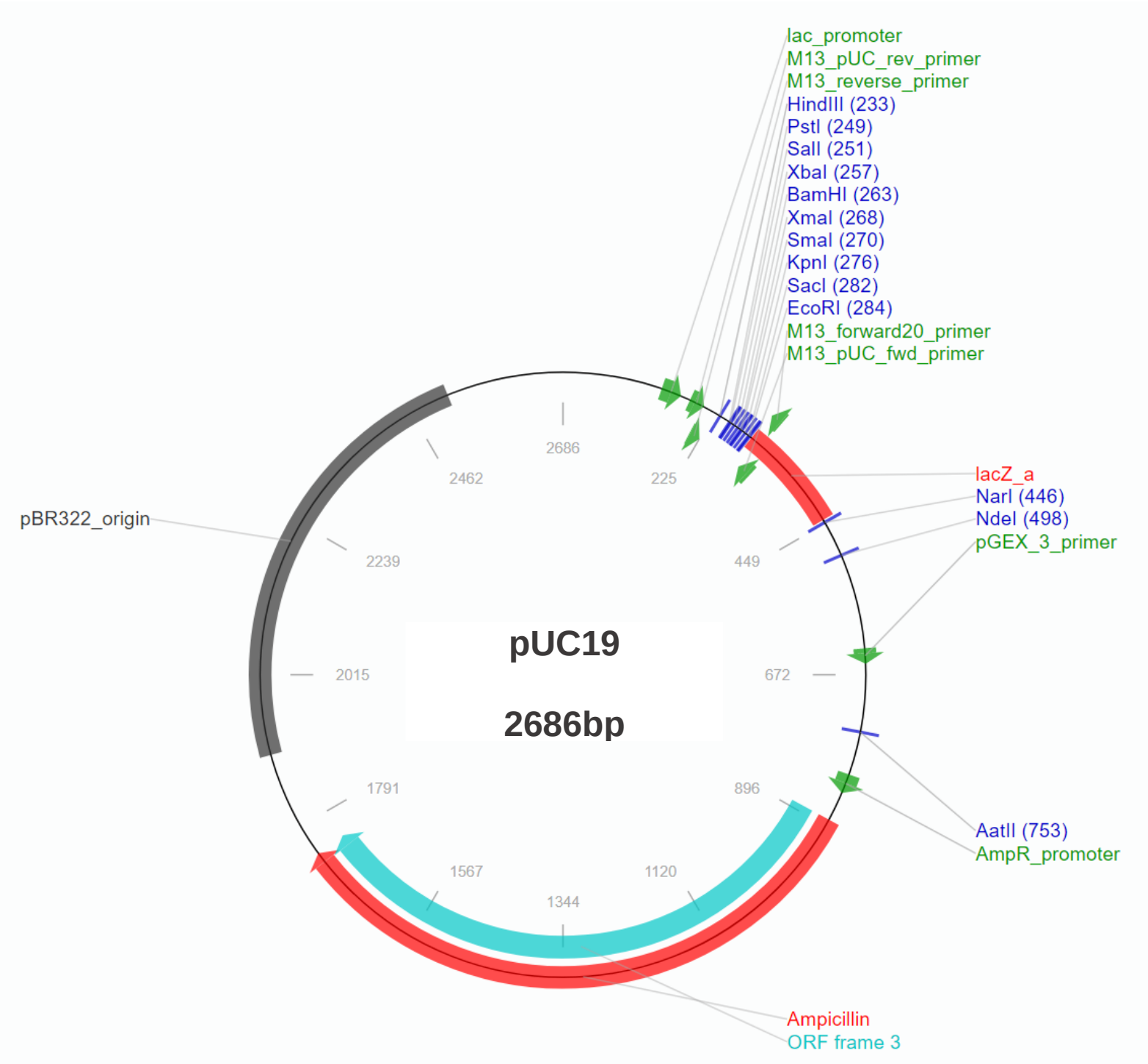

Figure 2.3: Plasmid map of puc19 positive control plasmid used to assess transformation efficiencies. Whilst completing bacterial transformations a negative and positive control was used. pUC19 was used to assess bacterial transformation efficiency and the use of a negative control ensured there was no bacterial contamination.

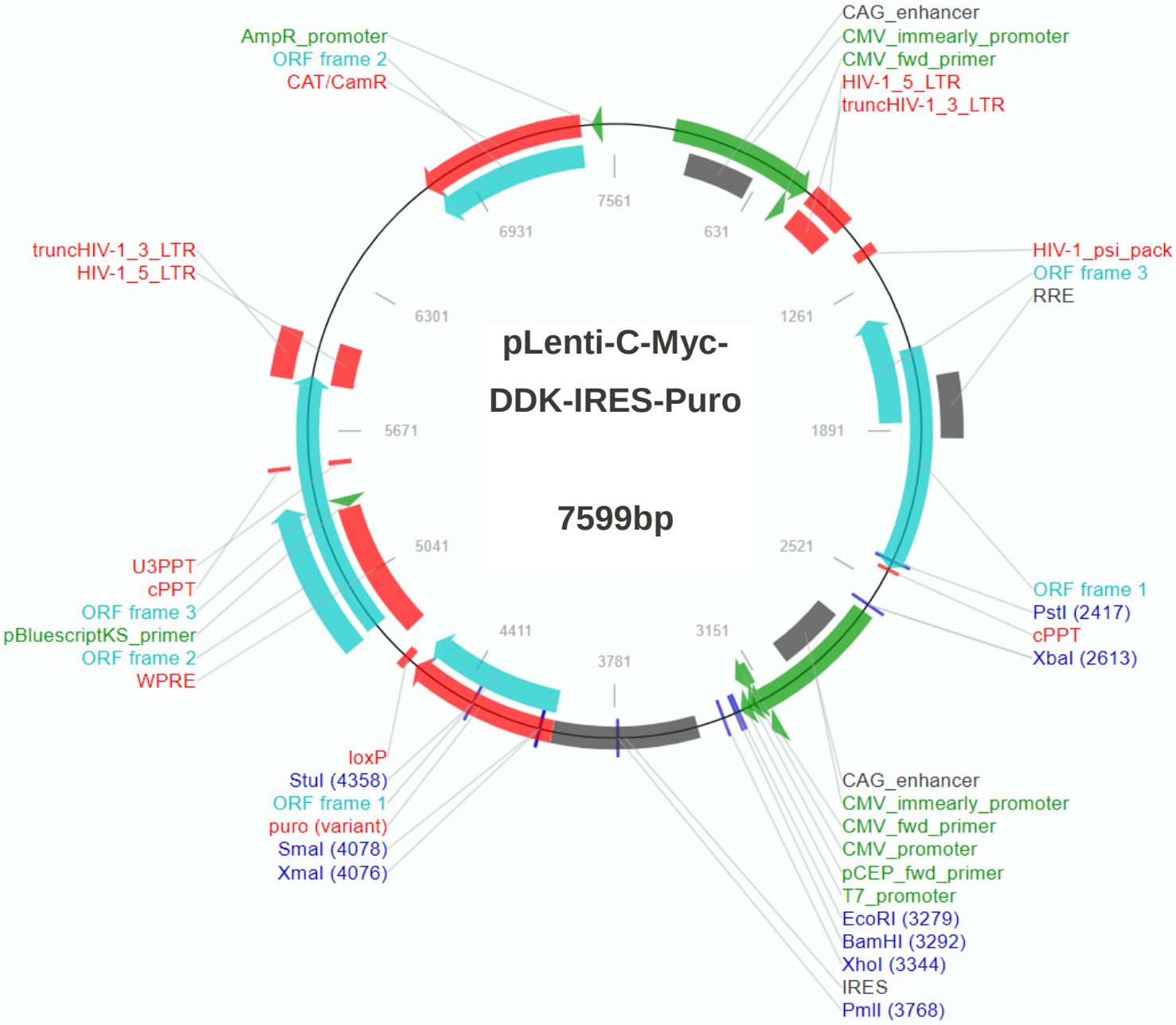

Figure 2.4: Plasmid map of pLenti positive control plasmid. HEK293T cells were transfected with pLenti-C-Myc-DDK-IRES-Puro and the Lenti-vpak plasmids as described in 2.3.7. The HepG2 control cells were transduced with the resultant lentiviral particles this ensured that the differences found were due to occludin or ZO2 expression and not due to lentiviral transduction.

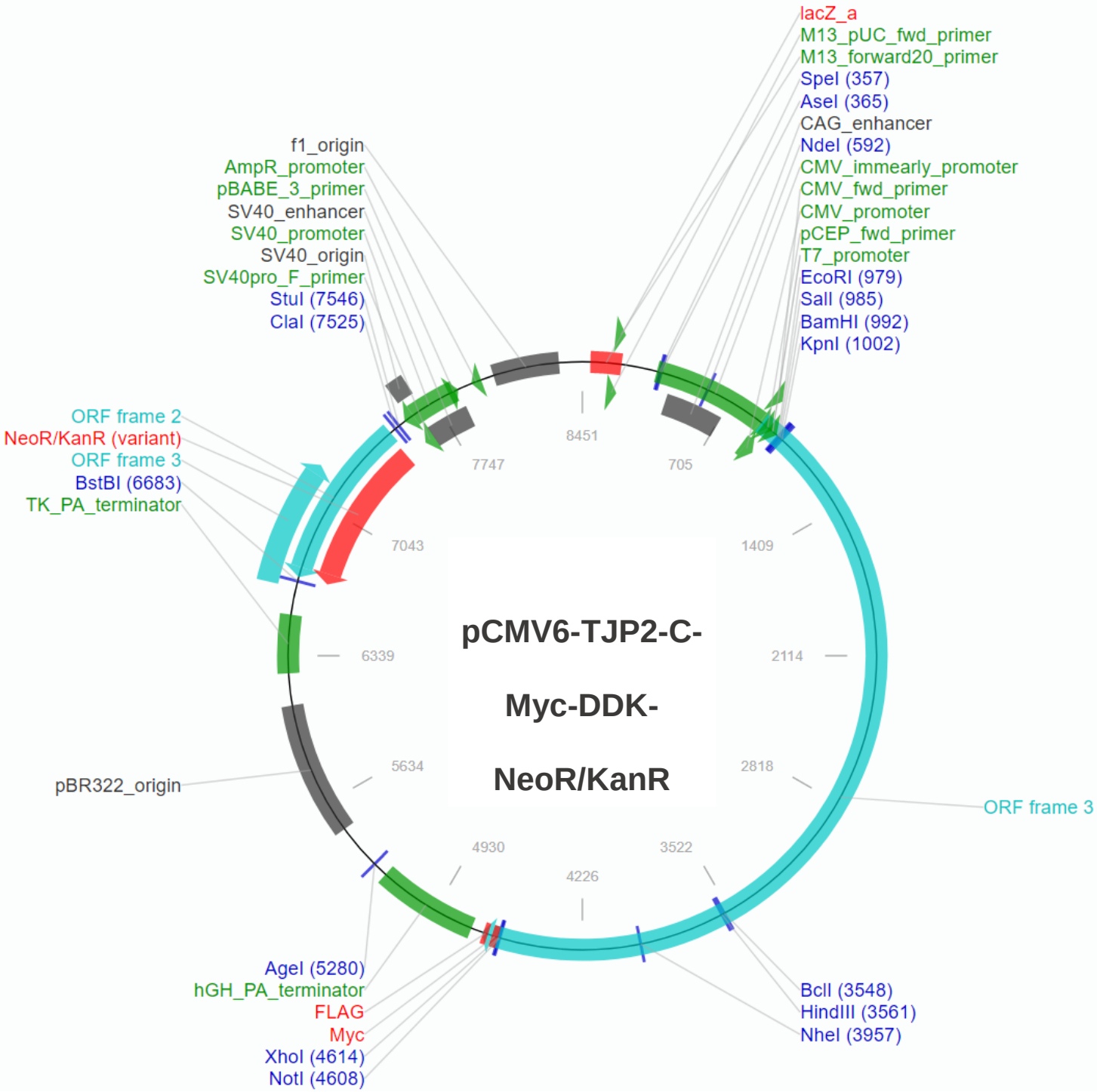

Figure 2.5: Plasmid map of TJP2-myc overexpression plasmid. Direct transfection of this plasmid on HepG2 cells was performed to induce ZO2 overexpression. The HepG2 cells were continually cultured in 1 mg/ml G418 to ensure that only the HepG2 cell that had integrated this plasmid were viable.

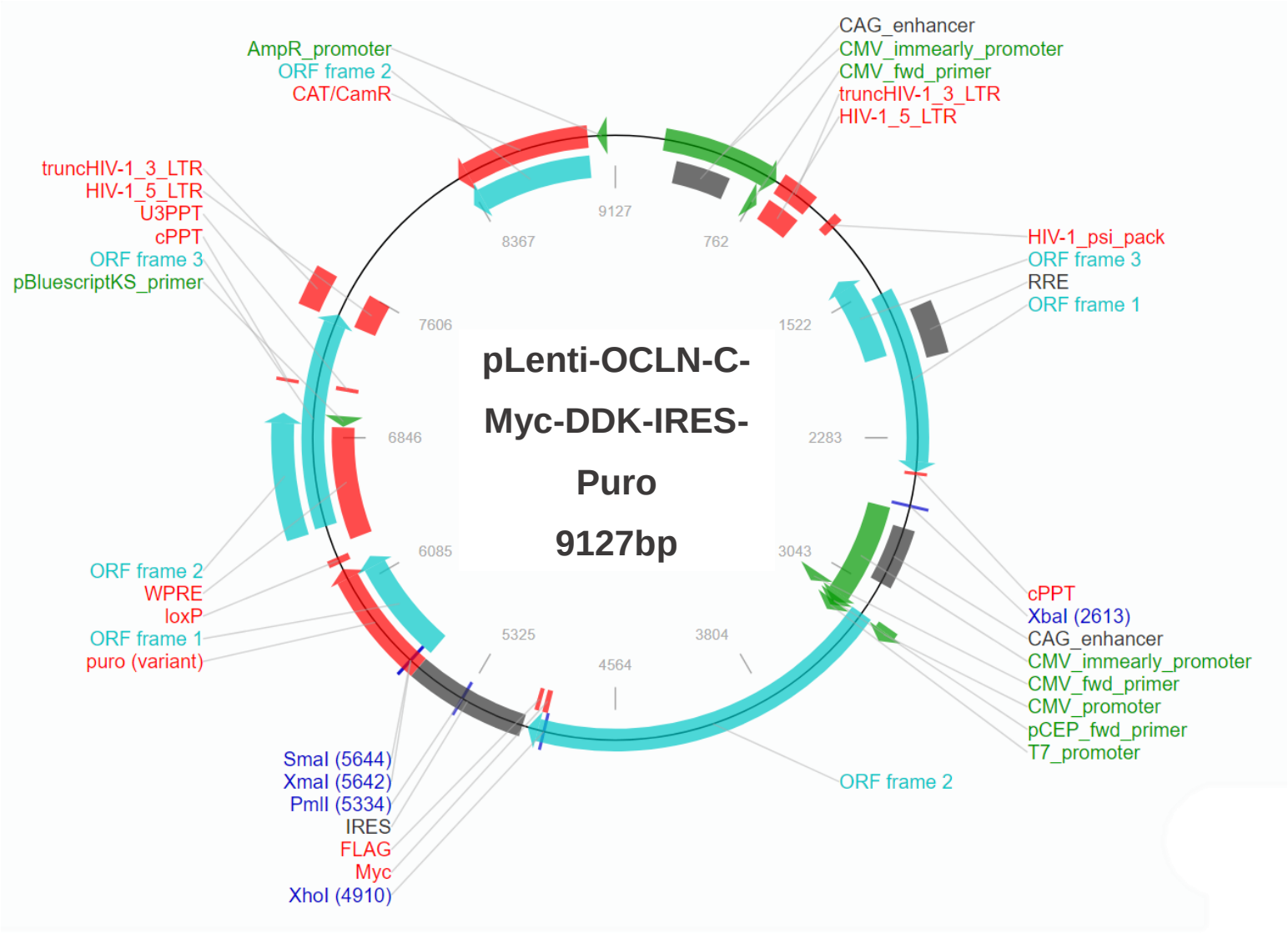

Figure 2.6: Plasmid map of pLenti OCLN-myc overexpression plasmid. HEK293T cells were transfected with pLenti-OCLN-C-Myc-DDK-IRES-Puro and the Lenti-vpak plasmids as described in 2.3.7. The HepG2 control cells were transduced with the resultant lentiviral particles. The cells were continually cultured with 4 µg/ml puromycin.

2.3.2 Preparation of competent *E. coli*

LB-agar plates were produced by melting LB-agar stock for 3 minutes in a microwave. Once molten the LB-agar was placed in a 55^{o}C water bath until the LB-agar was 55^{o}C (Chung et al. 1989). Once the LB-agar had cooled to 55^{o}C the bacterial selective antibiotic was added at the required concentration, displayed in Table 2.2. Immediately, the LB-agar was poured into Petri dishes and was left to sit in a laminar flow cabinet for 1 hour. LB-agar Petri dishes were stored at 4^{o}C for up to 4 weeks.

Antibiotic	Transformed Plasmid	Stock Concentration (mg/ml)	Working Concentration (µg/ml)
Ampicillin	pUC19	100	100
Chloramphenicol	Occludin Myc-DDK pCMV-Control	25 (in EtOH)	25
Kanamycin	TJP2 Myc-DDK	50	50

Table 2.2: Preparation of competent *E. coli*2.3.2 Preparation of competent E. coli, stock and working concentrations for bacterial selection after transformation, antibiotics were diluted directly in the broth/agar at 1:1000.

2.3.3 Competent *E. coli* DNA transformation.

LB-agar plates were warmed to 37^{o}C at the before the start of this protocol.

The Stbl3 was removed from the -80^{o}C freezer and thawed on wet ice for 10 minutes. While on ice 50 ng of DNA was added to the Stbl3 cells and mixed gently.

The same volume of sterile water was added to the negative control. The *E. coli* and DNA mixture were left to incubate on ice for 30 minutes. To heat shock the E.coli, the microcentrifuge tubes were placed in a 42^{o}C water bath for 45 seconds without shaking then immediately returned to ice for 2 minutes (Chung et al. 1989). To this 250 µl of the pre-warmed S.O.C medium was added and then incubated at 37^{o}C on an orbital shaker for 1 hour at 225 rpm. 35 µl of the transformed *E. coli* was streaked on separate LB-agar plates containing the selective antibiotic and was incubated face down at 37^{o}C for 18 hours (Invitrogen 2015).

2.3.4 Growing transformed *E. coli* in a liquid culture

The plasmid specific antibiotic was added at the working concentration to pre-warmed sterile LB-broth in a conical flask just before use.

A single colony was picked from positive colonies and inoculated the respective LB-broth. The negative control was taken from the negative control transformation plates and inoculated with a sterile loop into L-Broth containing the specific antibiotics. The conical flasks were incubated at 37^{o}C in an orbital shaking incubator for 18 hours at 225 rpm (Invitrogen 2015).

2.3.5 Isolation of plasmids using GeneJET plasmid miniprep kit.

GeneJET plasmid miniprep kit was acquired from Thermo Fisher and the method follows the protocol supplied with the kit (Thermo Scientific 2014). Before use 700 µl of 10 mg/ml RNase A solution was added to 70 ml resuspension buffer and stored at 4^{o}C. 170 ml of ethanol was added to 100 ml to the concentrated wash solution.

The 15 ml *E. coli* culture was centrifuged at 3000 x g for 10 minutes in a swinging bucket centrifuge, the LB-broth supernatant was discarded.

The cell pellet was resuspended by pipette in 250 µl resuspension buffer, the solution was transferred to a 2 ml microcentrifuge tube. 250 µl lysis solution was added and mixed via inversion of the tube 6 times, with care not to shear the chromosomal DNA. The RNAse A in the resuspension buffer degrades the RNA that was present in the cell lysate. The lysis buffer contains SDS and NaOH. SDS is an ionic detergent that solubilises the cell membrane and NaOH aids in the breakdown of the bacterial cell wall. NaOH also disrupts the hydrogen bonds in DNA resulting in single stranded DNA.

350 µl neutralisation solution was added and again mixed by inversion of the tube 6 times, with care not to shear the chromosomal DNA. The neutralisation solution neutralises the alkaline condition produced by the lysis buffer. This allows the reforming of double stranded DNA; the long strands of bacterial DNA do not reanneal and therefore do not dissolve. The potassium in the neutralisation solution precipitates the single stranded DNA. The microcentrifuge tube was centrifuged at 10000 x g for 5 minutes to pellet the cell debris and chromosomal DNA.

The supernatant was transferred into a GeneJET spin column without disturbing the pellet, the spin column was centrifuged at 10000 x g for 1 minute. The plasmid DNA reversibly binds to the silica membrane in the column.

500 µl wash solution 1 was pipetted into the spin column and centrifuged at 10000 x g for 45 seconds. The buffer contains isopropyl alcohol and guanidine hydrochloride with facilitates DNA silica binding.

500 µl wash solution 2 was pipetted into the spin column and centrifuged at 10000 x g for 45 seconds. Wash solution 2 contains ethanol, this removed any salts from the silica membrane and did not remove the plasmid DNA.

An additional centrifuge step at 10000 x g for 1 minute was done to remove residual wash solution. The spin column was placed into a fresh microcentrifuge tube and 50 µl of pre-warmed elution solution at 70^{o}C was pipetted into the spin column. The column was incubated at room temperature for 2 minutes then centrifuged at 13000 x g for a further 2 minutes. The DNA quantity was assessed using a Nanodrop and the plasmid was stored at -20^{o}C or used immediately.

2.3.6 Lentiviral production for the differential expression of occludin.

A lentiviral system was used for the differential expression of occludin. For occludin overexpression pLenti-OCLN-C-Myc-DDK-IRES-Puro plasmid was used and for shRNA silencing of occludin a pool of four shRNA plasmids specific to occludin was used from Santa Cruz Biotechnology.

Before the experiment a 6 well plate was coated in poly-l-lysine to facilitate HEK293T attachment to the base of the well. 1ml of 100µg/ml poly-l-sine was pipetted into the wells and the six-well plate was placed on a rocker for 5 minutes. The poly-l-lysine was removed and the wells were washed twice in PBS. The plates were left in the laminar flow cabinet for two hours to dry. HEK293T cells were trypsinised and counted as outlined in 2.2.3 and 2.3.4. $5x10^5$ HEK293T cells were seeded into each well in antibiotic-free medium and incubated overnight at 37^oC and 5 % CO_2 (OriGene 2015).

In a microcentrifuge tube 1 µg of shRNA or pCMV plasmid and 1.2 µg of packaging plasmids was diluted in 250 µl Optimem, mixed via pipetting. 10 µl of MegaTran transfection reagent supplied by OriGene (TT200002), was added and left to incubate at room temperature for 15 minutes. The media on the HEK293T cells was replaced with 1.75 ml fresh antibiotic-free medium during this incubation. The transfection mix was added dropwise to the cells and the plate was gently rocked to ensure the transfection mix was dispersed throughout the well. 18 hours after the addition of the transfection mix the media was removed and replaced with 2 ml fresh antibiotic-free media. 24 hours later the media was harvested and stored at 4^oC and 2 ml fresh antibiotic-free media was added to each well. After another 24 hours, the media was again harvested and pooled with the original harvested media to give a

total of 4 ml (OriGene 2015). The media was filter sterilised through a 0.44 µm filter to remove cellular debris. This media contained the virus and was added immediately on the HepG2 cells.

2.3.7 Lentiviral infection of HepG2 cells.

24 hours before the final lentiviral harvest a T25 cell culture flask containing $7x10^5$ HepG2 cells were cultured in antibiotic-free media was produced.

The media was removed from the T25 flask containing the HepG2 cells and replaced with 4 ml viral media. The viral media contained 8 µg/ml hexadimethrine bromide this countered the electrostatic charges between the viral particles and the HepG2 cells. 8 hours after the addition of the viral media, the cells were supplemented with 4 ml antibiotic-free media. The cell culture was incubated for an additional 24 hours, the spent media was removed and replaced with fresh medium containing antibiotics (OriGene 2015).

2.3.8 Generation of HepG2 cells overexpressing TJP2

This protocol used Fugene HD transfection reagent supplied by Promega and Optimem purchased from Fisher Scientific.

HepG2 cells were seeded at $3x10^5$/well in a six-well plate in antibiotic-free medium 24 hours before Fugene transfection.

4 µg of pCMV6-TJP2-C-Myc-DDK-NeoR/KanR plasmid was added to 250 µl Optimem and was vortexed, then incubated at room temperature for 5 minutes. The plasmid was transferred into a microcentrifuge tube containing 10 µl of Fugene in 240 µl Optimem, the transfection mix was vortexed and incubated at room temperature for an additional 20 minutes. The 500 µl plasmid liposome mix was

added dropwise into each well and the cells were incubated for 18 hours. The media containing the transfection mix was then removed and replaced with fresh media (Promega 2013).

2.3.9 Selecting for HepG2 cells with altered gene expression.

HepG2 cells that had successfully integrated the plasmid DNA were producing the protein of interest. The plasmid also encoded for a mammalian antibiotic resistance gene. The mammalian antibiotic was used to kill any cell that did not express the plasmid. (Kim et al. 2013).

After infection or transfection cells were incubated for 72 hours to allow transcription and translation of the antibiotic resistance gene. The cells were then subcultured equally into a 6 well plate containing the selective antibiotic at a range of concentrations. These concentrations were based off antibiotic kill curves previously calculated. The concentration used was the lowest concentration that resulted in complete cell death in untransformed cells, these concentrations are displayed in Table 2.3.

Antibiotic	Stock concentration (mg/ml)	Working concentration (µg/ml)
G418	1	1
Puromycin	4	4

Table 2.3: Antibiotic concentration used for the selection of positive transformed HepG2 cells. These antibiotics were used when culturing *E. coli* in broth and on agar plates.

The cells were continuously cultured with a selective antibiotic at the concentrations in Table 2.3 to ensure there was a selective pressure.

mRNA and protein analysis were completed on the cells growing in the selective antibiotic to ensure transcription and translation of the inserted gene. The cells were seeded at $2x10^5$ cells/well in a 6 well plate for 48 hours before mRNA expression analysis and 96 hours for protein expression analysis. HepG2 cells transformed with pLenti-C-Myc-DDK-IRES-Puro was used as a control. Once overexpression was confirmed cells culture medium contained the selective antibiotic as described in Table 2.3.

2.4 Generation of siRNAs for mRNA knockdown in HepG2 cells

siRNA Knockdown of ZO1 and ZO2 was completed before each experiment as siRNA knockdown was transient. The siRNA was transfected into the cells with DharmaFECT reagent. The protocol was conducted under usual sterile conditions and extra care was taken due to the use of antibiotic-free DMEM.

2.4.1 siRNA resuspension and dilution

This protocol was completed in a laminar flow cabinet in sterile conditions; extra care was taken due to the use of antibiotic-free medium. Lyophilised siRNA was resuspended and diluted before use. 5 nmol of siRNA was resuspended in 250 µl of 1x siRNA buffer by pipetting the solution taking care not to produce bubbles. The final siRNA concentration was 20 µM. The siRNA solution was placed on an orbital shaker at room temperature for 30 minutes. The siRNA was centrifuged and concentration was verified on a Nanodrop at 260 nm (Horizon 2018).

2.4.2 Transfection of ZO1 and ZO2 siRNA knockdown into HepG2 cells.

The following protocol is for a 1 well of a 6 well plate, the amounts were altered accordingly when needed. Cells cultured in antibiotic-free medium at $3.34x10^5$ cells/well of a 6 well plate. The cells were incubated overnight at 37°C and with 5 % CO_2.

After siRNA resuspension, the siRNA was diluted 1 in 4 with DEPC-treated water to make a working solution of 5 µM. 10 µl of the diluted siRNA was added to 190 µl of Optimem in a microcentrifuge tube. In a different tube, 10 µl of DharmaFECT transfection reagent was added to 190 µl of Optimem. Both siRNA and transfection reagent mixes were incubated separately at room temperature for 5 minutes. The 200 µl siRNA Optimem mix was added to the tube containing the DharmaFECT transfection reagent. The transfection reagent and siRNA were mixed by pipetting and then incubated for an additional 20 minutes at room temperature. All 400 µl of the transfection/siRNA mix was added dropwise to a single well of a six well plate containing 1600 µl antibiotic-free media. When the siRNA was added to the well the final concentration of siRNA was 25 nM in 2 ml (Dharmacon 2018).

2.5 RNA isolation and mRNA quantification

RNA isolated from the cells contains mRNA; this was used to determine expression levels of target genes. The mRNA was converted to cDNA pool before PCR determines the mRNA expression level. All PCR experiments followed The MIQE Guidelines: Minimum Information for Publication of Quantitative Real-Time PCR Experiments (Bustin et al. 2009).

2.5.1 RNA isolation for q-RT-PCR analysis.

RNases are enzymes that degrade RNA found on many surfaces, most notably bare skin. All steps were completed carefully to decrease any chance of RNase contamination. RNA was acquired from cells growing in a monolayer cultured in a six-well plate at 37^{o}C and 5 % CO_2. Isolation of RNA was completed through the protocol supplied by Bioline (Bioline 2017).

Cell lysis: Cells were lysed by adding 500 µl of TRIsure directly to each well. The lysate was pipetted several times to remove and lyse any cells still adhering to the plate. The TRIsure containing the cell contents from the well was transferred into a microcentrifuge tube and incubated at room temperature for 5 minutes to ensure full lysis.

Phase separation: 100 µl of chloroform was added to the cells lysed in TRIsure and tubes were vortexed for 15 seconds. The samples were incubated at room temperature for 3 minutes before being centrifuged at 10000 x g for 15 minutes resulting in three phases, a green phenol phase, an interphase and an upper aqueous phase. The uppermost phase contains the RNA. For smaller quantities of cells where the RNA yield was predicted to be much lower, the phase separation stage was completed twice. This was completed due to the upper aqueous phase being much smaller and there was a high risk of phenol contamination. The second phase separation was conducted in the same manner as before however there were only two phases formed. A clear colourless upper aqueous phase and a clear colourless lower chloroform phase. As before, the clear colourless upper aqueous

phase was transferred to a new microcentrifuge tube. The organic phase and interphase was retained for protein isolation.

RNA precipitation: The upper aqueous phase was carefully transferred to another microcentrifuge tube without removing any other phase. To this 500 µl of ice-cold isopropyl alcohol was added and the samples were incubated for 10 minutes at room temperature. After the 10-minute precipitation had taken place, the RNA was pelleted at 10000 x g for 10 minutes.

RNA wash: The supernatant was discarded then the RNA pellet was washed in 1 ml 75 % ethanol and vortexed for 15 seconds. The samples were centrifuged at 3700 x g for 5 minutes to pellet the RNA pellet again.

Re-solubilisation of RNA: The RNA sample was air dried for 5 minutes at room temperature to allow any remaining ethanol to evaporate. Once all ethanol had evaporated 50 µl of sterile dH_2O was added to re-solubilise the RNA.

RNA purity and yield: Spectrometry was used to quantify RNA yield, a Nanodrop quantified the concentration of nucleic acids through measuring absorption at 260 nm. The RNA purity was assessed on a T.A.E gel, 750 ng of RNA sample was pipetted per well on the agarose gel. The RNA bands were evaluated in a Bio-Rad transilluminator; the RNA was considered good quality if no RNA degradation had occurred and there was no genomic DNA contamination.

2.5.2 DNase treatment

The Turbo DNA-free kit from Ambion was used to remove any DNA contamination present in the RNA preparations (Ambion 2012).

Typically, 27 µl of RNA was transferred into a 0.5 ml PCR tube, to this 3 µl 10x turbo DNase buffer added and mixed by vortex. Once mixed 1 µl of turbo DNase (2U) was added and again mixed by vortexing. The PCR tube was placed into a PCR machine and incubated at 37^{o}C for 30 minutes. To inactivate, 3 µl DNase inactivation reagent was added and mixed by vortex. The reaction was incubated at room temperature for 5 minutes with occasional mixing by flicking the tube. The mix was centrifuged at 10000 x g for 1.5 minutes; the RNA is in the supernatant and transferred to a fresh RNAse/DNAse free tube. The remaining pellet containing the DNAse and inactivation reagent was discarded. As the concentration of nucleic acids have been altered the samples were processed on the Nanodrop once again. The RNA was run on a TAE gel to assess if the contaminating DNA had been removed and to ensure that the RNA had not been degraded in the process. To ensure the RNA did not degrade during electrophoresis DEPC treated H_2O was used to prepare the TAE buffer. The TAE buffer was autoclaved to inactivate the DEPC. The gel tank was washed with RNaseZAP, the electrophoresis tank was sprayed liberally with the RNaseZAP. The solution was discarded, and the tank was washed twice with DEPC-treated H_2O (Ambion 2012).

If the RNA sample was to be used in final investigations the RNA integrity was also assessed on 2100 Agilent bioanalyzer.

2.5.3 Assessing RNA integrity for q-RT-PCR and miRNA analysis.

RNA integrity and quality were assessed with the Agilent bioanalyzer and an RNA nanochip, also supplied by Agilent (Agilent Technologies 2013).

Before the experimental procedure, the RNA ladder was heat-denatured for 2 minutes at 70^{o}C, cooled on ice and 90 µl of RNase free water was added. Aliquots of 10 µl were prepared for storage at -80^{o}C. The analyser was also cleaned to remove any residual components from previous use. The electrode cleaner chip was loaded with 350 µl RNase-free water and placed in the bioanalyser the lid was closed for 5 minutes, the chip was removed and the lid remained open for 30 seconds to allow evaporation of any residual water.

The RNA gel was prepared by pipetting 550 µl of RNA gel matrix into the spin filter and centrifuged at 1500 x g for 10 minutes at room temperature. The filtered gel was aliquot into 8 RNase-free tubes and any unused aliquots stored at 4^{o}C for up to 4 weeks. The RNA dye concentrate was removed from 4^{o}C storage to equilibrate to room temperature for 30 minutes, the dye was then briefly vortexed and centrifuged and 1 µl of this was added to the gel aliquot. The solution was vortexed to mix and centrifuged at 13000 x g for 10 minutes at room temperature. A fresh RNA nanochip was placed into the priming station and 9 µl of the gel-dye matrix was pipetted into the well marked G. The plunger set to 1 ml was compressed to disperse the gel-dye matrix in the RNA nanochip. An additional 9 µl was pipette into the well marked G. To the well-marked with a ladder 5 µl of the RNA marker was added and then 1 µl ladder. To the 12 sample was 1 µl of RNA diluted to 500 ng/µl was loaded. The chip was vortexed for 1 minute at 2400 rpm. The RNA nanochip was placed into the bioanalyzer and the RNA quality was assessed (Agilent Technologies 2013).

2.5.4 cDNA synthesis for q-RT-PCR.

cDNA synthesis was carried out per the Bioline protocol supplied with the kit. A cDNA master mix was prepared on ice (Bioline 2014).

cDNA mix	µl
Oligo dt primers	1
10mM dNTP mix	1
5x RT buffer	4
Ribosafe RNase Inhibitor	1
Tetro Reverse Transcriptase (200u/µl)	1

Table 2.4: cDNA master mix components supplied with the Tetro cDNA synthesis kit supplied by Bioline. This table shows how much of each component was used for one reaction, if multiple cDNA synthesis reactions were being performed the amounts were scaled accordingly.

RNA samples were made to 1500 ng by dilution in DEPC-treated water on wet ice. This was added to the cDNA mix made as described in Table 2.4. The total volume was made to 20 µl with DEPC-treated water and was gently pipetted to ensure full mixing.

The samples were incubated at room temperature for 10 minutes as random hexamers were used. The samples were then placed into a heating block at 45^{o}C for 30 minutes where the RNA to cDNA conversion took place. The reaction is terminated by heating the samples to 85^{o}C for 5 minutes. The samples were stored on ice if used immediately for PCR or at -20^{o}C for long-term storage (Bioline 2014).

2.5.5 Primer design

Primers were designed using the NCBI database. A nucleotide search for the intended protein of interest in the Homo sapiens species was completed. The search term used was “(protein of interest) AND "*Homo sapiens*"[porgn:__txid9606]”. The relevant nucleotide sequence for the mRNA target was chosen. The pick primer option allowed automatic generation of primers within specific requirements. The PCR product length was set to a maximum of 200bp and the exon junction span was chosen to reduce the chance of genomic DNA amplification. Note, not all primers were available as exon spanning. The primers arrived in a lyophilised state; the stock was reconstituted in DEPC-treated water to a concentration of 1 mM. An aliquot of the stock was taken and diluted to give a working concentration of 10 µM. The aliquot of primer reduced the chance of primer contamination in the stock and minimised freeze-thaw cycles.

2.5.6 Primers used in mRNA expression analysis.

Homo sapiens cadherin 1 (CDH1), transcript variant 1, NM_004360.5
Product length = 89

Forward primer	1	CATGAGTGTCCCCCGGTATC	20
Template	2497	……	2561
Reverse primer	1	CAGTATCAGCCGCTTTCAGA	20
Template	2585	……	2566

	Length	Tm	GC%	Self-complementarity	Self 3' complementarity
Forward Primer	20	59.61	60.00	4.00	2.00
Reverse Primer	20	57.70	50.00	5.00	3.00

Homo sapiens cadherin 2 (CDH2), transcript variant 1, NM_001792.5
Product length = 97

Forward primer	1	TCGGGTAATCCTCCCAAATCA	21
Template	2161	……	2181
Reverse primer	1	CCACAATCCTGTCCACATCTG	21
Template	2257	……	2237

	Length	Tm	GC%	Self-complementarity	Self 3' complementarity
Forward Primer	21	58.52	47.62	3.00	1.00
Reverse Primer	21	58.64	52.38	4.00	4.00

Homo sapiens claudin 1 (CLDN1), NM_001792.5
Product length = 120

Forward primer	1	TGGTATGGCAATAGAATCGTTCA	23
Template	655	……	677
Reverse primer	1	TCCCAGAAGGCAGAGAGAAG	20
Template	774	……	755

	Length	Tm	GC%	Self-complementarity	Self 3' complementarity
Forward Primer	23	57.97	39.13	6.00	2.00
Reverse Primer	21	58.43	55.00	2.00	0.00

Homo sapiens glyceraldehyde-3-phosphate dehydrogenase (GAPDH), transcript variant 1, NM_002046.7
Product length = 87

Forward primer	1	TGCACCACCAACTGCTTAGC	20
Template	530	.....	677
Reverse primer	1	GGCATGGACTGTGGTCATGAG	21
Template	616	.....	596

	Length	Tm	GC%	Self-complementarity	Self 3' complementarity
Forward Primer	20	61.17	55.00	5.00	5.00
Reverse Primer	21	61.02	57.14	6.00	4.00

Homo sapiens gap junction protein alpha 1 (GJA1), NM_000165.5
Product length = 130

Forward primer	1	CAATTACAACAAGCAAGCAAGTG	23
Template	1100	.....	1122
Reverse primer	1	CTGGTTATCATCGGGGAAATCA	22
Template	1229	.....	1208

	Length	Tm	GC%	Self-complementarity	Self 3' complementarity
Forward Primer	23	57.68	39.13	4.00	2.00
Reverse Primer	22	57.91	45.45	4.00	4.00

Homo sapiens occludin (OCLN), transcript variant 1, NM_002538.3
Product length = 108

Forward primer	1	AGCAGCGGTGGTAACTTTG	19
Template	1541	.....	1559
Reverse primer	1	AGTTGTGTAGTCTGTCTCATAGTG	24
Template	1678	.....	1625

	Length	Tm	GC%	Self-complementarity	Self 3' complementarity
Forward Primer	19	58.37	52.63	4.00	0.00
Reverse Primer	24	57.74	41.67	3.00	2.00

Homo sapiens snail family transcriptional repressor 2 (SNAI2), NM_003068.5

Product length = 119

Forward primer	1	ACTCCGAAGCCAAATGACAAA	21
Template	1013	.....	1033
Reverse primer	1	CTCTCTCTGTGGGTGTGTGT	20
Template	1131	.....	1112

	Length	Tm	GC%	Self-complementarity	Self 3' complementarity
Forward Primer	21	58.42	42.86	4.00	0.00
Reverse Primer	20	58.96	55.00	1.00	0.00

Homo sapiens tight junction protein 1 (TJP1), transcript variant 1, NM_003257.4

Product length = 95

Forward primer	1	AAACAAGCCAGCAGAGACC	19
Template	3617	.....	3635
Reverse primer	1	CGCAGACGATGTTCATAGTTTC	22
Template	3711	.....	3690

	Length	Tm	GC%	Self-complementarity	Self 3' complementarity
Forward Primer	19	57.97	52.63	2.00	0.00
Reverse Primer	22	57.83	45.45	6.00	4.00

Homo sapiens tight junction protein 2 (TJP2), transcript variant 1, NM_004817.4

Product length = 77

Forward primer	1	GGCACAGTTGTCCCAGAGA	19
Template	1495	.....	1513
Reverse primer	1	GGGGCTGCTTTTGGTTGAG	19
Template	1571	.....	1553

	Length	Tm	GC%	Self-complementarity	Self 3' complementarity
Forward Primer	19	59.25	57.89	6.00	3.00
Reverse Primer	19	59.33	57.89	3.00	0.00

Homo sapiens twist family transcription factor 1 (TWIST1), transcript variant 1, NM_000474.4

Product length = 119

Forward primer	1	CTCAAGAGGTCGTGCCAATC	20
Template	1280	……	1299
Reverse primer	1	CCCAGTATTTTTATTTCTAAAGGTGTT	27
Template	1398	……	1372

	Length	Tm	GC%	Self-complementarity	Self 3' complementarity
Forward Primer	20	58.64	55.00	4.00	0.00
Reverse Primer	27	56.57	29.63	4.00	0.00

Homo sapiens zinc finger E-box binding homeobox 2 (ZEB2), transcript variant 1, NM_014795.4

Product length = 129

Forward primer	1	GTTATCCACAGCCTAGAGTTTTTATAT	27
Template	6457	……	6483
Reverse primer	1	GTTATCGCCTAGAGCCTTTCAA	22
Template	6585	……	6564

	Length	Tm	GC%	Self-complementarity	Self 3' complementarity
Forward Primer	27	57.22	33.33	4.00	4.00
Reverse Primer	22	58.21	58.21	4.00	3.00

Each primer was tested before use in experiments to ensure any PCR results would be reliable. A real time PCR would be run using GAPDH as a reference and dH_2O as a negative control along with the new untested primer. The PCR was run for 40 cycles and included a melt curve. If a single peak was produced, the PCR reaction mix would be run on a 2 % T.B.E agarose gel. If the primers had worked efficiently there was a single positive band, the band size was calculated by assessing it against a PCR marker (New England BioLabs N3234L).

2.5.7 Quantitative reverse transcriptase polymerase chain reaction (q-RT-PCR)

q-RT-PCR amplifies specific targets in the cDNA pool previously generated. A Bio-Rad CFX Connect™ Real-Time PCR Detection System is a thermal cycler that can detect fluorescence of a probe bound to the amplified DNA. A ratio between the constitutive reference gene GAPDH and target mRNA normalises expression levels between samples. All PCR reactions were a total of 10 µl and were amplified in a Hard-Shell® Low-Profile Thin-Wall 96-Well Skirted PCR Plate, acquired from Bio-Rad. The cDNA was diluted 1:5 with DEPC-treated and 1 µl was added to a premade master mix as described in Table 2.5 (Bio-Rad Laboratories 2017).

PCR mix	µl
Forward primer (1 µM)	1
Reverse primer (1 µM)	1
iTaq™ Universal SYBR® Green Supermix	5
DEPC-treated water	2
cDNA (1:5 dilution)	1

Table 2.5: PCR mix recipe used per well for q-RT-PCR. The master mix was supplied by Bio-Rad, iTaq™ Universal SYBR® Green Supermix. The master mix contained dNTPs, DNA polymerase, $MgCl_2$, SYBR green and chemical stabilisers. This table shows how much of each component was used for one reaction, if multiple PCR reactions were being performed the amounts were scaled accordingly.

The PCR mix was prepared as a master mix and placed into each well before the addition of the diluted cDNA to reduce pipetting error. The PCR mix was prepared on

wet ice under sterile conditions to minimise degradation and contamination. Before the plate was placed into the PCR machine, it was centrifuged at 100 x g to ensure all PCR mix was at the base of the well.

The Bio-Rad CFX Connect™ Real-Time PCR Detection System was controlled by Bio-Rad CFX Manager™ Software 3.1 under the following conditions outlined in Table 2.6.

Step	Temperature (°C)	Time (s)	Cycles
1. Initial Denaturation	95	120	1
2. Denaturation	95	5	
3. Annealing	60	30	40
Detection			
4. Denaturation	95	5	1
5. Melt curve	65-95	0.1°C/s	1

Table 2.6: q-RT-PCR PCR amplification protocol programmed on Bio-Rad CFX Manager™ Software 3.1. Due to the small PCR amplicon sizes negating the need for an elongation step, a two-step PCR was run.

Detection of the amplicon was executed at the end of step 4 after each cycle. The validity of the results was ensured through running each target in triplicate and running a negative control for each sample. A negative controlled contained all the same PCR components. However, the cDNA was replaced by DEPC-treated water. A melt curve further validated results; the amplicon was heated between 65°C and

95^{o}C. When the amplicon melts the PCR machine detects a loss of the fluorescent probe. When the PCR product is of the same length as intended there was a single peak produced when the fluorescence was lost.

2.5.8 Methodology of calculating relative expression of mRNA after RT-PCR, $2^{--\Delta\Delta CT}$ method.

Normalised gene expression was calculated by using the ΔΔCt method. The formula is listed here (Livak and Schmittgen 2001). Normalised expression allowed for the comparison between samples compared to the control. Expression of the gene is set to 1, the relative expression of the sample target is given as a fold change. For example, the control mRNA target was 1 and the normalised expression of the experimental target was 2. There is twice as much target mRNA in the experimental sample compared to the control.

$$\text{Normalised expression} = 2^{-\Delta\Delta Ct}$$

Where ΔΔCt = ΔCt (sample) – ΔCt (control)]

ΔCt (sample) = Ct value target (sample) – Ct value reference (sample)

ΔCt (control) = Ct value target (control) – Ct value reference (control)

The reference gene used was GAPDH, it was ensured that there GAPDH expression had <0.5 Ct change the control and all experimental groups.

2.6 RNA isolation, cDNA synthesis and q-RT-PCR for miRNA analysis.

As miRNA are approximately 22 nucleotides a column-based RNA extraction method was used to ensure extraction of the smaller RNA.

2.6.1 RNA isolation for miRNA analysis.

To extract small RNAs, RNA was extracted using the mirVana miRNA isolation kit purchased and acid-phenol:chloroform from Fisher Scientific (Ambion 2011). The total RNA isolation procedure was used. This was because the isolation of enrichment of small RNAs does not allow the critical evaluation of the RNA before miRNA analysis.

HepG2 cell experiments were terminated by washing the cells with PBS twice for 2 minutes and then adding 450 µl lysis/binding solution. The solution was pipetted vigorously to obtain a homogenous cell lysate. The lysate was transferred into a 2 ml RNase/DNase free tube. To this 45 µl miRNA homogenate additive and mixed by vortex, then left to incubate on ice for 10 minutes. 450 µl of acid-phenol:chloroform was added to the lysate and vortexed for 45 seconds to mix. The solution was centrifuged at 10000 x g for 5 minutes at room temperate to achieve phase separation. The upper aqueous phase was transferred to a fresh RNase/DNase free tube without disturbing the interphase and organic phase which was discarded.

To the aqueous phase collected, 560 µl 100 % ethanol was added and mixed by vortex. A maximum of 700 µl of the solution was applied to the RNA filter cartridge and centrifuged at 10000 x g for 15 seconds, the flow through was discarded. This was repeated until all the aqueous/ethanol solution had passed through the filter cartridge. 700 µl miRNA wash solution 1 was applied to the filter cartridge, centrifuged at 10000 x g for 7 seconds and the flow through was discarded. 500 µl miRNA wash solution 2/3 was applied to the filter cartridge, centrifuged at 10000 x g for 7 seconds and the flow through was discarded, then repeated. To remove any

residual wash buffer the filter cartridge was centrifuged again at 10000 x g for 1 minute. The filter cartridge was placed into a fresh RNase/DNase free tube and 100 µl of preheated 95^{o}C elution solution was added. The filter cartridge was centrifuged at maximum speed for 30 seconds to recover the RNA from the filter. The RNA concentration was assessed on the Nanodrop and samples were stored at -80^{o}C. An aliquot of 2000 ng of each sample was stored at -20^{o}C for analysis on the Agilent bioanalyzer and in a denaturing acrylamide gel (Ambion 2011).

2.6.2 Assessing small RNA quality and relative amounts through a denaturing acrylamide gel.

Denaturing acrylamide gels visualise the small RNA fraction of RNA, this assessed the RNA preparation and whether the small RNA fraction had been isolated.

An acrylamide gel was produced as described in 2.1.3 and placed into a Bio-Rad Mini-Protean Tetra Cell. 1000 ml of 1x TBE buffer was added to the cell. 1500 ng of RNA was mixed with equal volume gel loading dye and heated at 95^{o}C in a dry block for 3.5 minutes. The samples were loaded into separate wells. One well contained Thermo Scientific GeneRuler 50 bp DNA Ladder. The gel was run at 37 mA until the bromophenol blue dye front had migrated within 0.5 cm to bottom of the gel (Ambion 2011). The acrylamide gel was visualised under UV light in a Bio-Rad gel doc EZ and ImageLab 5.2.1 software. All PCR experiments followed The MIQE Guidelines: Minimum Information for Publication of Quantitative Real-Time PCR Experiments (Bustin et al. 2009).

2.6.3 cDNA synthesis for investigations in miRNA expression.

Megaplex RT primers and TaqMan microRNA reverse transcription kit were purchased from Fisher scientific. The RT reaction was completed without preamplification of miRNA and only TaqMan™ Array Human MicroRNA A Cards v2.0. This array was used, as it focused towards miRNA that are better characterised.

Megaplex RT primers, TaqMan microRNA RT kit and $MgCl_2$ were thawed on wet ice for 10 minutes. The following reagents were combined in a DNase/RNase free PCR tube, volumes stated in Table 2.7 are for one sample, for multiple samples the amounts were increased accordingly (Applied Biosystems 2011).

RT reaction mix components	Volume (µl)
Megaplex RT primers 10x	0.8
dNTPs with DTTP (100mM)	0.2
MultiScribe RT (50U/µl)	1.5
10x RT buffer	0.8
$MgCl_2$ (25mM)	0.9
RNase inhibitor (20U/µl)	0.1
dH_2O	0.2
Total	4.5

Table 2.7: Components and amounts to synthesise cDNA from miRNA. This table shows how much of each component was used for one reaction, if multiple cDNA synthesis reactions were being performed the amounts were scaled accordingly

The RT reaction mix was mixed by inverting the PCR tube 6 times, 3 µl of total RNA at a concentration of 330 ng/µl was added. The RT/RNA mix was incubated on ice for 5 minutes.

The tube was placed into the PCR machine and the thermal cycling protocol is outlined in Table 2.8.

Temperature (ºC)	Time (s)	Cycles
16	120	
42	60	40
50	1	
85	300	1
4	∞	1

Table 2.8: The RT reaction setting used for miRNA cDNA synthesis. The RT reaction was run on an Eppendorf Mastercycler nexus gradient PCR machine. Once completed the cDNA was used, if possible, immediately after the completion of the RT reaction.

cDNA was stored for a maximum of one week, miRNA PCR was typically completed as soon as possible after cDNA synthesis (Applied Biosystems 2011).

2.6.4 Quantitative reverse transcriptase polymerase chain reaction for miRNA analysis in a low-density TLDA microRNA assay.

The TaqMan universal master mix and TaqMan low-density array was supplied by Fisher scientific.

In a microcentrifuge tube the following reagents were combined and mixed by inverting the tube 6 times, volumes in Table 2.9 are for one microRNA array, volumes were altered accordingly when needed (Applied Biosystems 2018).

Component	Volume (µl)
TaqMan universal PCR master mix	450
RT cDNA product	6
dH_2O	444

Table 2.9: Components and volumes needed to run one microRNA array. This was the total amount needed for the full miRNA assay. The master mix, cDNA and H_2O were kept on ice when preparing the mix.

The low-density Taqman microRNA array removed from 4^{o}C storage to equilibrate to room temperature for 5 minutes. 100 µl of the master mix produced in Table 2.9 was pipetted into the 8 reservoirs. The array centrifuged to disperse the PCR reaction mix throughout the array; the array was inserted into a Sorvell centrifuge bucket facing outward. The plate was centrifuged at 330 x g for 1 minute with maximum up and down ramp rate settings. This step was repeated to ensure there was equal amounts of the PCR reaction mix throughout the array plate. The reservoirs were inspected to ensure that equal amounts of the sample had entered the array. The array plate is sealed with the plate sealer. Once sealed the reservoirs were cut off the array plate.

The low-density array was processed immediately in the Applied Biosystems 7900HT q-RT-PCR machine (Applied Biosystems 2018).

The plate was inserted into the PCR machine that had a TLDA block installed. The standard protocol for miRNA analysis was used though SDS 2.4.1 software. The SDS setup file supplied by Fisher Scientific was imported into the software, the setup file automatically labels the position of miRNA target and configures the thermal cycling settings, shown in Table 2.10 (Applied Biosystems 2018).

Step	Temperature (ºC)	Time (S)	Cycles
Uracil-N-glycosylase activation	50	120	1
Initial Denaturation	94.5	600	1
Denaturation	97	30	45
Annealing/Elongation	59.7	60	
Detection			

Table 2.10: Thermal cycling settings used for miRNA analysis PCR on an Applied Biosystems 7900HT PCR machine. The detection of fluorescence after the elongation step.

The results were imported to RQ manager 1.2.1, the miRNA targets were compared to the control sample the normalised against the value of the U6 target.

2.7 Immunocytochemistry

Protein localisation was assessed through antibody staining with secondary antibodies that have a probe that fluoresces when bound to primary antibodies. HepG2 cells were cultured in a 24 well plate with sterile glass slides in each well at $4x10^4$ cells. Procedures such as siRNA knockdown or occludin overexpression occurred before termination of the cells and immunocytochemistry staining.

2.7.1 Antibodies used in immunofluorescence experiments

Antibodies used in protein localisation studies are noted in Table 2.11, occludin, ZO1 and ZO2 were purchased from Invitrogen and MRP2 was purchased from Abcam. Displayed in Table 2.11 are the antibodies, class and expected kDa.

Target	1º/2º	Host	Concentration (mg/ml)	Class	Clone reference
Occludin	1º	Mouse	0.5	Monoclonal	OC-3F10
ZO1	1º	Mouse	0.5	Monoclonal	ZO1-1A12
ZO2	1º	Mouse	0.5	Monoclonal	3E8D9
MRP2	1º	Mouse	0.25	Monoclonal	M2 III-6
Mouse IgG	2º	Goat	2	Polyclonal GFP	A-11001

Table 2.11: Information of antibodies used in localisation of protein through immunofluorescence. Mouse monoclonal antibodies were used to increase specificity to the protein and reduce non-specific protein binding. All primary antibodies were not conjugated.

2.7.2 Experiment termination and fixing of cells

The spent DMEM media was removed from the 24 well plates and replaced with ice cold 500 µl of 3.7 % paraformaldehyde for 10 minutes at room temperature. The paraformaldehyde was discarded and the cells were washed with 500 µl PBS three times. The cells were immediately carried forward to the antibody staining procedure or stored at 4ºC (Abcam 2015).

2.7.3 Antibody staining

To reduce non-specific antibody binding the fixed cells were incubated with PBS with 5 % bovine serum albumin for 1 hour at room temperature. The cells were washed 3 times with 500 µl PBS for 5 minutes at room temperature.

Antibody	Concentration in 5 % BSA/PBS (µg/ml)
Mouse anti occludin	2.5
Mouse anti ZO1	7.5
Mouse anti ZO2	5

Table 2.12: Antibody dilutions for immunocytochemistry investigations. The dilutions were in 5 % BSA/PBS, typically in 350 µl. The antibody dilutions were prepared during the fixing of the cells, then stored at 4^{o}C until use.

The primary antibody was diluted in 350 µl PBS with 0.5 % w/v bovine serum albumin for 2 hours at room temperature, concentrations shown in Table 2.12 Following the incubation with the primary antibody thecells were washed again 3 times with PBS at room temperature. The secondary antibody Goat anti Mouse IgG Alexa Fluor 488 was diluted in 400 µl PBS with 0.5 % w/v bovine serum albumin and incubated for 1 hour at room temperature. To identify where the target protein was in relation to the cell DAPI nucleic acid stain was used, 2 µl of stock solution 1mg/ml was added to 8 µl PBS (Abcam 2015). When the secondary antibody incubation period had 5 minutes remaining 1 µl of the diluted DAPI solution was added to each well. The cells were washed finally 3 times with PBS at room temperature and the cells were mounted onto microscope slides with ProLong gold antifade mountant. Fluorescent images were acquired on a Nikon fluorescent microscope with a Microtec MDC-C1.3F microscope camera.

2.8 Protein analysis

Protein isolation continued from the RNA extraction protocol; the upper aqueous phase was removed for RNA analysis; the organic phase and interphase were retained for protein extraction.

2.8.1 Antibodies used in protein expression experiments.

Antibodies used in protein quantification studies are noted in Table 2.13, occludin (33-1500), ZO1 (33-9100) and ZO2 (37-4700) purchased from Invitrogen, phosphorylated Ser/Thr (ab17464) purchased from Abcam and Mouse HRP (7076) and Rabbit HRP (7074) from Cell Signalling Technology.

Target	1º/2º	Host	Concentration (mg/ml)	Class	Expected kDa
Occludin	1º	Mouse	0.5	Monoclonal	≈60
ZO1	1º	Mouse	0.5	Monoclonal	≈187
ZO2	1º	Mouse	0.5	Monoclonal	≈131
Phospho Ser/Thr	1º	Rabbit	0.25	Polyclonal	N/a
Mouse IgG 7076	2º	Horse	2	Polyclonal HRP	N/a
Rabbit IgG 7074	2º	Horse	2	Polyclonal HFP	N/a

Table 2.13: Primary antibodies product data used in immunocytochemistry investigations. Phospho Ser/Thr antibody is specific to phosphorylated serine or threonine amino acids surrounded by phenylalanine. Occludin, ZO1, ZO2 and Phospho Ser/Thr antibodies were not conjugated.

2.8.2 Protein isolation.

Any remaining aqueous phase was removed from the organic and interphase to reduce RNA contamination. To this 0.3 ml 100 % ethanol was added and mixed by

inversion. The samples were left to incubate for 5 minutes at room temperature to precipitate the DNA. The sample was centrifuged at 2000 x g for 5 minutes at 4^{o}C, the supernatant was retained into a fresh 2 ml microcentrifuge tube and the DNA pellet was discarded. The protein was precipitated by adding 1.5 ml to the sample and mixed on an orbital shaker at room temperature for 10 minutes; the sample was then centrifuged at 12000 x g for 10 minutes. The protein was washed twice in 0.3 M guanidine hydrochloride in 95 % ethanol by adding 2 ml to the protein pellet, mixing on an orbital shaker for 20 minutes at room temperature and then centrifuging at 7500 x g for 5 minutes at 4^{o}C. The protein pellet was washed again with 2 ml ethanol and mixed on an orbital shaker at 225 rpm room temperature for 20 minutes. Finally, the protein was pelleted by centrifuging at 7500 x g at 4^{o}C for 5 minutes. The protein was dried in a desiccator for 10 minutes, once dry the protein pellet was resuspended in 1 % SDS (Bioline 2017).

2.8.3 Protein gel electrophoresis and blotting.

Protein samples were diluted to 4 µg/µl in 1 % w/v SDS. This was mixed with Laemmli sample buffer 1:1 in a microcentrifuge tube and was incubated at 95^{o}C for 5 minutes in a dry bath. After 5 minutes, the samples were immediately cooled on ice.

Bio-Rad Any kD Mini-PROTEAN TGX Stain-Free gels were loaded into a Bio-Rad mini-protean tetra cell with 1000 ml of electrode buffer. One well per gel had 7 µl of precision plus protein dual colour standards as a control. The other wells were loaded with 20 µl of the sample, this equates to 40 µg of protein/well. The gel was run at 100 volts constant until the sample had migrated completely into the gel, once this had occurred the volts were increased to 200 volts constant. The gel

electrophoresis was run until the dye front had reached 0.5 cm from the base of the gel (Bio-Rad laboratories 2016).

2.8.4 Ensuring equal concentrations of protein was used between samples.

Bio-Rad Mini PROTEAN Stain-Free™ gels were used to separate proteins before blotting. These gels contain a trihalo compound, this enhanced the fluorescence of tryptophan amino acids when exposed to UV. This allowed for the visualisation of the gel without inhibiting downstream steps, a problem associated with traditional methods of protein lane staining such as Coomassie blue.

After separation of proteins on the SDS-PAGE gel but before blotting on to the PVDF membrane. The gel was removed from the cassette and exposed to UV light in the transilluminator for 5 minutes to activate the fluorescence of tryptophan. Once activated the transilluminator imaged the gel so total lane protein could be assessed between samples (Bio-Rad 2015).

2.8.5 Blotting of proteins from the SDS-PAGE to the PDVF membrane and antibody staining.

The protein gel was blotted onto a trans-blot® turbo mini PDVF in a trans-blot turbo system at 2.5 A and 25 V for 20 minutes. The blot was transferred into 5 % w/v MARVEL/TBST and placed in a 50 ml falcon tube overnight at 4^{o}C on a tube roller. The membrane is washed in 20 ml TBST once for 5 minutes at room temperature. Primary antibodies were diluted in 0.5 % w/v MARVEL/TBST and added to the membrane at the required concentrations for 2 hours at room temperature on the

tube roller. The blot was washed three times for 10 minutes with 20 ml TBST on the tube roller. The secondary antibody with an HRP conjugate was diluted in 0.5 % MARVEL/TBST and incubated on the tube roller for one hour at room temperature. The blot was washed finally for 10 minutes with 20 ml TBST three times at room temperature. The blot was developed using SuperSignal West Femto maximum sensitivity substrate by incubating with 0.5 ml of solutions A and B for 5 minutes in the dark. The blot was placed on the Bio-Rad transilluminator, using Image Lab 5.2.1, the chemi setting was set to signal accumulation mode. This exposed the blot until a band could be visualised by eye on the screen, the number of seconds was recorded an image was acquired. To attain a high resolution image with maximum clarity the exposure time was slightly modified to either increase exposure to attain brighter bands or decrease expose to decrease band intensity
(Bio-Rad laboratories 2018).

2.8.6 Protein molecular weight estimation.

When obtaining an image of the western blot a multichannel image was acquired. The chemiluminescence channel took an image of the HRP fluorescence of the target antibody and the colorimetric channel imaged the molecular markers. These two images were overlaid in ImageLab 5.2.1 (URL http://www.bio-rad.com/en-uk/product/image-lab-software?ID=KRE6P5E8Z), Figure 2.7.

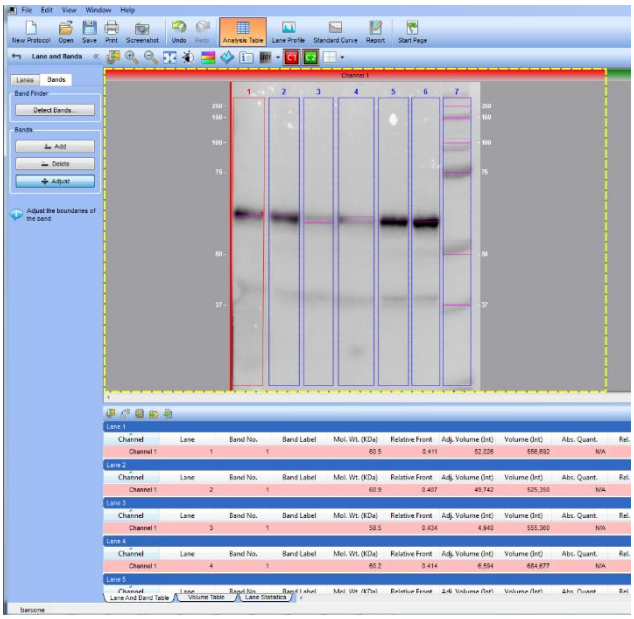

Figure 2.7: A multichannel blot in ImageLab 5.2.1. Lanes 1-6 show bands to target protein. Lane 7 shows the molecular weight marker Bio-Rad dual colour plus standards. The software automatically highlights bands in each well. From this the software can assess distance travelled between each marker and the band.

As shown in Figure 2.7, a blot was imported into ImageLab 5.2.1, using the lane find tool the software would highlight any lanes present on the blot. Then the detect band tool was used, this would mark each band on the blot. Using the molecular weight estimation tool, the protein standards lane was labelled and each band in the lane was assigned its molecular weight. The software measured the distance the molecular markers and the distance the positive bands had travelled down the gel.

Using the distances between the marker, the software was able to estimate the size of the target protein band.

2.9 Statistics used to analyse experimental data.

Wound healing and invasion assays used 3 biological repeats and 2 analytical repeats. For PCR investigations 2 biological repeats and 3 analytical repeats were used. Western blotting investigations used two biological repeats but no analytical repeats. Before completing statistical analysis on the results were assessed for anomalous results and it was ensured that data was normally distributed to ensure the results showed no skew.

All data statistics was calculated using Microsoft Excel and GraphPad 7.0.2 utilising the statistical tools of (standard error of the mean) S.E.M, P-values and mean.

The S.E.M was calculated by calculating the mean, standard deviation and count. This was completed by using the formula for S.E.M.

$$\sigma_M = \frac{\sigma}{\sqrt{N}}$$

σ_M = standard error of the mean

σ = the standard deviation of the original distribution

$\sqrt{N}$ = root of the sample size

This produced the standard error of the mean which was added to the graphs to show data variation. A low S.E.M implies the data was reliable but does not indicate any significant changes.

One-way analysis of variance was used to calculate if the results were statistically different from each other. GraphPad Prism 7.0.2. To test for significant changes between all variables a one-way analysis of variance with multiple comparisons was used. For invasion, migration and PCR investigations one-way analysis of variance was chosen so the means of two or more data sets could be compared. One-way analysis of variance produces an F-statistic, the ratio of means to the variance between samples. When only two means were being compared one-way analysis and t-tests are equivalent.

There are several assumptions needed for one-way analysis of variance, the measuring of an interval, two or more categorical groups and samples can only be used in one categorical group. Each investigation carried out followed all assumptions making this statistical test optimal to assess statistical differences.

When making multiple comparisons simultaneously a P value can show a significant difference due to chance. If there is a false positive in each comparison it is likely that there will be a P value showing significance.

Dunnett's post hoc test, is a Students t-statistic is computed for each experimental group. However, the issue here the error variance is pooled from the square of all errors. Dunnett's test uses the largest value of error in the Students t-statistic. This overcame the likelihood of false positives.

3. Analysis of Results

3.1 Generation of a HepG2 cell model with differential expression of tight junction protein occludin.

As described in 1.3.2 the downregulation of occludin expression correlates with a lower long-term survival and had a 2-fold higher change of HCC recurrence after treatment. Increased occludin correlates to a more positive outcome and shows increased long-term survival (Bouchagier et al. 2014; Orbán et al. 2008). To investigate the relationship between occludin expression and cancer cell behaviour a HepG2 model with differential occludin expression was produced.

The differential expression of occludin was produced through a lentiviral system outlined in, 2.3.7 Lentiviral infection of HepG2 cells. Occludin overexpression was achieved by using a plasmid containing occludin cDNA that had been inserted into a pLenti-C-Myc-DDK-IRES-Puro vector, supplied sequence validated from OriGene. Occludin knockdown was achieved with the use of four shRNA plasmids containing occludin shRNAs each containing a puromycin resistant gene, supplied by Santa Cruz Biotechnology sc-36117-SH.

Real-time PCR and Western blotting analysis were used as analytical tools to verify differential expression of occludin in the HepG2 model.

3.1.2 Quality control and statistical analysis for real-time PCR experiments.

For quality assurance the RNA was DNase treated using the TURBO DNA-free kit (Invitrogen) and the RNA samples were run on the Bioanalyzer (Agilent) with an RNA 6000 Nano chip. Only RNA samples that achieved an integrity score of >9 were used in cDNA reverse transcription.

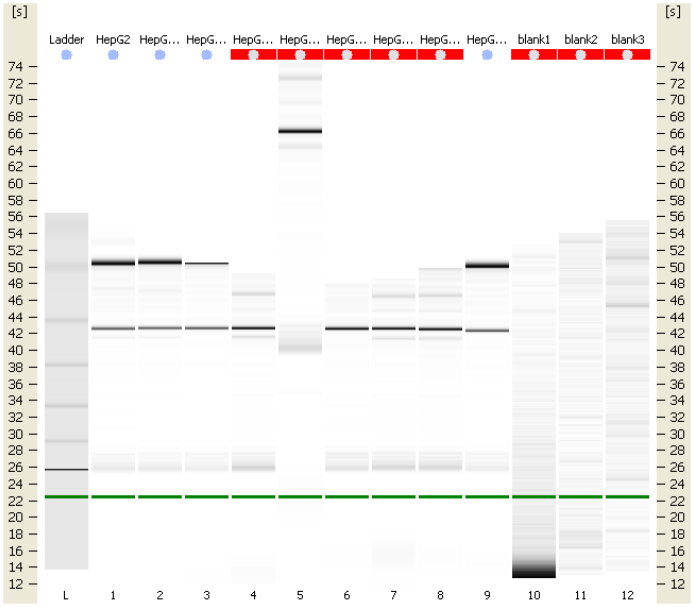

c. Ladder lane, RNA ladder; Lanes 1-9 RNA; Lanes 10-12 H_2O. This bioanalyzer plot shows optimal RNA isolations in lanes 1-3. Samples in lanes 4-7, show degraded RNA. Lanes 10-12 show that the H_2O had nucleic acid contamination.

Figure 3.1 shows, that the first three samples and sample 9 shows desired RNA extraction without contamination or degradation. Sample 5 shows little RNA has been extracted and instead DNA has contaminated the sample. Samples 4, 6, 7 and 8 show degraded RNA samples. Samples 10, 11, 12 are three different dH_2O samples that show contamination, dH_2O was tested before use in PCR. If the dH_2O result showed contamination the dH_2O was not used. Possible causes were contamination with primers from PCR reactions.

To ensure the PCR results were valid the PCR amplicon and melt curve was assessed. A melt curve was used to assess if the PCR was produced a single product that melted at an expected temperature.

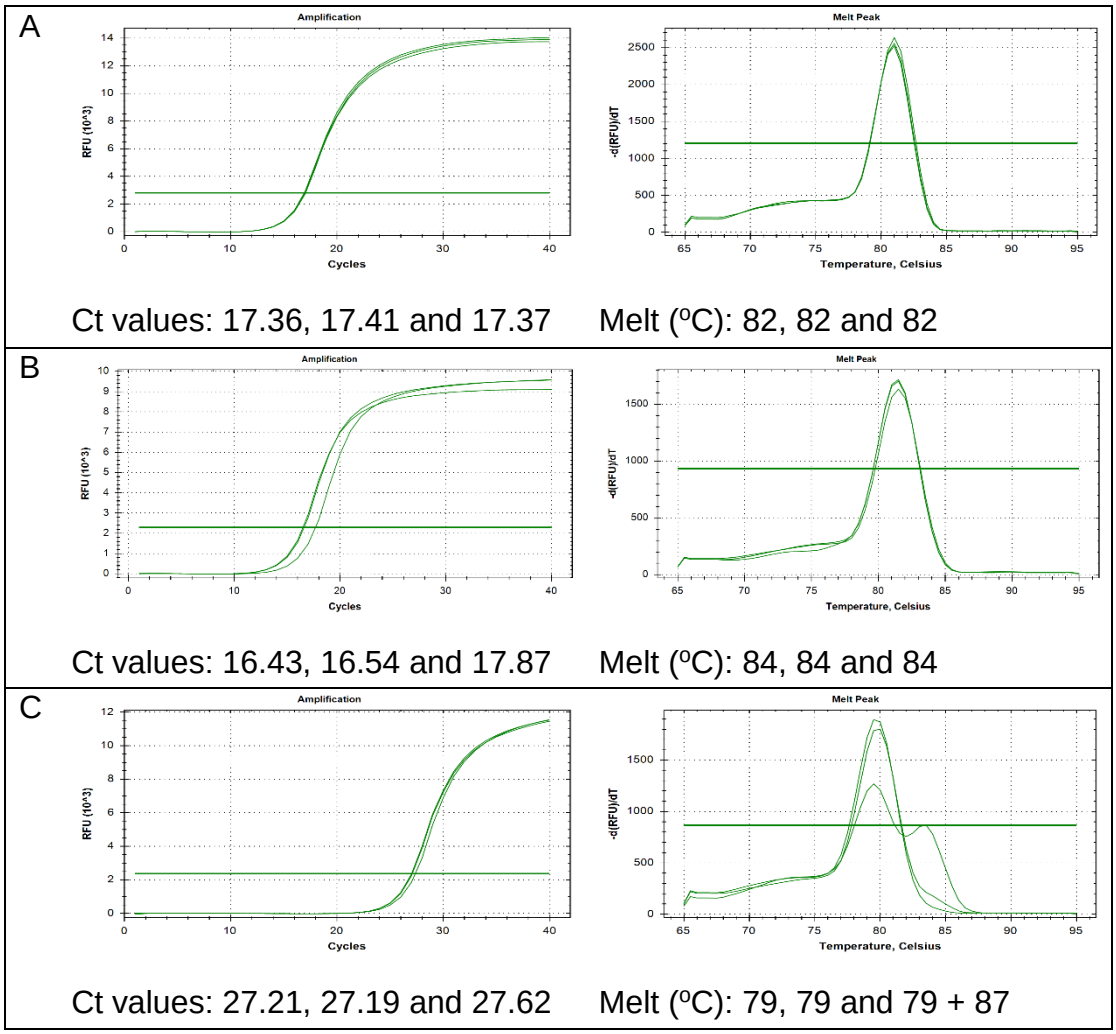

Figure 3.2: Quality control measures undertaken during PCR analysis. Panel A, shows an ideal PCR amplicon plot and melt curve; Panel B, shows technical replicates with a difference in CT value >0.5 and therefore cannot be used. Panel C, shows a desirable PCR amplicon plot with Ct values that are <0.5 cycles apart, however there were multiple products in a replicate and therefore could not be used.

When the PCR was complete the Ct value and melt curve was assess. Figure 3.2 shows three different PCR reactions,

Panel A, shows a desired PCR amplification plot where all three replicates with a Ct value <0.5 cycles and the respective melt peaks showing a single peak, therefore, a single product was synthesised during PCR.

Panel B, the melt peak in B shows a single product has been produced however the amplification plot shows an anomalous amplification plot. One out of the three technical replicates were outside of the exclusion criteria a Ct value <0.5 cycles between repeats. The lower Ct value, may be due incorrect cDNA or primer concentration in the PCR mix. The melt curve in panel B shows the same size PCR amplicon was produced.

Panel C, shows a desirable amplification plot but shows an anomalous melt peak. The double peak shows there are two products formed in the reaction most likely due to exogenous DNA or primer dimers. For both B and C, if the n number was >3 the anomalous result was discounted and the results was still used with an N of 2. If the n number was <3 the anomalous result could not be discounted and the PCR was deemed invalid and was repeated.

For this experiment HepG2 cells expressing pCMV-ve plasmids was used as a control and the PCR reaction had an N of 3. The CFX Manager software 3.1 produced the mean, Ct value and normalised gene expression (ΔΔCt). The software was used to assess if there was a 95 % confidence interval if so the results were deemed valid. The graphs were produced in GraphPad Prism 7.0.2. The statistical analysis was completed on the data imported to GraphPad, a two-tailed unpaired t-test was used to distinguish if there was any significant difference in expression.

3.1.3 Nomenclature used in experiments between occludin knockdown and overexpressing HepG2 cells.

These cell lines were used as test variables in investigations into altered occludin expression and the effect it has during HCC progression. HepG2 control had both a pCMV-ve expression plasmid to ensure a direct comparison between test and control could be made. Each model cell line was assigned a name which listed in Table 3.1.

	Altered gene expression	Nomenclature
HepG2	pCMV-ve	$HepG2^{Control}$
HepG2	OCLN+	$HepG2^{OCLN+}$
HepG2	shOCLN	$HepG2^{shOCLN}$

Table 3.1: Cell line and nomenclature for cell lines used in further investigations. OCLN+ HepG2 cells were lentivirally transduced with pLenti-OCLN-C-Myc-DDK-IRES-Puro and over expressed occludin. shOCLN HepG2 cells were lentivirally transduced with four shRNA plasmids to knockdown occludin mRNA.

$HepG2^{OCLN+}$ cells had a stable knock-in of occludin overexpression. As seen in Bouchagier et al. 2014, study into tight junction expression in HCC. Upregulation of occludin presented with a 2-fold increase of survival and disease free rates. Here occludin mRNA is overexpressed 4.23-fold higher than $HepG2^{Control}$. This is to try and allude to why increased occludin expression is coupled with better patient outcomes. Investigations by Orbán et al. 2008, show that occludin is downregulated in during HCC in the cancerous growth and surrounding field. This may be explained by down regulation of occludin to stop superinfection of HCV (Liu et al. 2009). To assess the effect this on hepatocytes a $HepG2^{shOCLN}$ model cell line was made with a stable knock down of occludin expression. Occludin mRNA expression was knocked down 4.23-fold.

3.1.4 Quantification of differential occludin expression in HepG2 cells.

HepG2 with pCMV-ve was used as a control to quantify differential expression of occludin in HepG2 cells with the use of occludin pLenti overexpression and shRNA silencing vectors.

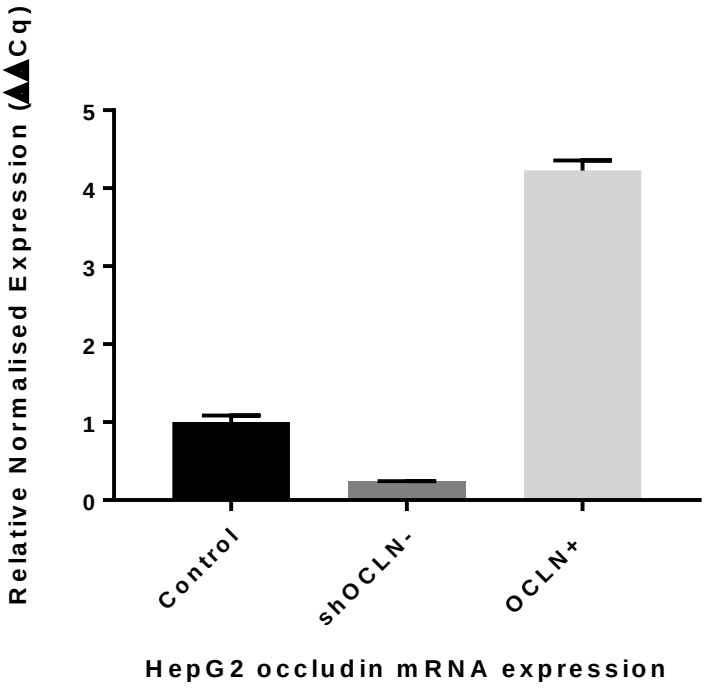

Figure 3.3: RT-PCR analysis to assess if HepG2 cells had been successfully transformed to HepG2 cells to knock-in and silence occludin. The mRNA data shows that occludin was overexpressed 4.23-fold and silence 4.23-fold compared to the HepG2 control.

As shown in, Figure 3.3, differential expression of occludin was confirmed at mRNA level via PCR normalised against GAPDH. Occludin expression was knocked down to 0.23-fold in shRNA occludin cells, P value 0.0124. HepG2 cells expressing occludin pLenti plasmid increased occludin mRNA expression 4.23-fold P-value 0.0023.

To confirm differential occludin expression Western blot analysis was performed on protein extracted from the same cell lysate from the mRNA expression experiments.

Western blot confirmed mRNA expression analysis and proved there was differential occludin expression in HepG2 cells, shown in Figure 3.4. The expected size of occludin is 60-65 kDa.

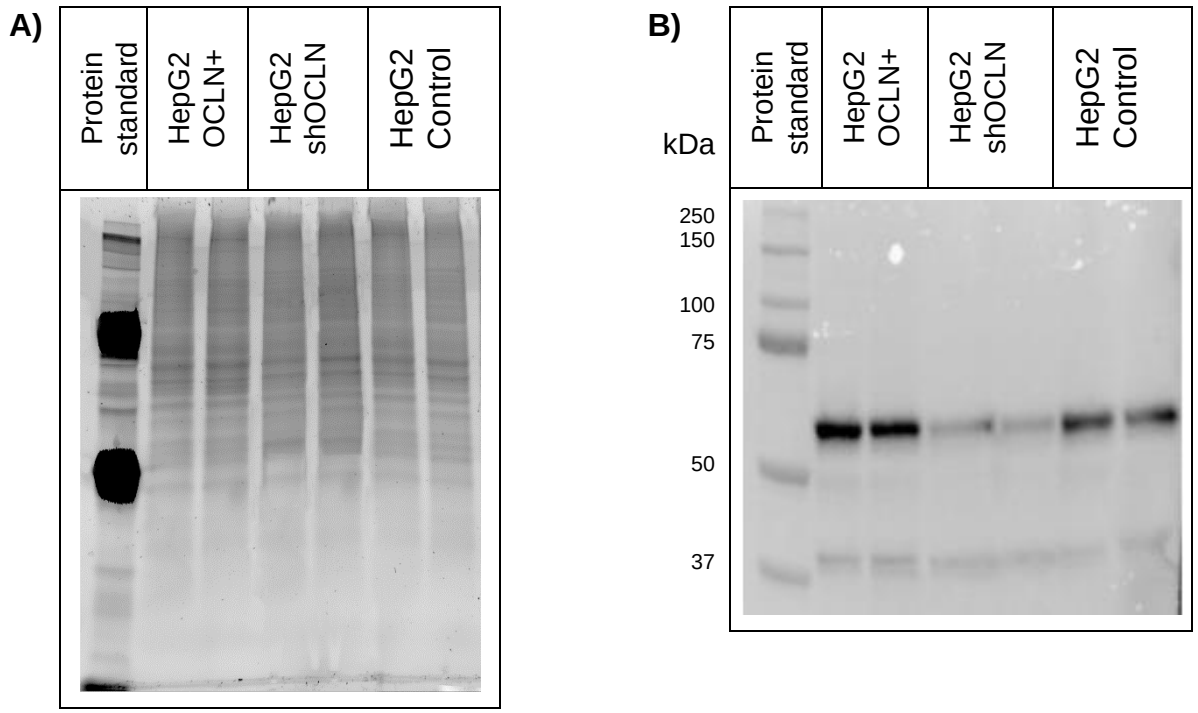

Figure 3.4: A. Total lane protein concentration assessed through fluorescence of tryptophan amino acids, after 5 minutes UV activation. B: Resultant Western blot from gel A, lane 1 is Bio-Rad dual colour plus protein standards; lanes 2 and 3 HepG2 cells overexpressing occludin; lanes 4 and 5, HepG2 cells with silenced occludin expression; lanes 6 and 7, HepG2 control cells. Lanes 2 and 3 show increased expression of occludin while lanes 4 and 5 show successful silencing of occludin in HepG2 cells.

Figure 3.4 A. shows, equal total lane protein between the three samples, HepG2 control, occludin overexpression and knockdown of occludin cells. There was equal concentration of protein loaded into each well, no protein degradation and a range of large to small proteins.

Figure 3.4, shows positive occludin bands at the expected 60-65 kDa size. HepG2^{shOCLN} protein, lanes 4 and 5, show a fainter band at the expected size of occludin, 60-65 kDa, compared to HepG2^{Control}. This proved that occludin successfully knocked down and non-specific antibody binding as the bands travelled the same distance through the SDS-PAGE. The lanes with HepG2^{OCLN+} cell protein, 2 and 3 has a darker band for occludin compared to HepG2^{Control}, lanes 4 and 5. This proved occludin was successfully overexpressed in HepG2^{OCLN+} cells.

3.2 Determining the expression of adhesion molecules in cells with altered tight junction associated gene expression *in vitro*.

Gene expression analysis gives an insight into how different disease states affect the disease pathophysiology. These insights can help identify potential targets for reducing disease progression or aid in accurately assessing how the disease will progress. The differences found in cell migration, invasion and cell polarity with differential tight junction associated protein expression may be found in gene analysis. Therefore, in the investigation PCR was used to analyse genes related to cell adhesion and migration.

All cell lines described in Table 3-11 were cultured 48 hours before investigations into gene expression.

Statistical analysis

The PCR used a technical replicate and n number of 3. The CFX Manager software automatically produces the mean CT, normalised gene expression (ΔΔCt), standard deviation. The software was used to see if there was a 95 % confidence interval if so the results were deemed valid. Graphs were produced in GraphPad Prism 7.0.2. To test for significant expression changes between all variables a one-way analysis of variance with multiple comparisons was used. To correct for the use multiple comparisons Dunnett's statistical hypothesis was used, all statistical analysis was calculated using GraphPad Prism 7.0.2.

3.2.1 Quantification of changes in adhesion associated molecules with differential expression of occludin in HepG2 cells.

The data represented in Figure 3.5 shows, the mRNA expression of genes associated with cellular adhesion. The expression of the cellular adhesion molecule

was tested in HepG2^{Control}, HepG2^{OCLN+} and HepG2^{shOCLN} cell lines. Each PCR reaction was assessed any targets with abnormalities, unreliable technical replicates were not included.

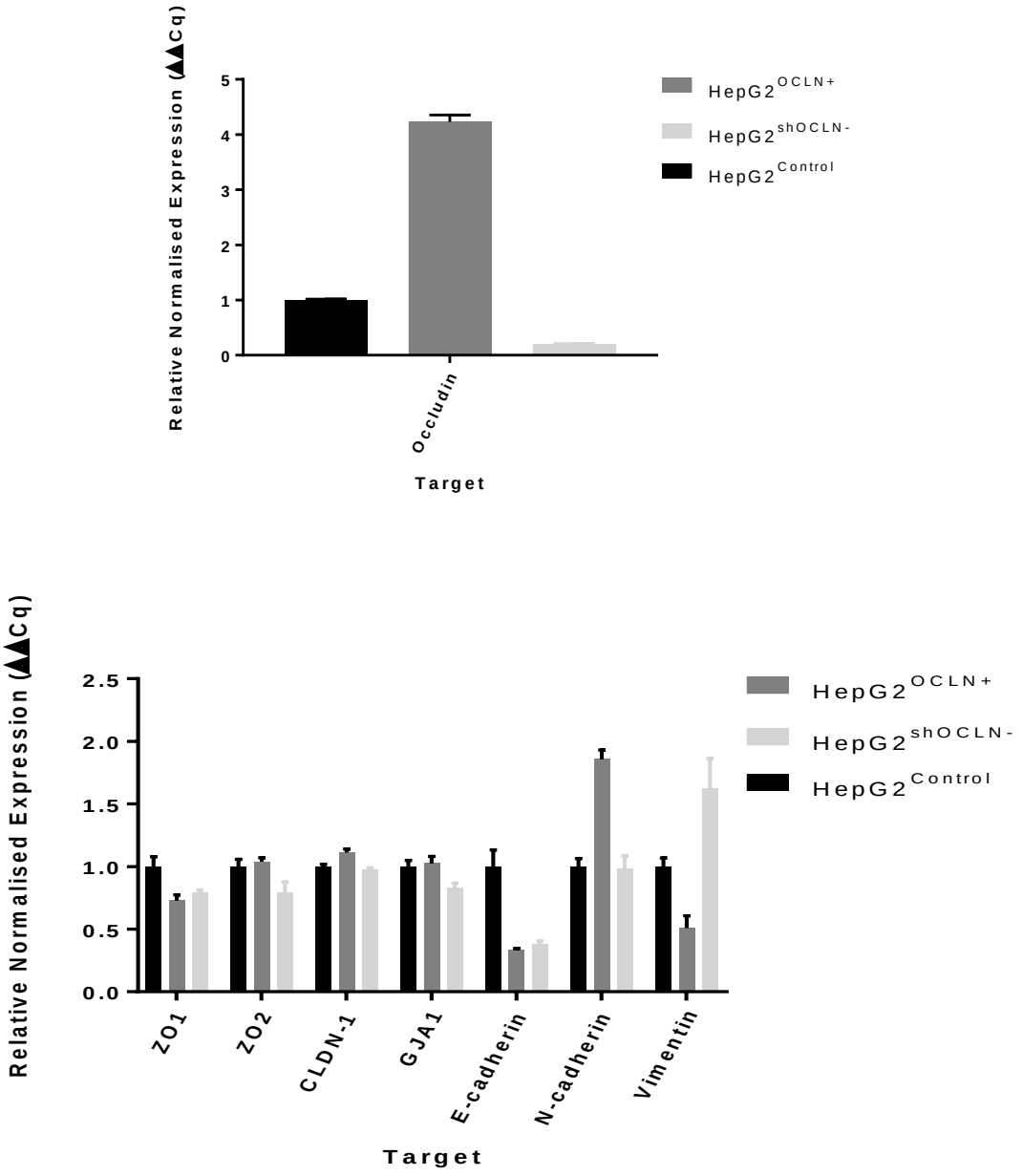

Figure 3.5: PCR analysis of adhesion molecules for HepG2 cells with differential occludin expression. RT-PCR quantified the relative expression of adhesion molecules after 48 hours culture in HepG2 cells with differential occludin expression. HepG2^{shOCLN} cells had decreased E-cadherin and increased vimentin expression, classically shown in EMT. Plotted here are mean and S.E.M values. A. shows occludin mRNA expression on a different graph due to the size of the axis.

As seen in Figure 3.5, HepG2^{OCLN} cells show an increase of 4.65-fold occludin expression, P value 0.0002. HepG2 cells with knocked down occludin expression, HepG2^{shOCLN}, showed a decrease to 0.13-fold of occludin mRNA expression, P value 0.0029.

Compared to HepG2^{Control}, HepG2^{OCLN+} cells had no significant change in mRNA expression for ZO1 0.73-fold expression P value 0.1065, ZO2 1.04-fold expression P value 0.9421, CLDN-1 1.11-fold expression P value 0.6245 and GJA1 1.02-fold expression P value 0.9785.

Compared to HepG2^{Control}, HepG2^{shOCLN} cells had no significant change in mRNA expression for ZO1 0.79-fold expression P value 0.2419, ZO2 0.79-fold expression P value 0.24, CLDN-1 0.97-fold expression P value 0.97, GJA1 0.82-fold expression P value 0.36 and N-cadherin 0.98-fold expression P value 0.98.

HepG2^{OCLN+} and HepG2^{shOCLN} cells downregulate E-cadherin expression to 0.33 and 0.37-fold expression P-valued 0.0002 and 0.0004 respectively. The only other significant differences between HepG2^{OCLN+} and HepG2^{shOCLN} cells was in the expression of N-cadherin, vimentin.

HepG2^{OCLN+} cells upregulate N-cadherin 1.85-fold expression while down regulating vimentin expression 2-fold P values 0.0001 and 0.0034 respectively. Conversely HepG2^{shOCLN} increases vimentin expression by 1.62-fold P-value 0.0034.

3.3.1 Migration rates of HepG2 cells with differential expression of occludin.

Differential expression of occludin alters E-cadherin, N-cadherin. An increase in vimentin mRNA expression and a decrease in E-cadherin mRNA expression is marker for the loss of epithelial polarity.

HepG2 cells were cultured in a six-well plate containing Ibidi 2 well silicone inserts with a defined cell-free gap at a concentration of $4x10^5$ cells per well with a N=6. After an initial 24-hour incubation period in a humidified chamber at 37^{o}C with 5 % CO_2, the inserts were removed with sterile forceps, 2ml fresh DMEM was added and time 0 images were taken. For the following 72 hours, the cells were maintained at 37^{o}C with 5 % CO_2. Every 24 hours the cell migration across the cell-free gap was monitored using the Microtec MDC-C1.3F microscope camera with a Nikon inverted microscope using a 4X objective.

Data displayed in Figure 3.6 shows, $HepG2^{Control}$ as the control with $HepG2^{OCLN+}$ and $HepG2^{shOCLN}$ as test variables. An increase in cell migration is seen if there is a decreased amount of cell-free gap left.

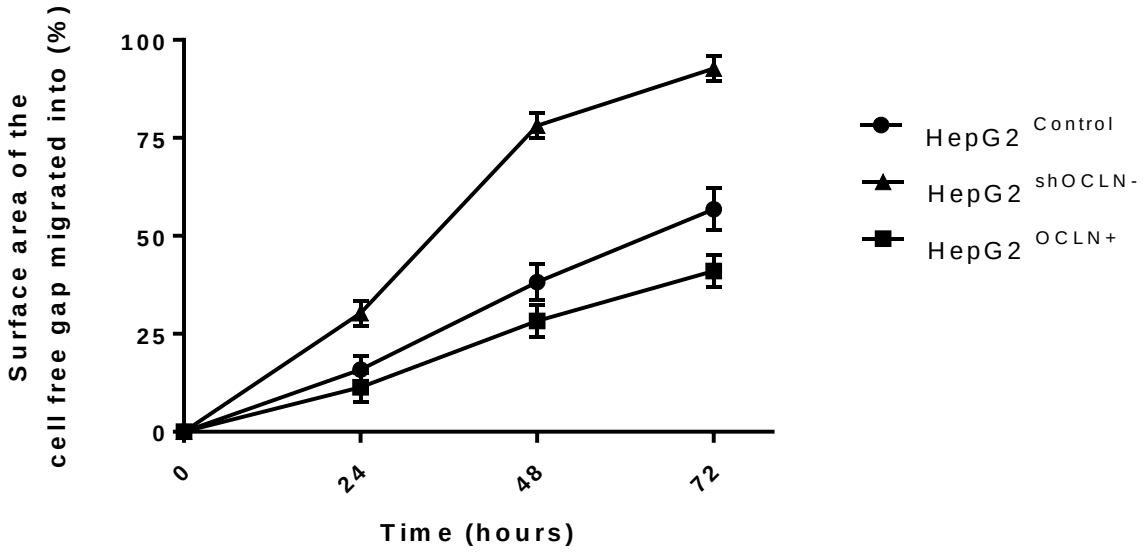

Figure 3.6: HepG2 rate of migration across a cell-free gap with differential occludin expression. Cells were cultured in Ibidi migration assay inserts for 24 hours prior to the first image being taken at time 0 hours. ImageJ was used to calculate the size of the cell free gap at time 0 hours, the time points how far in pixels the cells migrated into the cells free gap. HepG2^{shOCLN} cells have a much higher rate of migration than HepG2^{control} and HepG2^{OCLN+} cells.

HepG2^{Control} migrated into the cell-free gap at a linear rate, after 72 hours the cells had migrated into 56.82 % of the cell-free gap. HepG2^{OCLN+} cells also migrated into the cell-free gap at a linear rate, however slightly less than the control. Overall the HepG2^{OCLN+} cells migrated into 41.80 % of the cell-free gap, 15.02 % less than the control HepG2^{Control} with a P value 0.0189. HepG2^{shOCLN} showed much higher levels of migration after 48 hours, 78.14 % of the cell-free gap had closed. After 72 hours HepG2^{shOCLN} cells had migrated 92.74 % of the cell-free gap, this was 1.63 and 2.22 times faster than HepG2^{Control} HepG2^{OCLN+} respectively, P-value >000.1. This data shows that occludin expression influences migration in HepG2 cells, occludin overexpression can reduce motility whereas occludin silencing increases HepG2 cell motility.

3.4 Determining the rate of HepG2 rate of invasion in a 3D ECM with altered occludin *in vitro.*

Assays such as wound healing assays along a 2D surface are a measure of cell motility However, it does not give any representation if cells can invade. The ability for a cell to invade through the extracellular matrix is required during invasion. The PCR assay and motility assays show differential occludin expression had different outcomes in motility. The invasion assay was used to asses if the differential expression of occludin also had different outcomes concerning cell invasion. EMT and cell invasion through the basal laminar into the ECM are processes that occur with the progression of HCC; this gives HCC its low prognosis at later cancer stages (Dhir et al. 2016).

Occludin overexpressing HCC tumours are associated with a better prognosis and reduced infiltration of the Glisson's capsule (Bouchagier et al. 2014). To understand if this was directly linked to occludin expression, cell invasion experiments through an artificial ECM was completed.

The experiment was completed according to 2.2.8 cell invasion assay and incubated at 5 % CO_2 without disturbing the plate. Cell invasion was monitored using the Microtec MDC-C1.3F microscope camera with an Olympus inverted microscope with a 4X objective after the 72 hours.

Statistical analysis

The spheroid invasion data was processed in Excel, the mean, standard deviation and standard error of the mean were calculated. The mean of the control was set to

1.000 and all test variables were normalised against the control. The mean, standard error of the mean and N number was imported into GraphPad Prism 7.0.2, the graphs and the one-way analysis of variance were produced using the software.

3.4.1 Invasion rates and spheroid morphology of HepG2 cells with differential expression of occludin.

Data presented in Figure 3.7, had HepG2^{Control} as the control with HepG2^{OCLN+} and HepG2^{shOCLN} as test variables. An increase in spheroid diameter was correlated with increased invasion of cells into the matrix. HepG2^{Control} spheroid diameter was assessed, the mean diameter size was set to 1. The change in HepG2^{OCLN+} or HepG2^{scOCLN} spheroid size was compared to HepG2^{Control}. Spheroid size was calculated following 2.2.8.

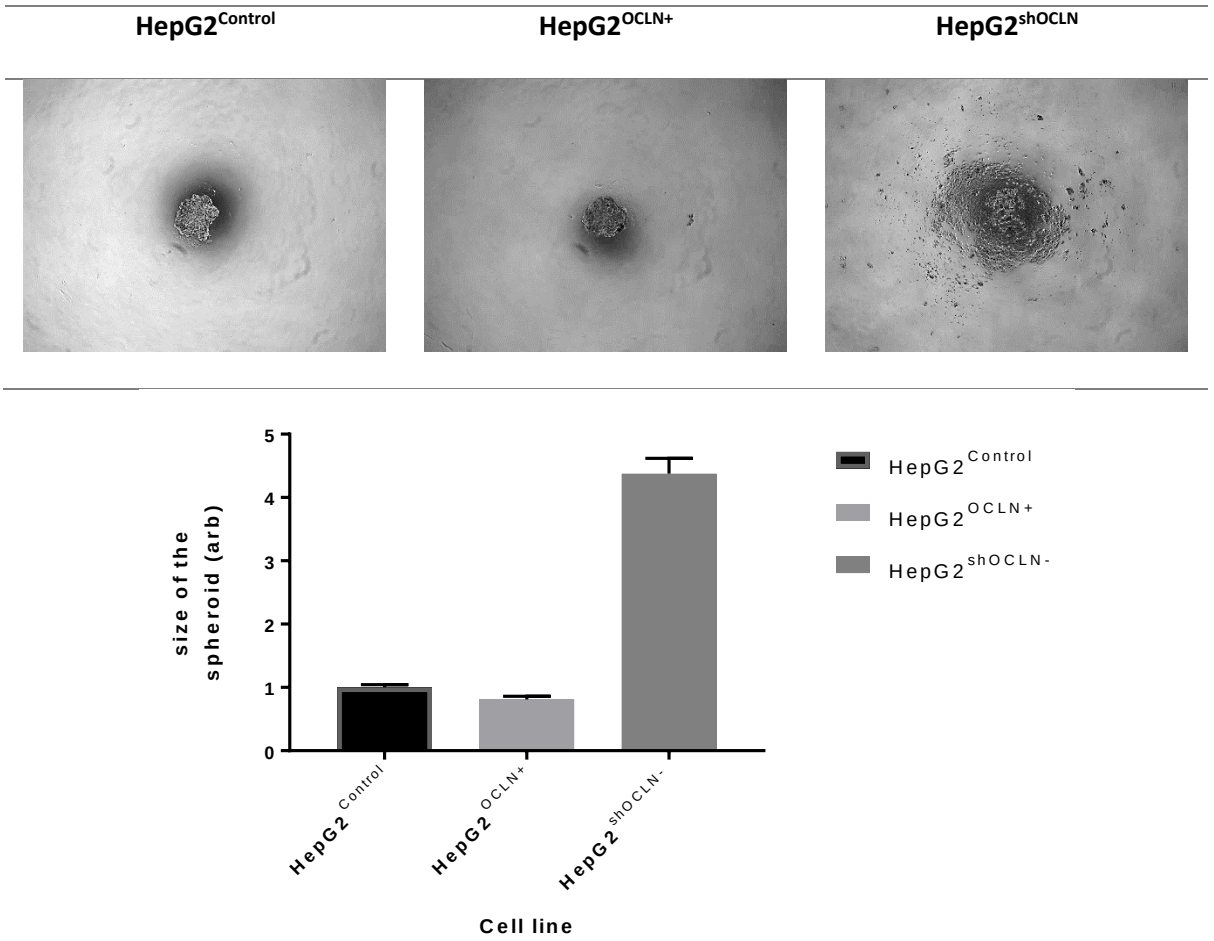

Figure 3.7: HepG2 invasiveness from spheroid into an ECM with differential occludin expression after 72 hours. A, shows a typical spheroid produced by each cell line in this investigation. ImageJ was used to calculate the diameter in pixels, the size of the spheroid was compared to HepG2Control. HepG2^{shOCLN} had lost much of its core spheroid unlike HepG2^{Control} and HepG2^{OCLN+}.

As displayed in Figure 3.7, HepG2^{OCLN+} cells maintained a spheroid shape and did not invade into the extracellular matrix. HepG2^{OCLN+} cells formed the smallest spheroid size; however, it was not significantly smaller than HepG2^{Control}, P value 0.9977. HepG2^{shOCLN} cells did not mention a single spheroid, after 72 hours, the cells had migrated into the matrix. The HepG2^{shOCLN} spheroid was 4.3-fold larger than the control, P value <0.001.

3.5 Determining if the altered expression of tight junction associated proteins affect cell polarity.

Epithelial cell polarity in hepatocytes as they form layer between sinusoidal blood and bile canaliculi. During cancer progression, apical-basal polarisation is lost, and cells generate anterior-posterior polarity. This allows the cells to have directional motility. The loss of functional tight junctions, resulting in the loss of epithelial polarity is seen in the development of HCC. The PCR screen and 2D/3D invasion assays suggest a loss of polarity in HepG2^{shOCLN} cells and maintenance of polarity in HepG2^{OCLN+} cells.

3.5.1 Bile canaliculi staining on HepG2 cells with altered tight junction associated proteins to assess whether cell polarity is maintained or lost.

HepG2 cells were grown on sterilised glass slides inside a 24 well plate at a concentration of $4x10^4$ cells/well. Cells were left for 96 hours to allow them to polarise then fixed in 4 % paraformaldehyde. The fixed cells and a primary antibody against MRP2 was added. MRP2 is a protein that is recruited to the bile canaliculi when liver cells are polarised. A secondary antibody with a GFP tag was used to locate the MRP2 primary antibody. Bile canaliculi stained green by targeting MRP2 and was counted in 5 fields of view under a fluorescent microscope at 20X magnification. This number was compared to the number of DAPI stained nuclei to give a ratio of cell/bile canaliculi. The images were overlaid in ImageJ and the ratio was taken from the resultant image shown in Figure 3.8. This was normalised against the control, the higher the ratio the more polarised the cells were.

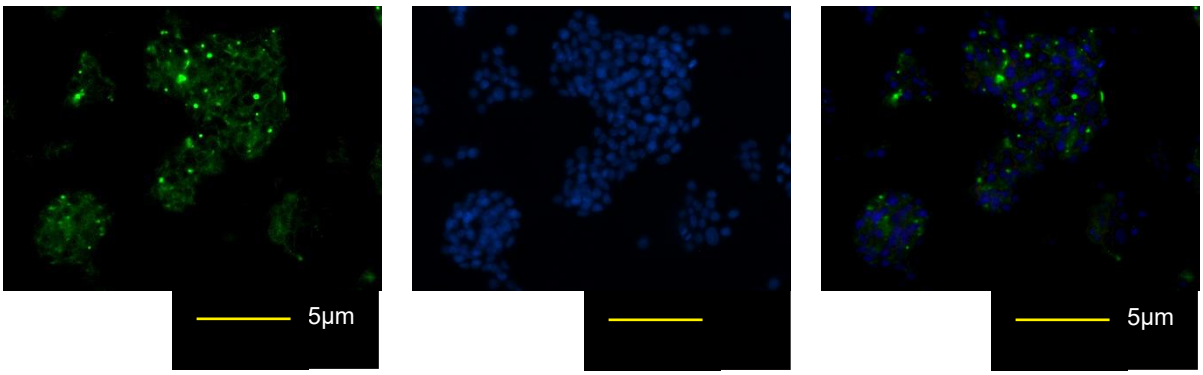

Figure 3.8: Single and composite image of bile canaliculi staining in HepG2 cells to DAPI nuclear stain to produce a ratio of bile canaliculi to nuclei ratio. MRP2 antibodies were used to assess the location and frequency of the TJs. MRP2 green and DAPI stain blue.

HepG2^{Control} was used as the control and HepG2^{OCLN+} and HepG2^{shOCLN} was used as the test variables. The higher the bile canaliculi/cell ratio, the more polarised the cells were.

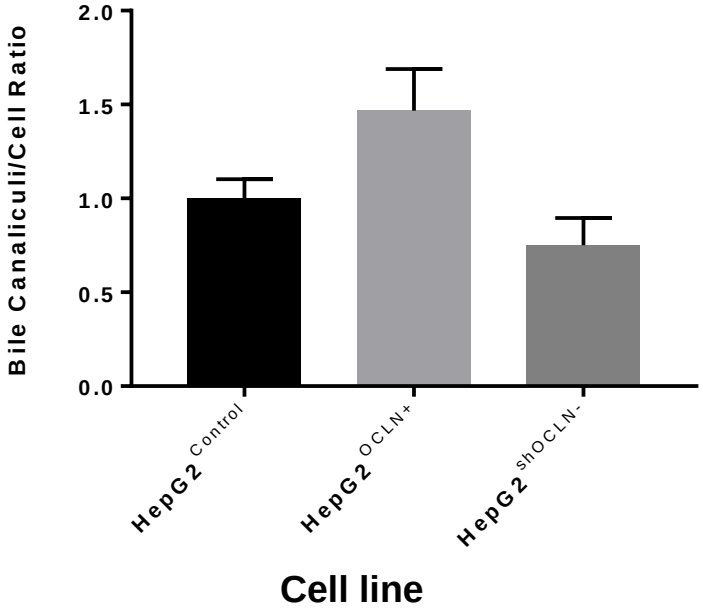

Figure 3.9: Bile canaliculi to cell ratio as a measure of cell polarity *in vitro* with differential expression of occludin. MRP2 recruit to the tight junction, therefore, a ratio of positive MRP2 to bile canaliculi can be calculated. Although HepG2^{OCLN+} have a higher MRP2 to bile canaliculi ratio there was no significant difference P value >0.05.

Figure 3.9 shows, HepG2^{shOCLN} cells had a decreased BC to nuclei ratio compared to the HepG2^{Control}, however, it was not significant, P value >0.05. HepG2^{OCLN+} cells increase BC to nuclei ratio 1.5-fold compared to HepG2^{control} showing higher MRP2 staining but this was not significant, P value 0.090. The difference in MRP2 positive areas is correlated to areas of higher cell density, shown in Figure 3.10.

Following the same procedure the BC:nuclei ratio was assessed in areas of low and high cell density were taken and results were formulated into Figure 3.10.

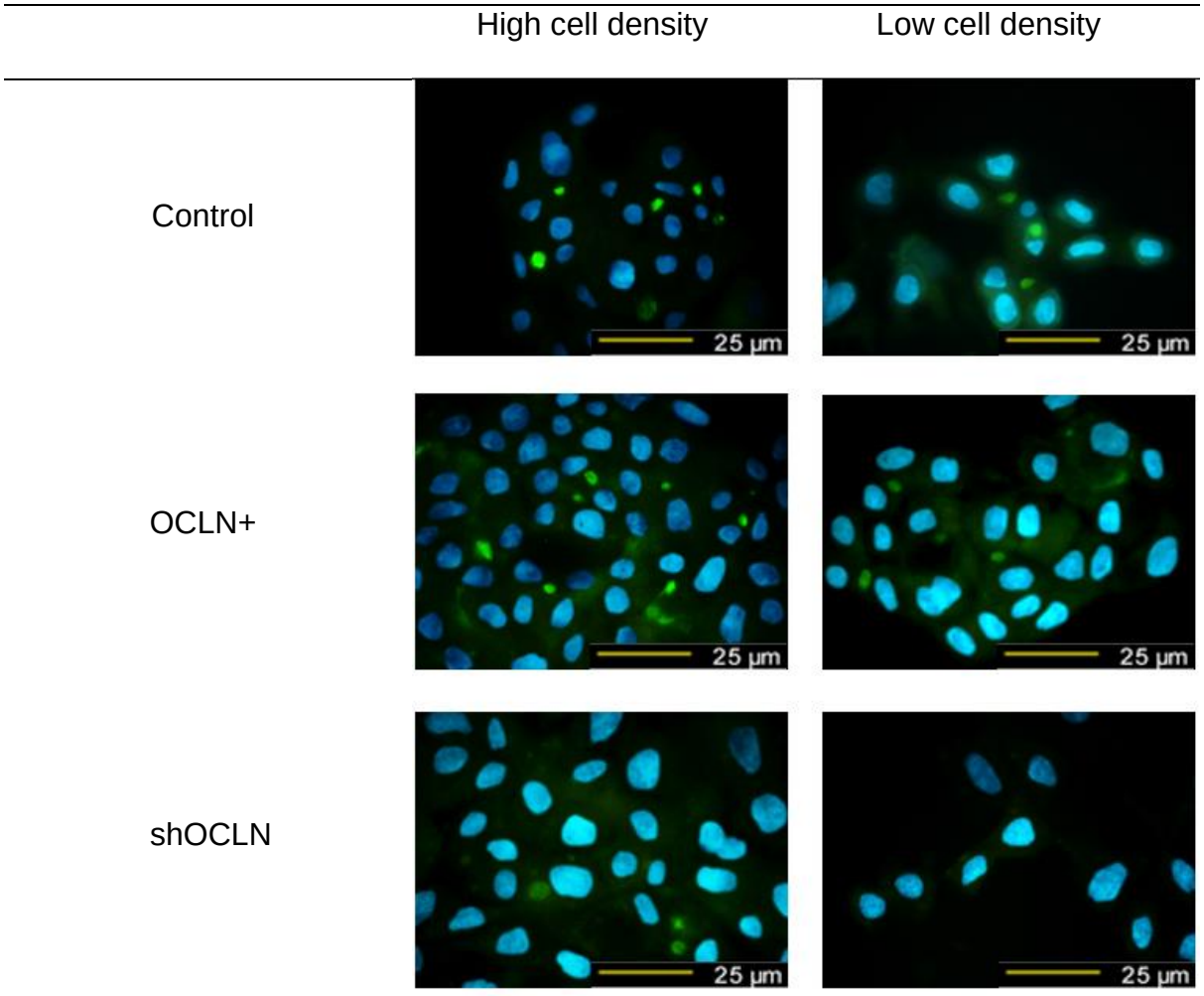

Figure 3.10: BC location concerning cell density with differential occludin expression. MRP2 antibodies were used to assess the location and frequency of the TJs. Areas of higher cell density show higher have an increase BC to nuclei ratio. MRP2 green and DAPI nuclei stain blue. Areas that had ≤6 nuclei/ 40 µm were considered as areas of low cell density.

HepG2^{Control} and HepG2^{OCLN+} cells show the same BC to nuclei ratio in areas of high and low cell density, shown in Figure 3.10. HepG2^{shOCLN} cells, did not significantly decrease the BC to nuclei compared to HepG2^{Control}. However, in areas of low cell density there is no staining of MRP2. HepG2^{Control} and HepG2^{OCLN+} had fewer areas on six well plate that had cells growing in low cell density compared to HepG2^{shOCLN}.

3.6 Investigation into the relationship between occludin, ZO1 and ZO2.

Progression of HCC is associated with the downregulation of ZO1 or loss of ZO2 expression. Differential expression of occludin experiments show that occludin does not have any regulation of ZO1 or ZO2 mRNA or protein expression.

As shown previously in Figure 3.5, knock down of occludin expression did not significantly downregulate ZO1 or ZO2 expression, shown again in, Figure 3.11.

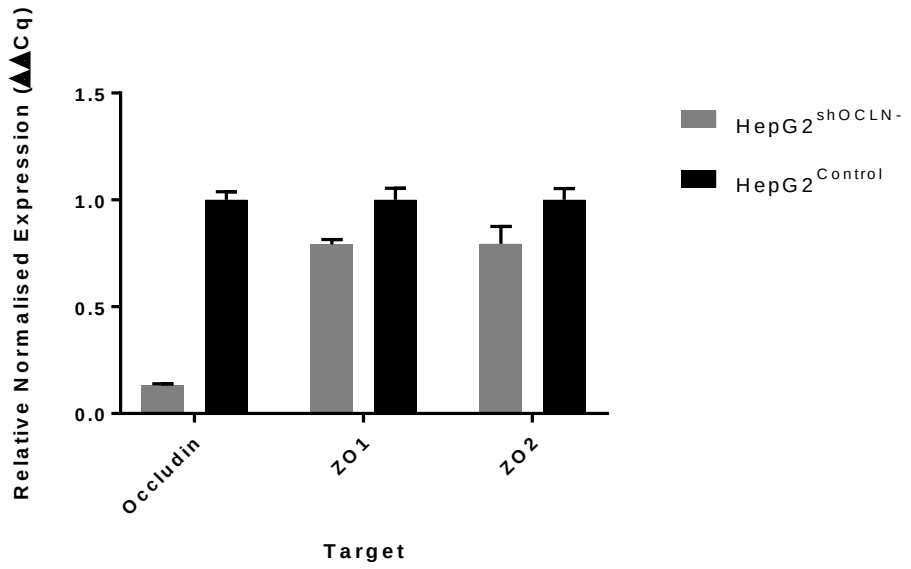

Figure 3.11: RT-PCR quantified the relative expression of ZO1 and ZO2 when occludin was knocked down in HepG2 cells. PCR analysis shows knockdown of occludin mRNA does not downregulate the expression of the scaffold proteins ZO1 or ZO2 in HepG2 cells. HepG2^{shOCLN} cells show successful knockdown of occludin.

The loss of occludin expression is also associated with the loss of zona occludens proteins (Orbán et al. 2008). However, there is no significant difference between the loss of occludin expression and the loss of ZO1 and ZO2 expression to 0.21-fold expression and 0.21-fold expression and decrease P values 0.2419 and 0.2485. To assess whether ZO1 or ZO2 expression regulated occludin expression or function ZO1/2 knockdown studies were completed.

3.7 Quantification and justification of ZO1 and ZO2 expression changes after knock-in and knockdown experiments in HepG2 cells.

The RNA and protein investigations were carried out following sections 2.5.7 and 2.8.3. Knockdown of ZO1 and ZO2 was accomplished with the use of siRNA, these siRNAs were a mix of four siRNAs for each target. To knockdown the gene in HepG2 cells the siRNAs were transfected into HepG2 cells using DharmaFect 4 reagent supplied by Dharmacon in accordance with, 2.4.2.

Statistical analysis and quality control.

For this experiment HepG2 cells transfected with scrambled siRNA was used as a control and the PCR reaction had an N of 3. The CFX Manager software automatically produces the mean CT, normalised gene expression (ΔΔCt). The software was used to see if there was a 95 % confidence interval. The graphs were produced in GraphPad Prism 7.0.2. The statistical analysis was completed on the data imported to GraphPad, a two-tailed unpaired t test was used to distinguish if there was any significant difference in expression.

3.7.1 Quantification of knockdown ZO1 in HepG2 cells.

HepG2 with scrambled siRNA was used as a control and HepG2 cells transfected independently with siRNAs targeting ZO1 as the test variable. Figure 3.12 shows mRNA expression of ZO1 in HepG2^{Control} and HepG2^{Control} cells that have been transfected with siRNA that targets ZO1 mRNA.

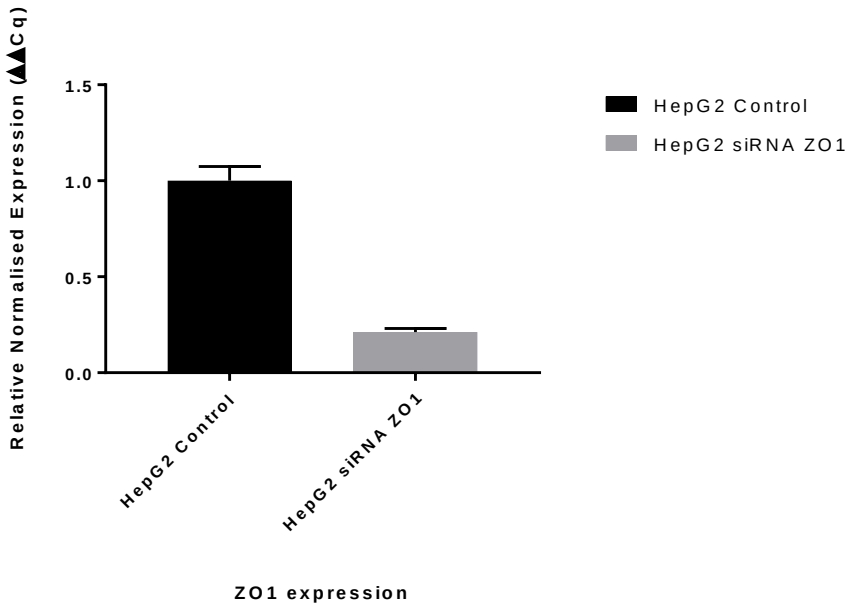

Figure 3.12: RT-PCR quantified the relative expression ZO1 mRNA after HepG2^{Control} cells were transfected with siRNA that target ZO1 mRNA. The HepG2 cells were cultured for 48 hours post ZO1 siRNA transfection. ZO1 was successfully knocked down to 4.73-fold P value <0.05.

Knockdown of ZO1 mRNA was confirmed by PCR analysis Figure 3.12, the expression of ZO1 was downregulated to 0.21-fold expression P-value 0.0093. To confirm knockdown of ZO1 Western blotting analysis was completed on protein extracted from the same cell lysates.

Western blot confirmed mRNA expression analysis and proved there was knocked down ZO1 expression in HepG2 cells, shown in Figure 3.13.

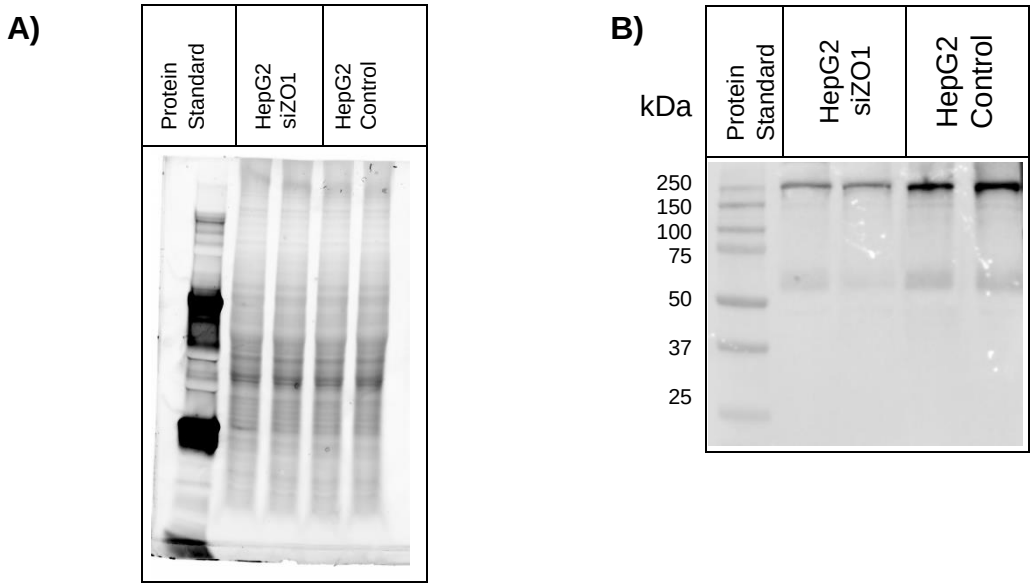

Figure 3.13: A: Total lane protein concentration assessed through fluorescence of tryptophan amino acids, after 5 minutes UV activation. B: Resultant Western blot from gel A, lane 1 is Bio-Rad dual colour plus protein standards; HepG2 cells transfected with ZO1 siRNA, lanes 2 and 3; HepG2 control lanes 4 and 5. HepG2 cells were used as a control transfected with scrambled siRNA. The test cells were HepG2 cells transfected with ZO1 siRNA reduced levels of ZO1 protein in lanes 2 and 3.

Figure 3.13 A, shows equal total lane protein between the two samples, HepG2 control and knockdown of ZO1. There was equal concentration of protein loaded into each well, no protein degradation and a range of large to small proteins.

Figure 3.13 B, shows positive ZO1 bands at ~220 kDa, HepG2 cells and lanes 4-5 show normal levels of ZO1 in HepG2 cells. Lanes 2-3 show, a decrease in ZO1 expression in HepG2 cells after transfection with ZO1 siRNA.

3.7.2 Quantification of differential ZO2 expression in HepG2 cells.

HepG2 expressing pCMV-ve transfected with scrambled siRNA was used as a control and HepG2 cells transfected independently with siRNAs targeting ZO2 as the test variable.

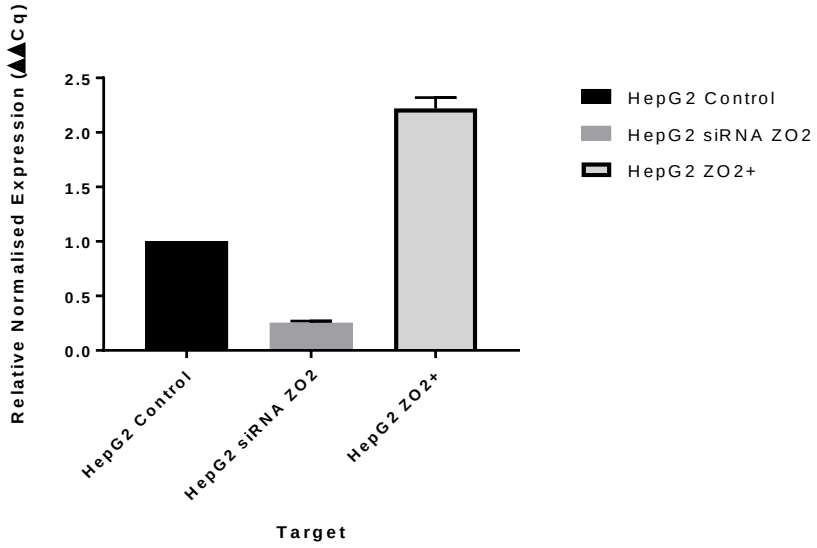

Figure 3.14: RT-PCR quantified the relative expression ZO2 mRNA after knockdown with siRNA in HepG2 cells. The cells were cultured for 48 hours post siRNA transfection. ZO1 was successfully knocked down to 3.91-fold P value <0.05. HepG2 cells with ZO2 knock in had a 2.22-fold increase in ZO2 mRNA expression.

Knockdown of ZO2 mRNA was confirmed by PCR analysis Figure 3.14, the expression of ZO2 was downregulated 0.31-fold expression P-value 0.0102. Expression of ZO2 mRNA increase in ZO2 overexpressing HepG2 cells 2.22-fold P-value 0.0075.

To confirm knockdown and overexpression of ZO2 Western blotting analysis was completed on protein extracted from the same cell lysates.

Western blot confirmed mRNA expression analysis. The blot showed that ZO2 had successfully been knocked down and over expressed at the protein level in HepG2 cells, displayed in Figure 3.15. The cells were cultured for 72 hours before lysis.

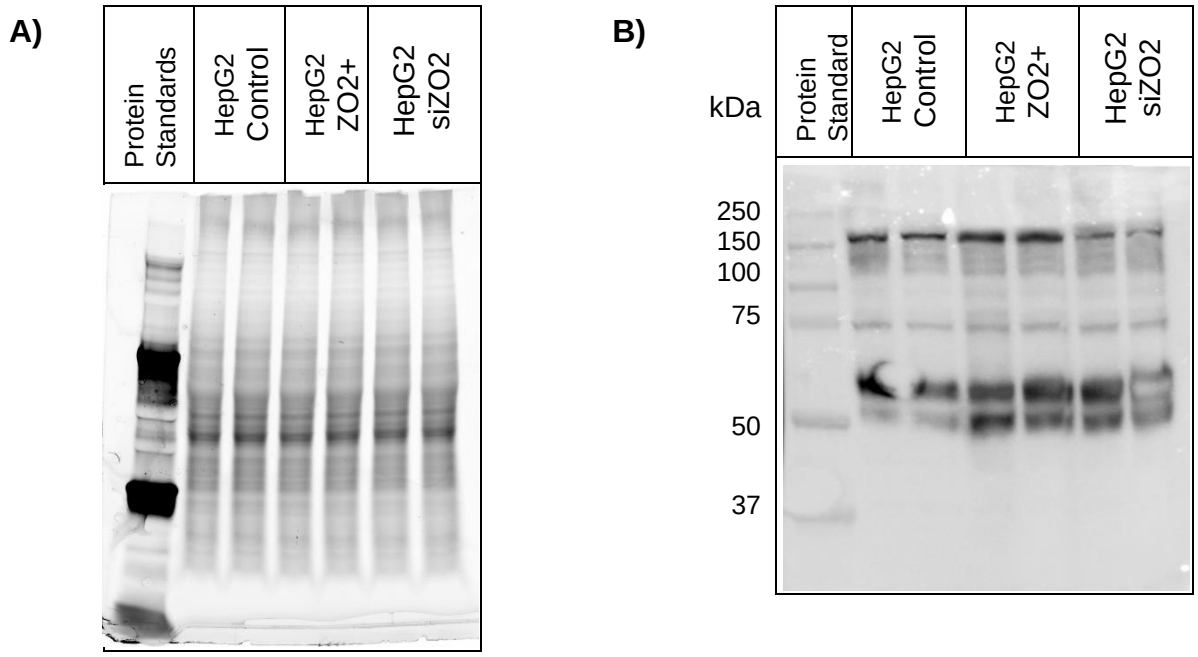

Figure 3.15: A: Total lane protein concentration assessed through fluorescence of tryptophan amino acids, after 5 minutes UV activation. B: Resultant Western blot from gel A, lane 1 is Bio-Rad dual colour plus protein standards; HepG2 control, lanes 2 and 3; HepG2 cells overexpressing ZO2, lanes 4 and 5; HepG2 cells transfected with ZO2 siRNA, lanes 6 and 7. B, shows the increased expression of ZO2 in lanes 4 and 5. Lanes 6 and 7 show ZO2 is successfully under expressed 72 hours post transfection.

Figure 3.15 A, shows equal total lane protein between the three samples, HepG2 control, overexpression of ZO2 and knockdown of ZO2. There was equal concentration of protein loaded into each well, no protein degradation and a range of large to small proteins. Figure 3.15 B, shows positive ZO2 bands at~160 kDa, HepG2 cells overexpressing ZO2, lanes 4 and 5 showed an increase in protein expression. HepG2 cells transfected with ZO2 siRNA, lanes 6 and 7, showed a decrease in ZO2 expression.

3.8 Cell lines used in further investigations.

These cell lines were used as test variables in investigations into altered TJ expression and HCC progression. HepG2 control had both a pCMV-ve expression plasmid and scrambled-ve siRNA to ensure a direct comparison between test and control could be made. Each cell line was assigned a name which is listed in Table 3.2 and is used during the analysis.

	Overexpressed	Knockdown	Nomenclature
HepG2	pCMV-ve	Scrambled-ve	$HepG2^{Control}$
HepG2	pCMV-ve	siZO1	$HepG2^{siZO1}$
HepG2	pCMV-ve	siZO2	$HepG2^{siZO2}$
HepG2	OCLN+	Scrambled-ve	$HepG2^{OCLN+}$
HepG2	OCLN+	siZO1	$HepG2^{OCLN+\ siZO1}$
HepG2	OCLN+	siZO2	$HepG2^{OCLN+\ siZO2}$
HepG2		shOCLN	$HepG2^{shOCLN}$
HepG2		shOCLN, siZO1	$HepG2^{shOCLN\ siZO1}$
HepG2		shOCLN, siZO2	$HepG2^{shOCLN\ siZO2}$
HepG2	ZO2+	Scrambled -ve	$HepG2^{ZO2+}$
HepG2	ZO2+	siZO1	$HepG2^{ZO2+\ siZO1}$
HepG2	ZO2+	shOCLN	$HepG2^{ZO2+\ shOCLN}$
HepG2	ZO2+	shOCLN, siZO1	$HepG2^{ZO2+\ shOCLN\ siZO1}$

Table 3.2: Cell line and nomenclature for use in the analysis. HepG2 cells were transformed with pCMV-ve plasmid and in knock down investigations transfected with scrambled-ve siRNA. Occludin and ZO2 overexpression was a stable transformation and were made before investigations were run. ZO1 and ZO2 knock down was only transient. Cells were cultured for 48 hours for mRNA investigations or 96 for protein investigations.

3.9 Identifying the relationship and regulation of occludin, ZO1 and ZO2 in HepG2 cells.

With HepG2^{Control} as the control for the investigation, HepG2^{OCLN+} and HepG2^{shOCLN} as test variables. The gene expression profiles associated with cellular adhesion or loss of adhesion. All amplification profiles were assessed, targets with abnormalities, unreliable technical replicates or insufficient PCR efficiency were not included.

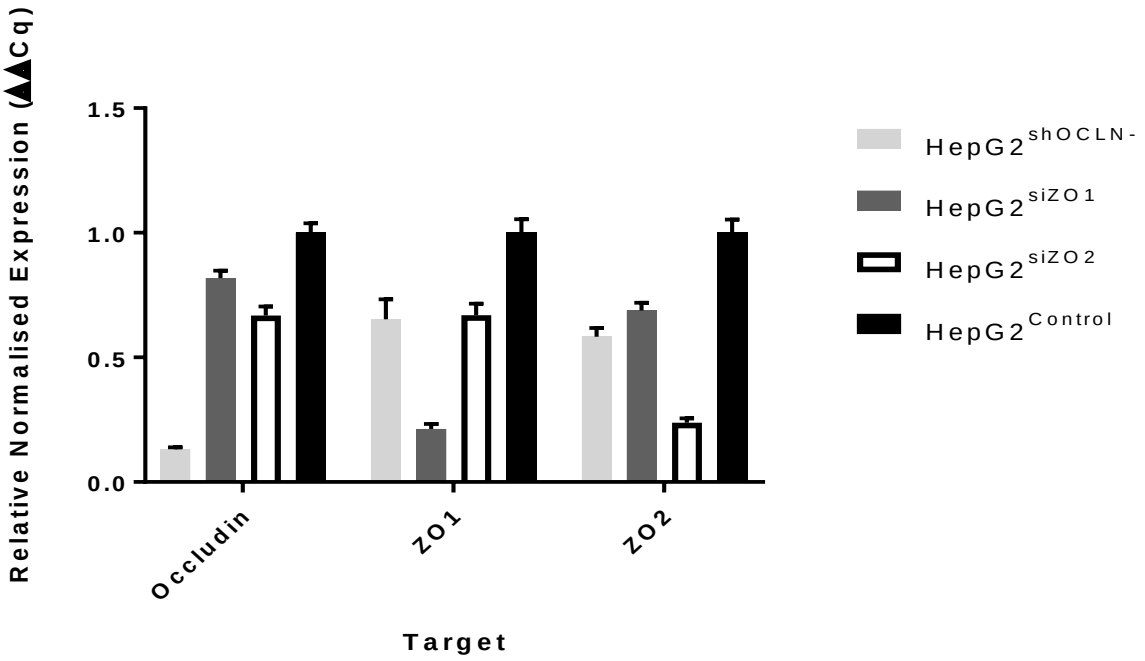

Figure 3.16: RT-PCR quantified the relative expression and relationship between the knockdown of occludin, ZO1 and ZO2 mRNA. Independent knockdown of occludin, ZO1 or ZO2 was not sufficient to knockdown the mRNA expression of the other two genes.

Knockdown of occludin, ZO1 and ZO2 was knocked down to 0.2-fold P values <0.05. The knockdown of occludin, ZO1 and ZO2 down regulates the expression of the other targets. However there is no significance, all P values >0.05. Figure 3.16 demonstrates the relationship and regulation between these three proteins is not at the mRNA level.

Occludin is also regulated by phosphorylation of Thr/Ser residues, the knockdown of ZO1 and ZO2 may be regulatory over occludin phosphorylation.

3.10 The effect of differential tight junction protein expression on the phosphorylation of the threonine and serine residues on occludin.

Occludin phosphorylation is essential for the assembly and maintenance of hepatocellular tight junctions. However, the phosphorylation of occludin is reversible and the dephosphorylation of the threonine and serine residues on occludin occurs in tight junction disassembly. The inverse is found on the tyrosine residues of occludin with an increase of phosphorylation of these residues associated with occludin tight junction disassociation. For correct occludin function it has been suggested there is probably an important ratio between phosphorylation of threonine, serine and tyrosine residues. This may help elucidate if occludin is responsible for the regulation of tight junction integrity. Moreover, the correct occludin localisation and phosphorylation has been proposed to be significant for direct occludin intracellular signalling.

3.10.1 Quantification of occludin threonine and serine phosphorylation with the differential occludin expression and the knockdown of ZO1 and ZO2 *in vitro.*

HepG2 cells were seeded at $2.5x10^5$ cells per well in a six-well plate in 2 ml complete media. The knockdown of ZO1 and ZO2 was initiated 24 hours after cell seeding, in accordance with 2.4.2. The following data used $HepG2^{Control}$ as the control with $HepG2^{OCLN+}$ and $HepG2^{shOCLN}$ as test variables. The total lane protein

gel to ensure equal protein concentration is shown in, Figure 3-17 and the resultant Western blot is displayed in Table 3.3.

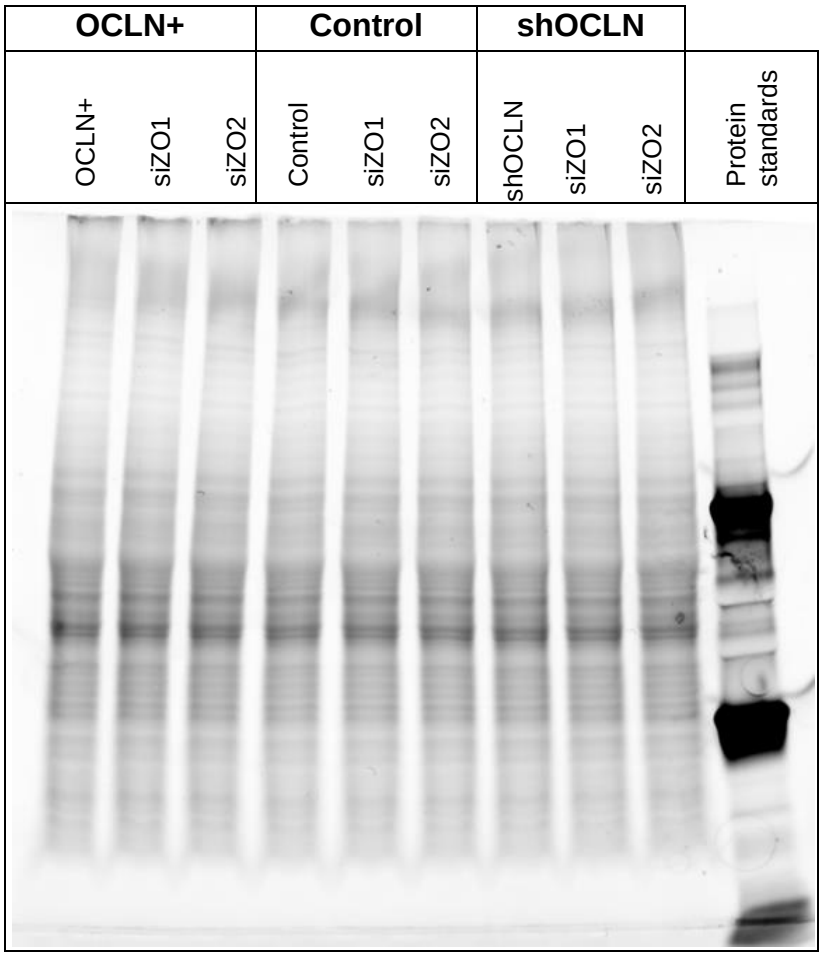

Figure 3.17: A: Total lane protein concentration assessed through fluorescence of tryptophan amino acids, after 5 minutes UV activation. The gel shows equal concentrations were loaded into each well from each cell line used. Protein samples run from lanes 1-9 $HepG2^{OCLN+}$, $HepG2^{OCLN+\ siZO1}$, $HepG2^{OCLN+\ siZO2}$, $HepG2^{Control}$, $HepG2^{siZO1}$, $HepG2^{siZO2}$, $HepG2^{shOCLN}$, $HepG2^{shOCLN\ siZO1}$, $HepG2^{shOCLN\ siZO2}$. The protein standards is in lane 10.

Figure 3.17 shows, equal concentrations of protein were loaded per well on the SDS-PAGE gel. There is no protein degradation and equal isolation of proteins at all sizes. This SDS-PAGE gel was used to blot for Table 3.3.

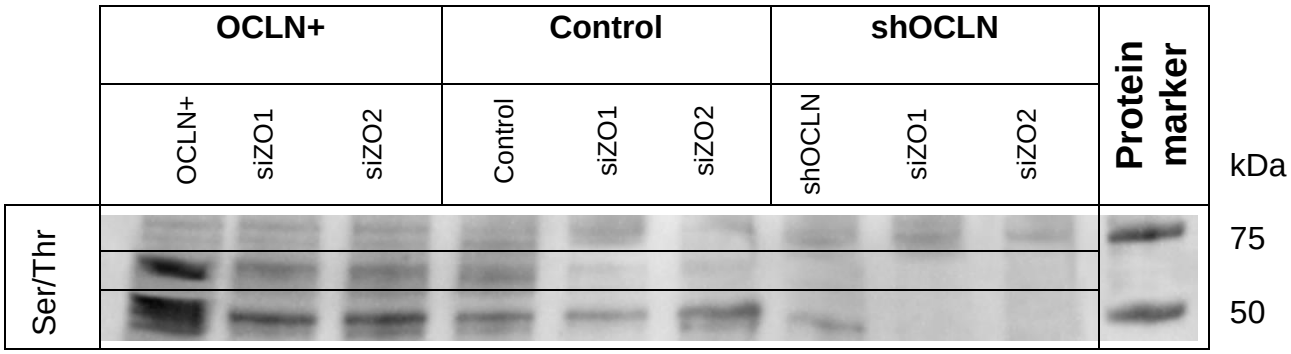

Table 3.3: Western blot for Ser/Thr phosphorylation of occludin. Phosphorylated Ser/Thr residues show a band at the correct size of 65kDa for occludin. Knockdown of ZO1 and ZO2 in HepG2^{Control} and HepG2^{shOCLN} cells show weak bands or no bands at the expected size. HepG2^{OCLN+} cells show increased phosphorylation of Ser/Thr compared to HepG2^{control}. HepG2^{OCLN+} cells with ZO1 or ZO2 knockdown still show a band at the expected size.

As shown in Table 3.3, occludin phosphorylation is altered with altered expression of ZO1 and ZO2. HepG2^{Control} were used to convey normal levels of phosphorylated Ser/Thr of occludin. When ZO1 and ZO2 was knocked down in HepG2^{Control} cells there was almost complete loss of Ser/Thr occludin phosphorylation.

Overexpression of occludin in HepG2 cells results in higher phosphorylation of occludin on Ser/Thr residues. When ZO1 or ZO2 was knocked down in HepG2^{OCLN+} cells there was a decrease in the level of occludin Ser/Thr phosphorylation. However, the levels appear similar to HepG2^{Control}.

In HepG2^{shOCLN} cells have knocked down expression of occludin, so as expected there is no phosphorylation of occludin. However, this showed that the positive bands are likely to be occludin in the other model cell lines as they have positive staining at the ≈65kDa mark.

3.11.1 Expression of markers of EMT with differential occludin expression and ZO1/2 knockdown.

Gene expression analysis of occludin, ZO1 and ZO2 showed no significant changes when a single gene was downregulated. The knockdown of ZO1 and ZO2 regulate occludin function by altering the occludin phosphorylation state. A PCR experiment analysing EMT genes ZEB2, SNAIL2 and TWIST1 was completed on all cell lines used in the phosphorylation investigation. This was done to attain whether a loss of ZO1/2 and therefore loss of occludin phosphorylation only affects cellular adhesion or it promotes a loss of the epithelial phenotype.

The gene expression was targeted to gene responsible for cellular adhesion. All PCR amplification profiles were assessed, targets with abnormalities, unreliable technical replicates or insufficient PCR was removed from analysis.

All cell lines described in Table 3.2, were cultured 48 hours before investigations into gene expression.

Statistical analysis

The PCR used a technical replicate and n number of 3. The CFX Manager software automatically produces the mean CT, normalised gene expression (ΔΔCt), standard deviation. The software was used to see if there was a 95 % confidence interval if so the results were deemed valid. Graphs were produced in GraphPad Prism 7.0.2. To test for significant expression changes between all variables a one-way analysis of variance with multiple comparisons was used. To correct for the use multiple comparisons Dunnett's statistical hypothesis was used, all statistical analysis was calculated using GraphPad Prism 7.0.2.

HepG2^{Control}, HepG2^{OCLN+} and HepG2^{shOCLN} model cell lines was used in this investigation. ZO1 and ZO2 mRNA expression was knocked down in accordance with 2.4.2. Results displayed in Figure 3.18,

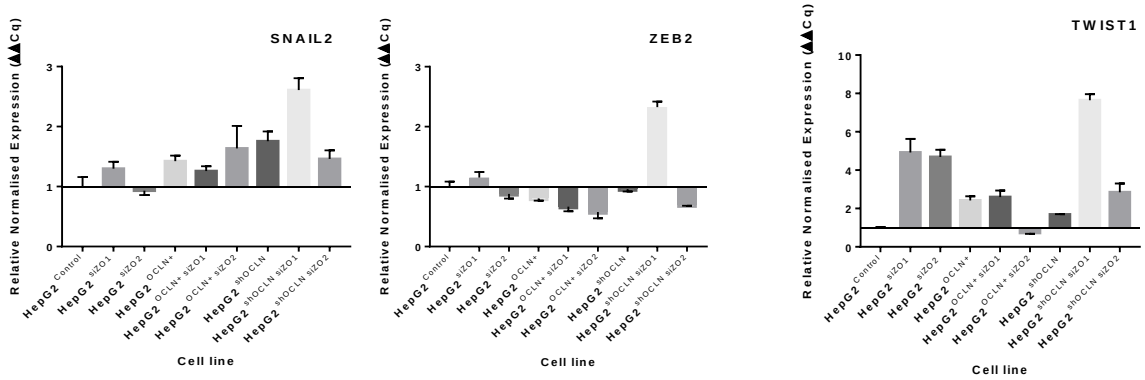

Figure 3.18: P: RT-PCR quantified the relative expression of 3 EMT genes SNAIL2, ZEB2 and TWIST1 when tight junction expression is altered. Overall HepG2$^{shOCLN\ siZO1}$ cells showed the highest increases of SNAIL2, ZEB2 and TWIST1. HepG2^{OCLN+} cells only increased the expression of TWIST1.

The expression of transcription factors SNAIL2, ZEB2 and TWIST1 are generally higher in knockdown occludin and ZO1/2 cells.

Figure 3.18 shows, SNAIL2 only has a significant increase in expression in HepG2^{shOCLN} and HepG2$^{shOCLN\ siZO1}$ cells increasing 1.75 and 2.60-fold respectively P values 0.0440 and 0.0001 respectively. There was no significant change in HepG2$^{OCLN+\ siZO1}$ 1.31-fold increase P value 0.8633 and HepG2$^{OCLN+\ siZO2}$ 1.2-fold increase P value 0.1116.

Expression of ZEB2 showed no change in expression with HepG2^{siZO1} 1.15-fold expression P value 0.6227 and HepG2^{siZO2} 0.87-fold expression P value 0.8076. Occludin overexpression did slightly decrease expression of ZEB2 but not significantly decreased to 0.8-fold but was not significant P-value of 0.3495 however knockdown of ZO1 and ZO2 in HepG2^{OCLN+} cells resulted in a down regulation of

ZEB2 expression 1.5 and 1.7-fold respectively P values 0.0334 and 0.0058. The expression of ZEB2 did not change significantly in HepG2^{shOCLN} cells, with 1.04-fold expression P value 0.9994 and HepG2$^{shOCLN\ siZO2}$ cells 0.56-fold expression, P value 0.0542. ZEB2 did show an increase in expression of 2.32-fold in HepG2$^{shOCLN\ siZO2}$ cells P-value 0.0001. This was the only significant increase of ZEB2 expression.

Knockdown of ZO1 increased ZEB2 expression 1.88-fold P-value 0.0002, combined with knockdown of occludin ZEB2 expression increase 1.98-fold P-value 0.0001, This did not occur with occludin and ZO2 knock down, there was no significant change in ZEB2 expression, P-value 0.2923.

TWIST1 expression is increased in all cell lines that knockdown ZO1 including occludin overexpression with an increase of 2.59-fold P-value 0.0318. As before with SNAIL2 knockdown occludin cell lines had the highest expression. TWIST1 expression in HepG2^{shOCLN} cells increased 1.6-fold P-value 0.0279 with ZO1 knockdown the expression of TWIST1 increased to 7.64-fold P-value 0.0001 and with ZO2 knockdown TWIST1 expression increased 2.84-fold P-value 0.0001.

All these data show a relationship between occludin and ZO1/2. The downregulation of occludin or ZO1/2 only invoked expression changes in TWIST1. When occludin and ZO1 was knocked down simultaneously it invoked the largest increases in ZEB2, SNAIL2 and TWIST1. Knockdown of occludin and ZO2 simultaneously did not invoke a large increase in ZEB2, SNAIL2 and TWIST1 as seen with ZO1. In fact, expression of ZEB2 and TWIST1 was lowest in HepG2$^{OCLN+\ siZO2}$ cells.

3.12.1 Quantification of changes in adhesion associated molecules with differential occludin expression and knockdown ZO1.

With HepG2^{Control} as the control for the investigation, HepG2$^{OCLN+\ siZO1}$ and HepG2$^{shOCLN\ siZO1}$ as test variables. The gene expression profiles molecules associated with cellular adhesion or loss of adhesion and displayed in Figure 3.19. All amplification profiles were assessed, targets with abnormalities, unreliable technical replicates or insufficient PCR efficiency were not included.

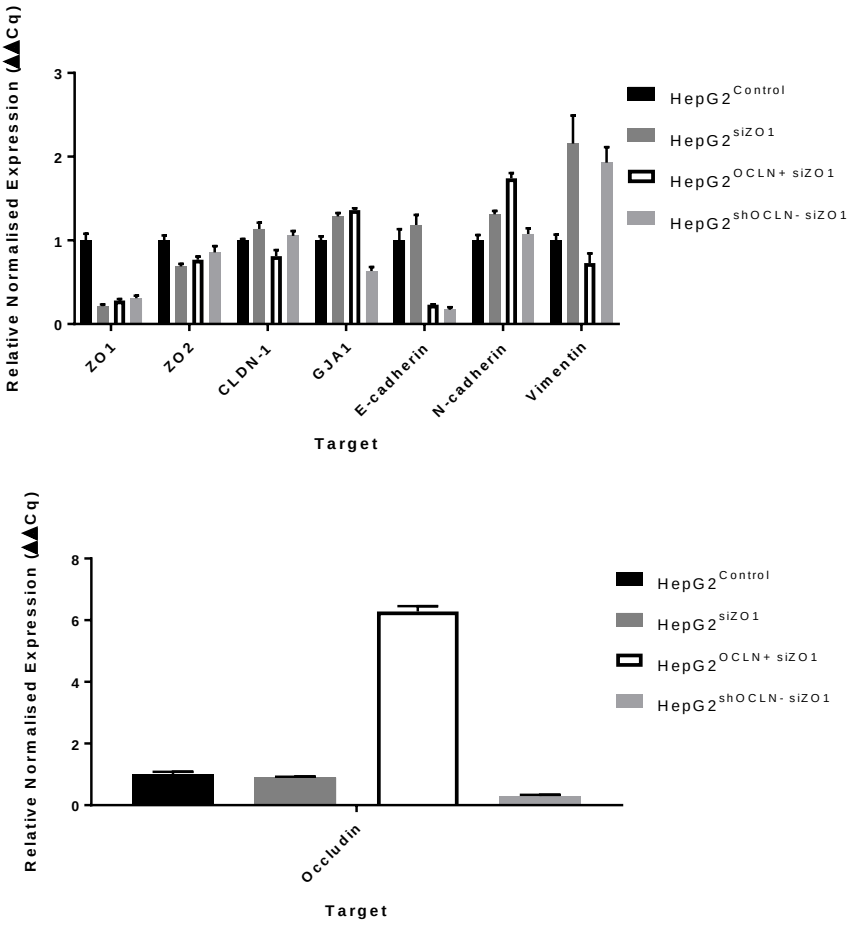

Figure 3.19: PCR analysis of adhesion molecules for HepG2 cells with differential occludin expression and knockdown of ZO1. RT-PCR quantified the relative expression of adhesion molecules after 48 hours culture in HepG2 cells with differential occludin expression. HepG2^{shOCLN} and HepG2$^{shOCLN\ siZO1}$ cells had decreased E-cadherin and increased vimentin expression, classically shown in EMT. Plotted here are mean and S.E.M values. Split into two graphs due to large axis difference.

There was no significant difference between all test variables in CLDN-1, GJA1 and ZO2 expression P values >0.05.

As shown in Figure 3.19, HepG2$^{OCLN+\ siZO1}$ cells as expected had an increase in occludin expression of 6.28-fold P-value 0.0001 and HepG2$^{shOCLN\ siZO1}$ cells occludin expression decreased to 0.29-fold P-value 0.0001. Again, as previously shown knockdown of ZO1 in HepG2 cells did not affect occludin expression, 0.90-fold expression P-value 0.9996.

Knockdown of ZO1 was significant in all cell lines with a knockdown of <0.33-fold expression in all cell lines P values all <0.0003.

Differential expression of occludin with ZO1 knockdown resulted in the downregulation of E-cadherin expression to 0.25-fold P values 0.0001. Knockdown of ZO1 independently does not alter E-cadherin 1.18-fold expression P-value 0.9622. This may highlight that occludin has a regulatory role over E-cadherin.

The main differences between these cell lines are in the epithelial and mesenchymal markers. HepG2$^{OCLN+\ siZO1}$ cells did not alter vimentin 0.72-fold expression P-value 0.9935 and increased N-cadherin expression 1.74-fold P-value 0.0001. HepG2^{siZO1} and HepG2$^{shOCLN\ siZO1}$ cells displayed an increase in vimentin expression of 2-fold P values 0.0001 and did not increase N-cadherin expression 1.08-fold expression P values 0.5316 and 0.9999.

3.12 Quantification of changes in adhesion associated molecules

Investigations were carried out in accordance with, 3.11 Quantification of changes in adhesion associated molecules with differential expression of occludin and ZO2 with knockdown of ZO1 in HepG2 cells.

3.12.2 Quantification of changes in adhesion associated molecules with differential occludin expression and knockdown ZO2.

With HepG2^{Control} as the control for the investigation, HepG2$^{OCLN+\ siZO2}$ and HepG2$^{shOCLN\ siZO2}$ as test variables. The gene expression profiles molecules associated with cellular adhesion or loss of adhesion and displayed in Figure 3.20. All amplification profiles were assessed, targets with abnormalities, unreliable technical replicates or insufficient PCR efficiency were not included.

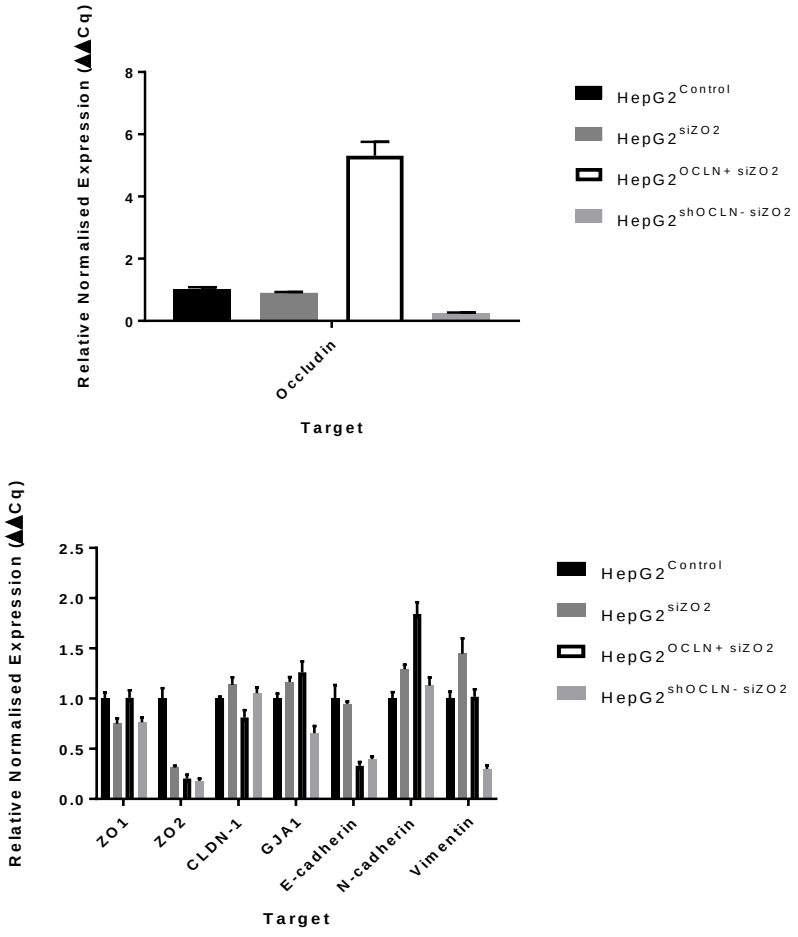

Figure 3.20: PCR analysis of adhesion molecules for HepG2 cells with differential occludin expression and knockdown of ZO2. RT-PCR quantified the relative expression of adhesion molecules after 48 hours culture in HepG2 cells with differential occludin expression. HepG2$^{shOCLN\ siZO2}$ cells had decreased E-cadherin and vimentin expression. Plotted here are mean and S.E.M values. Split into two graphs due to large axis difference.

Shown in Figure 3.20, HepG2^{siZO2} cells had a significant difference against the HepG2^{control} with two genes, ZO2 and vimentin. ZO2 as expected was knocked down to 0.31-fold expression P-value 0.0001. Vimentin had a slight increase in mRNA expression of 1.5-fold P-value 0.0021.

Differential expression of occludin with ZO2 knockdown does not alter ZO1 0.74-fold expression, GJA1 1.17-fold expression and CLDN-1 1.13-fold expression all P values >0.05. HepG2$^{OCLN+\ siZO2}$ cells did not alter the expression of GJA1 1.26-fold expression and vimentin 1.02-fold expression P values > 0.800.

HepG2$^{OCLN+\ siZO2}$ cells increased N-cadherin expression 1.84-fold P-value 0.0012. Both HepG2$^{OCLN+\ siZO2}$ and HepG2$^{shOCLN\ siZO2}$ cells decreased E-cadherin expression to 0.40-fold expression P values <0.01. HepG2$^{shOCLN\ siZO2}$ did not alter N-cadherin expression 1.13-fold expression P-value 0.9914 although interestingly decreased vimentin expression to 0.3-fold expression P-value 0.0008.

3.12.3 Quantification of changes in adhesion associated molecules with overexpression of ZO2 with the loss of occludin and ZO1.

With HepG2^{Control} as the control for the investigation, HepG2^{ZO2+}, HepG2$^{ZO2+\ siZO1}$, HepG2$^{ZO2+\ shOCLN}$ and HepG2$^{ZO2+\ shOCLN\ siZO2}$ as test variables. The gene expression profiles molecules associated with cellular adhesion or loss of adhesion and displayed in Figure 3.21. All amplification profiles were assessed, targets with abnormalities, unreliable technical replicates or insufficient PCR efficiency were not included.

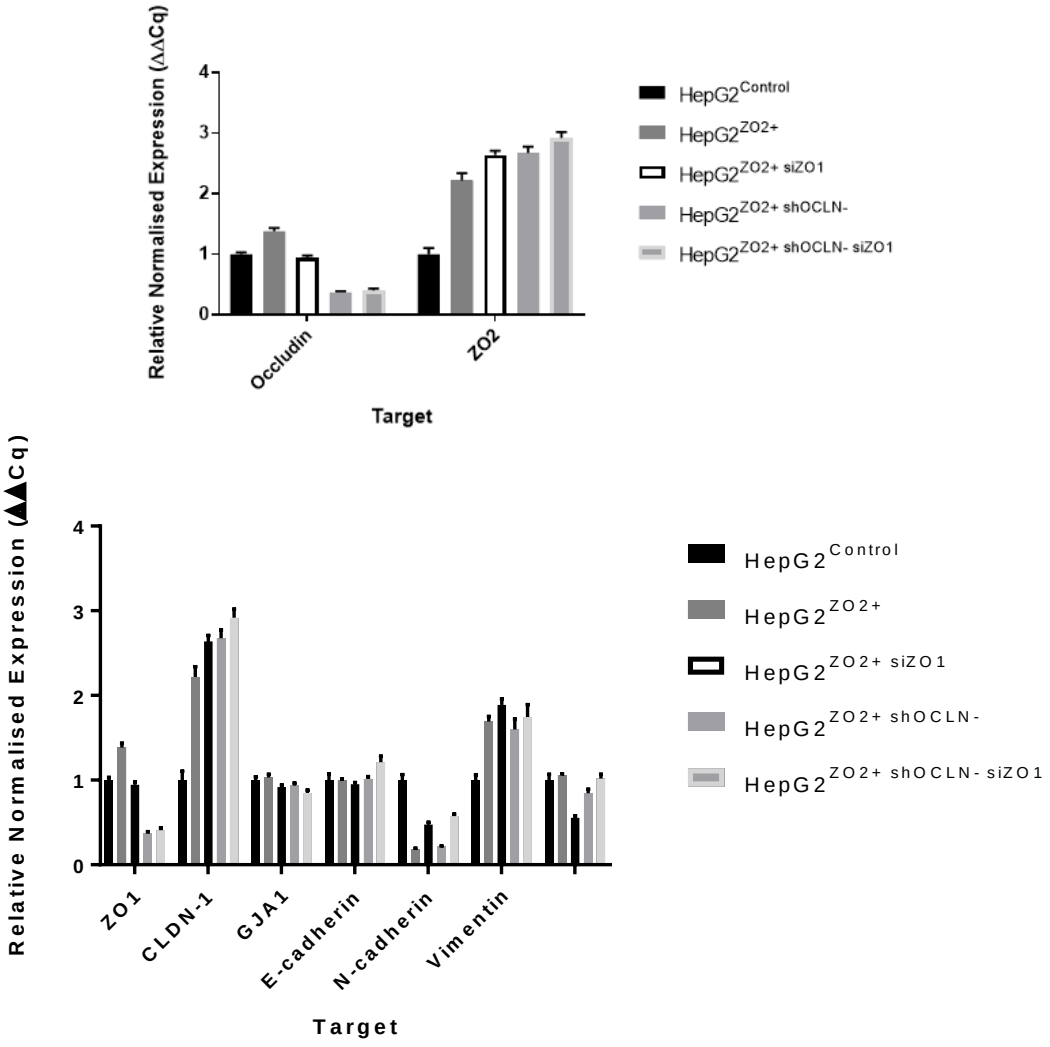

Figure 3.21: PCR analysis of adhesion molecules for HepG2 cells with differential ZO2 expression and knockdown of ZO1 and occludin. RT-PCR quantified the relative expression of adhesion molecules after 48 hours culture in HepG2 cells with differential occludin expression. All HepG2^{ZO2+} cells have increased N-cadherin and

decrease E-cadherin expression, classically shown in EMT. However, HepG2^{ZO2+} cells did not increase vimentin expression. Plotted here are mean and S.E.M values.

Shown in Figure 3.21, all test variables had increased levels of ZO2 mRNA expression, HepG2^{ZO2+} cells had an increase of 2.2-fold mRNA expression compared to HepG2^{Control}. All other cell lines tested had increased ZO2 mRNA expression that was significantly more than HepG2^{control} and HepG2^{ZO2+}, P values <0.0030.

Occludin mRNA expression was reduced in HepG2$^{ZO2+\ shOCLN}$ and HepG2$^{ZO2+\ shOCLN\ siZO1}$ cells to <0.37-fold expression, P values <0.0001. Occludin expression in HepG2^{ZO2+} cells shows a slight significant increase of 1.4-fold, P value 0.0133. In HepG2^{ZO2+} and HepG2$^{ZO2+\ siZO2}$ cells had no significant change in expression 1.38 and 0.94-fold expression, P values 0.8880 and 0.5175. HepG2$^{ZO2+\ siZO1}$ and HepG2$^{ZO2+\ shOCLN\ siZO1}$ cells show a decreased ZO1 mRNA expression to 0.5-fold expression, P values 0.0002 and <0.0001.

Figure 3.21 also shows the expression profile for E-cadherin and N-cadherin. In all cell lines E-cadherin was downregulated whereas N-cadherin was upregulated. E-cadherin expression had no significant difference between all cell lines and all are significantly decreased compared to the control P values, <0.0024.

Increased N-cadherin mRNA expression in all test cell lines was between 1.6 and 1.8-fold are significantly higher than the control, P values <0.0001. Vimentin mRNA levels show no significant difference in all test cell lines apart from HepG2$^{ZO2+\ siZO1}$ with a 1.8-fold decrease, P value, 0.0009. Figure 3.21 shows no mRNA expression change for claudin1 and GJA1 mRNA P values >0.05.

3.13 Determining the rate of migration across a 2D surface and invasion into a 3D matrix with altered occludin, ZO1 and ZO2 expression.

The gene expression profiles suggested occludin overexpression can inhibit a migratory phenotype and knockdown of occludin exacerbates the migratory phenotype with ZO1 and ZO2 knockdown. The expression profile of ZO2 overexpression suggests it inhibits the migratory phenotype even with the loss of occludin and ZO1 with increased N-cadherin and the inhibition of increased vimentin expression.

To confirm this 2D migration and 3D invasion assays were repeated to determine if ZO1 and ZO2 influence the migratory phenotype further. This experiment was completed in accordance with, 3.3.1 and 3.4.

3.13.1 HepG2 rate of migration and invasion with differential occludin expression and knockdown ZO1.

The following data had HepG2^{Control} as the control with HepG2^{siZO1}, HepG2$^{OCLN+\ siZO1}$ and HepG2$^{shOCLN\ siZO1}$ as test variables. Figure 3.22 shows an increase in cell migration is seen with a decreased amount of cell-free gap left and an increase in invasiveness if the size of spheroid/cell spread diameter increases. Spheroid size was calculated following 2.2.8.

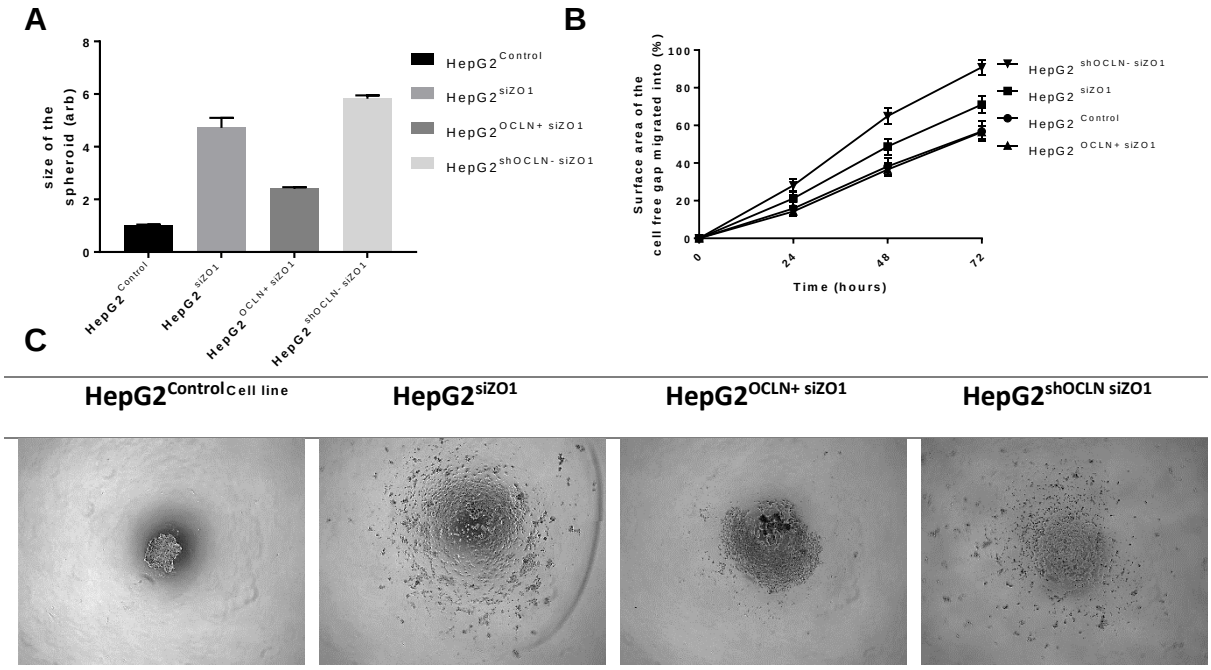

Figure 3.22: Graph A, HepG2 invasiveness from spheroid into an ECM with differential occludin expression with knockdown of ZO1. Graph B, the HepG2 rate of migration across a cell-free gap with differential occludin expression and ZO1 knockdown. C, visual comparisons of spheroid formation and invasion with differential occludin expression and knockdown of ZO1.

The knockdown of ZO1 increased cell motility, HepG2^{siZO1} migrated 71.05 % into the cell-free gap, this was an increase of 14.23 % compared to HepG2^{Control}, P value 0.0351. HepG2$^{shOCLN\ siZO1}$ migrated into a further 20 % of the cell free gap taking 90 % of the available space P-value 0.0001 and was significantly more than

independent ZO1 knockdown P-value 0.0017. This was mirrored in the invasion assay HepG2^{siZO1} and HepG2$^{shOCLN\ siZO1}$ showed the largest diameters with an increase of 4.7 and 5.8-fold respectively, P value <000.1, both showing loss of spheroid formation. Knockdown of ZO1 coupled with occludin silencing showed a more invasive cancer cell behaviour than knockdown of occludin by 1.2-fold, P value 0.0007.

HepG2$^{OCLN+\ siZO1}$ showed similar migration to the HepG2^{Control} with no significant difference, P value 0.9751. The same trend was seen in the invasion assay, however, the HepG2$^{OCLN+\ siZO1}$ spheroid increased 2.4-fold, P value <0.0001.

HepG2$^{OCLN+\ siZO1}$ displayed the least invasive cancer cell behaviour with ZO1 knockdown with a partial spheroid still formed. HepG2$^{shOCLN\ siZO1}$ and HepG2^{siZO1} lost the spheroid formation and limited cellular migrated outwards away from the spheroid.

3.13.2 HepG2 rate of migration and invasion with differential occludin expression and knockdown ZO2.

The following data had HepG2^{Control} as the control with HepG2^{siZO2}, HepG2$^{OCLN+\ siZO2}$ and HepG2$^{shOCLN\ siZO2}$ as test variables. Figure 3.23 shows an increase in cell migration is seen with a decreased amount of cell-free gap left and an increase in invasiveness if the size of spheroid/cell spread diameter increases. Spheroid size was calculated following 2.2.8.

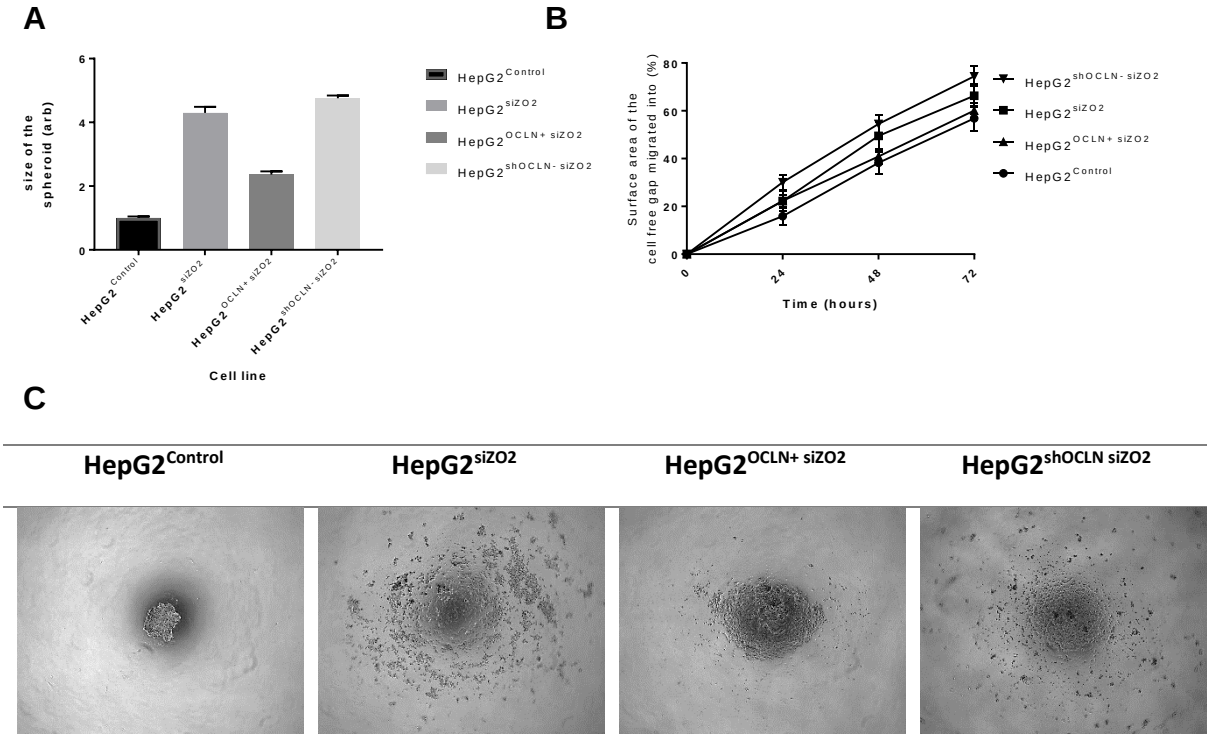

Figure 3.23: Graph A, HepG2 invasiveness from spheroid into an ECM with differential occludin expression with knockdown of ZO2. Graph B, the HepG2 rate of migration across a cell-free gap with differential occludin expression and ZO2 knockdown. C, visual comparisons of spheroid formation and invasion with differential occludin expression and knockdown of ZO2.

The pattern of results in Figure 3.22, shows a similar to the pattern of results in, Figure 3.23, the only difference is HepG2$^{OCLN+\ siZO2}$ has a higher rate of migration into the cell-free gap. However it is not significantly different, P value 0.9989. As

before with ZO1 knockdown HepG2^{siZO2} exhibited a higher rate of migration with HepG2$^{shOCLN\ siZO2}$ having the highest rate of migration compared to the control, P values <0.0001 and 0.0135.

All invasion test variables had larger diameters showing greater invasiveness. HepG2^{siZO2} and HepG2$^{shOCLN\ siZO2}$ had the largest cell spread diameters by 4.3 and 4.8-fold compared with HepG2^{control}, P value <0.0001. Although HepG2$^{shOCLN\ siZO2}$ showed more invasiveness than HepG2 ^{siZO2} it was not significantly different, P value 0.6491. HepG2$^{OCLN+\ siZO2}$ showed the least invasive cancer cell behaviour with ZO2 knockdown with a cell spread diameter increase against the control of 2.4-fold, P value <0.0001, this is also 1.8 and 2-fold less than HepG2^{siZO2} and HepG2^{shOCLN} respectively, P value <0.001. HepG2$^{OCLN+\ siZO2}$ maintained partial spheroid formation unlike HepG2^{siZO2} and HepG2$^{shOCLN\ siZO2}$ that showed complete loss of spheroid formation while HepG2$^{OCLN+\ siZO2}$ retained the spheroid core.

3.13.3 HepG2 rate of migration and invasion with differential occludin and ZO2 expression and knockdown ZO1.

The following data had HepG2^{Control} as the control with HepG2^{ZO2+}, HepG2$^{ZO2+\ siZO1}$ and HepG2$^{ZO2+\ siZO2}$ and HepG2$^{ZO2+\ shOCLN\ siZO2}$ as test variables. Graph X shows an increase in cell migration is seen with a decreased amount of cell-free gap left and an increase in invasiveness if the size of spheroid/cell spread diameter increases. Spheroid size was calculated following 2.2.8.

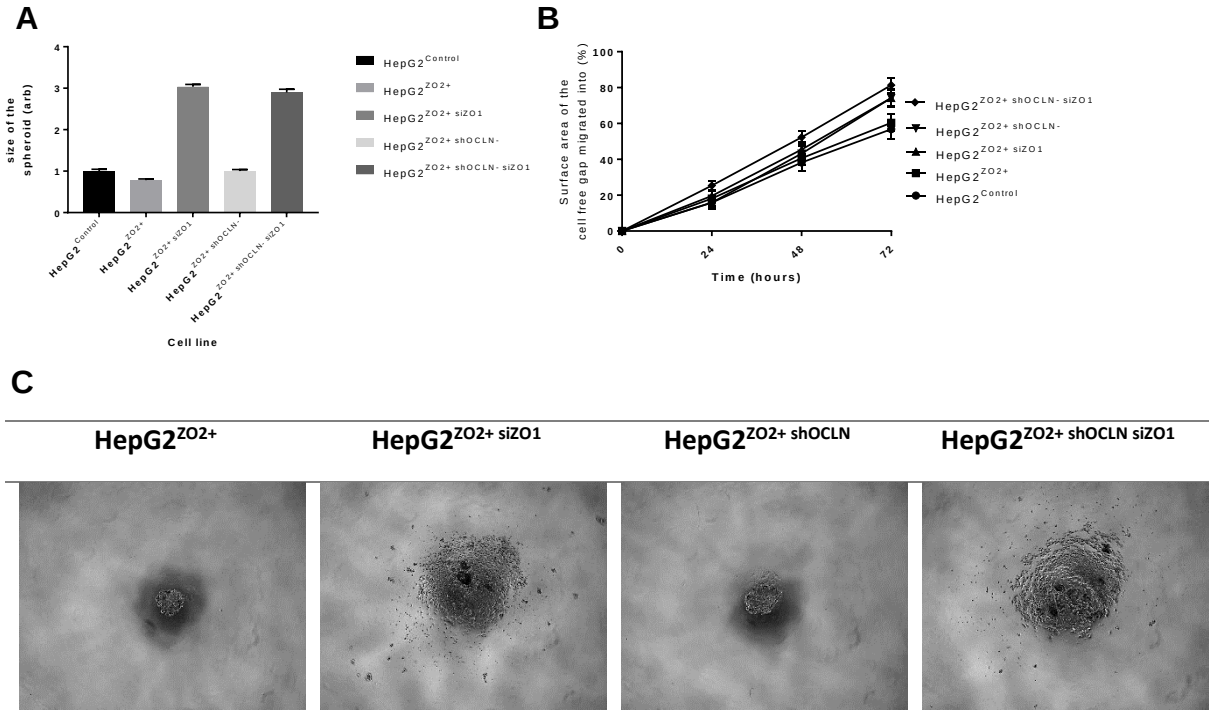

Figure 3.24: Graph A, HepG2 invasiveness from spheroid into an ECM with differential occludin and ZO2 expression with the ZO1 knockdown. Graph B, the HepG2 rate of migration across a cell-free gap with differential occludin and ZO2 expression and ZO1 knockdown. C, visual comparisons of spheroid formation and invasion with differential occludin and ZO2 expression with knockdown of ZO1.

HepG2^{Control} and HepG2^{ZO2+} show similar rates of motility with no significant difference, P value 0.9575. HepG2$^{ZO2+\ siZO1}$, HepG2$^{ZO2+\ shOCLN}$, HepG2$^{ZO2+\ shOCLN\ siZO1}$ exhibited similar migration rates compared to the control, however, had no significant difference in migration with each other, P values >0.999, 0.6331 and 0.6284.

However, the invasion assay showed a different pattern, ZO2 overexpression had no protective effect on the epithelial phenotype with ZO1 knockdown in the invasion assays.

With ZO1 knockdown, the diameter of cell spread increased with an increase of 3 and 2.9-fold for HepG2$^{ZO2+\ siZO1}$ and HepG2$^{ZO2+\ shOCLN\ siZO1}$ respectively, P value <0.0001, however, there was no significant difference between them, P-value >0.999. HepG2^{ZO2+} and HepG2$^{ZO2+\ shOCLN}$ formed complete spheroids with minimal invasion into the ECM. HepG2$^{ZO2+\ siZO1}$ and HepG2$^{ZO2+\ shOCLN\ siZO1}$ showed a more invasive cancer cell behaviour however a partial spheroid was formed and invasion was limited. Overall ZO2 overexpression did not inhibit invasion when ZO1 was knocked down but did inhibit invasion when occludin was knocked down.

3.14 Determining if the altered expression of ZO1 and ZO2 alter cell polarity with differential occludin expression.

Occludin expression had no significant effect on cell polarity shown in, Figure 3.10, however there were differences in BC to nuclei ratio in areas of low and high cell density. As the knockdown of ZO1 and ZO2 increased cell migration and exacerbated knockdown occludin migration the polarity investigation was repeated to see if ZO1/2 is responsible for the loss of cell polarity seen in the development of HCC.

$HepG2^{Control}$ was used as the control and $HepG2^{OCLN+}$ and $HepG2^{shOCLN}$ was used as the test variables. The control and test variables were subjected to siRNA knockdown of ZO1 and ZO2 to see if the cell junction anchorage had an effect of polarity. The higher the bile canaliculi/cell ratio, the more polarised the cells were. .

Bile canaliculi stained green by targeting MRP2 and was counted in 5 fields of view under a fluorescent microscope at 20X magnification. This number was compared to the number of DAPI stained nuclei to give a ratio of cell/bile canaliculi.

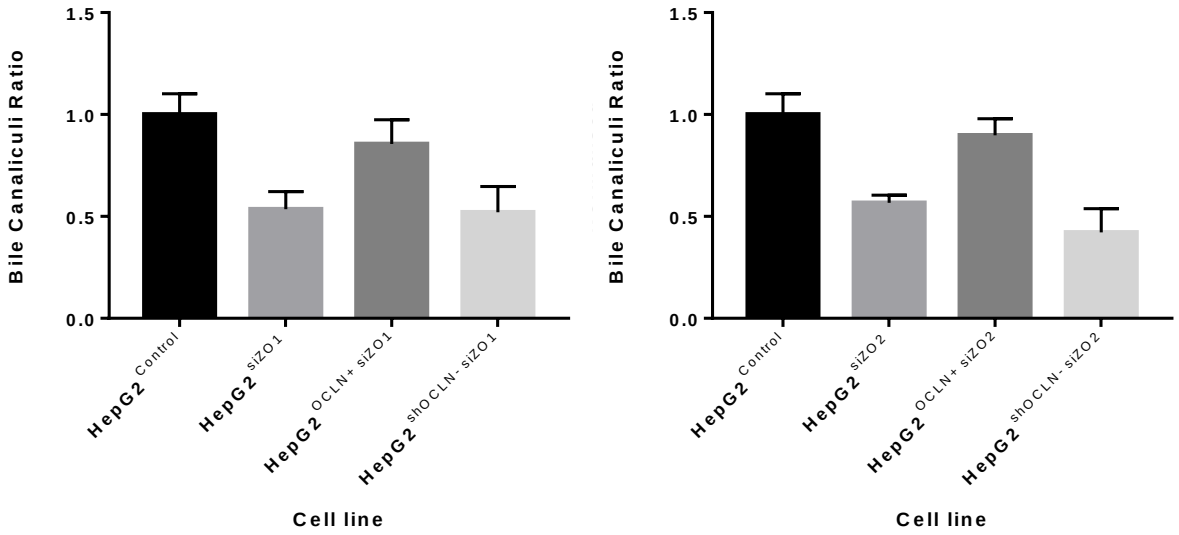

Figure 3.25: Bile canaliculi to cell ratio as a measure of cell polarity *in vitro* with differential expression of occludin and knockdown of ZO1 or ZO2. MRP2 recruit to the tight junction, therefore, a ratio of positive MRP2 to bile canaliculi can be calculated. Although HepG2^{OCLN+} have a higher MRP2 to bile canaliculi ratio there was no significant difference P value >0.05.

Occludin, ZO1 and ZO2 knockdown all result in the loss of approximately half the bile canaliculi, P values <0.05. The loss of occludin simultaneously with a loss of ZO1 and ZO2 does not significantly decrease nuclei to BC ratio further. Occludin overexpression with knockdown ZO1/2 rescued the phenotype with no significant difference between the controls, occludin expression with ZO1 knockdown resulted in a 14.5 % loss and knockdown ZO2 11.2 % loss, P values 0.7888 and 0.8516 respectively.

The same procedure was followed and assessed areas of high and low cell density areas for cells with differential occludin expression and knockdown of ZO1, results were formulated into Figure 3.26.

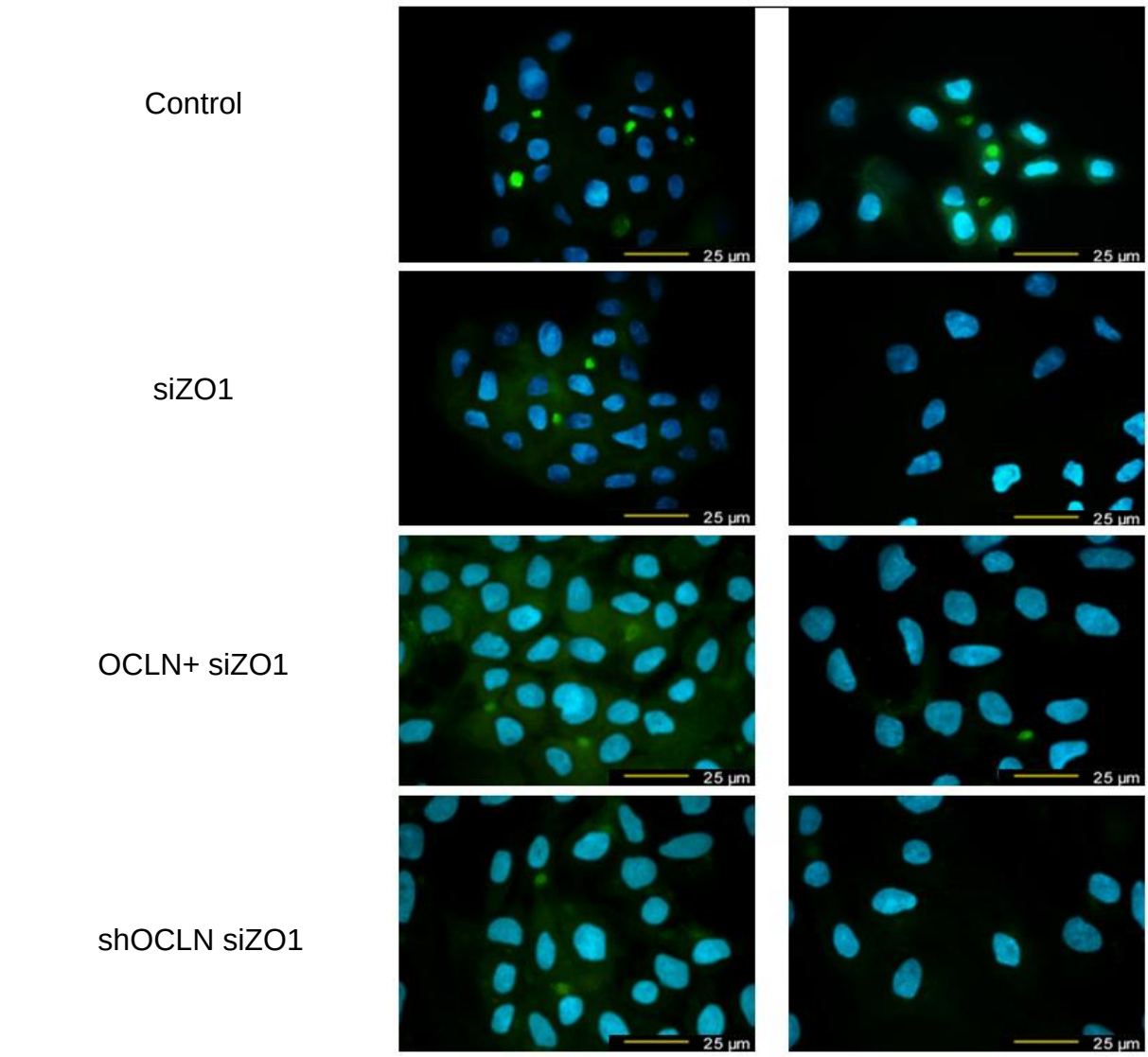

Figure 3.26: BC location concerning cell density with differential occludin expression and the knock down of ZO1. MRP2 antibodies were used to assess the location and frequency of the TJs. Areas of higher cell density show higher have an increase BC to nuclei ratio. MRP2 green and DAPI nuclei stain blue. Areas that had ≤6 nuclei/ 40 µm were considered as areas of low cell density.

The BC to nuclei ratio was altered in all cell lines with knockdown ZO1. In $HepG2^{Control}$ and $HepG2^{OCLN+\ siZO1}$ cells grew in areas of high cell density unlike

HepG2^{siZO1} and HepG2$^{shOCLN\ siZO1}$ cells. In HepG2^{siZO1} and HepG2$^{shOCLN\ siZO1}$ cells that were migrating into areas of cell free space often did not stain positive for MRP2.

The same procedure was followed and assessed areas of high and low cell density areas for cells with differential occludin expression and knockdown of ZO1, results were formulated into Figure 3.26.

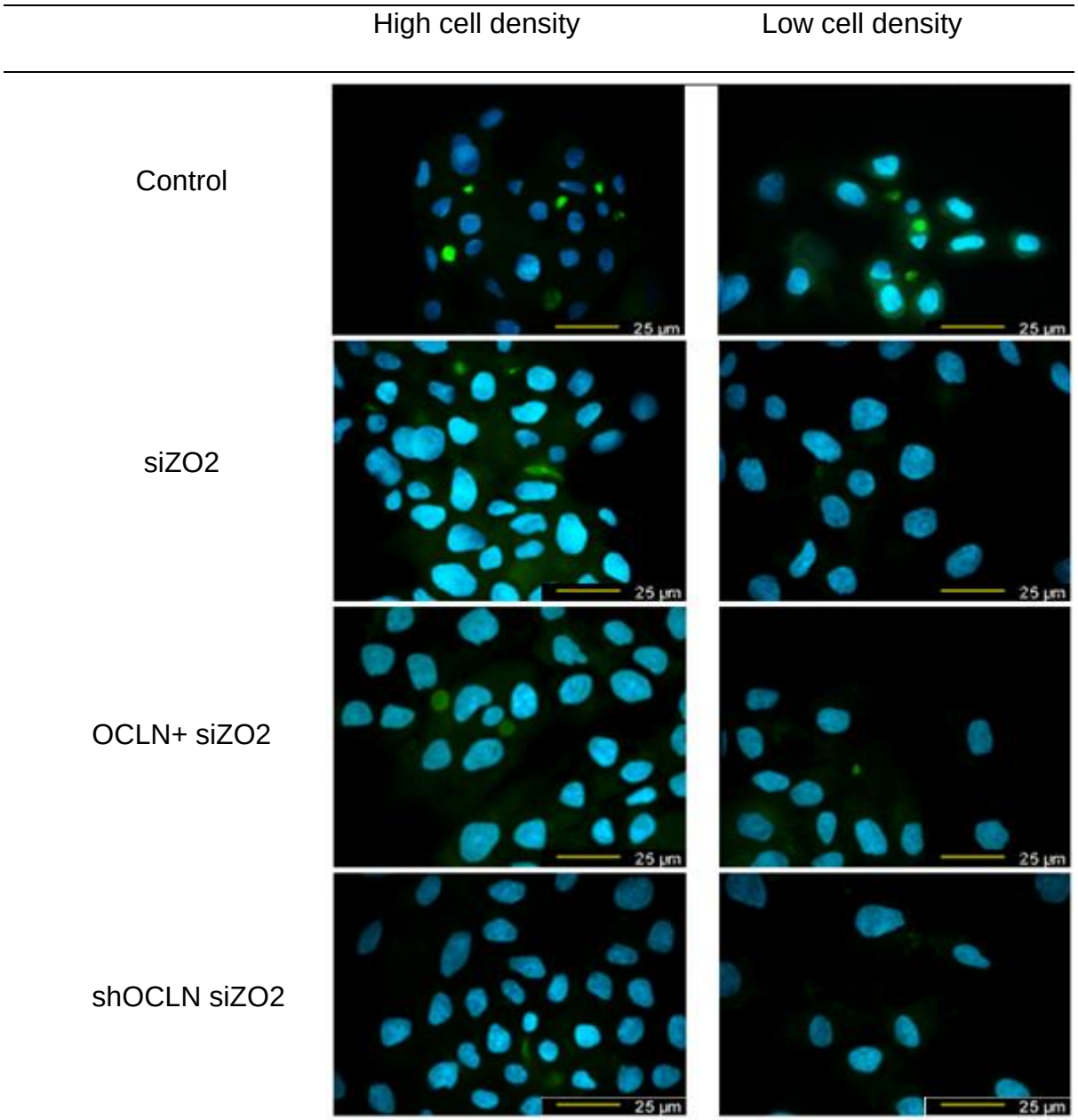

Figure 3.27: BC location concerning cell density with differential occludin expression and the knock down of ZO2. MRP2 antibodies were used to assess the location and frequency of the TJs. Areas that had ≤6 nuclei/ 40 µm were considered as areas of low cell density. MRP2 green and DAPI nuclei stain blue.

Knockdown ZO2 displays the same results as knockdown ZO1. HepG2$^{OCLN+\ siZO2}$ cells show limited migration into cell free areas and grow in high density groups. The knockdown of ZO2 in HepG2^{siZO2} and HepG2$^{shOCLN\ siZO2}$ did, however, change the staining pattern of MRP2, BCs did not always stain with a bright circular formation. Shown above in Figure 3.27 MRP2 stained along apical contact with the opposing cell.

3.14.1 Evaluating if overexpression of ZO2 with knockdown of occludin in HepG2 cells influences cell polarity *in vitro.*

HepG2^{Control} was used as the control and HepG2^{ZO2+} and HepG2$^{ZO2+\ shOCLN}$ was used as the test variables. The test variables were subjected to siRNA knockdown of ZO1 to see if the cell junction anchorage had an effect of polarity. The higher the bile canaliculi/cell ratio, the more polarised the cells were.

Bile canaliculi stained green by targeting MRP2 and was counted in 5 fields of view under a fluorescent microscope at 20X magnification. This number was compared to the number of DAPI stained nuclei to give a ratio of cell/bile canaliculi.

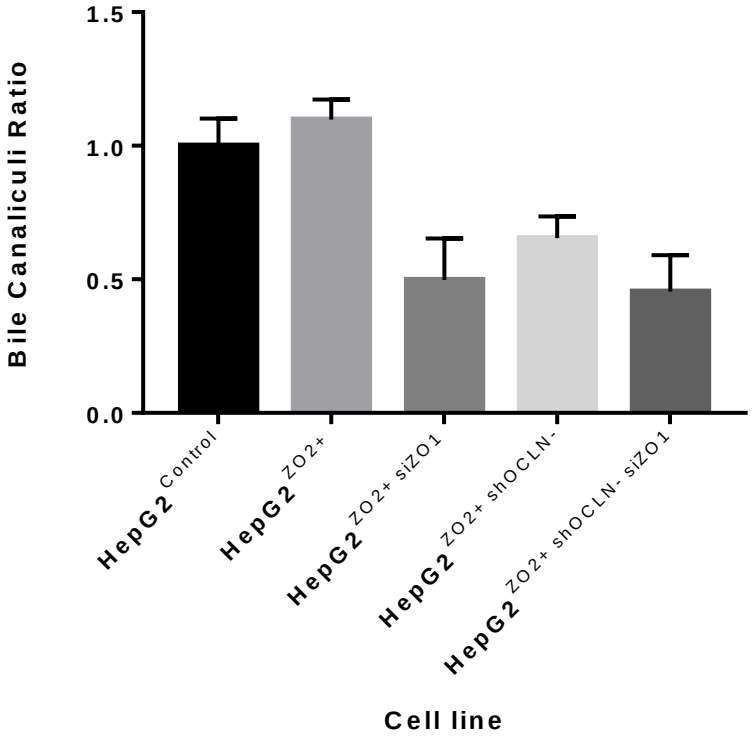

Figure 3.28: Bile canaliculi to cell ratio as a measure of cell polarity in HepG2 cells that have ZO2 overexpression, differential expression of occludin and knockdown of ZO1. MRP2 recruit to the tight junction, therefore, a ratio of positive MRP2 to bile canaliculi can be calculated. Although HepG2^{OCLN+} have a higher MRP2 to bile canaliculi ratio there was no significant difference P value >0.05.

Figure 3.28 shows, ZO2 overexpression has no significant effect on cell polarity, P value 0.9715. However, HepG2^{ZO2+} cells that had knocked down occludin expression showed a 45 % in the BCs, P value 0.0393. HepG2^{shOCLN} do not significantly change the BC ratio, Figure 3.28. This shows that ZO2 overexpression does not protect against the loss of functional tight junctions. HepG2$^{ZO2+\ siZO1}$, HepG2$^{ZO2+\ shOCLN}$ and HepG2$^{ZO2+\ shOCLN\ siZO1}$ had a marked decrease in BC to nuclei ratio, however, it was not significant, P value >0.05.

3.14.2 Overall analysis of cell polarity with altered tight junction associated protein expression.

The loss of occludin, ZO1 and ZO2 decreases the BC to nuclei ratio inferring a loss in cellular polarity and functional tight junctions. When occludin was knocked down simultaneously with ZO1 or ZO2 the same loss of BC to nuclei was seen, Figure 3.25. Occludin and ZO2 overexpression in HepG2 cells do not significantly increase the BC to nuclei ratio and therefore no increase of polarity, Figure 3.26. ZO2 overexpression does not protect against the loss of bile canaliculi when occludin, ZO1 or ZO2 expression was knocked down, Figure 3.26. However, occludin overexpression minimised the loss of BCs, Figure 3.25, when ZO1 or ZO2 expression was knocked down as the BC to nuclei ratio only decreased by 15 % against the HepG2^{Control}.

3.15 An investigation of the localisation of tight junctional proteins with differential occludin, ZO1 and ZO2 expression *in vitro*.

As the loss of occludin, ZO1 and ZO2 either independently or combined resulted in increased migration and invasion, Figures 3.6, 3.7, 3.22, 3.23 and 3.24. A cell polarity was conducted to assess whether functional tight junctions were forming, this assay showed that there were differences between each cell line, to investigate the relationship between occludin, ZO1 and ZO2 protein localisation, investigations through immunofluorescence was used.

The cells were seeded at 40000 cells/well on 13 mm dia. Menzel round coverslips in a 24 well plate. The relevant knockdowns were conducted after a 24-hour incubation period. The cells were incubated for a further 96 hours, this is the optimal time for assessing protein localisation after siRNA gene knockdown.

3.15.1 Localisation of occludin with differential occludin expression and knockdown of ZO1 and ZO2.

The following data was created at the same time with HepG2^{Control} as the control to show the correct localisation of occludin with differential occludin expression and knockdown of the ZO proteins. Figure 3.29, shows the localisation of occludin in HepG2^{control}, HepG2^{OCLN+} and HepG2^{shOCLN} cell lines. The mRNA expression of ZO1 and ZO2 was knocked down in these cells to ascertain a whether a change of occludin localisation occurred.

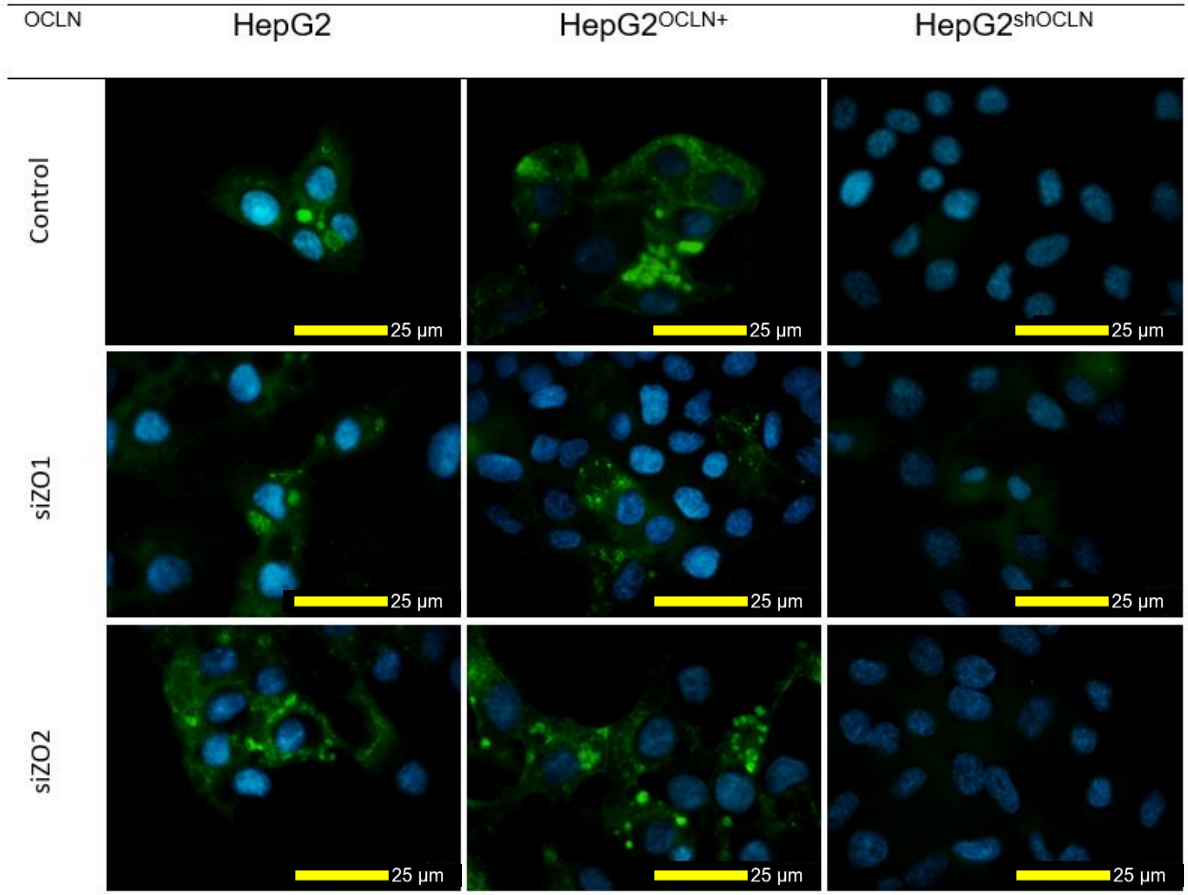

Figure 3.29: Localisation of occludin, in HepG2 cells with over and under expression of occludin. occludin localisation was assessed in HepG2, HepG2^{OCLN} and HepG2^{shOCLN} cells with knocked down ZO1 and ZO2 expression. These cells were cultured on cover slips for 96 hours post transfection. A knock down of ZO1, ZO2 or occludin resulted in the mislocalisation of ZO1. Green is secondary anti mouse conjugated to Alexa Fluor 488 and blue is DAPI nuclei counter stain.

As expected there is no positive protein staining of occludin in knockdown occludin HepG2 cells. HepG2^{Control} shows four polarised cells sharing a pseudo bile canalicular tight junction with occludin predominately concentrated within the single junction. Knockdown of ZO2 does not alter occludin tight junction localisation. ZO1 knockdown however appears to be more cytoplasmic.

With the overexpression of occludin there are still the single occludin tight junctions forming between cells, however, there are also multiple aggregates of occludin formed. The occludin appears to localise to the correct area but a lack of space appears to cause non-junctional cytoplasmic localised occludin. Again, knockdown of ZO2 does not alter occludin localisation unlike knockdown of ZO1. Interestingly the knockdown of ZO1 reduced occludin positive staining considerably, however, the remaining occludin appears to be junctional.

3.15.2 Localisation of ZO1 with differential occludin expression and knockdown of ZO1 and ZO2.

The following data was created at the same time with HepG2^{Control} as the control to show the correct localisation of ZO1 with differential occludin expression and knockdown of the ZO proteins. Figure 3.30, shows the localisation of ZO1 in HepG2^{control}, HepG2^{OCLN+} and HepG2^{shOCLN} cell lines. The mRNA expression of ZO1 and ZO2 was knocked down in these cells to ascertain a whether a change of ZO1 localisation occurred.

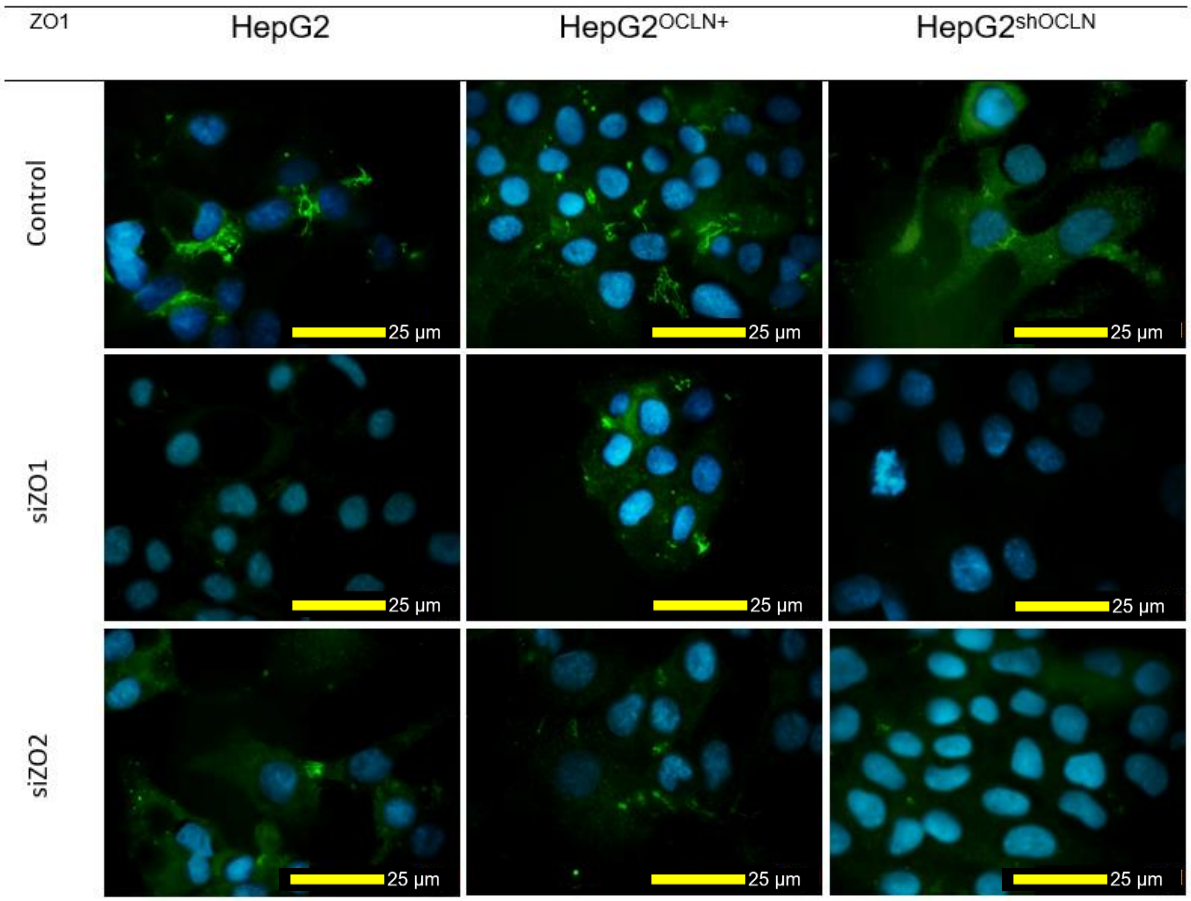

Figure 3.30: Localisation of ZO1, in HepG2 cells with over and under expression of occludin. ZO1 localisation was assessed in HepG2, HepG2^{OCLN} and HepG2^{shOCLN} cells with knocked down ZO1 and ZO2 expression. These cells were cultured on cover slips for 96 hours post transfection. A knock down of ZO1, ZO2 or occludin resulted in the mislocalisation of ZO1. Green is secondary anti mouse conjugated to Alexa Fluor 488 and blue is DAPI nuclei counter stain.

Figure 3.30 shows, in HepG2^{Control} cells, ZO1 predominantly localised around the tight junction, however, there was also ZO1 was in the cytoplasm. As expected HepG2 cells with knocked down ZO1 expression did not show any immunofluorescence labelling of ZO1. When ZO2 expression was knocked down in HepG2 cells ZO1 was only restricted to the sites of cell adhesion, however, less frequently than HepG2^{Control}.

HepG2^{OCLN+} cells showed ZO1 localising primarily to the adhesion sites between cells, there was less cytoplasmic ZO1 in HepG2^{OCLN+} cells compared to HepG2^{Control}. HepG2^{OCLN+} cells with knock down of ZO1 still show staining of ZO1, this suggests ZO1 was being recycled. Knockdown of ZO2 in HepG2^{OCLN+} cells restricts ZO1 to the tight junction.

HepG2^{shOCLN} cells, ZO1 is located at the membrane between neighbouring cells, this does not appear junctional but rather alongside the two opposing membranes. When ZO1 and ZO2 expressing is knocked down in HepG2^{shOCLN} cells, there is no immunofluorescence labelling of ZO1.

3.15.3 Localisation of ZO2 with differential occludin expression and knockdown of ZO1 and ZO2.

The following data was created at the same time with HepG2^{Control} as the control to show the correct localisation of ZO2 with differential occludin expression and knockdown of the ZO proteins. Figure 3.31, shows the localisation of ZO2 in HepG2^{control}, HepG2^{OCLN+} and HepG2^{shOCLN} cell lines. The mRNA expression of ZO1 and ZO2 was knocked down in these cells to ascertain a whether a change of ZO2 localisation occurred.

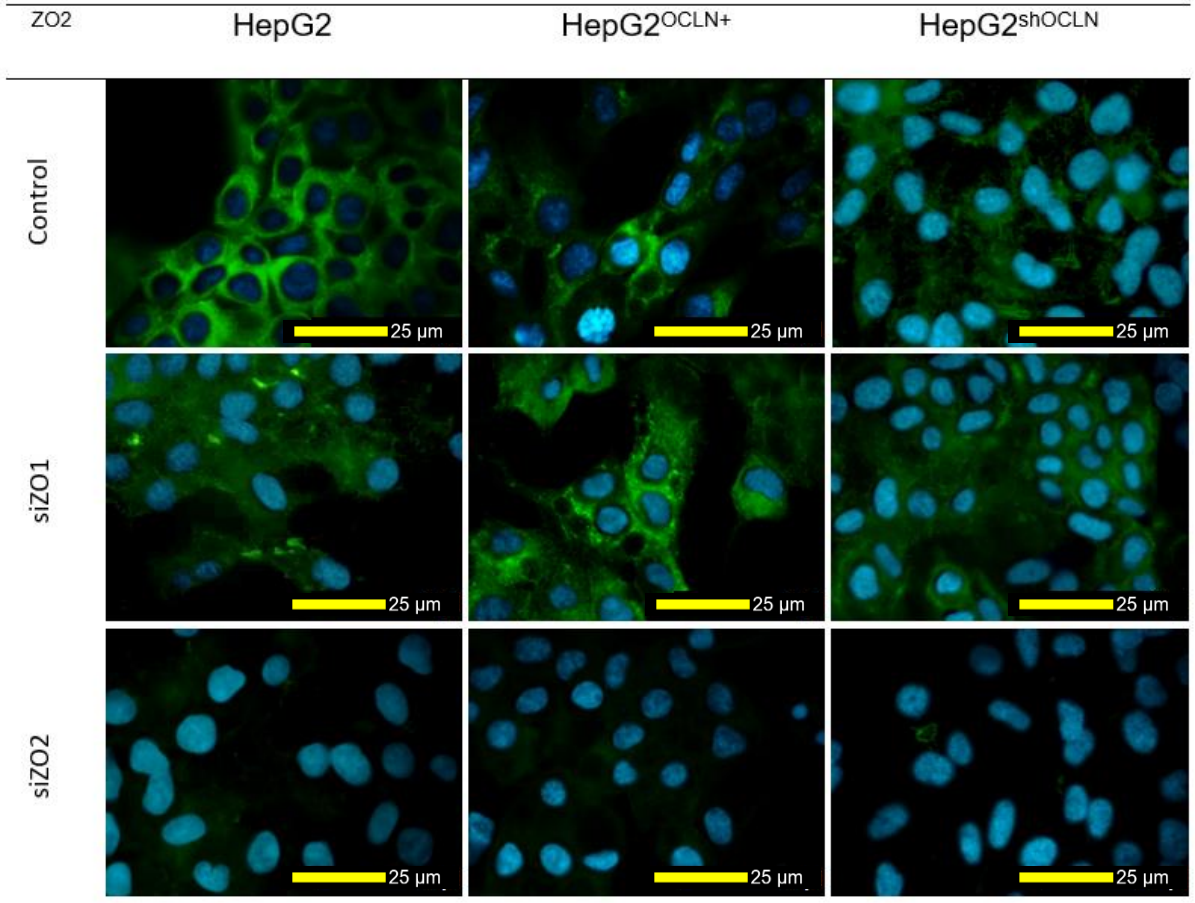

Figure 3.31: Localisation of ZO2, in HepG2 cells with over and under expression of occludin. ZO2 localisation was assessed in HepG2, HepG2^{OCLN} and HepG2^{shOCLN} cells with knocked down ZO1 and ZO2 expression. These cells were cultured on cover slips for 96 hours post transfection. ZO2 was more localised to the tight junctions when ZO1 expression was knocked down. Green is secondary anti mouse conjugated to Alexa Fluor 488 and blue is DAPI nuclei counter stain.

Figure 3.31 shows, in HepG2^{Control} cells, ZO2 predominantly localised at the membrane of the cell but had some specifically at the site of cell adhesion. Knockdown of ZO1 in HepG2 cells resulted in increased junctional specificity of ZO2.

HepG2^{OCLN+} cells showed ZO2 localising primarily to the adhesion sites between cells. When ZO1 expression was knocked down in HepG2^{OCLN+} cells, ZO2 lost junctional specificity and became membrane bound.

HepG2^{shOCLN} cells showed non-specific ZO2 localisation, the staining was predominantly cytoplasmic. This was also seen in HepG2^{shOCLN} cells with knocked down ZO1 expression. In cells where ZO2 was knocked down there was no positive immunofluorescence staining for ZO2.

3.15.4 Localisation of HepG2 occludin, ZO1 and ZO2 with knockdown ZO2 expression.

The following data was created at the same time with HepG2^{Control} as the control to show the correct localisation of occludin, ZO1 and ZO2. The investigation was to assess the whether occludin, ZO1 and ZO2 were localised correctly in HepG2^{ZO2+}. The localisation of ZO2 was also assessed in HepG2^{ZO2+} cells with knocked down occludin and ZO1 expression. Figure 3.32, shows the localisation of occludin, ZO1 and ZO2 in HepG2^{ZO2+} with knockdown occludin and ZO1 expression.

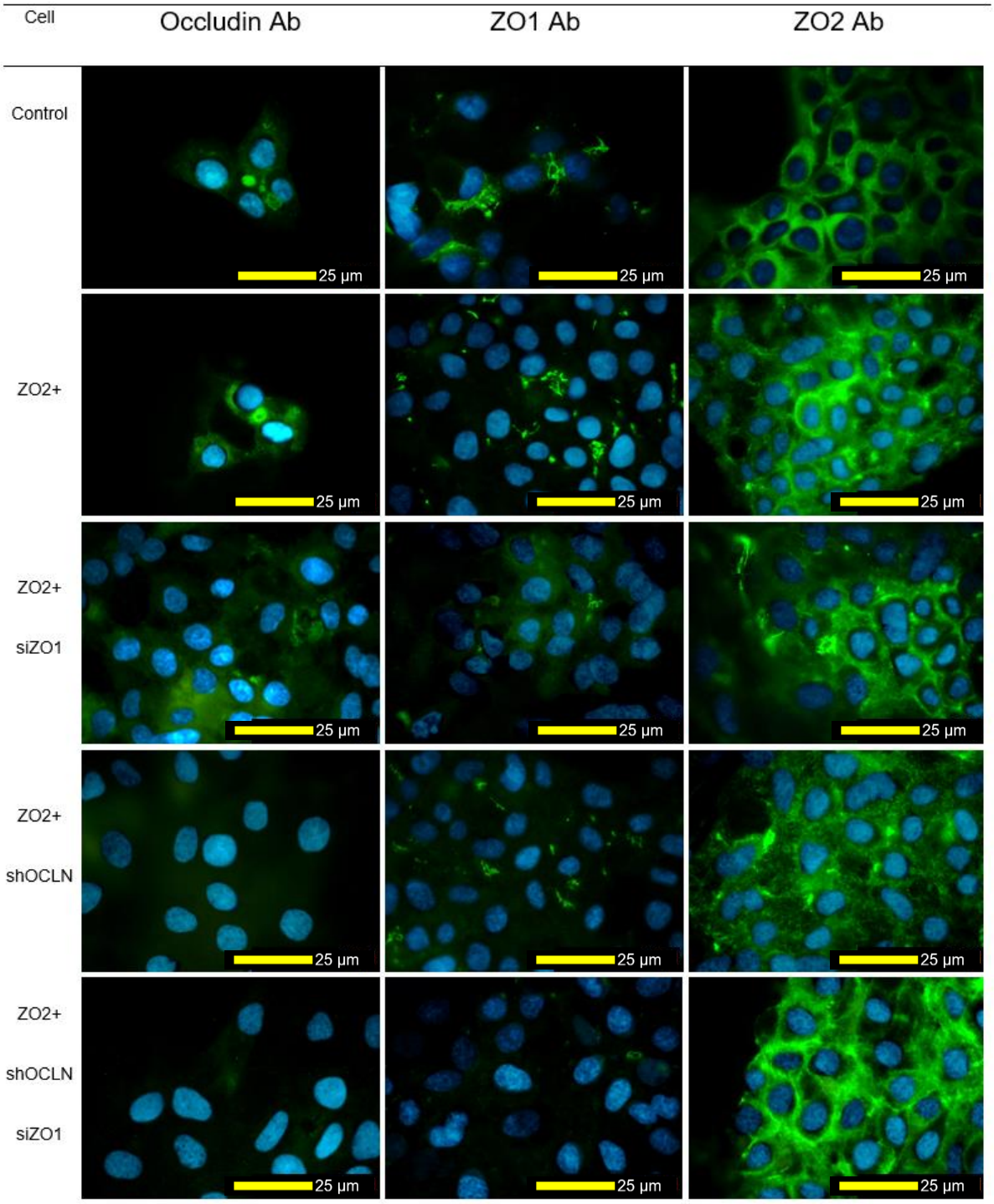

Figure 3.32: Different localisation of occludin, ZO1 and ZO2 when ZO2 is overexpressed in HepG2 cells. Green is secondary anti mouse conjugated to Alexa Fluor 488 and blue is DAPI nuclei counter stain. Columns are different antibody targets and rows are the different cell lines investigated.

As expected occludin knockdown cells do not show any visable flourscently labbled occludin. In HepG2^{ZO2+} cells, occludin was localised to the tight junction, however

when there was a loss of ZO1, tight junctions were not as defined showing slight mislocalisation. ZO1 localisation was correctly localised when ZO2 was overexpressed, as there were frequent ZO1 staining at the tight junction.

ZO2 overexpression resulted in a much higher concentration of ZO2 at the membrane but not was specific to the tight junction. The knockdown of ZO1 and occludin mRNA independently resulted in increased junctional ZO2 localisation. When ZO1 and occludin are knocked down simultaneously in HepG2^{ZO2+} cells, ZO2 was not localised immediately around the nucleus. However, ZO2 did not localise to the tight junction, ZO2 appeared to be located around the membrane.

These data show a clear influence on location and quantity between occludin, ZO1 and ZO2. Knockdown of occludin alone results in reduced junctional ZO1 and ZO2, this is compounded when occludin knockdown is coupled with a ZO1 or ZO2 knockdown. Occludin overexpression results in cellular aggregates of occludin located toward the junctions between neighbouring cells. The overexpression of occludin also increases junctional ZO1 when ZO2 is knocked down and vice versa.

The ZO2 overexpression correlation positively with the correct localisation of ZO1 and occludin. In fact, ZO2 overexpression had more influence on ZO1 localisation than occludin overexpression. The loss of occludin and ZO1 simultaneously resulted in limited ZO2 staining. When ZO2 was overexpressed however, the ZO2 localised to the plasma membrane and junctional sites to compensate.

A loss of ZO1 reduced occludin staining in control, occludin and ZO2 overexpressing cell lines.

3.16 Changes in miRNA profile in the HepG2 cell model with differential occludin expression and knockdown ZO1.

As hepatocellular carcinoma progresses into a more migratory and invasive cancer cell behaviour, there are changes in the miRNA profile. These changes in the miRNA profile within a patient could be analysed to work out disease progression, treatment and prognosis. miRNA responsible for a more cancerous phenotype are well known and if the miRNA profile could be altered the progression of the disease can be slowed. More importantly, these miRNA changes can occur early within the disease to allow early intervention. Occludin expression is influential in HCC progression, reduced occludin expression is associated with a higher tumour grade and infiltration of the Glisson's capsule. Occludin overexpression in HCC is linked to increased patient survival and disease-free rates (Bouchagier et al. 2014; Orbán et al. 2008). However, underlying molecular mechanisms of why this is are uncertain. To determine why an increase in occludin expression is associated with better patient outcomes, a miRNA screen was completed to provide a snapshot of post-transcriptional regulation. As the loss of occludin expression is coupled with the loss of ZO1 expression in HCC, ZO1 expression was also knocked down for this investigation.

$HepG2^{Control}$, $HepG2^{OCLN+\ siZO1}$ and $HepG2^{shOCLN\ siZO1}$ cells were cultured for 24 hours before the knockdown of ZO1 and then cultured for a further 48 hours. A PCR was completed to ensure there was sufficient knockdown of ZO1 before the miRNA profiling began. RNA extraction was completed using the Ambion mirVana miRNA isolation kit as described in 2.6.1. The cDNA was synthesised as described in 2.6.3 and the PCR was completed following 2.6. To ensure that the same amount of small

RNAs were present in the extraction of RNA a denaturing acrylamide gel electrophoresis was completed.

Statistical analysis

RQ manager software 1.2.1 supplied by Life Technologies was used to produce a mean CT, normalised gene expression and the software was used to assess if there was a 95 % confidence interval. To normalise the gene expression the U6 target was used as the reference gene, the rest of the genes were experimental targets. The mean, standard error of the mean and N number was imported into GraphPad Prism 7.0.2, the graphs and the ordinary one-way analysis of variance were produced.

3.16.1 Analysis of the quality of extracted miRNA.

For quality control, the RNA was DNase treated using the TURBO DNA-free kit (Invitrogen) and the RNA samples were run on the Bioanalyzer (Agilent) with an RNA 6000 Nano chip. Only RNA samples that achieved an integrity score of >9 were used in cDNA reverse transcription. From this 1500 ng of DNAse treated RNA was ran on a 15 % denaturing acrylamide gel shown in Figure 3.33. Figure 3.33 shows that the smaller RNAs were successfully extracted with equal quantities of 5.8S, 5S and tRNA and no RNA degradation.

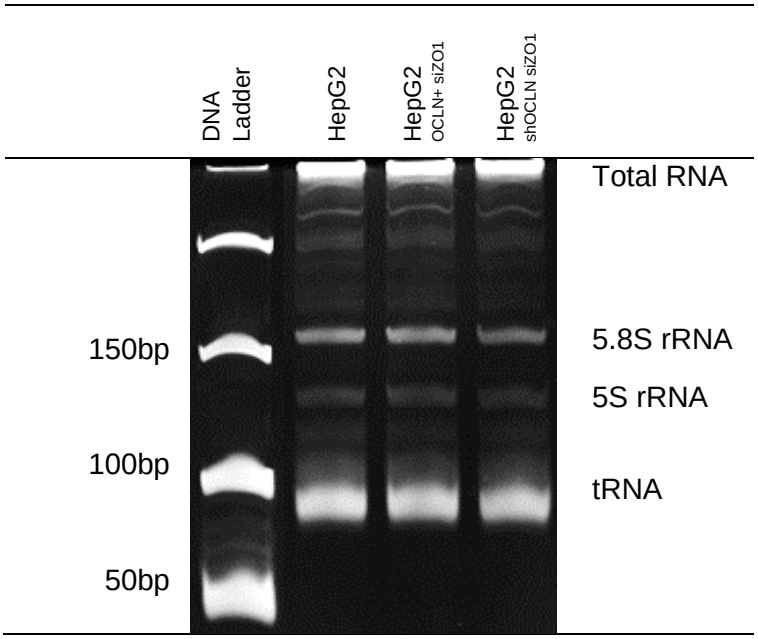

Figure 3.33: Denaturing acrylamide RNA gel to assess the extraction and quality of small RNA. This figure does not show miRNAs, however, it does show equal extraction of the smaller RNAs and that there was no RNA degradation in the extracted RNA.

The miRNA band is not visible on a denaturing acrylamide RNA gel, instead the gel shows the extraction quality of small RNAs. Figure 3.33 shows equal extraction of small RNAs with no RNA degradation. As the small RNAs were extracted successfully and at equal volumes the RNA quality was deemed to be satisfactory and therefore used in the miRNA expression analysis.

3.16.2 Grouping miRNAs to analyse the HepG2 cell model.

Using miRNA expression data initially taken from, Morishita and Masaki (2015) miRNA in hepatocellular carcinoma, allowed the selection of miRNA genes that have been shown to be influential in the progression of HCC (Morishita and Masaki 2015). For this miRNA analysis the miRNAs were split into two categories. Table 3.4 shows which miRNA where highlighted as influential in the progression of HCC and the category they were aligned to.

Associated with up regulation in HCC		Function	Associated with down regulation in HCC	
18a 130b 155 221	373 494 517a 519 590-5p	Apoptosis Proliferation Cell cycle progression	7a/b/c/d/f/g 26a 29a/b/c 99a 101 125a/b 195	200a/b/c 203 222 223 429 449 520e
21 22 26 106b 135a	182 183 186 485-3p	Metastasis Tumour suppression Invasion Carcinogenesis	15a/b/c 21 29b 34a 106b	139-5p 141 145 148a 152 198
(Dang et al. 2014; Gao and Liu 2014; Li et al. 2014; Meg et al. 2007; Morishita and Masaki 2015; Noh et al. 2013; Qiu et al. 2015; Tan et al. 2011; Toffanin et al. 2011; Wang et al. 2011; Wang et al. 2013; Wong et al. 2010; Yan et al. 2013; Zhang et al. 2012)				

Table 3.4: Categorisation of miRNA analysed based on their function in HCC progression.

3.16.3 Complete miRNA profile for HepG2 cells with differential expression of occludin and knockdown ZO1.

Appendix Figure 1, shows the complete miRNA profile that compares the effect of knockdown ZO1 with differential occludin expression on HepG2 cells. miRNA data were compared against $HepG2^{Control}$ cells and normalised with U6 snRNA expression. The test variables are $HepG2^{OCLN+\ siZO1}$ and $HepG2^{shOCLN\ siZO1}$, these RNA extracts were run on low-density TLDA microRNA assay Card A.

The miRNA expression varies between $HepG2^{Control}$ and the two experimental cell lines $HepG2^{OCLN+\ siZO1}$ and $HepG2^{shOCLN\ siZO1}$. A total of 126 different miRNAs were not expressed in all three cell lines and were excluded from the results. Out of the remaining 258 miRNAs, 85 showed no significant difference and a further 37 miRNAs were only slightly significant and are between 0.65-1.45-fold. This left a remaining 136 miRNAs that showed a clear significant difference in at least one of the experimental cell lines. These expression differences are analysed in 3.16.7, they are grouped by the cell lines that did or did not show expression.

The miRNA profiles of $HepG2^{OCLN+\ siZO1}$ and $HepG2^{shOCLN\ siZO1}$ was cross referenced against. Morishita and Masaki (2015) miRNA in hepatocellular carcinoma. This allowed for greater specificity in miRNA gene selection to analyse. Other miRNA associated with HCC were taken from the literature to add into the analysis.

3.16.4 miRNA that only expresses in HepG2^{Control} cells and does not express in and HepG2$^{OCLN+\ siZO1}$ or HepG2$^{shOCLN\ siZO1}$ cells.

Many of the miRNAs show no difference between the two test variables and the control. However there are some miRNA that shows a loss of miRNA expression or overexpression, the miRNA profiles Table 3.5, are those that only express in HepG2^{Control} cells and the expression is lost in HepG2$^{OCLN+\ siZO1}$ and HepG2$^{shOCLN\ siZO1}$. Data was selected if the expression was <0.25-fold and presented in chronological order.

	HepG2	HepG2$^{OCLN+\ siZO1}$			HepG2$^{shOCLN\ siZO1}$		
		Expression	SEM	P value	Expression	SEM	P value
hsa-miR-125a-3p	1	0.25	0.03	<0.005	0.25	0.04	<0.005
hsa-miR-125b	1	0.00	0.00	-	0.00	0.00	-
mmu-miR-153	1	0.00	0.00	-	0.00	0.00	-
hsa-miR-198	1	0.00	0.00	-	0.00	0.00	-
hsa-miR-302b	1	0.05	0.03	<0.005	0.00	0.00	-
hsa-miR-337-5p	1	0.00	0.00	-	0.00	0.00	-
hsa-miR-342-5p	1	0.00	0.00	-	0.00	0.00	-
hsa-miR-371-3p	1	0.19	0.06	<0.005	0.24	0.07	<0.005
hsa-miR-449b	1	0.00	0.00	-	0.00	0.00	-
hsa-miR-491-3p	1	0.00	0.00	-	0.00	0.00	-
hsa-miR-501-3p	1	0.00	0.00	-	0.00	0.00	-
hsa-miR-507	1	0.00	0.00	-	0.00	0.00	-
hsa-miR-512-5p	1	0.00	0.00	-	0.00	0.00	-
hsa-miR-525	1	0.00	0.05	<0.005	0.00	0.04	<0.005
hsa-miR-539	1	0.00	0.00	-	0.00	0.00	-
hsa-miR-561	1	0.00	0.00	-	0.00	0.00	-
hsa-miR-576-5p	1	0.00	0.00	-	0.00	0.00	-
hsa-miR-655	1	0.02	0.06	<0.005	0.01	0.07	<0.005
hsa-miR-891a	1	0.00	0.00	<0.005	0.00	0.00	<0.005

Table 3.5: List of the miRNAs that do not express in HepG2$^{OCLN+\ siZO1}$ and HepG2$^{shOCLN\ siZO1}$.

As the expression and SEM are 0, a P value cannot be calculated. These miRNAs only have a low expression in HepG2 cells with a Ct value that ranged from 33-39 and the average Ct value at 35.8. These miRNAs are a mix of tumour suppressors

and enhancers; there are no miRNA families that only express in HepG2^{Control} just individual miRNAs.

3.16.5 miRNA that only expresses in HepG2$^{shOCLN\ siZO1}$ and HepG2$^{OCLN+\ siZO1}$ cells and does not express in HepG2^{Control} cells.

The miRNA profiles, Table 3.6, are those that have no expression in HepG2^{Control} cells but express in HepG2$^{OCLN+\ siZO1}$ and HepG2$^{shOCLN\ siZO1}$. Data was selected if the expression was <0.25-fold and presented in chronological order.

	HepG2	HepG2$^{OCLN+\ siZO1}$			HepG2$^{shOCLN\ siZO1}$		
		Expression	SEM	P value	Expression	SEM	P value
hsa-miR-22	-	138986.3	40.23	<0.005	169045.5	25.14	<0.005
hsa-miR-98	-	1050.59	4.13	<0.005	434.18	3.36	<0.005
hsa-miR-154	-	145.07	2.36	<0.005	1489.28	4.60	<0.005
hsa-miR-410	-	555.49	3.24	<0.005	216.05	5.37	<0.005
hsa-miR-449	-	4200.79	8.66	<0.005	5838.31	15.95	<0.005
hsa-miR-504	-	21279.30	15.35	<0.005	842.88	4.54	<0.005
hsa-miR-511	-	368.86	4.57	<0.005	14.43	0.42	<0.005
hsa-miR-519e	-	49.20	2.65	<0.005	853.39	4.39	<0.005
hsa-miR-548c-5p	-	67.56	3.26	<0.005	29.55	0.91	<0.005
hsa-miR-642	-	548.71	0.99	<0.005	1149.28	4.39	<0.005
hsa-miR-888	-	20179.08	22.37	<0.005	13885.17	7.97	<0.005

Table 3.6: List of the miRNAs that are not expressed in HepG2^{Control} cells but express in both control variables.

All the miRNAs show a large increase of expression, displayed in Table 3.6, however, due to the miRNA being absent in the HepG2^{Control} cells a small difference in Ct value causes large fold changes. Only three of the miRNAs that are associated with progression of HCC, hsa-miR-410, 511 and 548c-5p, are expressed much higher in HepG2$^{OCLN+\ siZO1}$ than HepG2$^{shOCLN\ siZO1}$ cells.

There are 14 miRNAs that are only expressed in HepG2^{Control} and HepG2$^{OCLN+\ siZO1}$ cells, these miRNAs show no expression in HepG2$^{shOCLN\ siZO1}$, P values <0.005, shown in Table 3.7. Data was selected if the expression was <0.25-fold and presented in chronological order.

	HepG2	HepG2$^{OCLN+\ siZO1}$			HepG2$^{shOCLN\ siZO1}$		
		Expression	SEM	P value	Expression	SEM	P value
hsa-miR-9	1	2.635	0.059	>0.005	0.001	0	-
hsa-miR-23b	1	0.854	0.06	0.16	0.233	0.038	>0.005
mmu-miR-96	1	0.821	0.022	0.01	0.159	0.065	>0.005
hsa-miR-125a-5p	1	0.893	0.079	0.31	0.236	0.026	>0.005
hsa-miR-142-3p	1	1.784	0.049	>0.005	0.003	0	-
hsa-miR-199b	1	536.378	2.375	>0.005	0	0	-
hsa-miR-203	1	0.157	0.046	>0.005	0.008	0	-
hsa-miR-326	1	3.861	0.018	>0.005	0	0	-
hsa-miR-328	1	0.421	0.02	>0.005	0.191	0.08	>0.005
hsa-miR-361	1	0.742	0.045	0.03	0.228	0.05	>0.005
hsa-miR-376c	1	0.79	0.059	0.07	0.001	0	-
hsa-miR-381	1	4.893	0.074	>0.005	0.013	0.039	>0.005
hsa-miR-433	1	1.102	0.2	>0.005	0	0.021	>0.005
hsa-miR-520e	1	0.266	0.02	>0.005	0.027	0.037	>0.005
hsa-miR-520f	1	0.43	0.032	>0.005	0.095	0.048	>0.005
hsa-miR-582-5p	1	1.654	0.021	>0.005	0.179	0.024	>0.005
hsa-miR-629	1	0.814	0.073	0.13	0.159	0.04	>0.005
hsa-miR-616	1	14.093	0.226	>0.005	0.007	0	-

Table 3.7: List of the miRNAs that do not express in HepG2$^{shOCLN\ siZO1}$ cells but express in HepG2^{Control} and HepG2$^{OCLN+\ siZO1}$ cells.

Table 3.7 shows 14 miRNAs that are common to both HepG2^{Control} and HepG2$^{OCLN+\ siZO1}$, all but 5 miRNAs are protective against cancer. Of the 5 miRNAs in both HepG2^{Control} and HepG2$^{OCLN+\ siZO1}$ that aid in cancer progression hsa-miR-9, 96, 328, 376c and 616 there are three with lower expression compared to HepG2^{Control}. Of these three miRNAs hsa-miR-328 was significantly knocked down with P value <0.005. Two of the negative miRNAs showed no significant expression difference against HepG2^{Control}, hsa-miR-96 and 376c P values, 0.015 and 0.007 respectively.

The only negative miRNA with increased expression in hsa-miR-9 with a 2.36-fold increase, P-value 0.001.

The cancer protective miRNAs that only show expression in both HepG2^{Control} and HepG2$^{OCLN+\ siZO1}$ cells all show a significant increase in expression except hsa-miR-520e/f, 629 23b and 125a. Of these 5 miRNAs only 520e/f are significantly knocked down 0.266 and 0.433, P values, <0.005. hsa-miR-199b shows the largest expression increase of the miRNAs present in Table 3.8 with an increase of 536.4fold, P value <0.005, there is no expression was seen in HepG2$^{shOCLN\ siZO1}$.

There are 7 miRNAs that are only expressed in HepG2$^{OCLN+\ siZO1}$ cells and showed no expression in HepG2^{Control} and HepG2$^{shOCLN\ siZO1}$ cells, these are all significantly overexpressed compared to the HepG2^{Control} and HepG2$^{shOCLN\ siZO1}$, P values <0.005, shown in Table 3.8. Data was selected if the expression was <0.25-fold and presented in chronological order.

	HepG2	HepG2$^{OCLN+\ siZO1}$			HepG2$^{shOCLN\ siZO1}$		
		Expression	SEM	P value	Expression	SEM	P value
hsa-miR-299-3p	-	254.72	1.27	<0.005	0.00	0.00	-
hsa-miR-302c	-	136.52	4.31	<0.005	0.00	0.00	-
hsa-miR-411	-	16.88	0.91	<0.005	0.00	0.02	>0.99
hsa-miR-450b-5p	-	379221.8	41.86	<0.005	0.00	0.00	-
mmu-miR-499	-	1996.20	2.32	<0.005	0.00	0.00	-
hsa-miR-518a-3p	-	18.42	0.93	<0.005	0.00	0.00	-
hsa-miR-519c	-	543.44	5.33	<0.005	0.00	0.00	-

Table 3.8: List of the miRNAs that are only expressed in HepG2$^{OCLN+\ siZO1}$ cells.

All the miRNAs show a large increase of expression, however, due to the miRNA being absent in the HepG2^{Control} cells a small difference in Ct value causes large fold changes as with hsa-miR-411 and hsa-miR-518a-3p. However, the other miRNAs listed in Table 3.8, show a marked increase in miRNA expression indicating an

intentional increase in the miRNA expression. The miRNA, hsa-miR-411 is the only miRNA in Table 3.8 that aids in cell proliferation, hsa-mmir-499 and 518a-3p roles are still undefined and all the other miRNA in Table 3.9 have cancer suppressing roles all with P values < 0.005.

3.16.6 miRNA that express in HepG2^{Control} and HepG2$^{shOCLN\ siZO1}$ and do not express in HepG2$^{OCLN+\ siZO1}$.

There are 10 miRNAs that are only expressed in HepG2^{Control} and HepG2$^{OCLN+\ siZO1}$ cells; these miRNAs show no expression in HepG2$^{shOCLN\ siZO1}$, P values <0.005, shown in Table 3.9. Data was selected if the expression was <0.25-fold and presented in chronological order.

	HepG2	HepG2$^{OCLN+\ siZO1}$			HepG2$^{shOCLN\ siZO1}$		
		Expression	SEM	P value	Expression	SEM	P value
hsa-miR-33b	1	0.00	0.00	-	0.86	0.08	0.22
hsa-miR-99a	1	0.20	0.05	<0.005	1.26	0.05	<0.005
hsa-miR-323-3p	1	0.17	0.05	<0.005	0.90	0.04	0.15
hsa-miR-338-3p	1	0.01	0.00	-	6.42	0.08	<0.005
hsa-miR-383	1	0.00	0.00	-	2.68	0.07	<0.005
hsa-miR-505	1	0.00	0.00	-	1.45	0.04	0.01
hsa-miR-509-5p	1	0.09	0.01	<0.005	3.48	0.03	<0.005
hsa-miR-518d	1	0.00	0.04	<0.005	1.16	0.05	0.09
hsa-miR-518f	1	0.10	0.02	<0.005	0.91	0.08	0.38
hsa-miR-548d	1	0.04	0.08	<0.005	0.44	0.04	<0.005

Table 3.9: List of miRNAs that do not express in HepG2$^{OCLN+\ siZO1}$ cells but express in HepG2^{Control} and HepG2$^{shOCLN\ siZO1}$ cells.

Seven of the ten of the miRNAs in Table 3.9, express in both HepG2^{Control} and HepG2$^{shOCLN\ siZO1}$ cells and not in HepG2$^{OCLN+\ siZO1}$ cells show no significant change in expression P values >0.005. Of the remaining three miRNAs, hsa-miR-388-3p and 509-5p are cancer protective.

There are the 16 miRNAs that are only expressed in HepG2$^{shOCLN\ siZO1}$ cells, these are all significantly overexpressed compared to the HepG2^{Control} and HepG2$^{OCLN+\ siZO1}$, P values <0.005, shown in Table 3.10. Data was selected if the expression was <0.25-fold and presented in chronological order.

	HepG2	HepG2$^{OCLN+\ siZO1}$			HepG2$^{shOCLN\ siZO1}$		
		Expression	SEM	P value	Expression	SEM	P value
mmu-miR-187	-	0	0	-	200.11	7.23	<0.005
hsa-miR-193a-3p	-	0	0	-	437.42	7.45	<0.005
hsa-miR-208	-	0	0	-	424.79	6.28	<0.005
hsa-miR-363	-	0	0	-	13.38	0.11	<0.005
hsa-miR-369-3p	-	0	0	-	27.67	0.91	<0.005
hsa-miR-375	-	0	0	-	13.94	0.74	<0.005
hsa-miR-377	-	0	0	-	35062.86	13.54	<0.005
hsa-miR-382	-	0	0	-	447.32	3.74	<0.005
hsa-miR-384	-	0	0	-	7.01	0.09	<0.005
hsa-miR-409-5p	-	0	0	-	56420.95	30.37	<0.005
hsa-miR-487b	-	0	0	-	14.25	0.26	<0.005
hsa-miR-493	-	0	0	-	55.95	0.97	<0.005
hsa-miR-522	-	0	0	-	443.09	5.64	<0.005
hsa-miR-542-3p	-	0	0	-	7.17	0.33	<0.005
hsa-miR-589	-	0	0	-	276.35	6.25	<0.005
hsa-miR-627	-	0	0	-	27.54	1.85	<0.005

Table 3.10: List of miRNAs that are only expressed in HepG2$^{shOCLN\ siZO1}$ cells.

All the miRNAs show a large increase of expression, however, due to the miRNA being absent in the HepG2^{Control} cells a small difference in Ct value causes large fold changes as with hsa-miR-384 and hsa-miR-542-3p. From Table 3.10, 6 miRNAs aid in the progression of cancer (hsa-miR-208, 382, 409-5p, 487b, 522, 627), the other 10 miRNAs either have no seen function or a protective effect against liver cancer.

3.16.7 Expression of miRNAs that are altered in the progression hepatocellular carcinoma.

The miRNAs associated with a poor prognosis in HCC were selected from the review, miRNA in hepatocellular carcinoma. The miRNA was presented as typically upregulated or downregulated (Morishita and Masaki 2015). Their data was compared against expression in HepG2$^{OCLN+\ siZO1}$ and HepG2$^{shOCLN\ siZO1}$, and the results are presented in Figures 3.34, 3.35 and 3.36. miRNAs that have shown to result in a poor prognosis with either an increase or decrease according to Morishita and Masaki 2015 in expression are shown in the Figures 3.34 and below.

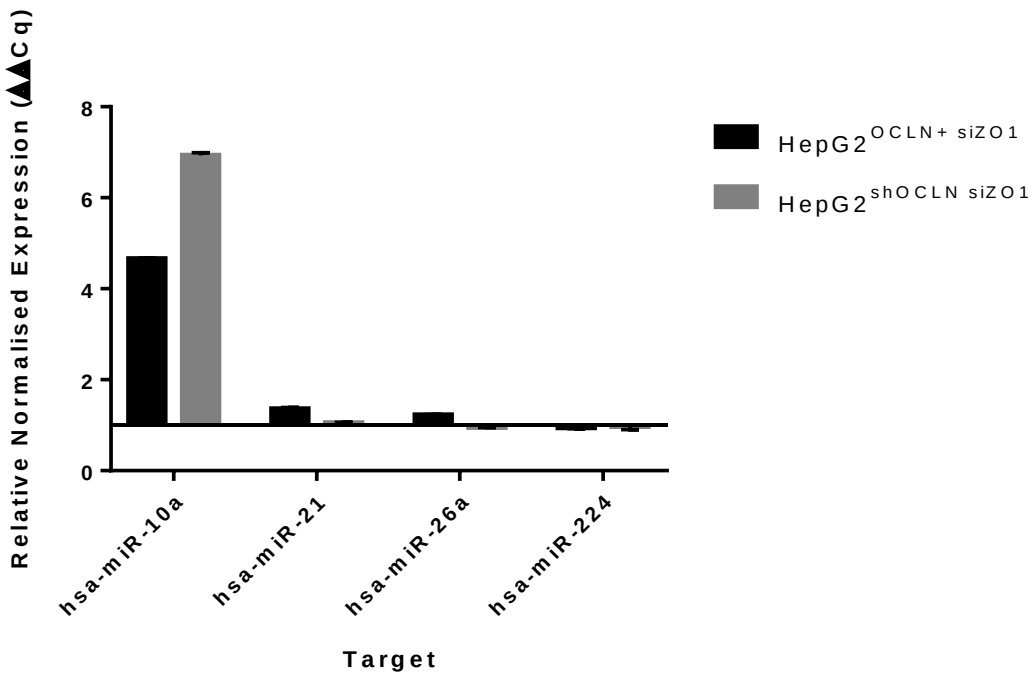

Figure 3.34: The relative expression of the miRNAs that are associated with worse patient outcomes in HCC, it their expression is altered. The cells were cultured for 48 hours post transfection of ZO1 siRNA. Only miR-10a shows a significant increase in expression HepG2$^{OCLN+\ siZO1}$ cells 4.6-fold and HepG2$^{shOCLN\ siZO1}$ cells 9.9-fold, P values <0.001.

Only miR-10a shows a significant change in expression with differential occludin expression and the knockdown of ZO1 with HepG2$^{OCLN+\ siZO1}$ increasing expression 4.6-fold and HepG2$^{shOCLN+\ siZO1}$ increasing expression 6.9-fold, P values <0.001.

3.16.8 Expression of miRNAs that are downregulated in the progression hepatocellular carcinoma.

Of the miRNAs that are associated with the progression of HCC when downregulated are shown in the Figure 3.35.

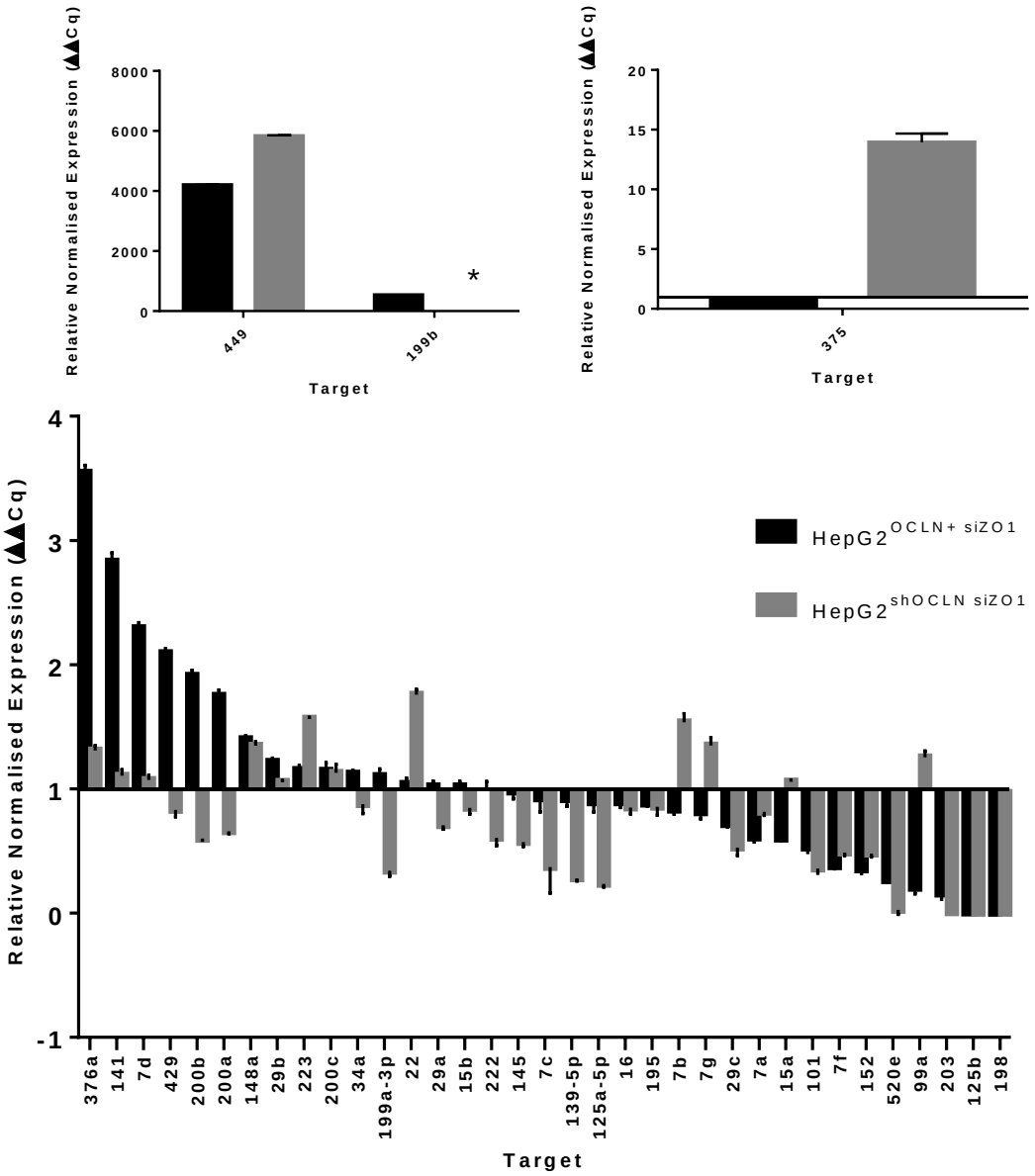

Figure 3.35: The relative expression of the miRNAs that are associated with worse patient outcomes in when expression is decreased in HCC. The cells were cultured for 48 hours post transfection of ZO1 siRNA. Overall 16 of the miRNAs show significant decreased expression in HepG2$^{shOCLN\ siZO1}$ cells whereas HepG2$^{OCLN\ siZO1}$ only decreased the expression of 10. miR-200a and -200b were up regulated in HepG2$^{OCLN+\ siZO1}$ cells but not in HepG2$^{shOCLN\ siZO1}$ cells. The figure was split to account for the large expression changes for miR-449, -199b, -375. * No expression for miRNA 199b in HepG2$^{shOCLN\ siZO1}$ cells.

Out of the 38 miRNAs that are associated with HCC progression when downregulated 10 are upregulated in HepG2$^{OCLN+\ siZO1}$ cells and a further 21 miRNAs show no significant change in expression. Conversely the loss of occludin and ZO1 results in a down regulation of 16 miRNA, however, there is an increase seen with 7 miRNAs. The large increase in expression of targets miR-449 and -199b are due to no expression in HepG2^{control} cells.

The in Figure 3.35 shows, most of the miRNA changes associated with a negative outcome when down regulated in HCC patients occurred in HepG2$^{shOCLN\ siZO1}$ cells. HepG2$^{OCLN+\ siZO1}$ protected against a decrease of miRNAs associated with HCC progression, by upregulating 8 of the miRNAs frequently downregulated in HCC. Occludin overexpression does not protect against the downregulation of 8 of the miRNAs screened possibly due to the knockdown of ZO1. HepG2$^{shOCLN+\ siZO1}$ cells showed an increased expression of miR-7b, -22, 223 and -375 which are typically downregulated during HCC progression.

3.16.9 Expression of miRNAs that are up regulated in the progression hepatocellular carcinoma.

Of the miRNAs that are associated with the progression of HCC, with an increase in expression are shown in the Figure 3.36. The graphs have been split to account for the large expression changes.

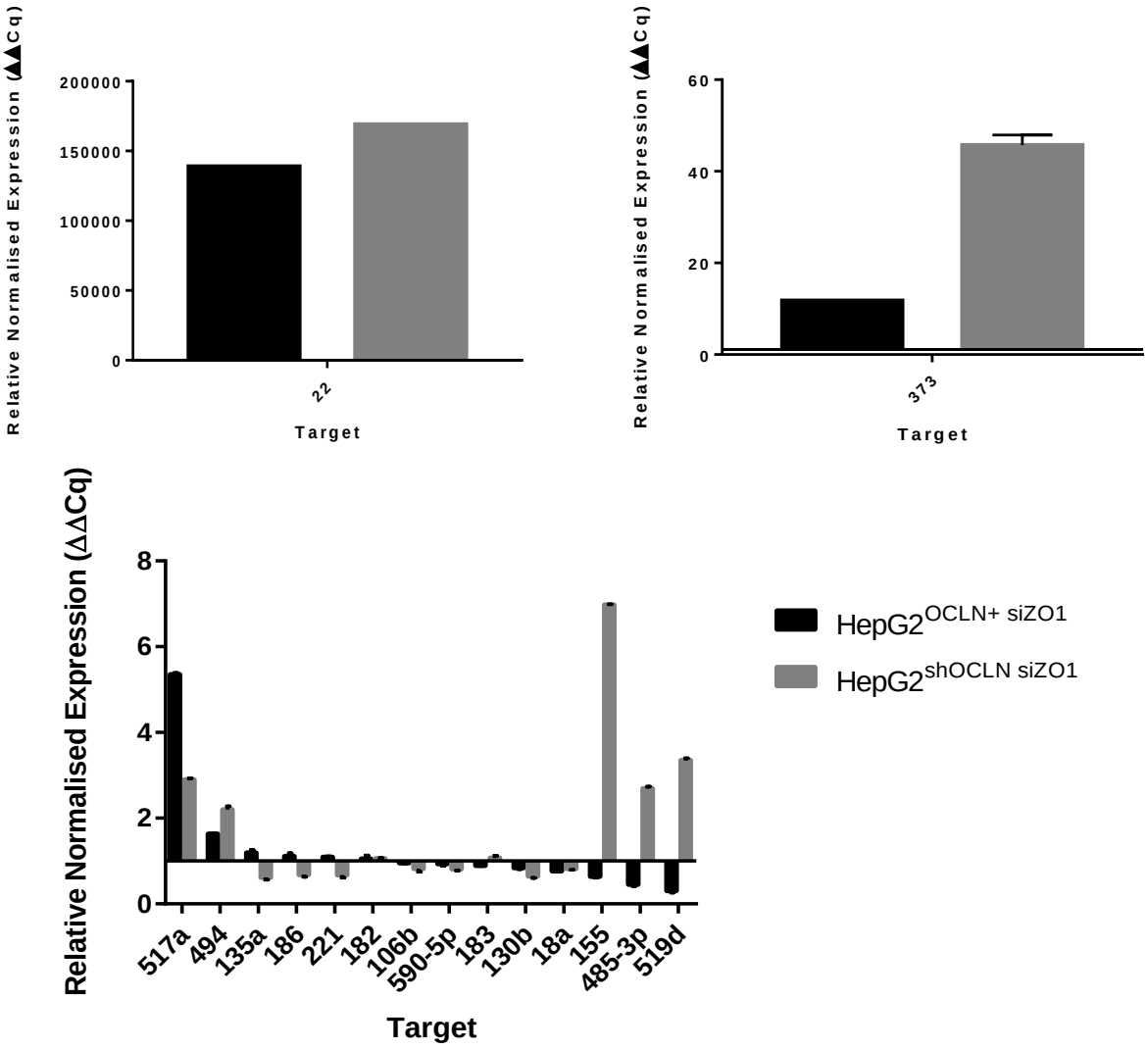

Figure 3.36: The relative expression of the miRNAs that are associated with worse patient outcomes in when expression is increased in HCC. HepG2$^{shOCLN\ siZO1}$ cells significantly increased the expression of 7 of the 15 miRNAs screened whereas HepG2$^{OCLN+\ siZO1}$ were only responsible for the increased expression of 4.

Occludin overexpression with ZO1 knockdown only increases 3 miRNAs associated with a poor prognosis. Occludin and ZO1 knockdown results in the increase of 7 miRNA associated with a poor prognosis. In the 3 miRNAs that were significantly downregulated in HepG2$^{OCLN+\ siZO1}$ cells, hsa-miR-155, 485-3p and 519d, the converse was seen in HepG2$^{shOCLN\ siZO1}$ cells with a significant increase in expression. The large increase in expression of targets miR-22 is due to no expression in HepG2^{control} cells.

This data shows occludin overexpression may protect against the effects on ZO1 knockdown in the HepG2 cell model, of the 16 miRNA genes that are typically down regulated in hepatocellular carcinoma only 4 are significantly downregulated with occludin overexpression with ZO1 knockdown.
Interestingly HepG2$^{OCLN+\ siZO1}$ invoked an increase of 5 out of the 16 miRNAs that HepG2$^{shOCLN\ siZO1}$ cells upregulated. Furthermore, HepG2$^{shOCLN\ siZO1}$ cells also upregulated 7 miRNAs normally associated with downregulation in HCC.

3.16.10 Interpretation of changes miRNA expression between HepG2$^{OCLN+\ siZO1}$ and HepG2$^{shOCLN\ siZO1}$.

Changes in occludin expression with knockdown of ZO1 in the HepG2 cell model invoked changes in miRNA expression. HepG2$^{OCLN+\ siZO1}$ cells showed no miRNA response or no change in 42/55 of the miRNAs selected for analysis, this clearly shows occludin overexpression is protective in HepG2 cells even when ZO1 is knocked down. Overall there were 55 miRNA targets that were highlighted to be influential in the progression of hepatocellular carcinoma. The HepG2$^{shOCLN\ siZO1}$ cell

model showed an increase in 7 of the 16 miRNAs chosen that a typically upregulated in HCC progression and downregulated in 16 of the 39-miRNA assessed that are typically downregulated in HCC.

3.17 Interpretation of results

The differential expression of occludin did not alter the expression of other tight junction related proteins significantly, however, there were differences in the expression of epithelial and mesenchymal cell markers, Figure 3.5. Knockdown of occludin decreased E-cadherin expression to 0.33-fold expression and increased vimentin expression 1.62-fold. HepG2 cells with occludin overexpression downregulated E-cadherin and vimentin expression 0.33-fold and 0.5-fold expression. HepG2 overexpressing occludin “switched” from E-cadherin to N-cadherin expression increasing N-cadherin expression 1.85-fold whereas knockdown occludin in HepG2 cells has no effect on N-cadherin expression.

The change in the HepG2 cells gene expression with differential occludin expression resulted in different morphological changes within the HepG2 cells. HepG2 cells with downregulated occludin expression had increased migration and invasion rates whereas occludin overexpression decreased the rates of invasion and migration. To understand how differential occludin expression resulted in the morphological changes displayed cell polarity assays were used. In areas of high cell density there was no change in cell polarity whereas in areas of low cell density occludin knockdown HepG2 cells did not generate polarity.

In HCC the downregulation of occludin is associated with the downregulation of ZO1 and ZO2. However, as figure 3.16 shows there is no significant change in mRNA of

occludin the knockdown of ZO1 and ZO2. The regulation of occludin is through its phosphorylation, which it loses during ZO1 and ZO2 knockdown.

The expression of EMT related genes SNAIL2, ZEB2 and TWIST1 was increased in HepG2 cells silenced for occludin combined with silenced ZO1 and ZO2 exhibited increased migration and invasion. HepG2 cells with occludin overexpression partially protected the against increased migration and invasion by not upregulating the EMT related genes, Figure 3.18, as such the invasion and migration rates were much low than knockdown occludin/ZO1/ZO2 cells.

Immunofluorescence investigations showed occludin overexpression forming cellular aggregates within the cells, Figure 3.29, they also form in knockout ZO1 and ZO2 cells. ZO1 localisation is not affected by occludin overexpression but does lose its ring formation with the loss of occludin. ZO2 will dual localises to the nucleus as well as more specific adhesion location. Silencing of ZO2 appeared to redistribute occludin along the edge of cellular contacts rather than maintaining the classical occludin hepatocyte localisation, Figure 3.31. The overexpression of ZO2, Figure 3.32, showed that ZO2 overexpression had little effect in overexpressing cells, however when occludin or ZO1 expression is silenced ZO2 becomes more localised at the tight junction, this may explain why migration and invasion rates were lower in ZO over expressing HepG2 cells Figure 3.24.

4. Discussion

Mortality of hepatocellular carcinoma remains high, even with early diagnosis and treatment, this is due to the capacity of HCC cells to metastasise and the recurrence of disease (Unal et al. 2016). Alterations in tight junction proteins occludin, the claudin family and ZO1/2 have all been implemented in the progression of HCC contributing to the increased hepatocyte metastasis and disease recurrence of HCC (Van Itallie et al. 2009).

Differential occludin expression in HCC has been linked with different outcomes in HCC, most importantly overall survival and the disease-free rate was approximately 2-fold higher in HCC with increased occludin expression (Bouchagier et al. 2014). This provides a need to determine the relationship between occludin, claudins and ZO proteins to provide insight into HCC disease progression to identify potential therapy.

The molecular differences that occur in the HepG2 cell model with differential occludin, ZO1 and ZO2 expression were directly linked to the diverse morphological phenotypes. It is important to note there are functional changes to the tight junctions that occur in hepatocytes grown in 2D culture. In a 3D culture hepatocytes form polarized epithelial cell sheets mediated through the generation of tight junctions (Tran et al. 2012). Hepatocytes cultured in this manner are shown to produce bipolar polarity shown through ZO1 staining and reorganise bile canalicular formation (Bierwolf et al. 2016). As such the 3D spheroid culturing of hepatocytes produced an experimental model that better resembles hepatocyte function *in vivo.*

4.1 ZO1 and ZO2 do not regulate occludin expression but rather the occludin activation state.

Gene expression investigations into the independent silencing of occludin or ZO1/2 does not significantly downregulate the mRNA expression of the other two genes,r. Figure 3.16 shows that occludin, ZO1 and ZO2 do not regulate the mRNA expression of each other however, Table 3.3 shows, ZO1 and ZO2 regulate occludin activation state.

Although there is no change in mRNA expression in occludin, ZO1/2 with independent silencing, there are diverse phenotypic alterations that occur especially related to migration and invasion; this complements the previously mentioned investigations with MDCK cells (McNeil et al. 2006; Van Itallie et al. 2009; McNeil et al. 2006). This led to the assumption regulation of tight junction proteins must occur at the protein level.

Currently, there is no literature directly linking ZO1/2 to the regulation of occludin phosphorylation. Knockdown of ZO1 and ZO2 reduced hyper Ser/Thr phosphorylation of occludin in a quiescent monolayer Table 3.3. After tight junction disruption PP2A dephosphorylates phosphorylated Thr residues and PP1α dephosphorylates pSer residues of occludin (Dörfel et al. 2013).

Dephosphorylation of occludin through ZO protein disruption has not been evaluated in hepatocytes until now but has been shown in Caco2 cells. Caco2 cells incubated with EGTA disrupts occludin/ZO binding and caused redistributed protein localisation. Pull-down assays confirmed occludin had become dephosphorylated as a result of the tight junction disruption (Seth et al. 2007). ZO protein disruption of the

tight junctions in hepatocytes may induce the same dephosphorylation response of PP2A and PP1α.

Occludin and claudins bind to SH3-hinge-GuK domain of ZO proteins coupling them to the perijunction cytoskeleton, this stabilises the tight junction a loss of either protein causes TJ disruption which is utilised in the progression of HCC (Van Itallie et al. 2009).

4.2 Loss of occludin is adequate to invoke increased migration and invasion but simultaneous ZO1-2 knockdown increases migration and invasion rates further.

Measuring cell migration into a cell-free gap does not distinguish between cell motility and proliferation; therefore the proliferative effects associated with changes in occludin expression must be taken into consideration (Glenn et al. 2016).

In MDCK occludin is internalised into the cell before cells migrate in wound healing assays; it appears the same process is seen in hepatocyte cell migration (Fletcher et al. 2012). HepG2 cells with silenced occludin expression had elevated migration rates compared to the control, Figure 3-17. HepG2 cells with occludin and either ZO1/2 knockdown showed higher rates of migration into the cell free gap than HepG2 cells with only occludin knockdown.

Knockdown of occludin in the HepG2 cell model increased cell migration and invasion but did not reduce overall cell polarity significantly. The high rate of cell migration into the cell-free gap when occludin expression in HepG2 cells was silenced could be attributed to increased proliferation. The knockdown of occludin reduces contact inhibition of proliferation, in hepatocytes, this occurs through

regulation of the Hippo signalling pathway. The Hippo pathway inhibits cell proliferation and survival through contact inhibition through YAP sequestration. YAP is a transcriptional regulator for genes responsible for cellular proliferation and apoptosis resistance (Wang et al. 2013). Angiomotin and endotubin compete for YAP binding; angiomotin sequesters YAP at the membrane and endotubin translocates YAP to the nucleus. In confluent epithelial cells, endotubin interacts with occludin at the tight junction and cannot compete with angiomotin for YAP binding (Cox et al. 2015). Furthermore, occludin overexpression can reverse dysregulation of cell contact inhibition this suggests occludin is integral for cell contact proliferation inhibition (Li and Mrsny 2000).

In the HepG2 cell model silencing of occludin did not alter cell polarity significantly, although there was reduced polarity in areas of low cell density. Proliferation and invasion may increase in regardless of cell polarity as silenced occludin would not sequester YAP at the tight junction. The increased migration and invasion can be attributed to cellular dedifferentiation.

HepG2^{shOCLN} and HepG2$^{shOCLN\ siZO1}$ cells PCR analysis showed there was a 42 % decrease in ZO2 expression, P value >0.05. Protein localisation of ZO2 in these cells show cytoplasmic staining for ZO2.

ZO2 that is perturbed from the tight junctions it translocates to the nucleus to form a transcriptome (Tapia et al. 2009). After EGF treatment in sparse cell culture PI3K activates AKT signalling. Downstream signalling from AKT phosphorylates SRPK which in turn phosphorylates ZO2. Further phosphorylation by PKCε and

O-GlcNAcylation of ZO2 in the nucleus induce exportation of ZO2 into the cytoplasm. Stabilisation of O-GlcNAc transferase by PUGNAc targets ZO2 for proteasome degradation (Quiros et al. 2013). Although this demonstrates ZO2 degradation after EGF signalling parallels can be made from tight junction disruption through occludin and ZO1 silencing. In Figure 3.30, HepG2^{siZO1} reduced junctional specificity of ZO2 however HepG2^{shOCLN} and HepG2$^{shOCLN\ siZO1}$ showed non-specific ZO2 immunofluorescence. This suggests the downregulation of occludin completely perturbs junctional ZO2 in HepG2 cells which may lead to ZO2 degradation.

4.3 Increased occludin expression partially protects against changes of protein localisation when ZO1/2 was knocked down in HepG2 cells.

Differential expression of occludin resulted in different localisation of ZO1 and ZO2. Occludin undergoes continuous endocytosis and degradation to maintain the tight junction steady state (Fletcher et al. 2014). Regulation of tight junction proteins through this manner provides extra regulatory protection for the tight junction. However, it can be exploited during cancer progression (Utech et al. 2010). Endocytosis of tight junction proteins through the Rab13 pathway results in occludin recycling or degradation of the internalised occludin via E3 ubiquitin-ligase Itch (Mutakami et al. 2009).

The Rab13 endocytosis pathway regulates clathrin-dependent endocytosis of occludin in epithelial cells, inhibition of this pathway causes an accumulation of intracellular occludin (Ioannou et al. 2016). Although the Rab13 pathway is not inhibited in the HepG2 cell model, the Rab13 pathway is continuously internalising

and recycling the excess occludin resulting in the intracellular aggregates seen in, Figure 3.29 and Figure 3.31 (Ioannou and McPherson 2016).

Occludin that is internalised in this manner does not localise to classical recycling endosomes but instead accumulates in intracellular storage compartments generating the aggregates seen. This creates a pool of paracellular membrane proteins that can be rapidly reinserted into the plasma membrane. Typically, the pool of paracellular membranes is minimal in a quiescent epithelial cell monolayer but as occludin can rapidly shift from a pool of paracellular membrane proteins to the paracellular membrane it is likely occludin regulates epithelial polarity and tight junction integrity (Morimoto et al. 2005; Fletcher et al. 2014).

Furthermore, cytoplasmic aggregates of occludin reverse the resistance of apoptosis in cells slowing proliferation. After disruption of tight junction cytoplasmic occludin forms a complex with death-inducing signalling complex (DISC) through the adaptor molecule FADD (Beeman et al. 2009).

The pool of occludin that is only present in HepG2^{OCLN+} cells might explain the difference in migration and invasion rates with differential occludin expression. Knockdown of ZO1 and ZO2 did not increase the motility of HepG2^{OCLN+} cells but did increase the invasiveness. The loss of ZO1/2 in knockout HepG2 cells exposes the occludin E3 binding site to allow degradation rather than recycling of occludin in the HepG2^{Control} cells. This demonstrates how knockout ZO1/2 cells perturbed occludin localisation creating a more invasive cancer cell behaviour similar to knockdown occludin.

The difference in 3D invasion and 2D migration with occludin overexpression with ZO1/2 knockdown can be attributed to the different localisation of occludin. In 3D cultures hepatocytes localise occludin along multiple apical domains similar to occludin localisation *in vivo*, this re-localisation of occludin may reduce the cellular pools of occludin (Molina-Jimenez et al. 2012).

4.4 ZO2 overexpression can partially rescue the occludin knockdown phenotype but cannot rescue the knockdown of the ZO1 phenotype.

ZO2 overexpression did not alter cellular polarity compared to $HepG2^{control}$. ZO2 overexpression reduced migration into the cell-free gap when occludin or ZO1 was knocked down.

Immunofluorescence staining of ZO2 in knockdown occludin or ZO1 cells reveals dual location of ZO2. This suggests that rather than stemming migration ZO2 is trafficked to the nucleus to provide its antiproliferative function by inhibiting Cyclin D1 by Cyclin D1 proteasome degradation (Oka et al. 2010; Gonzalez-Mariscal et al. 2009). ZO2 overexpression did not reduce migration/proliferation in $HepG2^{ZO2+\ shOCLN\ siZO1}$ cells suggesting reduced transcriptional activity ZO2. Immunofluorescence staining of ZO2 showed no subcellular ZO2 localisation agreeing with the theory of reduced transcriptional activity.

This could elucidate why knockdown occludin with ZO2 over expression reversed the invasive cancer cell behaviour of occludin knockdown cells but did not have an effect over ZO1 knockdown cells Figure 3.24.

4.4.1 Downregulation of ZO1 and ZO2 expression mediates a more migratory and invasive cancer cell behaviour.

Knockdown of ZO1/2 in HepG2 cells showed no staining of MRP2 in areas of low density suggesting a loss of cellular polarity Figure 3.26 and 3.27. If both ZO proteins are knocked down no tight junction strands are formed. This is because ZO proteins mediate the generation tight junction formation through occludin/claudin polymerisation (Umeda et al. 2006).

HepG2^{shOCLN} and HepG2$^{shOCLN\ siZO1}$cells grew more commonly in areas of low cell density, this can be seen in the invasion assay. This reflects the changes that occur during cancer metastasis and invasion through the ECM (Sharif et al 2015). During cancer progression there is a global downregulation of miRNAs, the tumour-supressing Hippo pathway regulates miRNA biogenesis in a cell-density-dependent manner (Mori et al. 2014). This may allude to why HepG2^{shOCLN} and HepG2$^{shOCLN\ siZO1}$ cells had increased invasive potential, Figures 3.6 and 3.22. Furthermore it could explain Figure 3.35, why HepG2$^{shOCLN\ siZO1}$ cells, showed a decrease in 16 out of 38 miRNAs known to have poor patient outcomes when down regulated.

In areas of high cell density, the correct localisation of ZO1/2 facilitates the polymerisation of claudins in the tight junction through the binding of their PDZ1 domain. If either ZO1 or ZO2 is independently down regulated there is protein compensation due to their overlapping functions and tight junction strands can still form. In areas of low cell density however, this does not occur (Umeda et al. 2006)

Correctly localised occludin, ZO1 and ZO2 are responsible for the regulation of the epithelial phenotype. Cytoskeletal proteins ZO1/2 as previously described are not just cytoskeletal adaptors for the occludin, claudin and JAM but regulate gene transcription as well. ZO1 and ZO2 share functional homology with regards to cellular adhesion the process of gene transcription regulation is different (Nie et al. 2009; Bauer et al. 2010; Nomme et al. 2011).

The MRP2 polarity assay on the HepG2 cell model with knockdown ZO1 displayed different levels of polarity across the cell surface. In areas of low HepG2 cell density, MRP2 staining was not present, Figure 3.26. In areas of low density when ZO1 expression is downregulated the expression of YBX3 is upregulated, moreover, if the cellular density is low YBX3 will pool in the nucleus (Ruan et al. 2014). YBX3 localisation to the nucleus has been shown to correlate with a higher tumour grade in HCC and in fact in a pre-cancerous state of HCC YBX3 nuclear localisation is associated with a poorer prognosis and increased metastasis (Gonzalez-Mariscal et al. 2016).

This effect is reversed with ZO1 overexpression denoting ZO1 can be solely responsible for the regulation of YBX3. ZO1 achieves this regulation when correctly localised, correct ZO1 localisation sequesters YBX3 transcription factor at the tight junction (Gonzalez-Mariscal et al. 2016). The sequestration of YBX3 promotes cellular differentiation and the inhibition of proliferation transcription protecting against the mesenchymal phenotype. YBX3 induces dedifferentiation and cell cycle progression in hepatocytes explains the increased rate of migration in knockdown

occludin, ZO1 and ZO2, Figure 3.22 and 3.23. HepG2 cells with occludin overexpression maintain ZO1 staining after treatment of siRNA ZO1 and had lower rates of migration and invasion. This can be attributed to occludin recycling and the formation of paraceullar membrane pools of proteins (Fletcher et al. 2014).

Occludin and ZO2 overexpression reversed the effects of ZO1 knockdown in motility assays but only partially in invasion assays Figure 3.34. This is likely due to depletion of ZO1 delaying the recruitment of the PATJ and Cdc42 GEF Tuba required for the 3D morphogenesis of tight junctions (Odenwald et al. 2017).
The inhibition of ZO1 binding to occludin in 3D cultures produces multiple apical lumens, therefore, occludin/ZO1 binding is essential in the correct morphogenesis of cellular lumens (Odenwald et al. 2017). As ZO2 overexpression only partially reverses the invasion rates during ZO1 knockdown, this shows ZO1 and ZO2 have overlapping functions but also fundamental differences, which is why the loss of ZO1 still induced morphological changes in ZO2 overexpressing cells (Gonzalez-Mariscal et al. 2010).

Knockdown of ZO2 produces similar rates of migration, invasion and polarity profile to knockdown ZO1, Figures 3.22, 3.23. Unlike ZO1, ZO2 regulates transcription directly by translocating to the nucleus and forming a transcriptome complex (Tapia et al. 2009). Loss of ZO2 expression promotes proliferation and motility whereas nuclear and junctional ZO2 inhibit motility and proliferation (Qiao et al. 2014). This is important because knockdown of ZO2 protein would mean there is a loss of cell proliferation regulation and motility.

When ZO2 is only localised to the tight junction, cells do not constitutively proliferate. Proliferating cells that are transitioning from G0-G1 phase relocalise ZO2 to the nucleus. The overexpression of occludin promotes more specific ZO2 localisation at the tight junctions suggesting a non-proliferative monolayer, even when the cells are sparse, Figure 3.31. HepG2^{OCLN+} cells reduced migration and invasion compared to HepG2^{control} and HepG2^{shOCLN}. HepG2$^{OCLN+\ siZO1}$ cells showed dual localisation of ZO2 in the HepG2 cell model, this provided both adhesion and transcriptional regulation over proliferation and migration associated with increased YBX3 activity. ZO2 regulates YBX3 activity inhibiting its function and thus decrease cellular proliferation (Huerta et al. 2007).

In sparse or readily proliferating cells ZO2 has dual localisation at the tight junction and in the nucleus (Tapia et al. 2009). Nuclear ZO2 interacts binds to c-myc E-box promotor and Siamois; this inhibits cell cycle progression through binding to downregulating cyclin D1 and inhibits the Wnt pathway (Balda and Matter 2009). The nuclear localisation of ZO2 also shuttles YAP, which is associated with cell proliferation and survival. However, ZO2 bound YAP inhibits any proto-oncogenic properties of YAP when translocating to the nucleus (Liu et al. 2012).

4.5 Increased expression of EMT transcription factors with occludin, ZO1 and ZO2 knockdown in HepG2 cells.

Hepatocellular carcinoma with elevated levels of TWIST1, SNAIL and ZEB expression is associated with poor prognosis and increased migration and invasion (Nagai et al. 2016). The independent knockdown of occludin, ZO1 and ZO2 overall did not result in large expression changes in the EMT associated transcription

factors as shown in, Figure 3.18. Occludin overexpression in HepG2 reduced the expression of the EMT transcription factors even when ZO1 and ZO2 was expression was silenced. Occludin and ZO1 silencing in combination resulted in the largest increases in all three EMT genes.

Classic tumour EMT transcription factors SNAIL, ZEB and TWIST are shown to work in tandem to promote tumour dissemination (Casas et al. 2011). The transcription factors promote EMT associated genes while suppressing epithelial genes. Supressed genes such as E-cadherin and β-catenin were downregulated in 62 % and 51.5 % of primary liver cancers respectively. This correlates with TWIST and SNAIL expression in primary liver cancers with 56.9 % and 80.9 % respectively (Yang et al. 2009; Jianni et al. 2016). Gene expression profiles of the EMT genes with differential occludin expression and the knockdown of ZO1/2 showed a significant increase in the EMT transcription factors, Figure 3.18 (Matsuo et al. 2009; Lan et al. 2016; Qi et al. 2016).

TWIST1 expression was highest in knockdown occludin cells with a combined knockdown of ZO1 or ZO2. Occludin and ZO1 simultaneous knockdown in HepG2 cells increased TWIST1 expression nearly 8-fold. The knockdown of ZO1/2 independently without changes in occludin expression still invoked and an increase of 4 and 2-fold. Interestingly, knockdown of occludin independently did not significantly alter TWIST1 expression, suggesting occludin silencing alone may to be sufficient enough to produce TWIST1 mediated cellular dedifferentiation (Matsuo et al. 2009). Well-differentiated hepatocellular HCC lines, such as HepG2 cells in a quiescent monolayer have low expression of TWIST and undifferentiated HCC lines high levels of ectopically expressed TWIST. When TWIST expression is induced in a

differentiated hepatocellular carcinoma cell line resembled undifferentiated cells (Matsuo et al. 2009). This suggests a knockdown of ZO1/2 resulting in increased TWIST1 expression would cause a loss of cellular differentiation leading to the motile phenotype displayed. TWIST overexpression in HCC cell lines does not promote proliferation, so the upregulation of TWIST1 expression is directly linked to the motile phenotype displayed.

SNAIL2/Slug has a functional role in haematopoietic stem cells derived from foetal liver and bone marrow but is upregulated in the progression of HCC. Generally SNAIL2 does not show significant mRNA expression changes with knockdown of ZO1/2 or overexpression of occludin. Only HepG2 cells silenced occludin and concurrent occludin/ZO1 knockdown displayed increased expression of SNAIL2. SNAIL2 overexpression in HepG2 cells increases cell proliferation, invasion and migration. Furthermore, SNAIL2 overexpression is directly linked to the upregulation of $CD133^{+}$ population in a HepG2 cell culture (Sun et al. 2014). The increased expression of SNAIL2, in $HepG2^{shOCLN\ siZO1}$ and $HepG2^{siZO1}$ cells would result in an increase the level of the $CD133^{+}$ population which would show occludin and ZO1 are important for maintaining cell differentiation. Within the HepG2 cell model this means that there are a proportion of cells that have stemness generated during dedifferentiation, the result in the liver during HCC would be a lower prognosis and increased chance of EMT and metastasis (Chan et al 2014).

Increase of ZEB2 mRNA was displayed in $HepG2^{shOCLN\ siZO1}$ cells, Figure 3.18. Increased expression of ZEB2 is initiated through three mechanisms a cytokine response, activation of the Wnt/β-catenin or Ras/ Mitogen-activated protein kinases

(MAPK) pathways. ZEB2 is a SMAD2 binding protein, the SMAD2/ZEB complex translocates to the nucleus and inhibits transcription of epithelial associated genes such as E-cadherin. Furthermore, increased ZEB2 expression results in the transcription of genes that are present in a mesenchymal cell such as vimentin (Browne et al. 2010). This could elucidate why HepG2$^{shOCLN\ siZO1}$ cells had decreased E-cadherin expression and increased vimentin expression, Figure 3.19.

The miRNA assay was used to elucidate how ZEB2 mRNA expression increased in HepG2$^{shOCLN\ siZO1}$ cells. ZEB2 expression is supressed by a variety of miRNAs such as the miR-200 family. HepG2$^{OCLN+\ siZO1}$ had approximately 3-fold higher expression of the miR-200 family than HepG2$^{shRNA\ siZO1}$ cells, this would explain the differences in ZEB2 expression in differential occludin HepG2 cell lines Figure 3.35 (Renthal et al. 2010).

The miRNA miR-139-5p regulates ZEB2 expression in hepatocytes (Qiu et al. 2015); the expression of miR-139-5p was not altered in HepG2$^{OCLN+\ siZO1}$and PCR data shows ZEB2 expression did not change. HepG2$^{shOCLN\ siZO1}$ cells downregulated miR-139-5p and therefore lost the regulation of ZEB2, as a result there was increased expression of ZEB2.

4.6 Gene expression analysis elucidates the morphological changes in the HepG2 cell model.

CLDN-1 did not show any difference in mRNA expression between all model cell lines, seen in Figure 3.19, 3.20 and 3.21. This does not mean CLDN-1 did not have a functional role in promoting the motile and invasive cancer cell behaviour.

Upregulation or a downregulation of CLDN-1 results in a more motile phenotype in hepatocytes, this shows that is not the expression of CLDN-1 that is important but its localisation (Stebbing et al. 2013). ZO1 is essential for correct localisation and polymerisation of occludin with CLDN-1/-2. CLDN-1/-2 formation of TJ stands is mediated through ZO protein PDZ1 domain binding to occludin and the SH3-GUK hinge binding to claudin (Tsukita et al. 2009). As such a knockdown of ZO1 in MDCK cells perturbs CLDN-1/2 localisation (Rodgers et al. 2013). However, CLDN-1 is overexpressed in 85 % of HCC cases and had low or weak expression in 13 % of HCC cases (Bouchagier et al. 2014). Further investigations between occludin and CLDN-1 by creating a differential CLDN-1 expressed HepG2 cell model would be needed to fully understand if expression of CLDN-1 has any influence when occludin and ZO protein expression is altered.

Gap junction expression was assessed using PCR analysis for Gap junction alpha-1 protein commonly known as connexin43 (GJA1). The expression of connexin43 showed no change in all cell lines. In metastatic HCC connexin43 expression is increased and has been shown to promote malignancy by inhibiting cell-cell communication (Zhang et al. 2007). HepG2 cells with knockdown occludin and ZO1/2 are the most invasive cancer cell behaviour and grow in a low cell dense manner. As connexin43 expression did not increase, it suggests there is no need to generate inhibition of cell-cell communication as it is already been inhibited through growing in low cell density.

Expression of E-cadherin and vimentin are used as a tool to assess EMT in cancers (Mani et al. 2008). During cancer progression and EMT it has been noted that there

is a switch from E-cadherin to N-cadherin which promotes a mesenchymal phenotype (Araki et al. 2011). However, in HCC this is not the case an increased expression of N-cadherin is associated with decreased metastatic potential and improved prognosis (Zhan et al. 2012; Liu et al. 2015). Figure 3.5 shows, expression of E-cadherin was not altered in HepG2 cell models with knockdown ZO1/2 in all other cell lines E-cadherin was notably downregulated, shown in Figures 3.19, 3.20 and 3.21. Occludin and ZO2 over expressing cell lines showed an increase in N-cadherin and decrease in vimentin whereas occludin knockdown showed the converse.

Figure 3.20 shows that knockdown of ZO2 in HepG2 cells mediates the E-cadherin to N-cadherin switch but does not upregulate vimentin. Figure 3.18 showed that the knockdown of ZO2 did not increase the expression of SNAIL2 and ZEB2 but did increase the expression of TWIST1 2.84-fold. This data taken together would imply that HepG2 cells with ZO2 knockdown do not fully undergo EMT, instead they would become metastable cells. A metastable cell is in a dynamic balance between epithelial and mesenchymal phenotypes, these cells have been shown to be able to initiate many of the pathways that are involved in cancer (Cicchini et al. 2015).

Knockdown occludin HepG2 cells had decreased E-cadherin expression and did not change N-cadherin expression. Conversely ZO2 and occludin overexpression had decreased E-cadherin expression but switched to N-cadherin expression. HepG2^{OCLN+} and HepG2^{ZO2+} increased N-cadherin expression by approx. 2-fold, knockdown of ZO1/2 did not change N-cadherin expression in HepG2^{OCLN+} and HepG2^{ZO2+}cells. Silenced occludin, ZO1 and ZO2 do not “switch” to N-cadherin expression and this can be seen in the vimentin expression. The switch of E to N

cadherin is associated with the increased expression of mesenchymal marker vimentin (Onder et al. 2008). Increased vimentin expression is associated with a much higher likelihood of HCC metastasis and is can elucidate why HepG2 cells with silenced occludin and ZO1 in combination where much more invasive (Zhai et al. 2014).

The invasion and migration rates in the HepG2 cell model directly associate with the expression of these three genes. The least invasive/migratory cell HepG2^{OCLN+} had a 1.85-fold increase in N-cadherin expression and 0.5-fold expression of vimentin. The most migratory phenotype HepG2$^{shOCLN\ siZO1}$ had a decrease in E-cadherin expression 4-fold and an increase in vimentin 2-fold.

4.7 Expression of miRNA families show knockdown of occludin and ZO1 promotes cancer HCC progression.

The let-7 family, consisting of 7a/b/c/d/f/g, is a tumour suppressive miRNA and is downregulated in hepatocellular carcinoma and levels of the let-7 family are significantly lower in HepG2 cells than immortalised liver cell lines (Wang et al. 2011). Although the tumour suppressive mechanisms of the let-7 family have not been elucidated it is known that they are responsible for inhibiting the oncogenes Ras and c-Myc which are responsible for increased proliferation in HCC (Chang et al. 2009; Ji et al. 2010; Kaposi-Novak et al. 2009; Aravelli et al. 2008). The let-7 family and c-Myc are in a regulatory balance with over each other so a decrease in one will result in the increase of the other. Increased expression of c-Myc in HepG2

cells causing a downregulation of the let-7 by binding to their E-box 3 domain (Wang et al. 2011).

Figure 3.35 shows, that in HepG2$^{OCLN+\ siZO1}$ and HepG2$^{shOCLN\ siZO1}$ cells the let-7 cluster was predominantly downregulated. HepG2$^{OCLN+\ siZO1}$ showed significant upregulation for only one member of the family let-7d and HepG2$^{shOCLN\ siZO1}$ displayed significant upregulation of let-7b. This shows expression loss of ZO1 was detrimental to let-7 miRNA protection against proliferation, this could explain the increased migration and invasion rates displayed by these cells. Although let-7b showed increased expression in HepG2$^{shOCLN\ siZO1}$ cells, Figure 3.35, this did not inhibit cell migration. HepG2$^{OCLN+\ siZO1}$ cells had slower migration rates than HepG2$^{shOCLN\ siZO1}$ cells but did not show an increase in let-7b. This may suggest that the migration assay was not influenced by proliferation. Colon cancer associated transcript 1 (CCAT1) is markedly increased in HCC and is a molecular sponge for the let-7 family. An increase of CCAT1 is associated with a poor prognosis of HCC and microvascular invasion (Deng et al. 2015). The work displayed in Figure 3.35 suggests that occludin overexpression can overcome multiple factors of HCC progression other than reducing migration rates.

The miR-15 family is another family of tumour suppressor miRNA consisting of mir-15a/b/c and miR195 (Chung et al. 2010). Decreased expression of the miR-15 family has been attributed to HBx-induced anchorage-independent, growth and apoptosis resistance and low HCC reoccurrence (Chung et al. 2010). Like the let-7 family the miR-15 family expression appears to be downregulated by c-Myc, although the mechanism of regulation is currently unknown (Wu et al. 2011). Another

method of deregulation of the miR-15 family is infection with HBV, but again the method of miRNome reprogramming with HBV infection is poorly understood (Wang et al. 2013).

There was no signification change in expression of the miR-15 family in HepG2^{OCLN+} and HepG2^{shOCLN} cell lines, displayed in Figure 3.35. However, this experimental model does not consider coinfection with hepatitis virus, further research would be needed to see if this family of miRNAs are affected following differential occludin expression.

The miR-200 family in hepatocytes was found to inhibit EMT and hepatocellular carcinoma cell migration, an upregulation of the miR-200 family miRNAs in the advanced stages of HCC has been shown to reduce cancer metastasis. Increased miR-200 family expression in hepatocytes is associated is directly linked to increased expression of H19, miR-141 and miR-429 resulting in a more favourable outcome with HCC (Zhang et al. 2012).

Figure 3.336 showed, HepG2$^{OCLN+\ siZO1}$ had significantly higher expression of miR-200a/b, miR-141 and miR-429 in comparison to HepG2$^{shOCLN\ siZO1}$ and HepG2^{control}. There was no significant difference in in miR-200c between the two test cell lines and control. This suggests occludin overexpression is can be solely responsible promoting decreased metastasis and increased disease outcome.

As shown in Figure 3.36, the miR-29 family consisting of a/b/c, is also a tumour suppressive miRNA family inhibiting oncogenes and apoptosis resistance by

targeting cell division cycle 42 (CDC42), myeloid cell leukaemia sequence 1 (Mcl-1) and phosphoinositide-3-kinase regulatory subunit 1 (PIK3R1) (Fornari et al. 2008; Mott et al. 2007; Park et al. 2009). How miR-29 family become dysregulated in hepatocarcinogenesis and miR-29 function is not currently known in hepatocytes (Xiong et al. 2010).

HepG2$^{OCLN+\ siZO1}$ cells had significantly higher expression of miR-29a/b and no significant change in expression in miR-29c unlike HepG2$^{shOCLN\ siZO1}$ cells that downregulated miR29a/b and did not alter the expression of miR-29c, Figure 3.36. miR29a/c expression are evidently more positively expressed in HepG2$^{OCLN+\ siZO1}$ cells and provides the control of apoptosis and cell cycle progression that is aberrant in HepG2$^{shOCLN\ siZO1}$ cells.

4.7 When occludin and ZO1 are knocked down in the HepG2 cell line miRNAs promote cyclin D1 expression and proliferation.

The cellular processes of apoptosis, proliferation and cell cycle progression are completely different mechanisms for achieving the same objective to increase tumour size (Evan et al. 2001).

Cell cycle progression and proliferation in HCC are controlled by the cyclin family mediated by upstream targets activating cyclin (Mann et al. 2009). Cyclin D is responsible for the expression of S-phase and GS-phase, G_2/M phase proteins and pro-oncogenic signalling through FOXM1 activation (Van Arsdale et al. 2015). The AKT pathway is activated by PIP3, in a normal quiescent epithelia PIP3/AKT activation is inhibited by PTEN (Chen et al. 2009).

The miRNA profile showed miRNAs activating the AKT pathway and downregulating tumour suppressor PTEN in HepG2$^{shOCLN\ siZO1}$. There is partial protection in HepG2$^{OCLN+\ siZO1}$, showing occludin can be protective against cell proliferation. Cyclin D1 and D2 are regulated by miR-26a, miR-195 and miR-520e (Li 2012; Xu et al. 2009; Chen et al.2011). In HepG2$^{shOCLN\ siZO1}$ there was signification downregulation of miR-26a and miR-520e while in HepG2$^{OCLN+\ siZO1}$ the expression was unchanged. The PTEN regulation of the AKT pathway is inhibited by the upregulation of miR-155/miR-519d/mir-494 and a down downregulation of miR-222 (Fornari et al. 2012; Xie et al.2012; Garofalo et al. 2009; Liu et al 2015); these miRNAs displayed the same expression in HepG2$^{shOCLN\ siZO1}$cells. In the occludin overexpressing cells the expression of these miRNA was unchanged.

There is also miRNA regulation upstream and downstream of the Cyclin D pathway that regulates hepatocyte proliferation in hepatocellular carcinoma. Table 4.1, shows miRNA that were associated as important in HCC (Morishita and Masaki 2015) that also have a regulative role on the Cyclin D pathway.

miRNA	Target	Function in HCC proliferation
miR-99a	PLK1	Downstream of Cyclin B1 allowing the progression of G_2/M-phase.
miR-101	Fos	Forms a transcription complex with c-Jun promoting Cyclin D1 expression.
miR-429	Wnt pathway	Activated Wnt pathway produces a transcription complex of CTNNB1 promoting Cyclin D1 expression.
miR-125a/b	Sirtuin7	Sirtuin7 is a transcription factor that inhibits cyclin D1.
miR-221	P27	Cyclin D1 induction of migration requires p27. miR-221 increases p27 activity.
miR26a	Cyclin D2	Activates Cyclin D2 promoting proliferation

(Zhang et al. 2014; Li et al. 2009; Tang et al. 2015; Kim et al. 2013; Fornari et al. 2008; Chen et al. 2011)

Table 4.1: Changes in other miRNA that involve regulation over Cyclin D1 in HCC. The table shows miRNA, its target and the function in cellular proliferation of the target.

In HepG2$^{shOCLN\ siZO1}$cells miR-99a, miR-101, miR-125a/b is negatively expressed promoting a further proliferative state. Interestingly the overexpression of occludin showed a downregulation of these miRNA but did upregulate miR-429 2-fold. As miR-429 inhibits Cyclin D1 upstream the downstream miRNA would not be as effective at exerting their functions regarding Cyclin D1 (Tashiro et al. 2007).

Other miRNAs identified as important in HCC progression aid cell cycle progression and resistance to apoptosis without modulating Cyclin D. Cell cycle progression promoting miRNA, miR-373 via PPP6C a negative regulator of cell cycle control allowing G_2/M phase transition increased in HepG2$^{shOCLN\ siZO1}$ and HepG2$^{OCLN+\ siZO1}$ cells (Wie et al. 2013).

The increased proliferation mediated by miRNA in HepG2$^{shOCLN\ siZO1}$ and HepG2$^{OCLN+\ siZO1}$ cells conforms to the protein localisation, migration and invasion assay results. As described the knockdown of ZO1 relocalises YBX3 to the nucleus which increases cell proliferation through transcription of proliferative genes including Cyclin D1 (Dupasquier et al. 2014). The increased Cyclin D expression and activation mediated through changes in miRNA suggests an increased cell proliferative state. HepG2$^{OCLN+\ siZO1}$ cells regulated upstream Cyclin D1 expression through increased miR-429 expression, this can also be attributed to the loss of ZO1 and increased YBX3 transcription.

In HCC progression the downregulation of miR-203 a regulator of survivin and upregulation of miR-517a a MAPK activator desensitises hepatocytes to apoptosis (Wei et al. 2013; Liu et al 2013). The expression of both miRNAs showed HepG2$^{OCLN+\ siZO1}$ and HepG2$^{shOCLN\ siZO1}$ cells miRNA mediated apoptosis resistance. However, as previously described when occludin is overexpressed in hepatocytes occludin overexpression sensitises the cells to apoptosis through the intracellular aggregates forming a complex with DISC (Beeman et al. 2009). HepG2$^{shOCLN\ siZO1}$ cells do not have occludin apoptosis sensitivity so the miRNA miR-517a and miR-203 would be able to exhibit their apoptosis resistance in hepatocytes.

This data showed that the downregulation of occludin and ZO1 have a negative impact on cell cycle progression and cell proliferation the overexpression of occludin offers some protection by modulating the miRNA profile. The downregulation of ZO1 mediates cell proliferation through YBX3 transcription (Nie et al. 2012), occludin expression appears to have a signalling feature allowing for changes in miRNA to protect against cell proliferation. The downregulation of occludin produces a miRNA profile that shows a dysregulation of cell cycle progression. This could be a determining factor which shows occludin expressing HCC survival and reoccurrence rates 2-fold higher than occludin down regulation (Bouchagier et al. 2014).

4.8 When occludin and ZO1 are knocked down in the HepG2 cell model miRNAs promote invasion and metastasis.

HepG2 cells with knockdown occludin and ZO1 knockdown modulate the miRNA profile to a more metastatic and invasive cancer cell behaviour. Interestingly differential occludin expression and knockdown of ZO1 did not decrease the miRNA expression of the miRNA featured in Table 4.2.

miRNA	Target	Function in HCC proliferation
miR-21	PTEN	Inhibits the Cyclin D pathway upstream by reversing PIP3 phosphorylation.
miR-34a	c-Met	Activates oncogenic pathways such as STAT3 and RAS.
miR-148	Wnt pathway	Inhibits Wnt pathway activity.
miR-135a	FOX1	FOX1 upregulates proliferation
miR-186	Hippo pathway	The hippo pathway regulates cell proliferation, miR-186 inhibits the hippo pathway.
miR-182	TP53INP1	Increased miR-182 upregulates TP53INP1 drug resistance activity.
miR-186	P21	P21 is important mediator of Cyclin D1, miR-186 inhibits this function.

(Meng et al. 2007; Zhu et al. 2012; Tan et al. 2014; Zeng et al. 2016; Ruan et al. 2016; Yau ey al. 2013; Qin et al. 2014)

Table 4.2: miRNA that do not change in expression with differential occludin expression and the knockdown of ZO1. The table shows the miRNA, its target and the function the target has in cellular proliferation.

However, there are miRNAs that have altered expression due to the differential expression of occludin and knockdown ZO1. Although miR-148, a Wnt pathway inhibitor does not display a change in expression 2 other miRNAs important in HCC development do these are miR-152 and miR-198. They are both significantly down

regulated in both HepG2$^{OCLN+\ siZO1}$ and HepG2$^{shOCLN\ siZO1}$ cells the Wnt pathway negatively influences HCC progression promoting cellular proliferation.

A miR-485-3p that inhibits the metastatic protein, metastasis-associated protein 1, an increased expression of metastasis-associated protein 1 increases cellular dedifferentiation and therefore metastasis. The expression of miR-485-3p was upregulated in HepG2$^{shOCLN\ siZO1}$ however with increased expression of the EMT makers TWIST, ZEB2 and SNAI2 the cellular dedifferentiation would still likely occur, Figure 3-18 (Qin et al. 2014).

These data show that differential occludin expression and the knockdown of ZO1 does not modulate the miRNA profile in HCC associated miRNAs with regards to tumour metastasis and invasion. This could be attributed to the loss of cellular adhesion and the resultant proliferation mediating cellular invasion.

4.9 Wider implications for liver disease with differential expression of occludin and ZO2 with ZO1 knockdown.

4.9.1 Progressive familial intrahepatic cholestasis

Inherited mutations in TJP2 can cause progressive familial intrahepatic cholestasis (PFIC), a disorder with a typical onset in children under two years old that leads the development of liver cirrhosis. There are three types of PFIC categorised by which gene has mutated, type 1 the ATP8B1 gene coding for FIC1, type 2 the ABCB11 gene coding for BSEP and type 3 the ABCB4 gene coding for MDR3 (Bosetti et al. 2014). Mutations in ZO2 is now understood to also disrupt hepatobiliary function

similarly to the mutations in ABCB11 and therefore a direct cause of PFIC2 and predispose childhood HCC (Dezsőfi and Knisely 2014; Sambrotta et al. 2014).

Currently it is not known whether the loss of ZO2 attributes towards the disease state or the biliary dysfunction. Here I have not demonstrated that the loss of ZO2 results in HCC, however I have demonstrated a loss in ZO2 influences the disease state negatively. Using the data from Table 3.3 it shows that silencing ZO2 dephosphorylates occludin, the reduced occludin function. This shows that HCC developed through PFIC would be a more invasive cancer cell behaviour especially if occludin or ZO1 become downregulated.

NASH, cholangitis and other liver diseases that can lead to HCC and the role of TJ modulation (Liu et al. 2009). This would need to be explored as to whether decreased occludin expression through these diseases is a trigger for HCC development.

4.9.2 Experimental design improvements.

When occludin is knocked down in HCC does not become completely silenced this is why the shRNA stable downregulation of occludin approach was taken. However limitations occurred due to only being able to create a single knockdown of gene with shRNA in a HepG2 cell, thus the use of siRNA for ZO1 and ZO2. To negate these issues genome editing for knock out could be used, Class 2 Clustered Regularly Interspaced Short Palindromic Repeat (CRISPR).

RNA interference gene silencing is mediated by 20-25 nucleotide double stranded DNA that are transfected in exogenously, siRNA or generated by short hairpin forming precursors, shRNA. siRNA and shRNA forms a complex with RNA-induced

silencing complex (RISC) which unwinds the DNA. The anti-sense strand can now target taget mRNA for endonucleolytic cleavage. When this occurs shRNA have transcriptional repression of the mRNA and siRNA have temporary gene silencing (Rao et al 2009). The issues with siRNA and shRNA are they can have non-specific off target effect resulting in the knockdown of another gene. This is why CRISPR is now being used (Rao et al. 2009).

The molecular mechanism of CRISPR knockout is different to shRNA or siRNA knockdown and results in complete gene silencing. CRIPR contains two components a guide RNA and endonuclease protein cas9. The guide RNA is a short synthetic RNA with a ~20 nucleotide spacer which specific to a target in the DNA and a sequence that cas9 can recognise. The guide RNA and Cas9 form a complex, the guide RNA targets the protospacer adjacent motif and DNA target, this results in a double stranded break. Following the double stranded break there are one of two DNA repair mechanisms activated non-homologous end joining pathway (prone to error) and homology directed repair pathway. This will result in one of four outcomes, the DNA is repaired correctly, insertion, deletion or frameshift. This results in the introduction of premature stop codons in the gene (Ran et al. 2013).

Work with CRISPR has already been started on HCC and TJs, complete occludin knockout restricts HCV entry (Shirasago et al. 2016). Future work involving CRISPR see 4.9.3.

4.10 Final conclusions

In this project occludin was observed to be an important cellular adhesion molecule, however its role on cell signalling was not elucidated and this needs to be

understood to understand how HCC progresses. Further downregulation of ZO1 and ZO2 increased migration and invasion displayed when occludin was also knocked down. This research showed that there is a regulatory function of ZO1 and ZO2 and that occludin phosphorylation would usefully be explored further. Occludin upregulation may be useful to target for therapeutic intervention and may in the future have benefit to subsets of patients with HCC.

4.11 Further research

This PhD project has given insight to the relationship between occludin, ZO1 and ZO2 in hepatocytes. However, there are a few unanswered questions that would be beneficial to answer.

4.11.1 Investigating the relationship between occludin, ZO1 and ZO2 in liver biopsies.

There is currently no research into looking at the expression and activation state of occludin, ZO1 and ZO2 in tandem in HCC patient liver biopsies. Quantification of tumour grade, metastasis and survival rate would allow research to focus in on the clinicopathological features of hepatocellular carcinoma directly responsible from occludin, ZO1 and ZO2.

The regulation of occludin activation state by ZO1 and ZO2 is unknown. Here I draw parallels between disruption of the tight junction when ZO1/2 are knocked down and EGTA disruption of tight junctions (Seth et al. 2007). However, as ZO1 and ZO2 knockdown is associated with diverse phenotypic effects such as overexpression of

EMT transcription factors and increase proliferation, there could be indirect regulation of occludin phosphorylation state.

4.11.2 Mimicry of the tumour microenvironment and coculture with non-parenchymal cells.

The HCC tumour has environmental responses that enact their functions upon the hepatocytes during the progression of disease. These are angiogenesis, inflammation, fibrosis, hypoxia and other cellular components of the tumour environment.

The tumour microenvironment regulates occludin delineated tight junctions. Vascular endothelial growth factor (VEGF) which reduces pseudicanaliculi and TGF-β which dephosphorylates occludin via PP2A. This would be able to investigate if occludin overexpression is as effective with inflammatory signals (Budi et al. 2016; Yang and Poon, 2008).

Investigations into PFIC2 show a correlation between truncating TJP2 mutations and the progression of HCC (Zhou et al. 2015). It is not known whether ZO2 deficiency directly or indirectly causes HCC progression to PFIC2 (Sambrotta and Thompson 2015). The downregulation of ZO2 in the HepG2 cell model increased the migratory/invasive cancer cell behaviour while regulating epithelial/mesenchymal genes. Here I show a downregulation of ZO2 expression can exacerbate a mesenchymal phenotype. I also show ZO2 directly increased the expression of TWIST1 which promotes dedifferentiated cell types, Figure 3.18. Tumorigenesis investigations should be used to ascertain if hepatocytes deficient of ZO2 are solely responsible for the progression of PFIC to HCC.

The loss of Occludin, ZO1 or ZO2 singularly or simultaneously provides a platform for EMT resulting in a more invasive cancer cell behaviour. These results show how stable Occludin expression can reduce hepatocyte motility and invasion. Several further investigations are needed, not into the role of Occludin but into the miRNAs that Occludin overexpressing and knockdown cells had altered. This research gives a novel insight into two miRNA profiles one of a hepatocellular carcinoma cell associated with a poor prognosis and one that reverses the phenotype. This allows for the development of a non-invasive test to for HCC but also a way to establish an idea of hepatocyte cell motility and invasiveness. However, further work should be aimed at using miRNA mimickers and antagomirs on the miRNAs identified. miRNA gene therapy provides an alternative approach to traditional chemotherapy and radiotherapy by correcting the altered regulatory and signalling pathways (Wang and Wu 2009).

4.11.3 Using CRISPR technologies

To further this work CRISPR should be used for investigations involving migration or invasion. The total length of time of a migration or invasion assay is longer than siRNA knockdown, especially during spheroid formation. This was not detrimental as the effects were still seen, however, to be more reliable HepG2 cells would require knockout of occludin and then validate the knockout. This would require PCR amplification, subcloning and then sequencing. Once validated knockout ZO1 or ZO2 and revalidate. This would allow migration and 3D invasion assays to run from start to end point with knockout occludin, ZO1 and ZO2.

4.11.4 Use of primary hepatocytes, induced pluripotent stem cells to investigate the role occludin, ZO1 and ZO2 in patients with HCC and PFIC.

This work did not assess the level of occludin, ZO1 or ZO2 in liver biopsy or primary hepatocytes. Future research would aim to acquire primary hepatocytes from healthy individuals and patients with HCC. This study only evaluated normalised expression of mRNA as HepG2 cells are not indicative of a normal healthy hepatocyte to compare gene expression.

Stem cells from extracted form urine can be reprogramed to produce induced pluripotent stem cells (iPS). These iPS cells can easily be acquired from an individual that is suffering from a disease of the liver and cannot undergo a biopsy procedure (Zhou et al. 2011). Using iPS cells or primary hepatocytes would allow for the quantification of mRNA copy that is indicative of a typical hepatocyte.

First a primer efficiency test would be run, a set of 1:10 serial dilutions of either cDNA or primer would be used to produce a standard curve. A line of best fit would be added to the standard curve, using the equation to the line the primer efficiency can be calculated above 90 % is optimal.

The standard curve PCR should be targeting *in vitro* transcribed RNA to work out quantification. Absorption of the *in vitro* transcribed RNA at 260 nm would give a concentration, using the molecular weight it can be converted into copy number. As the copy number is known and PCR results in a doubling of PCR amplicon. To

compare two mRNA copies of similar efficacy the $2^{-\Delta\Delta CT}$ method can be used if not the Plaffl method would need to be used (Larionov et al. 2005).

4.11.5 Using primary hepatocytes or iPS cells to produce a tissue model system to assess the effect of tight junction disruption.

To model the function of occludin, ZO1 and ZO2 with liver iPS or primary hepatocytes 3D culture should be used. Primary hepatocytes cannot be cultured for long periods of time they begin to differentiate into fibroblasts 3-5 days post initial culture, unless immortalised. By producing a bio-printed 3D model for primary hepatocytes 3 days after initial culture produce albumin and continue to do so for over two week showing retained hepatic function (Kim et al. 2017). This novel research method would be used to model a healthy and disease liver model system. By knocking out occludin, ZO1 or ZO2 it would be possible to assess how tight junction disruption affects the cell or if there is induction of cholestasis.

Immunofluorescence investigations or fluorescently protein knock-in would allow in real time to track the localisation of the protein. This would be beneficial in investigations into the HCC tumour microenvironment. Treatment with cytokines in a 3D model system would allow for real-time viewing of how TJs are disrupted. Using Z-stack imaging a 3D image can be produced to make a 3D image of the cell model system. To further this investigations into HCV entry via CD81/claudin-1/occludin complexes to work out additional binding partners. To achieve this Förster resonance energy transfer microscopy would need to be used.

Bibliography

Abcam (2015) *Immunocytochemistry and Immunofluorescence Protocol Procedure for Staining of Cell Cultures using Immunofluorescence*.: Abcam

Abdel-Misih, S. R. and Bloomston, M. (2010) 'Liver Anatomy'*. Surgical Clinics of North America* 90 (4), 643-653

Adachi, M., Inoko, A., Hata, M., Furuse, K., Umeda, K., Itoh, M., and Tsukita, S. (2006) 'Normal Establishment of Epithelial Tight Junctions in Mice and Cultured Cells Lacking Expression of ZO-3, a Tight-Junction MAGUK Protein'*. Molecular and Cellular Biology* 26 (23), 9003-9015

Agilent Technologies (2013) *Agilent RNA 6000 Nano Kit Guide*. Germany: Agilent Technologies

Aigner, K., Dampier, B., Descovich, L., Mikula, M., Sultan, A., Schreiber, M., Mikulits, W., Brabletz, T., Strand, D., Obrist, P., Sommergruber, W., Schweifer, N., Wernitznig, A., Beug, H., Foisner, R., and Eger, A. (2007) 'The Transcription Factor ZEB1 (deltaEF1) Promotes Tumour Cell Dedifferentiation by Repressing Master Regulators of Epithelial Polarity'*. Oncogene* 26 (49), 6979-6988

Al-Amoudi, A., Castano-Diez, D., Devos, D. P., Russell, R. B., Johnson, G. T., and Frangakis, A. S. (2011) 'The Three-Dimensional Molecular Structure of the Desmosomal Plaque'*. Proceedings of the National Academy of Sciences of the United States of America* 108 (16), 6480-6485

Aleman, S., Rahbin, N., Weiland, O., Davidsdottir, L., Hedenstierna, M., Rose, N., Verbaan, H., Stål, P., Carlsson, T., and Norrgren, H. (2013) 'A Risk for

Hepatocellular Carcinoma Persists Long-Term After Sustained Virologic Response in Patients with Hepatitis C–associated Liver Cirrhosis'. *Clinical Infectious Diseases* 57 (2), 230-236

Aljameeli, A., Thakkar, A., and Shah, G. (2017) 'Calcitonin Receptor Increases Invasion of Prostate Cancer Cells by Recruiting Zonula Occludens-1 and Promoting PKA-Mediated TJ Disassembly'. *Cellular Signalling* 36, 1-13

Ambion (2012) *TURBO DNA-Free™ Kit TURBO™ DNase Treatment and Removal Reagents*. G edn. Carlsbad, California: Thermo Fisher

Ambion (2011) *MirVana™ miRNA Isolation Kit*. Carlsbad, California: Thermo Fisher

Applied Biosystems (2011) *TaqMan® Small RNA Assays TaqMan® MicroRNA Assays TaqMan® siRNA Assays Custom TaqMan® Small RNA Assays Protocol*. Carlsbad, California: Thermo Fisher

Applied Biosystems (2018) *Megaplex™ Primer Pools USER GUIDE for MicroRNA Expression Analysis for use with TaqMan® Array Cards*.: Thermo Fisher

Araki, K., Shimura, T., Suzuki, H., Tsutsumi, S., Wada, W., Yajima, T., Kobayahi, T., Kubo, N., and Kuwano, H. (2011) 'E/N-Cadherin Switch Mediates Cancer Progression Via TGF-Beta-Induced Epithelial-to-Mesenchymal Transition in Extrahepatic Cholangiocarcinoma'. *British Journal of Cancer* 105 (12), 1885-1893

Aravalli, R. N., Steer, C. J., and Cressman, E. N. (2008) 'Molecular Mechanisms of Hepatocellular Carcinoma'. *Hepatology* 48 (6), 2047-2063

Ardito, F., Giuliani, M., Perrone, D., Troiano, G., and Lo Muzio, L. (2017) 'The Crucial Role of Protein Phosphorylation in Cell Signaling and its use as Targeted Therapy'. International Journal of Molecular Medicine 40 (2), 271-280

Baeriswyl, V. and Christofori, G. (eds.) (2009) *Seminars in Cancer Biology*. 'The Angiogenic Switch in Carcinogenesis': Elsevier

Baffy, G., Brunt, E. M., and Caldwell, S. H. (2012) 'Hepatocellular Carcinoma in Non-Alcoholic Fatty Liver Disease: An Emerging Menace'*. Journal of Hepatology* 56 (6), 1384-1391

Bai, D. and Wang, A. H. (2014) 'Extracellular Domains Play Different Roles in Gap Junction Formation and Docking Compatibility'*. The Biochemical Journal* 458 (1), 1-10

Balbuena, P., Li, W., and Ehrich, M. (2011) 'Assessments of Tight Junction Proteins Occludin, Claudin 5 and Scaffold Proteins ZO1 and ZO2 in Endothelial Cells of the Rat blood–brain Barrier: Cellular Responses to Neurotoxicants Malathion and Lead Acetate'. Neurotoxicology 32 (1), 58-67

Balda, M. S. and Matter, K. (2009) 'Tight Junctions and the Regulation of Gene Expression'*. Biochimica Et Biophysica Acta (BBA)-Biomembranes* 1788 (4), 761-767

Balda, M. S. and Matter, K. (2016) 'Tight Junctions as Regulators of Tissue Remodelling'*. Current Opinion in Cell Biology* 42, 94-101

Balda, M. S., Gonzalez-Mariscal, L., Matter, K., Cereijido, M., and Anderson, J. M. (1993) 'Assembly of the Tight Junction: The Role of Diacylglycerol'. *The Journal of Cell Biology* 123 (2), 293-302

Bauer, H., Zweimueller-Mayer, J., Steinbacher, P., Lametschwandtner, A., and Bauer, H. C. (2010) 'The Dual Role of Zonula Occludens (ZO) Proteins'. *Journal of Biomedicine & Biotechnology* 2010, 402593

Bazzoni, G. and Dejana, E. (2004) 'Endothelial Cell-to-Cell Junctions: Molecular Organization and Role in Vascular Homeostasis'. *Physiological Reviews* 84 (3), 869-901

Beeman, N. E., Baumgartner, H. K., Webb, P. G., Schaack, J. B., and Neville, M. C. (2009) 'Disruption of Occludin Function in Polarized Epithelial Cells Activates the Extrinsic Pathway of Apoptosis Leading to Cell Extrusion without Loss of Transepithelial Resistance'. *BMC Cell Biology* 10 (1), 85

Begus-Nahrmann, Y., Hartmann, D., Kraus, J., Eshraghi, P., Scheffold, A., Grieb, M., Rasche, V., Schirmacher, P., Lee, H. W., Kestler, H. A., Lechel, A., and Rudolph, K. L. (2012) 'Transient Telomere Dysfunction Induces Chromosomal Instability and Promotes Carcinogenesis'. *The Journal of Clinical Investigation*122 (6), 2283-2288

Berx, G. and van Roy, F. (2009) 'Involvement of Members of the Cadherin Superfamily in Cancer'. *Cold Spring Harbor Perspectives in Biology* 1 (6), a003129

Bewley, M. C., Tash, B. R., Tian, F., and Flanagan, J. M. (2013) 'A Complex Affair: Attraction and Repulsion make Occludin and ZO-1 Function!'. *Tissue Barriers* 1 (1), 1217-1223

Bierwolf, J., Volz, T., Lütgehetmann, M., Allweiss, L., Riecken, K., Warlich, M., Fehse, B., Kalff, J. C., Dandri, M., and Pollok, J. (2016) 'Primary Human Hepatocytes Repopulate Livers of Mice After in Vitro Culturing and Lentiviral-Mediated Gene Transfer'. *Tissue Engineering Part A* 22 (9-10), 742-753

Bioline (2014) *Tetro cDNA Synthesis Kit Reaction Guidelines*.: Bioline

Bioline (2017) *Protocol for the Isolation of RNA using TRIsure*.: Bioline

Bio-Rad Laboratories (2017) *ITaq Universal SYR Green Supermix*.: Bio-Rad

Bio-Rad Laboratories (2015) *Image Lab Software how to Obtain Stain-Free Gel and Blot Images*.: Bio-Rad

Bio-Rad Laboratories (2016) *Http://www.Bio-Rad.com/webroot/web/pdf/lsr/literature/Bulletin_6376.Pdf*.: Bio-Rad

Blonski, W., Kotlyar, D. S., and Forde, K. A. (2010) 'Non-Viral Causes of Hepatocellular Carcinoma'. *World Journal of Gastroenterology* 16 (29), 3603-3615

Bosetti, C., Turati, F., and La Vecchia, C. (2014) 'Hepatocellular Carcinoma Epidemiology'. *Best Practice & Research Clinical Gastroenterology* 28 (5), 753-770

Bouchagier, K. A., Assimakopoulos, S. F., Karavias, D. D., Maroulis, I., Tzelepi, V., Kalofonos, H., Karavias, D. D., Kardamakis, D., Scopa, C. D., and Tsamandas, A. C. (2014) 'Expression of Claudins-1, -4, -5, -7 and Occludin in Hepatocellular Carcinoma and their Relation with Classic Clinicopathological Features and Patients' Survival'. *In Vivo (Athens, Greece)* 28 (3), 315-326

Brandner, J. M., Poetzl, C., Schmage, P., Hauswirth, U., and Moll, I. (2008) 'A (Leaky?) Barrier: Tight Junction Proteins in Skin Diseases'. *Drug Discovery Today: Disease Mechanisms* 5 (1), e39-e45

Browne, G., Sayan, A. E., and Tulchinsky, E. (2010) 'ZEB Proteins Link Cell Motility with Cell Cycle Control and Cell Survival in Cancer'. *Cell Cycle* 9 (5), 886-891

Bryant, D. M. and Mostov, K. E. (2008) 'From Cells to Organs: Building Polarized Tissue'. *Nature Reviews.Molecular Cell Biology* 9 (11), 887-901

Budi, E. H., Xu, J., and Derynck, R. (2016) 'Regulation of TGF-β Receptors'. *TGF-β Signaling: Methods and Protocols*, 1-33

Burkhart, D. L. and Sage, J. (2008) 'Cellular Mechanisms of Tumour Suppression by the Retinoblastoma Gene'. *Nature Reviews.Cancer* 8 (9), 671

Bustin, S. A., Benes, V., Garson, J. A., Hellemans, J., Huggett, J., Kubista, M., Mueller, R., Nolan, T., Pfaffl, M. W., Shipley, G. L., Vandesompele, J., and Wittwer, C. T. (2009) 'The MIQE Guidelines: Minimum Information for Publication of Quantitative Real-Time PCR Experiments'. *Clinical Chemistry* 55 (4), 611-622

Calkins, C. C. and Setzer, S. V. (2007) 'Spotting Desmosomes: The First 100 Years'. *Journal of Investigative Dermatology* 127, E2-E3

Cao, Y., Chang, H., Li, L., Cheng, R., and Fan, X. (2007) 'Alteration of Adhesion Molecule Expression and Cellular Polarity in Hepatocellular Carcinoma'. *Histopathology* 51 (4), 528-538

Cao, X., Surma, M. A., and Simons, K. (2012) 'Polarized Sorting and Trafficking in Epithelial Cells'. *Cell Research* 22 (5), 793-805

Carulli, L. and Anzivino, C. (2014) 'Telomere and Telomerase in Chronic Liver Disease and Hepatocarcinoma'. *World Journal of Gastroenterology* 20 (20), 6287-6292

Casas, E., Kim, J., Bendesky, A., Ohno-Machado, L., Wolfe, C. J., and Yang, J. (2011) 'SNAIL2 is an Essential Mediator of Twist1-Induced Epithelial Mesenchymal Transition and Metastasis'. *Cancer Research* 71 (1), 245-254

Castello, G., Scala, S., Palmieri, G., Curley, S. A., and Izzo, F. (2010) 'HCV-Related Hepatocellular Carcinoma: From Chronic Inflammation to Cancer'. *Clinical Immunology* 134 (3), 237-250

Chan, A. W., Tong, J. H., Chan, S. L., Lai, P., and To, K. (2014) 'Expression of Stemness Markers (CD133 and EpCAM) in Prognostication of Hepatocellular Carcinoma'. *Histopathology* 64 (7), 935-950

Chang, T. C., Zeitels, L. R., Hwang, H. W., Chivukula, R. R., Wentzel, E. A., Dews, M., Jung, J., Gao, P., Dang, C. V., Beer, M. A., Thomas-Tikhonenko, A., and

Mendell, J. T. (2009) 'Lin-28B Transactivation is Necessary for Myc-Mediated Let-7 Repression and Proliferation'. *Proceedings of the National Academy of Sciences of the United States of America* 106 (9), 3384-3389

Chen, J., Wang, Q., Fu, X., Huang, X., Chen, X., Cao, L., Chen, L., Tan, H., Li, W., and Bi, J. (2009) 'Involvement of PI3K/PTEN/AKT/mTOR Pathway in Invasion and Metastasis in Hepatocellular Carcinoma: Association with MMP-9'. *Hepatology Research* 39 (2), 177-186

Chen, L., Zheng, J., Zhang, Y., Yang, L., Wang, J., Ni, J., Cui, D., Yu, C., and Cai, Z. (2011) 'Tumor-Specific Expression of microRNA-26a Suppresses Human Hepatocellular Carcinoma Growth Via Cyclin-Dependent and-Independent Pathways'. *Molecular Therapy* 19 (8), 1521-1528

Chen, Y. W., Li, C. H., Zhang, A. Q., Yang, S. Z., Zhang, W. Z., and Dong, J. H. (2012) 'Preserving Hepatic Artery Flow during Portal Triad Blood Inflow Occlusion Reduces Liver Ischemia-Reperfusion Injury in Rats'. *Journal of Surgical Research* 174 (1), 150-156

Chiba, H., Osanai, M., Murata, M., Kojima, T., and Sawada, N. (2008) 'Transmembrane Proteins of Tight Junctions'. *Biochimica Et Biophysica Acta (BBA)-Biomembranes* 1778 (3), 588-600

Chishti, M. S., Bhatti, A., Tamim, S., Lee, K., McDonald, M., Leal, S. M., and Ahmad, W. (2008) 'Splice-Site Mutations in the TRIC Gene Underlie Autosomal Recessive Nonsyndromic Hearing Impairment in Pakistani Families'. *Journal of Human Genetics* 53 (2), 101-105

Chung, C. T., Niemela, S. L., and Miller, R. H. (1989) 'One-Step Preparation of Competent Escherichia Coli: Transformation and Storage of Bacterial Cells in the Same Solution'. *Proceedings of the National Academy of Sciences of the United States of America* 86 (7), 2172-2175

Chung, G. E., Yoon, J., Myung, S. J., Lee, J., Lee, S., Lee, S., Kim, S., Hwang, S. Y., Lee, H., and Kim, C. Y. (2010) 'High Expression of microRNA-15b Predicts a Low Risk of Tumor Recurrence Following Curative Resection of Hepatocellular Carcinoma'. *Oncology Reports* 23 (1), 113-119

Ciana, A., Meier, K., Daum, N., Gerbes, S., Veith, M., Lehr, C., and Minetti, G. (2010) 'A Dynamic Ratio of the α and α− Isoforms of the Tight Junction Protein ZO-1 is Characteristic of Caco-2 Cells and Correlates with their Degree of Differentiation'. *Cell Biology International* 34 (6), 669-678

Cicchini, C., Amicone, L., Alonzi, T., Marchetti, A., Mancone, C., and Tripodi, M. (2015) 'Molecular Mechanisms Controlling the Phenotype and the EMT/MET Dynamics of Hepatocyte'. *Liver International* 35 (2), 302-310

Claudel, T., Zollner, G., Wagner, M., and Trauner, M. (2011) 'Role of Nuclear Receptors for Bile Acid Metabolism, Bile Secretion, Cholestasis, and Gallstone Disease'. *Biochimica Et Biophysica Acta (BBA)-Molecular Basis of Disease* 1812 (8), 867-878

Coleman, W. B. (2003) 'Mechanisms of Human Hepatocarcinogenesis'. *Current Molecular Medicine* 3 (6), 573-588

Cooper, A. and Shaul, Y. (2006) 'Clathrin-Mediated Endocytosis and Lysosomal Cleavage of Hepatitis B Virus Capsid-Like Core Particles'. *The Journal of Biological Chemistry* 281 (24), 16563-16569

Cox, C. M., Mandell, E. K., Stewart, L., Lu, R., Johnson, D. L., McCarter, S. D., Tavares, A., Runyan, R., Ghosh, S., and Wilson, J. M. (2015) 'Endosomal Regulation of Contact Inhibition through the AMOT:YAP Pathway'. *Molecular Biology of the Cell* 26 (14), 2673-2684

Crettol, S., Petrovic, N., and Murray, M. (2010) 'Pharmacogenetics of Phase I and Phase II Drug Metabolism'. *Current Pharmaceutical Design* 16 (2), 204-219

Cultrex (2013) *Cultrex® Invasion Matrix and 3D Culture Qualified 96 Well Spheroid Formation Plate*. Gaithersburg, Maryland: Trevigen

Cummins, P. M. (2012) 'Occludin: One Protein, Many Forms'. *Molecular and Cellular Biology* 32 (2), 242-250

Dahmani, R., Just, P., and Perret, C. (2011) 'The Wnt/β-Catenin Pathway as a Therapeutic Target in Human Hepatocellular Carcinoma'. *Clinics and Research in Hepatology and Gastroenterology* 35 (11), 709-713

Dang, Y. W., Zeng, J., He, R. Q., Rong, M. H., Luo, D. Z., and Chen, G. (2014) 'Effects of miR-152 on Cell Growth Inhibition, Motility Suppression and Apoptosis Induction in Hepatocellular Carcinoma Cells'. *Asian Pacific Journal of Cancer Prevention : APJCP* 15 (12), 4969-4976

Deng, L., Yang, S., Xu, F., and Zhang, J. (2015) 'Long Noncoding RNA CCAT1 Promotes Hepatocellular Carcinoma Progression by Functioning as Let-7 Sponge'*. Journal of Experimental & Clinical Cancer Research* 34 (1), 18

Dezsőfi, A. and Knisely, A. S. (2014) 'Liver Biopsy in Children 2014: Who, Whom, what, when, Where, Why?'*. Clinics and Research in Hepatology and Gastroenterology* 38 (4), 395-398

Dharmacon (2018) *DharmaFECT™ Transfection Reagents—siRNA Transfection Protocol*. Waterbeach, Cambridge: Horizon

Dhir, M., Melin, A. A., Douaiher, J., Lin, C., Zhen, W. K., Hussain, S. M., Geschwind, J. F., Doyle, M. B., Abou-Alfa, G. K., and Are, C. (2016) 'A Review and Update of Treatment Options and Controversies in the Management of Hepatocellular Carcinoma'*. Annals of Surgery* 263 (6), 1112-1125

Diaz-Gonzalez, A., Reig, M., and Bruix, J. (2016) 'Treatment of Hepatocellular Carcinoma'*. Digestive Diseases (Basel, Switzerland)* 34 (5), 597-602

Dixon, L. J., Barnes, M., Tang, H., Pritchard, M. T., and Nagy, L. E. (2013) 'Kupffer Cells in the Liver'*. Comprehensive Physiology*

Dörfel, M. J., Westphal, J. K., Bellmann, C., Krug, S. M., Cording, J., Mittag, S., Tauber, R., Fromm, M., Blasig, I. E., and Huber, O. (2013) 'CK2-Dependent Phosphorylation of Occludin Regulates the Interaction with ZO-Proteins and Tight Junction Integrity'*. Cell Communication and Signaling*11 (1), 40

Dörfel, M. J. and Huber, O. (2012) 'A Phosphorylation Hotspot within the Occludin C-terminal Domain'. *Annals of the New York Academy of Sciences*1257 (1), 38-44

Dorfel, M. J. and Huber, O. (2012) 'Modulation of Tight Junction Structure and Function by Kinases and Phosphatases Targeting Occludin'. *Journal of Biomedicine & Biotechnology* 2012, 807356

Dröge, C., Schaal, H., Engelmann, G., Wenning, D., Häussinger, D., and Kubitz, R. (2016) 'Exon-Skipping and mRNA Decay in Human Liver Tissue: Molecular Consequences of Pathogenic Bile Salt Export Pump Mutations'. *Scientific Reports* 6, 24827

Duncan, A. W., Dorrell, C., and Grompe, M. (2009) 'Stem Cells and Liver Regeneration'. *Gastroenterology* 137 (2), 466-481

Dupasquier, S., Delmarcelle, A., Marbaix, E., Cosyns, J., Courtoy, P. J., and Pierreux, C. E. (2014) 'Validation of Housekeeping Gene and Impact on Normalized Gene Expression in Clear Cell Renal Cell Carcinoma: Critical Reassessment of YBX3/ZONAB/CSDA Expression'. *BMC Molecular Biology*15 (1), 9

Edelblum, K. L. and Turner, J. R. (2009) 'The Tight Junction in Inflammatory Disease: Communication Breakdown'. *Current Opinion in Pharmacology* 9 (6), 715-720

El–Serag, H. B. and Rudolph, K. L. (2007) 'Hepatocellular Carcinoma: Epidemiology and Molecular Carcinogenesis'. *Gastroenterology* 132 (7), 2557-2576

Elias, B. C., Suzuki, T., Seth, A., Giorgianni, F., Kale, G., Shen, L., Turner, J. R., Naren, A., Desiderio, D. M., and Rao, R. (2009) 'Phosphorylation of Tyr-398 and Tyr-402 in Occludin Prevents its Interaction with ZO1 and Destabilizes its Assembly at the Tight Junctions'*. The Journal of Biological Chemistry* 284 (3), 1559-1569

Evan, G. I. and Vousden, K. H. (2001) 'Proliferation, Cell Cycle and Apoptosis in Cancer'*. Nature* 411 (6835), 342

Evans, M. J., von Hahn, T., Tscherne, D. M., Syder, A. J., Panis, M., Wölk, B., Hatziioannou, T., McKeating, J. A., Bieniasz, P. D., and Rice, C. M. (2007) 'Claudin-1 is a Hepatitis C Virus Co-Receptor Required for a Late Step in Entry'*. Nature* 446 (7137), 801

Falk, M. M., Bell, C. L., Andrews, R. M. K., and Murray, S. A. (2016) 'Molecular Mechanisms Regulating Formation, Trafficking and Processing of Annular Gap Junctions'*. BMC Cell Biology* 17 (1), S22

FARQUHAR, M. G. and PALADE, G. E. (1963) 'Junctional Complexes in various Epithelia'*. The Journal of Cell Biology* 17, 375-412

Ferlay, J., Shin, H., Bray, F., Forman, D., Mathers, C., and Parkin, D. M. (2010) 'Estimates of Worldwide Burden of Cancer in 2008: GLOBOCAN 2008'*. International Journal of Cancer* 127 (12), 2893-2917

Findley, M. K. and Koval, M. (2009) 'Regulation and Roles for claudin-family Tight Junction Proteins'*. IUBMB Life* 61 (4), 431-437

Fitamant, J., Kottakis, F., Benhamouche, S., Tian, H. S., Chuvin, N., Parachoniak, C. A., Nagle, J. M., Perera, R. M., Lapouge, M., and Deshpande, V. (2015) 'YAP Inhibition Restores Hepatocyte Differentiation in Advanced HCC, Leading to Tumor Regression'. *Cell Reports* 10 (10), 1692-1707

Fletcher, S. J., Iqbal, M., Jabbari, S., Stekel, D., and Rappoport, J. Z. (2014) 'Analysis of Occludin Trafficking, Demonstrating Continuous Endocytosis, Degradation, Recycling and Biosynthetic Secretory Trafficking'. *PloS One* 9 (11), e111176

Fletcher, S. J., Poulter, N. S., Haining, E. J., and Rappoport, J. Z. (2012) 'Clathrin-mediated Endocytosis Regulates Occludin, and Not Focal Adhesion, Distribution during Epithelial Wound Healing'. *Biology of the Cell* 104 (4), 238-256

Fornari, F., Gramantieri, L., Ferracin, M., Veronese, A., Sabbioni, S., Calin, G., Grazi, G., Giovannini, C., Croce, C., and Bolondi, L. (2008) 'MiR-221 Controls CDKN1C/p57 and CDKN1B/p27 Expression in Human Hepatocellular Carcinoma'. *Oncogene* 27 (43), 5651-5661

Fornari, F., Milazzo, M., Chieco, P., Negrini, M., Marasco, E., Capranico, G., Mantovani, V., Marinello, J., Sabbioni, S., and Callegari, E. (2012) 'In Hepatocellular Carcinoma miR-519d is up-regulated by p53 and DNA Hypomethylation and Targets CDKN1A/p21, PTEN, AKT3 and TIMP2'. *The Journal of Pathology* 227 (3), 275-285

Friedman, S. L. (2008) 'Hepatic Stellate Cells: Protean, Multifunctional, and Enigmatic Cells of the Liver'. *Physiological Reviews* 88 (1), 125-172

Fulda, S. (2009) 'Tumor Resistance to Apoptosis'. *International Journal of Cancer* 124 (3), 511-515

Furuse, M., Hata, M., Furuse, K., Yoshida, Y., Haratake, A., Sugitani, Y., Noda, T., Kubo, A., and Tsukita, S. (2002) 'Claudin-Based Tight Junctions are Crucial for the Mammalian Epidermal Barrier: A Lesson from Claudin-1-Deficient Mice'. *The Journal of Cell Biology* 156 (6), 1099-1111

Furuse, M., Fujita, K., Hiiragi, T., Fujimoto, K., and Tsukita, S. (1998) 'Claudin-1 and -2: Novel Integral Membrane Proteins Localizing at Tight Junctions with no Sequence Similarity to Occludin'. *The Journal of Cell Biology* 141 (7), 1539-1550

Furuse, M., Fujimoto, K., Sato, N., Hirase, T., Tsukita, S., and Tsukita, S. (1996) 'Overexpression of Occludin, a Tight Junction-Associated Integral Membrane Protein, Induces the Formation of Intracellular Multilamellar Bodies Bearing Tight Junction-Like Structures'. *Journal of Cell Science* 109 (Pt 2) (Pt 2), 429-435

Gardner, T. W., Antonetti, D. A., Barber, A. J., LaNoue, K. F., Levison, S. W., and Penn State Retina Research Group (2002) 'Diabetic Retinopathy: More than Meets the Eye'. Survey of Ophthalmology 47, S253-S262

Gao, H. and Liu, C. (2014) 'MiR-429 Represses Cell Proliferation and Induces Apoptosis in HBV-Related HCC'. *Biomedicine & Pharmacotherapy* 68 (8), 943-949

Gao, Z., Li, M., He, W., and Li, W. (eds.) (2013) *Proceedings of the 2013 International Meeting on Molecular Biology of Hepatitis B Viruses, Shanghai,*

China. 'Hepatitis B Virus may Enter HepG2 Cells Complemented with Human NTCP Via Macropinocytosis'

Garofalo, M., Di Leva, G., Romano, G., Nuovo, G., Suh, S., Ngankeu, A., Taccioli, C., Pichiorri, F., Alder, H., and Secchiero, P. (2009) 'MiR-221&222 Regulate TRAIL Resistance and Enhance Tumorigenicity through PTEN and TIMP3 Downregulation'*. Cancer Cell* 16 (6), 498-509

Ghouri, Y. A., Mian, I., and Rowe, J. H. (2017) 'Review of Hepatocellular Carcinoma: Epidemiology, Etiology, and Carcinogenesis'*. Journal of Carcinogenesis* 16

Giampazolias, E. and Tait, S. W. (2016) 'Mitochondria and the Hallmarks of Cancer'*. The FEBS Journal* 283 (5), 803-814

Gissen, P. and Arias, I. M. (2015) 'Structural and Functional Hepatocyte Polarity and Liver Disease'*. Journal of Hepatology* 63 (4), 1023-1037

Glenn, H. L., Messner, J., and Meldrum, D. R. (2016) 'A Simple Non-Perturbing Cell Migration Assay Insensitive to Proliferation Effects'*. Scientific Reports*6, 31694

Gong, X. Q., Nakagawa, S., Tsukihara, T., and Bai, D. (2013) 'A Mechanism of Gap Junction Docking Revealed by Functional Rescue of a Human-Disease-Linked Connexin Mutant'*. Journal of Cell Science* 126 (Pt 14), 3113-3120

Gonzalez-Mariscal, L., Miranda, J., Ortega-Olvera, J. M., Gallego-Gutierrez, H., Raya-Sandino, A., and Vargas-Sierra, O. (2016) 'Zonula Occludens Proteins in Cancer'*. Current Pathobiology Reports* 4 (3), 107-116

Gonzalez-Mariscal, L., Miranda, J., Ortega-Olvera, J. M., Gallego-Gutierrez, H., Raya-Sandino, A., and Vargas-Sierra, O. (2016) 'Involvement of Tight Junction Plaque Proteins in Cancer'. *Current Pathobiology Reports* 4 (3), 117-133

Gonzalez-Mariscal, L., Bautista, P., Lechuga, S., and Quiros, M. (2012) 'ZO-2, a Tight Junction Scaffold Protein Involved in the Regulation of Cell Proliferation and Apoptosis'. *Annals of the New York Academy of Sciences* 1257 (1), 133-141

Gumbiner, B., Lowenkopf, T., and Apatira, D. (1991) 'Identification of a 160-kDa Polypeptide that Binds to the Tight Junction Protein ZO-1'. *Proceedings of the National Academy of Sciences of the United States of America* 88 (8), 3460-3464

HAHN-STRÖMBERG, V., Edvardsson, H., Bodin, L., and FRANZEÉN, L. (2009) 'Tumor Volume of Colon Carcinoma is Related to the Invasive Pattern but Not to the Expression of Cell Adhesion Proteins'. *Apmis* 117 (3), 205-211

Hai, H., Tamori, A., and Kawada, N. (2014) 'Role of Hepatitis B Virus DNA Integration in Human Hepatocarcinogenesis'. *World Journal of Gastroenterology* 20 (20), 6236-6243

Hainaut, P. and Plymoth, A. (2013) 'Targeting the Hallmarks of Cancer: Towards a Rational Approach to Next-Generation Cancer Therapy'. *Current Opinion in Oncology* 25 (1), 50-51

Hanahan, D. and Weinberg, R. A. (2011) 'Hallmarks of Cancer: The Next Generation'. *Cell* 144 (5), 646-674

Hannezo, E., Prost, J., and Joanny, J. F. (2014) 'Theory of Epithelial Sheet Morphology in Three Dimensions'. *Proceedings of the National Academy of Sciences of the United States of America* 111 (1), 27-32

Harris, T. J. and Tepass, U. (2010) 'Adherens Junctions: From Molecules to Morphogenesis'. *Nature Reviews Molecular Cell Biology* 11 (7), 502-514

Hartsock, A. and Nelson, W. J. (2008) 'Adherens and Tight Junctions: Structure, Function and Connections to the Actin Cytoskeleton'. *Biochimica Et Biophysica Acta (BBA)-Biomembranes* 1778 (3), 660-669

Haskins, J., Gu, L., Wittchen, E. S., Hibbard, J., and Stevenson, B. R. (1998) 'ZO-3, a Novel Member of the MAGUK Protein Family found at the Tight Junction, Interacts with ZO-1 and Occludin'. *The Journal of Cell Biology* 141 (1), 199-208

Herr, K. J., Tsang, Y. H., Ong, J. W., Li, Q., Yap, L. L., Yu, W., Yin, H., Bogorad, R. L., Dahlman, J. E., Chan, Y. G., Bay, B. H., Singaraja, R., Anderson, D. G., Koteliansky, V., Viasnoff, V., and Thiery, J. P. (2014) 'Loss of Alpha-Catenin Elicits a Cholestatic Response and Impairs Liver Regeneration'. *Scientific Reports* 4, 6835

Higashi, Y., Suzuki, S., Sakaguchi, T., Nakamura, T., Baba, S., Reinecker, H., Nakamura, S., and Konno, H. (2007) 'Loss of Claudin-1 Expression Correlates with Malignancy of Hepatocellular Carcinoma'. *Journal of Surgical Research* 139 (1), 68-76

Hobbs, R. P. and Green, K. J. (2012) 'Desmoplakin Regulates Desmosome Hyperadhesion'. *The Journal of Investigative Dermatology* 132 (2), 482-485

Horizon (2018) *SiRNA Resuspension Protocol*. Waterbeach, Cambridge: Horizon

Hoshida, Y., Villanueva, A., and Llovet, J. M. (2009) 'Molecular Profiling to Predict Hepatocellular Carcinoma Outcome'. *Expert Review of Gastroenterology & Hepatology* 3 (2), 101-103

Huang, H. C., Chen, C. C., Chang, W. C., Tao, M. H., and Huang, C. (2012) 'Entry of Hepatitis B Virus into Immortalized Human Primary Hepatocytes by Clathrin-Dependent Endocytosis'. *Journal of Virology* 86 (17), 9443-9453

Huerta, M., Munoz, R., Tapia, R., Soto-Reyes, E., Ramirez, L., Recillas-Targa, F., Gonzalez-Mariscal, L., and Lopez-Bayghen, E. (2007) 'Cyclin D1 is Transcriptionally Down-Regulated by ZO2 Via an E Box and the Transcription Factor c-Myc'. *Molecular Biology of the Cell* 18 (12), 4826-4836

Hussain, S., Schwank, J., Staib, F., Wang, X., and Harris, C. (2007) 'TP53 Mutations and Hepatocellular Carcinoma: Insights into the Etiology and Pathogenesis of Liver Cancer'. *Oncogene* 26 (15), 2166

Ibidi (2018) Culture-Insert 2 Well [online] available from <https://ibidi.com/img/cms/products/labware/open_removable/E_8XXXX_CI_2Well/IN_8XXXX_CultureInsert_2Well.pdf;>

Ibidi (2015) Generation of Spheroids [online] available from <https://ibidi.com/img/cms/support/AN/AN32_Generation_of_spheroids.pdf;>

Ibidi Culture-Insert Family [online] available from <http://ibidi.com/xtproducts/en/ibidi-Labware/Open-Slides-Dishes:-Removable-Chambers/Culture-Insert-Family> [04/03 2014]

Iden, S. and Collard, J. G. (2008) 'Crosstalk between Small GTPases and Polarity Proteins in Cell Polarization'. *Nature Reviews Molecular Cell Biology* 9 (11), 846-859

Ikenouchi, J., Sasaki, H., Tsukita, S., Furuse, M., and Tsukita, S. (2008) 'Loss of Occludin Affects Tricellular Localization of Tricellulin'. *Molecular Biology of the Cell* 19 (11), 4687-4693

Ikenouchi, J., Matsuda, M., Furuse, M., and Tsukita, S. (2003) 'Regulation of Tight Junctions during the Epithelium-Mesenchyme Transition: Direct Repression of the Gene Expression of claudins/occludin by Snail'. *Journal of Cell Science* 116 (Pt 10), 1959-1967

ImageJ (2018) Wound Healing Tool [online] available from <http://dev.mri.cnrs.fr/projects/imagej-macros/wiki/Wound_Healing_Tool;>

Indra, I., Hong, S., Troyanovsky, R., Kormos, B., and Troyanovsky, S. (2013) 'The Adherens Junction: A Mosaic of Cadherin and Nectin Clusters Bundled by Actin Filaments'. *Journal of Investigative Dermatology* 133 (11), 2546-2554

Invitrogen (2015) *One Shot™ Stbl3™ Chemically Competent E. Coli*. Carlsbad, California: ThermoFigher

Ioannou, M. S., Girard, M., and McPherson, P. S. (2016) 'Rab13 Traffics on Vesicles Independent of Prenylation'. *The Journal of Biological Chemistry* 291 (20), 10726-10735

Ioannou, M. S. and McPherson, P. S. (2016) 'Regulation of Cancer Cell Behavior by the Small GTPase Rab13'. *The Journal of Biological Chemistry* 291 (19), 9929-9937

Jaeschke, H. (2008) 'Toxic Responses of the Liver'. *Casarett's & Doull's Toxicology: The Basic Science of Poisoning*, 557-582

Jain, S., Suzuki, T., Seth, A., Samak, G., and Rao, R. (2011) 'Protein Kinase Czeta Phosphorylates Occludin and Promotes Assembly of Epithelial Tight Junctions'. *The Biochemical Journal* 437 (2), 289-299

Ji, J., Zhao, L., Budhu, A., Forgues, M., Jia, H., Qin, L., Ye, Q., Yu, J., Shi, X., and Tang, Z. (2010) 'Let-7g Targets Collagen Type I α2 and Inhibits Cell Migration in Hepatocellular Carcinoma'. *Journal of Hepatology* 52 (5), 690-697

Jüngst, C., Berg, T., Cheng, J., Green, R. M., Jia, J., Mason, A. L., and Lammert, F. (2013) 'Intrahepatic Cholestasis in Common Chronic Liver Diseases'. *European Journal of Clinical Investigation* 43 (10), 1069-1083

Kalluri, R. and Weinberg, R. A. (2009) 'The Basics of Epithelial-Mesenchymal Transition'. *The Journal of Clinical Investigation* 119 (6), 1420-1428

Kamarajah, S., Patten, D., Wadkin, J., Coldham, C., Bhogal, R., Shetty, S., and Weston, C. (2016) *. PWE-041 Reduced Expression of TJP-2 is Associated with Chronic Liver Disease and Hepatic Malignancy*

Kaposi-Novak, P., Libbrecht, L., Woo, H. G., Lee, Y. H., Sears, N. C., Coulouarn, C., Conner, E. A., Factor, V. M., Roskams, T., and Thorgeirsson, S. S. (2009) 'Central Role of c-Myc during Malignant Conversion in Human Hepatocarcinogenesis'*. Cancer Research* 69 (7), 2775-2782

Katsuno, T., Umeda, K., Matsui, T., Hata, M., Tamura, A., Itoh, M., Takeuchi, K., Fujimori, T., Nabeshima, Y., Noda, T., Tsukita, S., and Tsukita, S. (2008) 'Deficiency of Zonula Occludens-1 Causes Embryonic Lethal Phenotype Associated with Defected Yolk Sac Angiogenesis and Apoptosis of Embryonic Cells'*. Molecular Biology of the Cell* 19 (6), 2465-2475

Kedinger, V., Sansregret, L., Harada, R., Vadnais, C., Cadieux, C., Fathers, K., Park, M., and Nepveu, A. (2009) 'P110 CUX1 Homeodomain Protein Stimulates Cell Migration and Invasion in Part through a Regulatory Cascade Culminating in the Repression of E-Cadherin and Occludin'*. The Journal of Biological Chemistry* 284 (40), 27701-27711

Kew, M. C. (2014) 'Hepatocellular Carcinoma: Epidemiology and Risk Factors'*. Journal of Hepatocellular Carcinoma* 1, 115-125

Kim, J. K., Noh, J. H., Jung, K. H., Eun, J. W., Bae, H. J., Kim, M. G., Chang, Y. G., Shen, Q., Park, W. S., and Lee, J. Y. (2013) 'Sirtuin7 Oncogenic Potential in

Human Hepatocellular Carcinoma and its Regulation by the Tumor Suppressors MiR-125a-5p and MiR-125b'. *Hepatology* 57 (3), 1055-1067

Kim, S., Choi, J., Park, C., and Jeong, J. (2010) 'Ethyl Pyruvate Stabilizes Hypoxia-Inducible Factor 1 Alpha Via Stimulation of the TCA Cycle'. *Cancer Letters* 295 (2), 236-241

Kim, Y., Jung, Y., Kim, T., and Kim, H. (2013) 'Alu-Related Transcript of TJP2 Gene as a Marker for Colorectal Cancer'. *Gene* 524 (2), 268-274

King, J. M., Tan, C. J. P., Thomason, N. C., White, A. R., Shen, L., and Turner, J. R. (2016) 'Zonula Occludens-1 ZU5 Domain Contributes Essential Stabilizing Interactions at the Tight Junction'. *The FASEB Journal* 30 (1_supplement), 1250.7-1250.7

Kim, Y., Kang, K., Jeong, J., Paik, S. S., Kim, J. S., Park, S. A., Kim, W. D., Park, J., and Choi, D. (2017) 'Three-Dimensional (3D) Printing of Mouse Primary Hepatocytes to Generate 3D Hepatic Structure'. Annals of Surgical Treatment and Research 92 (2), 67-72

Knasmüller, S., Parzefall, W., Sanyal, R., Ecker, S., Schwab, C., Uhl, M., Mersch-Sundermann, V., Williamson, G., Hietsch, G., and Langer, T. (1998) 'Use of Metabolically Competent Human Hepatoma Cells for the Detection of Mutagens and Antimutagens'. *Mutation Research/Fundamental and Molecular Mechanisms of Mutagenesis* 402 (1), 185-202

Konopka, G., Tekiela, J., Iverson, M., Wells, C., and Duncan, S. A. (2007) 'Junctional Adhesion Molecule-A is Critical for the Formation of Pseudocanaliculi and

Modulates E-Cadherin Expression in Hepatic Cells'. *The Journal of Biological Chemistry* 282 (38), 28137-28148

Konrad, M., Schaller, A., Seelow, D., Pandey, A. V., Waldegger, S., Lesslauer, A., Vitzthum, H., Suzuki, Y., Luk, J. M., and Becker, C. (2006) 'Mutations in the Tight-Junction Gene Claudin 19 (CLDN19) are Associated with Renal Magnesium Wasting, Renal Failure, and Severe Ocular Involvement'. *The American Journal of Human Genetics* 79 (5), 949-957

Krause, G., Protze, J., and Piontek, J. (eds.) (2015) *Seminars in Cell & Developmental Biology*. 'Assembly and Function of Claudins: Structure–function Relationships Based on Homology Models and Crystal Structures': Elsevier

Kudo, M. (2013) 'Early Hepatocellular Carcinoma: Definition and Diagnosis'. *Liver Cancer* 2 (2), 69-72

Lal-Nag, M. and Morin, P. J. (2009) 'The Claudins'. *Genome Biology* 10 (8), 235

Lan, T., Chang, L., Wu, L., and Yuan, Y. (2016) 'Downregulation of ZEB2-AS1 Decreased Tumor Growth and Metastasis in Hepatocellular Carcinoma'. *Molecular Medicine Reports* 14 (5), 4606-4612

Landy, J., Ronde, E., English, N., Clark, S. K., Hart, A. L., Knight, S. C., Ciclitira, P. J., and Al-Hassi, H. O. (2016) 'Tight Junctions in Inflammatory Bowel Diseases and Inflammatory Bowel Disease Associated Colorectal Cancer'. *World Journal of Gastroenterology* 22 (11), 3117-3126

LaQuaglia, M. J., Grijalva, J. L., Mueller, K. A., Perez-Atayde, A. R., Kim, H. B., Sadri-Vakili, G., and Vakili, K. (2016) 'Yap Subcellular Localization and Hippo Pathway Transcriptome Analysis in Pediatric Hepatocellular Carcinoma'. *Scientific Reports* 6, 30238

Larionov, A., Krause, A., and Miller, W. (2005) 'A Standard Curve Based Method for Relative Real Time PCR Data Processing'. BMC Bioinformatics 6 (1), 62

Law, P. T., Ching, A. K., Chan, A. W., Wong, Q. W., Wong, C., To, K., and Wong, N. (2012) 'MiR-145 Modulates Multiple Components of the Insulin-Like Growth Factor Pathway in Hepatocellular Carcinoma'. *Carcinogenesis* 33 (6), 1134-1141

LeCluyse, E. L., Witek, R. P., Andersen, M. E., and Powers, M. J. (2012) 'Organotypic Liver Culture Models: Meeting Current Challenges in Toxicity Testing'. *Critical Reviews in Toxicology* 42 (6), 501-548

Lee, N. P. and Luk, J. M. (2010) 'Hepatic Tight Junctions: From Viral Entry to Cancer Metastasis'. *World Journal of Gastroenterology* 16 (3), 289-295

Lemmon, M. A. and Schlessinger, J. (2010) 'Cell Signaling by Receptor Tyrosine Kinases'. *Cell* 141 (7), 1117-1134

Li, J., Fu, H., Xu, C., Tie, Y., Xing, R., Zhu, J., Qin, Y., Sun, Z., and Zheng, X. (2010) 'MiR-183 Inhibits TGF-β1-Induced Apoptosis by Downregulation of PDCD4 Expression in Human Hepatocellular Carcinoma Cells'. *BMC Cancer* 10 (1), 354

Li, N., Fu, H., Tie, Y., Hu, Z., Kong, W., Wu, Y., and Zheng, X. (2009) 'MiR-34a Inhibits Migration and Invasion by Down-Regulation of c-Met Expression in Human Hepatocellular Carcinoma Cells'. *Cancer Letters* 275 (1), 44-53

Li, Y., Fanning, A. S., Anderson, J. M., and Lavie, A. (2005) 'Structure of the Conserved Cytoplasmic C-Terminal Domain of Occludin: Identification of the ZO1 Binding Surface'. *Journal of Molecular Biology* 352 (1), 151-164

Li, B. A. (2012) 'A Novel Tumor Suppressor miRNA miR-520e Contributes to Suppression of Hepatoma'. *Acta Pharmacologica Sinica* 33 (1), 3-4

Li, D., Liu, X., Lin, L., Hou, J., Li, N., Wang, C., Wang, P., Zhang, Q., Zhang, P., Zhou, W., Wang, Z., Ding, G., Zhuang, S. M., Zheng, L., Tao, W., and Cao, X. (2011) 'MicroRNA-99a Inhibits Hepatocellular Carcinoma Growth and Correlates with Prognosis of Patients with Hepatocellular Carcinoma'. *The Journal of Biological Chemistry* 286 (42), 36677-36685

Li, D. and Mrsny, R. J. (2000) 'Oncogenic Raf-1 Disrupts Epithelial Tight Junctions Via Downregulation of Occludin'. *The Journal of Cell Biology* 148 (4), 791-800

Lie, P. P., Cheng, C. Y., and Mruk, D. D. (2010) 'Crosstalk between Desmoglein-2/desmocollin-2/Src Kinase and Coxsackie and Adenovirus receptor/ZO1 Protein Complexes, Regulates Blood-Testis Barrier Dynamics'. *The International Journal of Biochemistry & Cell Biology* 42 (6), 975-986

Liu, A. M., Wong, K., Jiang, X., Qiao, Y., and Luk, J. M. (2012) 'Regulators of Mammalian Hippo Pathway in Cancer'. *Biochimica Et Biophysica Acta (BBA)-Reviews on Cancer* 1826 (2), 357-364

Liu, K., Liu, S., Zhang, W., Jia, B., Tan, L., Jin, Z., and Liu, Y. (2015) 'MiR-494 Promotes Cell Proliferation, Migration and Invasion, and Increased Sorafenib Resistance in Hepatocellular Carcinoma by Targeting PTEN'. *Oncology Reports* 34 (2), 1003-1010

Liu, K., Liu, S., Zhang, W., Jia, B., Tan, L., Jin, Z., and Liu, Y. (2015) 'MiR-494 Promotes Cell Proliferation, Migration and Invasion, and Increased Sorafenib Resistance in Hepatocellular Carcinoma by Targeting PTEN'. *Oncology Reports* 34 (2), 1003-1010

Liu, R., Xu, X., Huang, J., Fei, Q., Chen, F., Li, Y., and Han, Z. (2013) 'Down-Regulation of miR-517a and miR-517c Promotes Proliferation of Hepatocellular Carcinoma Cells Via Targeting Pyk2'. *Cancer Letters* 329 (2), 164-173

Liu, S., Yang, W., Shen, L., Turner, J. R., Coyne, C. B., and Wang, T. (2009) 'Tight Junction Proteins Claudin-1 and Occludin Control Hepatitis C Virus Entry and are Downregulated during Infection to Prevent Superinfection'. *Journal of Virology* 83 (4), 2011-2014

Liu, W., Yeh, S., Lu, C., Yu, S., Chen, H., Lin, C., Chen, D., and Chen, P. (2009) 'MicroRNA-18a Prevents Estrogen Receptor-α Expression, Promoting Proliferation of Hepatocellular Carcinoma Cells'. *Gastroenterology* 136 (2), 683-693

Liu, Y., Liang, B., Guan, Y., You, J., Zhu, L., Chen, X., and Huang, Z. (2015) 'Loss of N-Cadherin is Associated with Loss of E-Cadherin Expression and Poor

Outcomes of Liver Resection in Hepatocellular Carcinoma'. *Journal of Surgical Research* 194 (1), 167-176

Liu, Y., Ding, Y., Huang, J., Wang, S., Ni, W., Guan, J., Li, Q., Zhang, Y., Ding, Y., and Chen, B. (2014) 'MiR-141 Suppresses the Migration and Invasion of HCC Cells by Targeting Tiam1'. *PloS One* 9 (2), e88393

Liu, S., Yang, W., Shen, L., Turner, J. R., Coyne, C. B., and Wang, T. (2009) 'Tight Junction Proteins Claudin-1 and Occludin Control Hepatitis C Virus Entry and are Downregulated during Infection to Prevent Superinfection'. *Journal of Virology* 83 (4), 2011-2014

Lujambio, A., Akkari, L., Simon, J., Grace, D., Tschaharganeh, D. F., Bolden, J. E., Zhao, Z., Thapar, V., Joyce, J. A., and Krizhanovsky, V. (2013) 'Non-Cell-Autonomous Tumor Suppression by p53'. *Cell* 153 (2), 449-460

Luissint, A., Artus, C., Glacial, F., Ganeshamoorthy, K., and Couraud, P. (2012) 'Tight Junctions at the Blood Brain Barrier: Physiological Architecture and Disease-Associated Dysregulation'. Fluids and Barriers of the CNS 9 (1), 23

Luo, D., Wang, Z., Wu, J., Jiang, C., and Wu, J. (2014) 'The Role of Hypoxia Inducible Factor-1 in Hepatocellular Carcinoma'. *BioMed Research International* 2014, 409272

Ma, S., Tang, K. H., Chan, Y. P., Lee, T. K., Kwan, P. S., Castilho, A., Ng, I., Man, K., Wong, N., and To, K. (2010) 'MiR-130b Promotes CD133 Liver Tumor-Initiating Cell Growth and Self-Renewal Via Tumor Protein 53-Induced Nuclear Protein 1'. *Cell Stem Cell* 7 (6), 694-707

Macovei, A., Radulescu, C., Lazar, C., Petrescu, S., Durantel, D., Dwek, R. A., Zitzmann, N., and Nichita, N. B. (2010) 'Hepatitis B Virus Requires Intact Caveolin-1 Function for Productive Infection in HepaRG Cells'. *Journal of Virology* 84 (1), 243-253

Major, J. M., Sargent, J. D., Graubard, B. I., Carlos, H. A., Hollenbeck, A. R., Altekruse, S. F., Freedman, N. D., and McGlynn, K. A. (2014) 'Local Geographic Variation in Chronic Liver Disease and Hepatocellular Carcinoma: Contributions of Socioeconomic Deprivation, Alcohol Retail Outlets, and Lifestyle'. *Annals of Epidemiology* 24 (2), 104-110

Malaguarnera, G., Giordano, M., Nunnari, G., Bertino, G., and Malaguarnera, M. (2014) 'Gut Microbiota in Alcoholic Liver Disease: Pathogenetic Role and Therapeutic Perspectives'. *World Journal of Gastroenterology* 20 (44), 16639-16648

Maly, I. P. and Landmann, L. (2008) 'Bile Duct Ligation in the Rat Causes Upregulation of ZO-2 and Decreased Colocalization of Claudins with ZO-1 and Occludin'. Histochemistry and Cell Biology 129 (3), 289-299

Mani, S. A., Guo, W., Liao, M., Eaton, E. N., Ayyanan, A., Zhou, A. Y., Brooks, M., Reinhard, F., Zhang, C. C., and Shipitsin, M. (2008) 'The Epithelial-Mesenchymal Transition Generates Cells with Properties of Stem Cells'. *Cell* 133 (4), 704-715

Mann, C. D., Neal, C. P., Garcea, G., Manson, M. M., Dennison, A. R., and Berry, D. P. (2007) 'Prognostic Molecular Markers in Hepatocellular Carcinoma: A Systematic Review'. *European Journal of Cancer* 43 (6), 979-992

Marchiando, A. M., Shen, L., Graham, W. V., Weber, C. R., Schwarz, B. T., Austin, J. R.,2nd, Raleigh, D. R., Guan, Y., Watson, A. J., Montrose, M. H., and Turner, J. R. (2010) 'Caveolin-1-Dependent Occludin Endocytosis is Required for TNF-Induced Tight Junction Regulation in Vivo'. *The Journal of Cell Biology* 189 (1), 111-126

Mariano, C., Sasaki, H., Brites, D., and Brito, M. A. (2011) 'A Look at Tricellulin and its Role in Tight Junction Formation and Maintenance'. *European Journal of Cell Biology* 90 (10), 787-796

Martin, T. A. (ed.) (2014) *Seminars in Cell & Developmental Biology*. 'The Role of Tight Junctions in Cancer Metastasis': Elsevier

Martin, T. A., Mason, M. D., and Jiang, W. G. (2011) 'Tight Junctions in Cancer Metastasis'. *Front Biosci* 16, 898-936

Martin, T. A., Mansel, R. E., and Jiang, W. G. (2010) 'Loss of Occludin Leads to the Progression of Human Breast Cancer'. *International Journal of Molecular Medicine* 26 (5), 723-734

Martin, T. A., Watkins, G., Mansel, R. E., and Jiang, W. G. (2004) 'Loss of Tight Junction Plaque Molecules in Breast Cancer Tissues is Associated with a Poor Prognosis in Patients with Breast Cancer'. *European Journal of Cancer* 40 (18), 2717-2725

Martin-Belmonte, F. and Mostov, K. (2008) 'Regulation of Cell Polarity during Epithelial Morphogenesis'. *Current Opinion in Cell Biology* 20 (2), 227-234

Martinez-Outschoorn, U. E., Pestell, R. G., Howell, A., Tykocinski, M. L., Nagajyothi, F., Machado, F. S., Tanowitz, H. B., Sotgia, F., and Lisanti, M. P. (2011) 'Energy Transfer in" Parasitic" Cancer Metabolism: Mitochondria are the Powerhouse and Achilles' Heel of Tumor Cells'. *Cell Cycle* 10 (24), 4208-4216

Martin-Padura, I., Lostaglio, S., Schneemann, M., Williams, L., Romano, M., Fruscella, P., Panzeri, C., Stoppacciaro, A., Ruco, L., Villa, A., Simmons, D., and Dejana, E. (1998) 'Junctional Adhesion Molecule, a Novel Member of the Immunoglobulin Superfamily that Distributes at Intercellular Junctions and Modulates Monocyte Transmigration'. *The Journal of Cell Biology* 142 (1), 117-127

Matsuo, N., Shiraha, H., Fujikawa, T., Takaoka, N., Ueda, N., Tanaka, S., Nishina, S., Nakanishi, Y., Uemura, M., and Takaki, A. (2009) 'Twist Expression Promotes Migration and Invasion in Hepatocellular Carcinoma'. *BMC Cancer* 9 (1), 240

Matter, K., Aijaz, S., Tsapara, A., and Balda, M. S. (2005) 'Mammalian Tight Junctions in the Regulation of Epithelial Differentiation and Proliferation'. *Current Opinion in Cell Biology* 17 (5), 453-458

McNeil, E., Capaldo, C. T., and Macara, I. G. (2006) 'Zonula Occludens-1 Function in the Assembly of Tight Junctions in Madin-Darby Canine Kidney Epithelial Cells'. *Molecular Biology of the Cell* 17 (4), 1922-1932

Meng, F., Henson, R., Wehbe–Janek, H., Ghoshal, K., Jacob, S. T., and Patel, T. (2007) 'MicroRNA-21 Regulates Expression of the PTEN Tumor Suppressor Gene in Human Hepatocellular Cancer'. *Gastroenterology* 133 (2), 647-658

Meng, W. and Takeichi, M. (2009) 'Adherens Junction: Molecular Architecture and Regulation'. *Cold Spring Harbor Perspectives in Biology* 1 (6), a002899

Meredith, L. W., Wilson, G. K., Fletcher, N. F., and McKeating, J. A. (2012) 'Hepatitis C Virus Entry: Beyond Receptors'. *Reviews in Medical Virology* 22 (3), 182-193

Meşe, G., Richard, G., and White, T. W. (2007) 'Gap Junctions: Basic Structure and Function'. *Journal of Investigative Dermatology* 127 (11), 2516-2524

Mirzayans, R., Andrais, B., Scott, A., and Murray, D. (2012) 'New Insights into p53 Signaling and Cancer Cell Response to DNA Damage: Implications for Cancer Therapy'. *BioMed Research International* 2012

Mistry, M., Parkin, D., Ahmad, A. S., and Sasieni, P. (2011) 'Cancer Incidence in the United Kingdom: Projections to the Year 2030'. *British Journal of Cancer* 105 (11), 1795

Mittal, S. and El-Serag, H. B. (2013) 'Epidemiology of Hepatocellular Carcinoma: Consider the Population'. *Journal of Clinical Gastroenterology* 47 Suppl, S2-6

Molina-Jimenez, F., Benedicto, I., Thi, V. L. D., Gondar, V., Lavillette, D., Marin, J. J., Briz, O., Moreno-Otero, R., Aldabe, R., and Baumert, T. F. (2012) 'Matrigel-Embedded 3D Culture of Huh-7 Cells as a Hepatocyte-Like Polarized System to Study Hepatitis C Virus Cycle'. *Virology* 425 (1), 31-39

Morgan, C., Jenkins, S. A., Kynaston, H. G., and Doak, S. H. (2013) 'The Role of Adhesion Molecules as Biomarkers for the Aggressive Prostate Cancer Phenotype'. *PloS One* 8 (12), e81666

Morimoto, S., Nishimura, N., Terai, T., Manabe, S., Yamamoto, Y., Shinahara, W., Miyake, H., Tashiro, S., Shimada, M., and Sasaki, T. (2005) 'Rab13 Mediates the Continuous Endocytic Recycling of Occludin to the Cell Surface'. *The Journal of Biological Chemistry* 280 (3), 2220-2228

Morishita, A. and Masaki, T. (2015) 'MiRNA in Hepatocellular Carcinoma'. *Hepatology Research* 45 (2), 128-141

Mori, M., Triboulet, R., Mohseni, M., Schlegelmilch, K., Shrestha, K., Camargo, F. D., and Gregory, R. I. (2014) 'Hippo Signaling Regulates Microprocessor and Links Cell-Density-Dependent miRNA Biogenesis to Cancer'. Cell 156 (5), 893-906

Mott, J. L., Kobayashi, S., Bronk, S. F., and Gores, G. J. (2007) 'Mir-29 Regulates Mcl-1 Protein Expression and Apoptosis'. *Oncogene* 26 (42), 6133-6140

Mukendi, C., Dean, N., Lala, R., Smith, J. J., Bronner, M. E., and Nikitina, N. V. (2016) 'Evolution of the Vertebrate Claudin Gene Family: Insights from a Basal Vertebrate, the Sea Lamprey'. *International Journal of Developmental Biology* 60 (1-3), 39-51

Murakami, T., Felinski, E. A., and Antonetti, D. A. (2009) 'Occludin Phosphorylation and Ubiquitination Regulate Tight Junction Trafficking and Vascular Endothelial Growth Factor-Induced Permeability'. *The Journal of Biological Chemistry* 284 (31), 21036-21046

Nagai, T., Arao, T., Matsumoto, K., Sakai, K., Kudo, K., Kaneda, H., Tamura, D., Aomatsu, K., Kimura, H., and Fujita, Y. (2012) *. Impact of TJP-1 and TWIST Expression on Post-Operative Prognosis in Hepatocellular Carcinoma*

Nagai, T., Arao, T., Nishio, K., Matsumoto, K., Hagiwara, S., Sakurai, T., Minami, Y., Ida, H., Ueshima, K., Nishida, N., Sakai, K., Saijo, N., Kudo, K., Kaneda, H., Tamura, D., Aomatsu, K., Kimura, H., Fujita, Y., Haji, S., and Kudo, M. (2016) 'Impact of Tight Junction Protein ZO1 and TWIST Expression on Postoperative Survival of Patients with Hepatocellular Carcinoma'*. Digestive Diseases (Basel, Switzerland)* 34 (6), 702-707

Nelson, W. J. (2009) 'Remodeling Epithelial Cell Organization: Transitions between Front-Rear and Apical-Basal Polarity'*. Cold Spring Harbor Perspectives in Biology* 1 (1), a000513

Németh, Z., Szász, A. M., Somorácz, Á., Tátrai, P., Németh, J., Győrffy, H., Szíjártó, A., Kupcsulik, P., Kiss, A., and Schaff, Z. (2009) 'Zonula Occludens-1, Occludin, and E-Cadherin Protein Expression in Biliary Tract Cancers'*. Pathology & Oncology Research* 15 (3), 533

Németh, Z., Szász, A. M., Tátrai, P., Németh, J., Györffy, H., Somorácz, Á., Szíjártó, A., Kupcsulik, P., Kiss, A., and Schaff, Z. (2009) 'Claudin-1,− 2,− 3,− 4,− 7,− 8, and− 10 Protein Expression in Biliary Tract Cancers'*. Journal of Histochemistry & Cytochemistry* 57 (2), 113-121

Neuveut, C., Wei, Y., and Buendia, M. A. (2010) 'Mechanisms of HBV-Related Hepatocarcinogenesis'*. Journal of Hepatology* 52 (4), 594-604

Ni, Y., Lempp, F. A., Mehrle, S., Nkongolo, S., Kaufman, C., Fälth, M., Stindt, J., Königer, C., Nassal, M., and Kubitz, R. (2014) 'Hepatitis B and D Viruses Exploit Sodium Taurocholate Co-Transporting Polypeptide for Species-Specific Entry into Hepatocytes'. *Gastroenterology* 146 (4), 1070-1083. e6

Nie, M., Balda, M. S., and Matter, K. (2012) 'Stress- and Rho-Activated ZO1-Associated Nucleic Acid Binding Protein Binding to p21 mRNA Mediates Stabilization, Translation, and Cell Survival'. *Proceedings of the National Academy of Sciences of the United States of America* 109 (27), 10897-10902

Nie, M., Aijaz, S., Leefa Chong San, I. V., Balda, M. S., and Matter, K. (2009) 'The Y-Box Factor ZONAB/DbpA Associates with GEF-H1/Lfc and Mediates Rho-Stimulated Transcription'. *EMBO Reports* 10 (10), 1125-1131

Niessen, C. M. and Gottardi, C. J. (2008) 'Molecular Components of the Adherens Junction'. *Biochimica Et Biophysica Acta (BBA)-Biomembranes* 1778 (3), 562-571

Noh, J. H., Chang, Y. G., Kim, M. G., Jung, K. H., Kim, J. K., Bae, H. J., Eun, J. W., Shen, Q., Kim, S., and Kwon, S. H. (2013) 'MiR-145 Functions as a Tumor Suppressor by Directly Targeting Histone Deacetylase 2 in Liver Cancer'. *Cancer Letters* 335 (2), 455-462

Nomme, J., Fanning, A. S., Caffrey, M., Lye, M. F., Anderson, J. M., and Lavie, A. (2011) 'The Src Homology 3 Domain is Required for Junctional Adhesion Molecule Binding to the Third PDZ Domain of the Scaffolding Protein ZO1'. *The Journal of Biological Chemistry* 286 (50), 43352-43360

Nordenstedt, H., White, D. L., and El-Serag, H. B. (2010) 'The Changing Pattern of Epidemiology in Hepatocellular Carcinoma'. *Digestive and Liver Disease* 42, S206-S214

Nusrat, A., Brown, G. T., Tom, J., Drake, A., Bui, T. T., Quan, C., and Mrsny, R. J. (2005) 'Multiple Protein Interactions Involving Proposed Extracellular Loop Domains of the Tight Junction Protein Occludin'. *Molecular Biology of the Cell* 16 (4), 1725-1734

Odenwald, M. A., Choi, W., Buckley, A., Shashikanth, N., Joseph, N. E., Wang, Y., Warren, M. H., Buschmann, M. M., Pavlyuk, R., Hildebrand, J., Margolis, B., Fanning, A. S., and Turner, J. R. (2017) 'ZO1 Interactions with F-Actin and Occludin Direct Epithelial Polarization and Single Lumen Specification in 3D Culture'. *Journal of Cell Science* 130 (1), 243-259

Oka, T., Remue, E., Meerschaert, K., Vanloo, B., Boucherie, C., Gfeller, D., Bader, G. D., Sidhu, S. S., Vandekerckhove, J., Gettemans, J., and Sudol, M. (2010) 'Functional Complexes between YAP2 and ZO2 are PDZ Domain-Dependent, and Regulate YAP2 Nuclear Localization and Signalling'. *The Biochemical Journal* 432 (3), 461-472

Onder, T. T., Gupta, P. B., Mani, S. A., Yang, J., Lander, E. S., and Weinberg, R. A. (2008) 'Loss of E-Cadherin Promotes Metastasis Via Multiple Downstream Transcriptional Pathways'. *Cancer Research* 68 (10), 3645-3654

Ooshio, T., Fujita, N., Yamada, A., Sato, T., Kitagawa, Y., Okamoto, R., Nakata, S., Miki, A., Irie, K., and Takai, Y. (2007) 'Cooperative Roles of Par-3 and Afadin in

the Formation of Adherens and Tight Junctions'. *Journal of Cell Science* 120 (Pt 14), 2352-2365

Orbán, E., Szabó, E., Lotz, G., Kupcsulik, P., Páska, C., Schaff, Z., and Kiss, A. (2008) 'Different Expression of Occludin and ZO1 in Primary and Metastatic Liver Tumors'. *Pathology & Oncology Research* 14 (3), 299-306

OriGene (ND) Lenti-Vpak Lentiviral Packaging Kit Application Guide. Rockville, Maryland: OriGene Technologies, Inc Palakkan, A. A., Drummond, R., Anderson, R. A., Greenhough, S., Tv, K., Hay, D. C., and Ross, J. A. (2015) 'Polarisation and Functional Characterisation of Hepatocytes Derived from Human Embryonic and Mesenchymal Stem Cells'. Biomedical Reports 3 (5), 626-636

Ortiz, G. G., Pacheco-Moisés, F. P., Macías-Islas, M. Á., Flores-Alvarado, L. J., Mireles-Ramírez, M. A., González-Renovato, E. D., Hernández-Navarro, V. E., Sánchez-López, A. L., and Alatorre-Jiménez, M. A. (2014) 'Role of the blood–brain Barrier in Multiple Sclerosis'. *Archives of Medical Research* 45 (8), 687-697

Palakkan, A. A., Drummond, R., Anderson, R. A., Greenhough, S., Tv, K., Hay, D. C., and Ross, J. A. (2015) 'Polarisation and Functional Characterisation of Hepatocytes Derived from Human Embryonic and Mesenchymal Stem Cells'. *Biomedical Reports* 3 (5), 626-636

Paris, L., Tonutti, L., Vannini, C., and Bazzoni, G. (2008) 'Structural Organization of the Tight Junctions'. *Biochimica Et Biophysica Acta (BBA)-Biomembranes* 1778 (3), 646-659

Park, S., Lee, J. H., Ha, M., Nam, J., and Kim, V. N. (2009) 'MiR-29 miRNAs Activate p53 by Targeting p85α and CDC42'. *Nature Structural & Molecular Biology* 16 (1), 23-29

Paschoud, S., Bongiovanni, M., Pache, J., and Citi, S. (2007) 'Claudin-1 and Claudin-5 Expression Patterns Differentiate Lung Squamous Cell Carcinomas from Adenocarcinomas'. *Modern Pathology* 20 (9), 947

Paul, A., Danley, M., Saha, B., Tawfik, O., and Paul, S. (2015) 'PKCzeta Promotes Breast Cancer Invasion by Regulating Expression of E-Cadherin and Zonula Occludens-1 (ZO1) Via NFkappaB-p65'. *Scientific Reports* 5, 12520

Peng, C., Guo, W., Ji, T., Ren, T., Yang, Y., Li, D., Qu, H. y., Li, X., Tang, S., and Yan, T. (2009) 'Sorafenib Induces Growth Inhibition and Apoptosis in Human Synovial Sarcoma Cells Via Inhibiting the RAF/MEK/ERK Signaling Pathway'. Cancer Biology & Therapy 8 (18), 1729-1736

Peng, Y. and Axelrod, J. D. (2012) 'Asymmetric Protein Localization in Planar Cell Polarity: Mechanisms, Puzzles, and Challenges'. *Current Topics in Developmental Biology* 101, 33-53

Pereira, D. M., Rodrigues, P. M., Borralho, P. M., and Rodrigues, C. M. (2013) 'Delivering the Promise of miRNA Cancer Therapeutics'. *Drug Discovery Today* 18 (5), 282-289

Perz, J. F., Armstrong, G. L., Farrington, L. A., Hutin, Y. J., and Bell, B. P. (2006) 'The Contributions of Hepatitis B Virus and Hepatitis C Virus Infections to

Cirrhosis and Primary Liver Cancer Worldwide'. *Journal of Hepatology* 45 (4), 529-538

Ploss, A., Evans, M. J., Gaysinskaya, V. A., Panis, M., You, H., de Jong, Y. P., and Rice, C. M. (2009) 'Human Occludin is a Hepatitis C Virus Entry Factor Required for Infection of Mouse Cells'. *Nature* 457 (7231), 882-886

Poisson, J., Lemoinne, S., Boulanger, C., Durand, F., Moreau, R., Valla, D., and Rautou, P. (2017) 'Liver Sinusoidal Endothelial Cells: Physiology and Role in Liver Diseases'. *Journal of Hepatology* 66 (1), 212-227

Promega (2013) *FuGENE® HD Transfection Reagent Instructions for use of Products E2311 and E2312*. Madison, Wisconsin: Promega

Qi, J., Li, T., Bian, H., Li, F., Ju, Y., Gao, S., Su, J., Ren, W., and Qin, C. (2016) 'SNAI1 Promotes the Development of HCC through the Enhancement of Proliferation and Inhibition of Apoptosis'. *FEBS Open Bio* 6 (4), 326-337

Qian, Y. and Prehoda, K. E. (2006) 'Interdomain Interactions in the Tumor Suppressor Discs Large Regulate Binding to the Synaptic Protein Gukholder'. *The Journal of Biological Chemistry* 281 (47), 35757-35763

Qiao, X., Roth, I., Féraille, E., and Hasler, U. (2014) 'Different Effects of ZO1, ZO2 and ZO-3 Silencing on Kidney Collecting Duct Principal Cell Proliferation and Adhesion'. *Cell Cycle* 13 (19), 3059-3075

Qin, J., Luo, M., Qian, H., and Chen, W. (2014) 'Upregulated miR-182 Increases Drug Resistance in Cisplatin-Treated HCC Cell by Regulating TP53INP1'. *Gene* 538 (2), 342-347

Qiu, G., Lin, Y., Zhang, H., and Wu, D. (2015) 'MiR-139-5p Inhibits epithelial–mesenchymal Transition, Migration and Invasion of Hepatocellular Carcinoma Cells by Targeting ZEB1 and ZEB2'. *Biochemical and Biophysical Research Communications* 463 (3), 315-321

Qiu, G., Xie, X., Xu, F., Shi, X., Wang, Y., and Deng, L. (2015) 'Distinctive Pharmacological Differences between Liver Cancer Cell Lines HepG2 and Hep3B'. *Cytotechnology* 67 (1), 1-12

Quiros, M., Alarcon, L., Ponce, A., Giannakouros, T., and Gonzalez-Mariscal, L. (2013) 'The Intracellular Fate of Zonula Occludens 2 is Regulated by the Phosphorylation of SR Repeats and the phosphorylation/O-GlcNAcylation of S257'. *Molecular Biology of the Cell* 24 (16), 2528-2543

Raleigh, D. R., Marchiando, A. M., Zhang, Y., Shen, L., Sasaki, H., Wang, Y., Long, M., and Turner, J. R. (2010) 'Tight Junction-Associated MARVEL Proteins marveld3, Tricellulin, and Occludin have Distinct but Overlapping Functions'. *Molecular Biology of the Cell* 21 (7), 1200-1213

Ran, F. A., Hsu, P. D., Wright, J., Agarwala, V., Scott, D. A., and Zhang, F. (2013) 'Genome Engineering using the CRISPR-Cas9 System'. Nature Protocols 8 (11), 2281

Rao, D. D., Vorhies, J. S., Senzer, N., and Nemunaitis, J. (2009) 'SiRNA Vs. shRNA: Similarities and Differences'. Advanced Drug Delivery Reviews 61 (9), 746-759

Raoul, J., Bruix, J., Greten, T. F., Sherman, M., Mazzaferro, V., Hilgard, P., Scherubl, H., Scheulen, M. E., Germanidis, G., and Dominguez, S. (2012) 'Relationship between Baseline Hepatic Status and Outcome, and Effect of Sorafenib on Liver Function: SHARP Trial Subanalyses'*. Journal of Hepatology* 56 (5), 1080-1088

Renthal, N. E., Chen, C. C., Williams, K. C., Gerard, R. D., Prange-Kiel, J., and Mendelson, C. R. (2010) 'MiR-200 Family and Targets, ZEB1 and ZEB2, Modulate Uterine Quiescence and Contractility during Pregnancy and Labor'*. Proceedings of the National Academy of Sciences of the United States of America* 107 (48), 20828-20833

Reshetnyak, V. I. (2013) 'Physiological and Molecular Biochemical Mechanisms of Bile Formation'*. World Journal of Gastroenterology* 19 (42), 7341-7360

Revenu, C. and Gilmour, D. (2009) 'EMT 2.0: Shaping Epithelia through Collective Migration'*. Current Opinion in Genetics & Development* 19 (4), 338-342

Rodgers, L. S., Beam, M. T., Anderson, J. M., and Fanning, A. S. (2013) 'Epithelial Barrier Assembly Requires Coordinated Activity of Multiple Domains of the Tight Junction Protein ZO1'*. Journal of Cell Science* 126 (Pt 7), 1565-1575

Ruan, T., He, X., Yu, J., and Hang, Z. (2016) 'MicroRNA-186 Targets Yes-Associated Protein 1 to Inhibit Hippo Signaling and Tumorigenesis in Hepatocellular Carcinoma'*. Oncology Letters* 11 (4), 2941-2945

Ruan, Y. C., Wang, Y., Da Silva, N., Kim, B., Diao, R. Y., Hill, E., Brown, D., Chan, H. C., and Breton, S. (2014) 'CFTR Interacts with ZO1 to Regulate Tight Junction Assembly and Epithelial Differentiation through the ZONAB Pathway'. *Journal of Cell Science* 127 (Pt 20), 4396-4408

Saitou, M., Furuse, M., Sasaki, H., Schulzke, J. D., Fromm, M., Takano, H., Noda, T., and Tsukita, S. (2000) 'Complex Phenotype of Mice Lacking Occludin, a Component of Tight Junction Strands'. *Molecular Biology of the Cell* 11 (12), 4131-4142

Salt, M. B., Bandyopadhyay, S., and McCormick, F. (2014) 'Epithelial-to-Mesenchymal Transition Rewires the Molecular Path to PI3K-Dependent Proliferation'. *Cancer Discovery* 4 (2), 186-199

Sambrotta, M. and Thompson, R. J. (2015) 'Mutations in TJP2, Encoding Zona Occludens 2, and Liver Disease'. *Tissue Barriers* 3 (3), e1026537

Sambrotta, M., Strautnieks, S., Papouli, E., Rushton, P., Clark, B. E., Parry, D. A., Logan, C. V., Newbury, L. J., Kamath, B. M., and Ling, S. (2014) 'Mutations in TJP2 Cause Progressive Cholestatic Liver Disease'. *Nature Genetics* 46 (4), 326-328

Sanyal, A. J., Yoon, S. K., and Lencioni, R. (2010) 'The Etiology of Hepatocellular Carcinoma and Consequences for Treatment'. *The Oncologist* 15 Suppl 4, 14-22

Schuppan, D. and Afdhal, N. H. (2008) 'Liver Cirrhosis'. *The Lancet* 371 (9615), 838-851

Seth, A., Sheth, P., Elias, B. C., and Rao, R. (2007) 'Protein Phosphatases 2A and 1 Interact with Occludin and Negatively Regulate the Assembly of Tight Junctions in the CACO-2 Cell Monolayer'. *The Journal of Biological Chemistry* 282 (15), 11487-11498

Shabbir, A., Lee, J., Lee, M., Park, D. J., and Kim, H. H. (2010) 'Combined Suture Retraction of the Falciform Ligament and the Left Lobe of the Liver during Laparoscopic Total Gastrectomy'. *Surgical Endoscopy* 24 (12), 3237-3240

Sharif, G. M., Schmidt, M. O., Yi, C., Hu, Z., Haddad, B. R., Glasgow, E., Riegel, A. T., and Wellstein, A. (2015) 'Cell Growth Density Modulates Cancer Cell Vascular Invasion Via Hippo Pathway Activity and CXCR2 Signaling'. Oncogene 34 (48), 5879

Shirasago, Y., Shimizu, Y., Tanida, I., Suzuki, T., Suzuki, R., Sugiyama, K., Wakita, T., Hanada, K., Yagi, K., and Kondoh, M. (2016) 'Occludin-Knockout Human Hepatic huh7. 5.1-8-Derived Cells are Completely Resistant to Hepatitis C Virus Infection'. Biological and Pharmaceutical Bulletin 39 (5), 839-848

Sibulesky, L. (2013) 'Normal Liver Anatomy'. *Clinical Liver Disease* 2 (S1), S1-S3

Singh, A. B., Sharma, A., and Dhawan, P. (2010) 'Claudin Family of Proteins and Cancer: An Overview'. *Journal of Oncology* 2010, 541957

Smittenaar, C. R., Petersen, K. A., Stewart, K., and Moitt, N. (2016) 'Cancer Incidence and Mortality Projections in the UK Until 2035'. *British Journal of Cancer* 115 (9), 1147-1155

Solaini, G., Sgarbi, G., and Baracca, A. (2011) 'Oxidative Phosphorylation in Cancer Cells'. Biochimica Et Biophysica Acta (BBA)-Bioenergetics 1807 (6), 534-542

Spadaro, D., Tapia, R., Jond, L., Sudol, M., Fanning, A. S., and Citi, S. (2014) 'ZO Proteins Redundantly Regulate the Transcription Factor DbpA/ZONAB'. *The Journal of Biological Chemistry* 289 (32), 22500-22511

Staehelin, L. A. (1973) 'Further Observations on the Fine Structure of Freeze-Cleaved Tight Junctions'. *Journal of Cell Science* 13 (3), 763-786

Stebbing, J., Filipović, A., and Giamas, G. (2013) 'Claudin-1 as a Promoter of EMT in Hepatocellular Carcinoma'. *Oncogene* 32 (41), 4871-4872

Steed, E., Balda, M. S., and Matter, K. (2010) 'Dynamics and Functions of Tight Junctions'. *Trends in Cell Biology* 20 (3), 142-149

Stevenson, B. R., Siliciano, J. D., Mooseker, M. S., and Goodenough, D. A. (1986) 'Identification of ZO1: A High Molecular Weight Polypeptide Associated with the Tight Junction (Zonula Occludens) in a Variety of Epithelia'. *The Journal of Cell Biology* 103 (3), 755-766

Subramanian, V. S., Marchant, J. S., Ye, D., Ma, T. Y., and Said, H. M. (2007) 'Tight Junction Targeting and Intracellular Trafficking of Occludin in Polarized Epithelial Cells'. *American Journal of Physiology.Cell Physiology* 293 (5), C1717-26

Sun, Y., Song, G., Sun, N., Chen, J., and Yang, S. (2014) 'Slug Overexpression Induces Stemness and Promotes Hepatocellular Carcinoma Cell Invasion and Metastasis'. *Oncology Letters* 7 (6), 1936-1940

Sundstrom, J. M., Tash, B. R., Murakami, T., Flanagan, J. M., Bewley, M. C., Stanley, B. A., Gonsar, K. B., and Antonetti, D. A. (2009) 'Identification and Analysis of Occludin Phosphosites: A Combined Mass Spectrometry and Bioinformatics Approach'. *Journal of Proteome Research* 8 (2), 808-817

Suzuki, T., Elias, B. C., Seth, A., Shen, L., Turner, J. R., Giorgianni, F., Desiderio, D., Guntaka, R., and Rao, R. (2009) 'PKC Eta Regulates Occludin Phosphorylation and Epithelial Tight Junction Integrity'. *Proceedings of the National Academy of Sciences of the United States of America* 106 (1), 61-66

Tabibian, J. H., Masyuk, A. I., Masyuk, T. V., O'Hara, S. P., and LaRusso, N. F. (2013) 'Physiology of Cholangiocytes'. *Comprehensive Physiology*

Tabrizian, P., Jibara, G., Shrager, B., Schwartz, M., and Roayaie, S. (2015) 'Recurrence of Hepatocellular Cancer After Resection: Patterns, Treatments, and Prognosis'. *Annals of Surgery* 261 (5), 947-955

Tan, S., Li, R., Ding, K., Lobie, P. E., and Zhu, T. (2011) 'MiR-198 Inhibits Migration and Invasion of Hepatocellular Carcinoma Cells by Targeting the HGF/c-MET Pathway'. *FEBS Letters* 585 (14), 2229-2234

Tang, J., Li, L., Huang, W., Sui, C., Yang, Y., Lin, X., Hou, G., Chen, X., Fu, J., and Yuan, S. (2015) 'MiR-429 Increases the Metastatic Capability of HCC Via Regulating Classic Wnt Pathway rather than epithelial–mesenchymal Transition'. *Cancer Letters* 364 (1), 33-43

Tapia, R., Huerta, M., Islas, S., Avila-Flores, A., Lopez-Bayghen, E., Weiske, J., Huber, O., and Gonzalez-Mariscal, L. (2009) 'Zona Occludens-2 Inhibits Cyclin

D1 Expression and Cell Proliferation and Exhibits Changes in Localization Along the Cell Cycle'. *Molecular Biology of the Cell* 20 (3), 1102-1117

Tashiro, E., Tsuchiya, A., and Imoto, M. (2007) 'Functions of Cyclin D1 as an Oncogene and Regulation of Cyclin D1 Expression'. *Cancer Science* 98 (5), 629-635

Terry, S. J., Zihni, C., Elbediwy, A., Vitiello, E., Leefa Chong San, I. V., Balda, M. S., and Matter, K. (2011) 'Spatially Restricted Activation of RhoA Signalling at Epithelial Junctions by p114RhoGEF Drives Junction Formation and Morphogenesis'. *Nature Cell Biology* 13 (2), 159-166

Thermo Scientific (2014) *GeneJET Plasmid Miniprep Kit #K0502, #K0503*. Carlsbad, California: Thermo Fisher

Thompson, P. D., Tipney, H., Brass, A., Noyes, H., Kemp, S., Naessens, J., and Tassabehji, M. (2010) 'Claudin 13, a Member of the Claudin Family Regulated in Mouse Stress Induced Erythropoiesis'. *PloS One* 5 (9), e12667

Tian, X., Liu, Z., Niu, B., Zhang, J., Tan, T. K., Lee, S. R., Zhao, Y., Harris, D. C., and Zheng, G. (2011) 'E-cadherin/beta-Catenin Complex and the Epithelial Barrier'. *Journal of Biomedicine & Biotechnology* 2011, 567305

Tirkes, T., Sandrasegaran, K., Patel, A. A., Hollar, M. A., Tejada, J. G., Tann, M., Akisik, F. M., and Lappas, J. C. (2012) 'Peritoneal and Retroperitoneal Anatomy and its Relevance for Cross-Sectional Imaging'. *Radiographics* 32 (2), 437-451

Tobioka, H., Tokunaga, Y., Isomura, H., Kokai, Y., Yamaguchi, J., and Sawada, N. (2004) 'Expression of Occludin, a Tight-Junction-Associated Protein, in Human Lung Carcinomas'. *Virchows Archiv* 445 (5), 472-476

Toffanin, S., Hoshida, Y., Lachenmayer, A., Villanueva, A., Cabellos, L., Minguez, B., Savic, R., Ward, S. C., Thung, S., and Chiang, D. Y. (2011) 'MicroRNA-Based Classification of Hepatocellular Carcinoma and Oncogenic Role of miR-517a'. *Gastroenterology* 140 (5), 1618-1628. e16

Toren, P. and Zoubeidi, A. (2014) 'Targeting the PI3K/Akt Pathway in Prostate Cancer: Challenges and Opportunities'. *International Journal of Oncology* 45 (5), 1793-1801

Tran, N. M., Dufresne, M., Duverlie, G., Castelain, S., Défarge, C., Paullier, P., and Legallais, C. (2012) 'An Appropriate Selection of a 3D Alginate Culture Model for Hepatic Huh-7 Cell Line Encapsulation Intended for Viral Studies'. *Tissue Engineering Part A* 19 (1-2), 103-113

Treyer, A. and Müsch, A. (2013) 'Hepatocyte Polarity'. *Comprehensive Physiology*

Tsukita, S., Yamazaki, Y., Katsuno, T., and Tamura, A. (2008) 'Tight Junction-Based Epithelial Microenvironment and Cell Proliferation'. *Oncogene* 27 (55), 6930

Tsukita, S., Katsuno, T., Yamazaki, Y., Umeda, K., Tamura, A., and Tsukita, S. (2009) 'Roles of ZO-1 and ZO-2 in Establishment of the Belt-like Adherens and Tight Junctions with Paracellular Permselective Barrier Function'. *Annals of the New York Academy of Sciences* 1165 (1), 44-52

Umeda, K., Ikenouchi, J., Katahira-Tayama, S., Furuse, K., Sasaki, H., Nakayama, M., Matsui, T., Tsukita, S., Furuse, M., and Tsukita, S. (2006) 'ZO1 and ZO2 Independently Determine Where Claudins are Polymerized in Tight-Junction Strand Formation'. *Cell* 126 (4), 741-754

Unal, E., Idilman, I. S., Akata, D., Ozmen, M. N., and Karcaaltincaba, M. (2016) 'Microvascular Invasion in Hepatocellular Carcinoma'. *Diagnostic and Interventional Radiology (Ankara, Turkey)* 22 (2), 125-132

Utech, M., Mennigen, R., and Bruewer, M. (2010) 'Endocytosis and Recycling of Tight Junction Proteins in Inflammation'. *Journal of Biomedicine & Biotechnology* 2010, 484987

Van Itallie, C. M., Aponte, A., Tietgens, A. J., Gucek, M., Fredriksson, K., and Anderson, J. M. (2013) 'The N and C Termini of ZO1 are Surrounded by Distinct Proteins and Functional Protein Networks'. *The Journal of Biological Chemistry* 288 (19), 13775-13788

Van Itallie, C. M., Fanning, A. S., Holmes, J., and Anderson, J. M. (2010) 'Occludin is Required for Cytokine-Induced Regulation of Tight Junction Barriers'. *Journal of Cell Science* 123 (Pt 16), 2844-2852

Van Itallie, C. M., Fanning, A. S., Bridges, A., and Anderson, J. M. (2009) 'ZO1 Stabilizes the Tight Junction Solute Barrier through Coupling to the Perijunctional Cytoskeleton'. *Molecular Biology of the Cell* 20 (17), 3930-3940

van Mil, S. W., van der Woerd, Wendy L, van der Brugge, G., Sturm, E., Jansen, P. L., Bull, L. N., van den Berg, Inge ET, Berger, R., Houwen, R. H., and Klomp, L.

W. (2004) 'Benign Recurrent Intrahepatic Cholestasis Type 2 is Caused by Mutations in ABCB11'. *Gastroenterology* 127 (2), 379-384

VanArsdale, T., Boshoff, C., Arndt, K. T., and Abraham, R. T. (2015) 'Molecular Pathways: Targeting the Cyclin D-CDK4/6 Axis for Cancer Treatment'. *Clinical Cancer Research : An Official Journal of the American Association for Cancer Research* 21 (13), 2905-2910

Verslype, C., Rosmorduc, O., Rougier, P., and ESMO Guidelines Working Group (2012) 'Hepatocellular Carcinoma: ESMO–ESDO Clinical Practice Guidelines for Diagnosis, Treatment and Follow-Up'. *Annals of Oncology* 23 (suppl_7), vii41-vii48

Vesely, M. D., Kershaw, M. H., Schreiber, R. D., and Smyth, M. J. (2011) 'Natural Innate and Adaptive Immunity to Cancer'. *Annual Review of Immunology* 29, 235-271

Vesuna, F., van Diest, P., Chen, J. H., and Raman, V. (2008) 'Twist is a Transcriptional Repressor of E-Cadherin Gene Expression in Breast Cancer'. *Biochemical and Biophysical Research Communications* 367 (2), 235-241

Vinken, M., Decrock, E., De Vuyst, E., De Bock, M., Vandenbroucke, R. E., De Geest, B. G., Demeester, J., Sanders, N. N., Vanhaecke, T., and Leybaert, L. (2010) 'Connexin32 Hemichannels Contribute to the Apoptotic-to-Necrotic Transition during Fas-Mediated Hepatocyte Cell Death'. *Cellular and Molecular Life Sciences* 67 (6), 907-918

Visvader, J. E. (2011) 'Cells of Origin in Cancer'. *Nature* 469 (7330), 314

Wanders, R. J. A. and Waterham, H. R. (2006) 'Biochemistry of Mammalian Peroxisomes Revisited'. *Annual Review of Biochemistry* 75 (1), 295-332

Wang, C., Wang, Y., Fan, C., Xu, F., Sun, W., Liu, Y., and Jia, J. (2011) 'MiR-29c Targets TNFAIP3, Inhibits Cell Proliferation and Induces Apoptosis in Hepatitis B Virus-Related Hepatocellular Carcinoma'. *Biochemical and Biophysical Research Communications* 411 (3), 586-592

Wang, J., Park, J., Wei, Y., Rajurkar, M., Cotton, J. L., Fan, Q., Lewis, B. C., Ji, H., and Mao, J. (2013) 'TRIB2 Acts Downstream of Wnt/TCF in Liver Cancer Cells to Regulate YAP and C/EBPα Function'. *Molecular Cell* 51 (2), 211-225

Wang, Y., Jiang, L., Ji, X., Yang, B., Zhang, Y., and Fu, X. D. (2013) 'Hepatitis B Viral RNA Directly Mediates Down-Regulation of the Tumor Suppressor microRNA miR-15a/miR-16-1 in Hepatocytes'. *The Journal of Biological Chemistry* 288 (25), 18484-18493

Wang, Z., Lin, S., Li, J. J., Xu, Z., Yao, H., Zhu, X., Xie, D., Shen, Z., Sze, J., Li, K., Lu, G., Chan, D. T., Poon, W. S., Kung, H. F., and Lin, M. C. (2011) 'MYC Protein Inhibits Transcription of the microRNA Cluster MC-Let-7a-1~let-7d Via Noncanonical E-Box'. *The Journal of Biological Chemistry* 286 (46), 39703-39714

Wayne Rasband (29 January 2019) *Platform Independent Download* [online] available from <https://imagej.nih.gov/ij/download.html>

Wege, H. and Brummendorf, T. H. (2007) 'Telomerase Activation in Liver Regeneration and Hepatocarcinogenesis: Dr. Jekyll Or Mr. Hyde?'. *Current Stem Cell Research & Therapy* 2 (1), 31-38

Wei, W., Wanjun, L., Hui, S., Dongyue, C., Xinjun, Y., and Jisheng, Z. (2013) 'MiR-203 Inhibits Proliferation of HCC Cells by Targeting Survivin'. *Cell Biochemistry and Function* 31 (1), 82-85

Wells, A., Yates, C., and Shepard, C. R. (2008) 'E-Cadherin as an Indicator of Mesenchymal to Epithelial Reverting Transitions during the Metastatic Seeding of Disseminated Carcinomas'. *Clinical & Experimental Metastasis* 25 (6), 621-628

Willott, E., Balda, M. S., Fanning, A. S., Jameson, B., Van Itallie, C., and Anderson, J. M. (1993) 'The Tight Junction Protein ZO-1 is Homologous to the Drosophila Discs-Large Tumor Suppressor Protein of Septate Junctions'. *Proceedings of the National Academy of Sciences of the United States of America* 90 (16), 7834-7838

Wirtz-Peitz, F. and Zallen, J. A. (2009) 'Junctional Trafficking and Epithelial Morphogenesis'. *Current Opinion in Genetics & Development* 19 (4), 350-356

Wong, Q. W., Ching, A. K., Chan, A. W., Choy, K. W., To, K. F., Lai, P. B., and Wong, N. (2010) 'MiR-222 Overexpression Confers Cell Migratory Advantages in Hepatocellular Carcinoma through Enhancing AKT Signaling'. *Clinical Cancer Research : An Official Journal of the American Association for Cancer Research* 16 (3), 867-875

Woo, H. Y., Min, A. L., Choi, J. Y., Bae, S. H., Yoon, S. K., and Jung, C. K. (2011) 'Clinicopathologic Significance of the Expression of Snail in Hepatocellular Carcinoma'. *The Korean Journal of Hepatology* 17 (1), 12-18

Wu, G., Yu, F., Xiao, Z., Xu, K., Xu, J., Tang, W., Wang, J., and Song, E. (2011) 'Hepatitis B Virus X Protein Downregulates Expression of the miR-16 Family in Malignant Hepatocytes in Vitro'. *British Journal of Cancer* 105 (1), 146-153

Wu, H., Feng, W., Chen, J., Chan, L., Huang, S., and Zhang, M. (2007) 'PDZ Domains of Par-3 as Potential Phosphoinositide Signaling Integrators'. *Molecular Cell* 28 (5), 886-898

Wu, N., Liu, X., Xu, X., Fan, X., Liu, M., Li, X., Zhong, Q., and Tang, H. (2011) 'MicroRNA-373, a New Regulator of Protein Phosphatase 6, Functions as an Oncogene in Hepatocellular Carcinoma'. *The FEBS Journal* 278 (12), 2044-2054

Xie, Q., Chen, X., Lu, F., Zhang, T., Hao, M., Wang, Y., Zhao, J., McCrae, M. A., and Zhuang, H. (2012) 'Aberrant Expression of microRNA 155 may Accelerate Cell Proliferation by Targeting sex-determining Region Y Box 6 in Hepatocellular Carcinoma'. *Cancer* 118 (9), 2431-2442

Xiong, Y., Fang, J., Yun, J., Yang, J., Zhang, Y., Jia, W., and Zhuang, S. (2010) 'Effects of MicroRNA-29 on Apoptosis, Tumorigenicity, and Prognosis of Hepatocellular Carcinoma'. *Hepatology* 51 (3), 836-845

Xu, J., Kausalya, P. J., Phua, D. C., Ali, S. M., Hossain, Z., and Hunziker, W. (2008) 'Early Embryonic Lethality of Mice Lacking ZO2, but Not ZO-3, Reveals Critical and Nonredundant Roles for Individual Zonula Occludens Proteins in Mammalian Development'. *Molecular and Cellular Biology* 28 (5), 1669-1678

Xu, T., Zhu, Y., Xiong, Y., Ge, Y., Yun, J., and Zhuang, S. (2009) 'MicroRNA-195 Suppresses Tumorigenicity and Regulates G1/S Transition of Human Hepatocellular Carcinoma Cells'. *Hepatology* 50 (1), 113-121

Yan, H., Dong, X., Zhong, X., Ye, J., Zhou, Y., Yang, X., Shen, J., and Zhang, J. (2014) 'Inhibitions of Epithelial to Mesenchymal Transition and Cancer Stem cells-like Properties are Involved in miR-148a-mediated anti-metastasis of Hepatocellular Carcinoma'. *Molecular Carcinogenesis* 53 (12), 960-969

Yan, Y., Luo, Y., Wan, H., Wang, J., Zhang, P., Liu, M., Li, X., Li, S., and Tang, H. (2013) 'MicroRNA-10a is Involved in the Metastatic Process by Regulating Eph Tyrosine Kinase Receptor A4-Mediated epithelial-mesenchymal Transition and Adhesion in Hepatoma Cells'. *Hepatology* 57 (2), 667-677

Yang, H., Cho, M. E., Li, T. W., Peng, H., Ko, K. S., Mato, J. M., and Lu, S. C. (2013) 'MicroRNAs Regulate Methionine Adenosyltransferase 1A Expression in Hepatocellular Carcinoma'. *The Journal of Clinical Investigation* 123 (1), 285-298

Yang, J. D., Kim, W. R., Coelho, R., Mettler, T. A., Benson, J. T., Sanderson, S. O., Therneau, T. M., Kim, B., and Roberts, L. R. (2011) 'Cirrhosis is Present in most Patients with Hepatitis B and Hepatocellular Carcinoma'. *Clinical Gastroenterology and Hepatology* 9 (1), 64-70

Yang, M., Chen, C., Chau, G., Chiou, S., Su, C., Chou, T., Peng, W., and Wu, J. (2009) 'Comprehensive Analysis of the Independent Effect of Twist and Snail in Promoting Metastasis of Hepatocellular Carcinoma'. *Hepatology* 50 (5), 1464-1474

Yang, Z. F. and Poon, R. T. (2008) 'Vascular Changes in Hepatocellular Carcinoma'. *The Anatomical Record* 291 (6), 721-734

Yang, H., Cho, M. E., Li, T. W., Peng, H., Ko, K. S., Mato, J. M., and Lu, S. C. (2013) 'MicroRNAs Regulate Methionine Adenosyltransferase 1A Expression in Hepatocellular Carcinoma'. *The Journal of Clinical Investigation* 123 (1), 285-298

Yau, W. L., Lam, C. S. C., Ng, L., Chow, A. K. M., Chan, S. T. C., Chan, J. Y. K., Wo, J. Y. H., Ng, K. T. P., Man, K., and Poon, R. T. P. (2013) 'Over-Expression of miR-106b Promotes Cell Migration and Metastasis in Hepatocellular Carcinoma by Activating Epithelial-Mesenchymal Transition Process'. *PloS One* 8 (3), e57882

Yu, A. S., McCarthy, K. M., Francis, S. A., McCormack, J. M., Lai, J., Rogers, R. A., Lynch, R. D., and Schneeberger, E. E. (2005) 'Knockdown of Occludin Expression Leads to Diverse Phenotypic Alterations in Epithelial Cells'. *American Journal of Physiology.Cell Physiology* 288 (6), C1231-41

Zeng, Y., Liang, X., Zhang, G., Jiang, N., Zhang, T., Huang, J., Zhang, L., and Zeng, X. (2016) 'MiRNA-135a Promotes Hepatocellular Carcinoma Cell Migration and Invasion by Targeting Forkhead Box O1'. *Cancer Cell International* 16 (1), 63

Zhai, X., Zhu, H., Wang, W., Zhang, S., Zhang, Y., and Mao, G. (2014) 'Abnormal Expression of EMT-Related Proteins, S100A4, Vimentin and E-Cadherin, is Correlated with Clinicopathological Features and Prognosis in HCC'. *Medical Oncology* 31 (6), 1-9

Zhan, D., Wei, S., Liu, C., Liang, B., Ji, G., Chen, X., Xiong, M., and Huang, Z. (2012) 'Reduced N-cadherin Expression is Associated with Metastatic Potential and Poor Surgical Outcomes of Hepatocellular Carcinoma'. *Journal of Gastroenterology and Hepatology* 27 (1), 173-180

Zhang, D., Kaneda, M., Nakahama, K., Arii, S., and Morita, I. (2007) 'Connexin 43 Expression Promotes Malignancy of HuH7 Hepatocellular Carcinoma Cells Via the Inhibition of cell–cell Communication'. *Cancer Letters* 252 (2), 208-215

Zhang, J., Jin, H., Liu, H., Wang, B., Wang, R., Ding, M., Yang, Y., Li, L., Fu, S., and Xie, D. (2014) 'MiRNA-99a Directly Regulates AGO2 through Translational Repression in Hepatocellular Carcinoma'. *Oncogenesis* 3 (4), e97

Zhang, L., Yang, F., Yuan, J., Yuan, S., Zhou, W., Huo, X., Xu, D., Bi, H., Wang, F., and Sun, S. (2012) 'Epigenetic Activation of the MiR-200 Family Contributes to H19-Mediated Metastasis Suppression in Hepatocellular Carcinoma'. *Carcinogenesis* 34 (3), 577-586

Zhang, W., Kong, G., Zhang, J., Wang, T., Ye, L., and Zhang, X. (2012) 'MicroRNA-520b Inhibits Growth of Hepatoma Cells by Targeting MEKK2 and Cyclin D1'. *PLoS*

Zhou, T., Benda, C., Duzinger, S., Huang, Y., Li, X., Li, Y., Guo, X., Cao, G., Chen, S., Hao, L., Chan, Y. C., Ng, K. M., Ho, J. C., Wieser, M., Wu, J., Redl, H., Tse, H. F., Grillari, J., Grillari-Voglauer, R., Pei, D., and Esteban, M. A. (2011) 'Generation of Induced Pluripotent Stem Cells from Urine'. Journal of the American Society of Nephrology : JASN 22 (7), 1221-1228One 7 (2), e31450

Zhou, S., Hertel, P. M., Finegold, M. J., Wang, L., Kerkar, N., Wang, J., Wong, L. C., Plon, S. E., Sambrotta, M., and Foskett, P. (2015) 'Hepatocellular Carcinoma Associated with tight-junction Protein 2 Deficiency'*. Hepatology* 62 (6), 1914-1916

Zhu, X., Dong, Q., Zhang, X., Deng, B., Jia, H., Ye, Q., Qin, L., and Wu, X. (2012) 'MicroRNA-29a Suppresses Cell Proliferation by Targeting SPARC in Hepatocellular Carcinoma'*. International Journal of Molecular Medicine* 30 (6), 1321-1326

Zyrek, A. A., Cichon, C., Helms, S., Enders, C., Sonnenborn, U., and Schmidt, M. A. (2007) 'Molecular Mechanisms Underlying the Probiotic Effects of Escherichia Coli Nissle 1917 Involve ZO-2 and PKCζ Redistribution Resulting in Tight Junction and Epithelial Barrier Repair'*. Cellular Microbiology* 9 (3), 804-816

Appendix, Figure 1: miRNA profile for HepG2 cells with differential occludin expression and knockdown ZO1.

	HepG2	$HepG2^{OCLN+ siZO1}$			$HepG2^{shOCLN siZO1}$		
		Expression	SEM	P value	Expression	SEM	P value
hsa-let-7a		0.609	0.037	0.00883	0.816	0.029	0.02395
hsa-let-7b		0.833	0.036	0.04346	1.536	0.070	0.01663
hsa-let-7c		0.925	0.111	0.00701	0.371	0.210	0.00444
hsa-let-7d		2.295	0.043	0.00110	1.073	0.036	0.17977
hsa-let-7e		0.641	0.034	0.00885	0.576	0.029	0.00464
hsa-let-7f		0.378	0.022	0.00124	0.488	0.024	0.00219
hsa-let-7g		0.811	0.052	0.06806	1.349	0.065	0.03298
hsa-miR-9		2.635	0.059	0.00130	0.001	0.000	-
hsa-miR-10a		4.654	0.020	0.00003	6.930	0.062	0.00109
hsa-miR-10b		12.977	0.474	0.00156	3.765	0.074	0.00071
hsa-miR-15a		0.599	0.017	0.00179	1.060	0.013	0.04387
hsa-miR-15b		1.021	0.040	0.65197	0.847	0.050	0.09225
hsa-miR-16		0.892	0.042	0.12377	0.850	0.051	0.09877
hsa-miR-17		0.934	0.049	0.31032	0.908	0.080	0.36909
hsa-miR-18a		0.768	0.013	0.00312	0.824	0.026	0.02113
hsa-miR-18b		0.645	0.063	0.03008	0.615	0.062	0.02496
hsa-miR-19a		1.406	0.069	0.02768	1.234	0.023	0.00952
hsa-miR-19b		1.034	0.077	0.70196	1.723	0.030	0.00424
hsa-miR-20a		0.851	0.019	0.01587	0.816	0.071	0.12219
hsa-miR-20b		1.390	0.009	0.00053	1.311	0.056	0.03092
hsa-miR-21		1.358	0.035	0.00942	1.051	0.014	0.06778
hsa-miR-22	No Exp	138986.3	40.234	<0.0001	169045.5	25.144	<0.0001
hsa-miR-23b		0.854	0.060	0.13541	0.233	0.038	0.00367
hsa-miR-24		0.953	0.045	0.40591	0.524	0.028	0.00344
hsa-miR-25		0.875	0.068	0.20741	0.910	0.047	0.19559
hsa-miR-26a		1.225	0.012	0.00283	0.957	0.009	0.04112
hsa-miR-26b		1.150	0.035	0.05036	0.855	0.020	0.01849
hsa-miR-27a		0.949	0.052	0.43012	0.378	0.025	0.00319
hsa-miR-27b		0.736	0.012	0.00206	0.623	0.009	0.00056
hsa-miR-28		1.071	0.043	0.24050	1.059	0.072	0.49864
hsa-miR-28-3p		1.255	0.057	0.04650	0.858	0.036	0.05867
hsa-miR-29a		1.022	0.040	0.63753	0.707	0.030	0.01032
hsa-miR-29b		1.218	0.031	0.01962	1.057	0.010	0.02942
hsa-miR-29c		0.717	0.021	0.00546	0.527	0.062	0.01675
hsa-miR-30b		1.236	0.014	0.00350	1.068	0.037	0.20747
hsa-miR-30c		1.124	0.025	0.03832	0.986	0.023	0.60465
hsa-miR-32		1.058	0.034	0.23014	1.084	0.070	0.35300

	HepG2	HepG2$^{OCLN+ siZO1}$			HepG2$^{shOCLN siZO1}$		
		Expression	SEM	P value	Expression	SEM	P value
hsa-miR-33b		0.004	0.000	-	0.860	0.079	0.21837
hsa-miR-34a		1.122	0.028	0.04884	0.877	0.075	0.24268
hsa-miR-34c		3551.6	2.355	<0.00000	764.86	1.174	0.00000
hsa-miR-92a		1.204	0.031	0.02232	1.151	0.074	0.17809
hsa-miR-95		248.79	1.233	0.00002	134.51	1.178	0.00007
hsa-miR-98	No Exp	1050.5	4.132	0.00001	434.17	3.355	0.00006
hsa-miR-99a		0.203	0.048	0.00360	1.255	0.050	0.03636
hsa-miR-99b		1.058	0.052	0.38073	0.308	0.045	0.00420
mmu-miR-93		1.016	0.029	0.63655	1.167	0.066	0.12708
mmu-miR-96		0.821	0.022	0.01477	0.159	0.065	0.00459
hsa-miR-101		0.529	0.040	0.00410	0.358	0.036	0.00313
hsa-miR-103		0.880	0.018	0.02176	0.757	0.038	0.02359
hsa-miR-106a		0.822	0.024	0.01769	0.992	0.050	0.88758
hsa-miR-106b		0.957	0.011	0.05964	0.821	0.074	0.13671
hsa-miR-107		1.333	0.044	0.01701	1.202	0.035	0.02873
hsa-miR-122		1.040	0.046	0.47621	1.758	0.042	0.00305
hsa-miR-125a-		0.249	0.033	0.00192	0.249	0.041	0.00296
hsa-miR-125a-		0.893	0.079	0.30832	0.236	0.026	0.00238
hsa-miR-125b		0.004	0.000	-	0.003	0.000	-
hsa-miR-126		1.878	0.049	0.00310	0.368	0.015	0.00056
hsa-miR-128a		0.904	0.070	0.30383	0.576	0.032	0.00564
hsa-miR-130a		0.680	0.054	0.02731	0.732	0.034	0.01571
hsa-miR-130b		0.846	0.037	0.05316	0.653	0.050	0.02013
hsa-miR-132		1.441	0.057	0.01629	0.864	0.036	0.06347
hsa-miR-135a		1.192	0.065	0.09804	0.618	0.057	0.02154
hsa-miR-135b		1.226	0.031	0.01830	0.710	0.035	0.01425
hsa-miR-136		5.289	0.022	0.00002	1.262	0.078	0.07835
hsa-miR-138		1.099	0.077	0.32730	0.849	0.049	0.09113
hsa-miR-139-		0.918	0.058	0.29299	0.280	0.020	0.00077
mmu-miR-140		0.921	0.025	0.08723	0.922	0.055	0.29190
hsa-miR-140-		1.249	0.063	0.05845	1.164	0.071	0.14715
hsa-miR-141		2.831	0.068	0.00137	1.107	0.048	0.15559
hsa-miR-142-		1.784	0.049	0.00388	0.003	0.000	-
hsa-miR-143-		3.744	0.037	0.00018	1.341	0.051	0.02164
hsa-miR-145		0.980	0.060	0.77058	0.573	0.037	0.00742
hsa-miR-146a		1.187	0.025	0.01740	0.352	0.020	0.00102
hsa-miR-146b		1.041	0.051	0.50580	0.828	0.042	0.05477
hsa-miR-146b-		0.678	0.056	0.02893	1.485	0.017	0.00122
hsa-miR-148a		1.401	0.027	0.00450	1.348	0.034	0.00941
hsa-miR-148b		0.965	0.034	0.41149	0.451	0.030	0.00426
hsa-miR-149		1.588	0.026	0.00194	0.628	0.075	0.03832
hsa-miR-150		0.001	0.000	-	0.140	0.052	0.00363
hsa-miR-152		0.353	0.034	0.00489	0.479	0.028	0.00287

	HepG2	HepG2$^{OCLN+ siZO1}$			HepG2$^{shOCLN siZO1}$		
		Expression	SEM	P value	Expression	SEM	P value
mmu-miR-153		0.002	0.000	-	0.002	0.000	-
hsa-miR-154	No Exp	145.06	2.358	0.00026	1489.2	4.596	0.00001
hsa-miR-155		0.644	0.031	0.00749	6.977	0.013	0.00000
hsa-miR-181a		1.864	0.031	0.00468	0.978	0.011	0.18350
hsa-miR-181c		6.956	0.016	0.00000	0.520	0.025	0.00767
hsa-miR-182		1.053	0.077	0.56237	1.059	0.014	0.05195
hsa-miR-183		0.896	0.014	0.01764	1.067	0.055	0.34735
hsa-miR-184		1.322	0.059	0.03197	0.990	0.078	0.90971
hsa-miR-185		0.774	0.039	0.02851	0.855	0.055	0.11878
hsa-miR-186		1.107	0.079	0.30832	0.682	0.050	0.02384
mmu-miR-187	No Exp	0.000	0.000	-	200.10	7.231	0.00130
hsa-miR-190		6.566	0.045	0.00006	4.113	0.059	0.00035
hsa-miR-191		0.874	0.041	0.09157	0.936	0.054	0.35768
hsa-miR-192		1.076	0.066	0.36859	1.090	0.016	0.03018
hsa-miR-193a-	No Exp	0.000	0.000	-	437.41	7.449	0.00029
hsa-miR-193a-		2.324	0.031	0.00054	1.514	0.049	0.00896
hsa-miR-193b		0.765	0.014	0.00353	0.472	0.010	0.00171
hsa-miR-194		1.474	0.019	0.00160	1.138	0.025	0.03128
hsa-miR-195		0.881	0.021	0.02975	0.856	0.068	0.16839
hsa-miR-196b		0.454	0.028	0.00198	0.435	0.012	0.00118
hsa-miR-197		1.149	0.062	0.13815	0.705	0.043	0.02059
hsa-miR-198		0.002	0.000	-	0.002	0.000	-
hsa-miR-199a-		1.104	0.057	0.20962	0.341	0.043	0.00440
hsa-miR-199b		536.37	2.375	0.00002	0.000	0.000	
hsa-miR-200a		1.750	0.046	0.00374	0.660	0.020	0.00344
hsa-miR-200b		1.910	0.045	0.00243	0.598	0.010	0.00067
hsa-miR-200c		1.146	0.067	0.16116	1.129	0.070	0.20667
hsa-miR-202		0.655	0.031	0.00797	2.425	0.043	0.00090
hsa-miR-203		0.157	0.046	0.00307	0.008	0.000	-
hsa-miR-204		0.792	0.011	0.00278	0.900	0.075	0.31400
hsa-miR-208	No Exp	0.000	0.000	-	424.78	6.282	0.00021
hsa-miR-218		1.724	0.015	0.00042	0.559	0.019	0.00185
hsa-miR-221		1.087	0.021	0.05362	0.676	0.065	0.03797
hsa-miR-222		1.000	0.059	>0.9999	0.606	0.063	0.02462
hsa-miR-223		1.153	0.036	0.05115	1.565	0.012	0.00045
hsa-miR-224		0.948	0.027	0.19396	0.974	0.070	0.74597
hsa-miR-296		0.838	0.018	0.01212	1.107	0.055	0.19113
hsa-miR-299-	No Exp	254.72	1.265	0.00002	0.000	0.000	-
hsa-miR-301		0.913	0.016	0.03219	0.569	0.030	0.00481
hsa-miR-301b		0.886	0.069	0.24030	0.557	0.015	0.00114
hsa-miR-302a		32.851	1.631	0.00261	140.28	3.332	0.00057
hsa-miR-302b		0.050	0.034	0.00127	0.002	0.000	-
hsa-miR-302c	No Exp	136.52	4.311	0.00099	0.000	0.000	-

	HepG2	HepG2$^{OCLN+ siZO1}$			HepG2$^{shOCLN siZO1}$		
		Expression	SEM	P value	Expression	SEM	P value
hsa-miR-320		1.079	0.079	0.42265	0.924	0.041	0.20496
hsa-miR-323-		0.166	0.048	0.00329	0.902	0.043	0.15029
hsa-miR-324-		0.830	0.059	0.10229	0.858	0.051	0.10841
hsa-miR-324-		0.810	0.055	0.07454	1.042	0.010	0.05228
hsa-miR-326		3.861	0.018	0.00004	0.000	0.000	-
hsa-miR-328		0.421	0.020	0.00119	0.191	0.080	0.00463
hsa-miR-330		0.633	0.030	0.00661	1.001	0.033	0.97857
hsa-miR-331		1.059	0.067	0.47142	0.767	0.030	0.01617
hsa-miR-331-		0.879	0.024	0.03716	0.441	0.016	0.00081
hsa-miR-335		0.703	0.059	0.03727	0.874	0.025	0.03718
hsa-miR-337-		0.004	0.000	-	0.003	0.000	-
hsa-miR-338-		0.008	0.000	-	6.423	0.077	0.00020
hsa-miR-339-		1.154	0.074	0.17290	1.043	0.033	0.32239
hsa-miR-339-		1.051	0.061	0.49109	0.913	0.047	0.20537
hsa-miR-340		1.285	0.063	0.04555	0.927	0.048	0.26769
hsa-miR-342-		1.681	0.041	0.00360	1.541	0.077	0.01966
hsa-miR-342-		0.004	0.000	-	0.003	0.000	-
hsa-miR-345		0.733	0.019	0.00502	0.734	0.017	0.00406
hsa-miR-361		0.742	0.045	0.02910	0.228	0.050	0.00416
hsa-miR-362		1.822	0.050	0.00368	1.403	0.012	0.00088
hsa-miR-362-		0.354	0.019	0.00146	1.236	0.051	0.04366
hsa-miR-363	No Exp	0.000	0.000	-	13.383	0.111	0.00068
hsa-miR-365		0.767	0.014	0.00359	0.454	0.026	0.00202
hsa-miR-367		46.948	1.537	0.00111	57.038	3.218	0.00328
hsa-miR-369-	No Exp	0.000	0.000	-	27.672	0.912	0.00189
hsa-miR-371-		0.193	0.059	0.00053	0.238	0.074	0.00493
hsa-miR-372		0.877	0.010	0.00654	0.492	0.010	0.00038
hsa-miR-373		11.778	0.035	0.00001	45.702	2.221	0.00245
hsa-miR-374		1.182	0.040	0.04506	0.978	0.065	0.76724
mmu-miR-		0.646	0.079	0.04636	0.888	0.010	0.00787
hsa-miR-375	No Exp	0.000	0.000	-	13.944	0.737	0.00364
hsa-miR-376a		3.545	0.060	0.00055	1.309	0.038	0.01478
hsa-miR-376c		0.790	0.059	0.07066	0.001	0.000	-
hsa-miR-377	No Exp	0.000	0.000	-	35062.8	13.537	<0.0000
mmu-miR-379		1.579	0.032	0.00304	2.380	0.037	0.00071
hsa-miR-381		4.893	0.074	0.00036	0.013	0.039	0.00155
hsa-miR-382	No Exp	0.000	0.000	-	447.32	3.738	0.00007
hsa-miR-383		0.004	0.000	-	2.678	0.073	0.00188
hsa-miR-384	No Exp	0.000	0.000	-	7.014	0.091	0.00016
hsa-miR-409-	No Exp	0.000	0.000	-	56420.9	30.374	<0.0000
hsa-miR-410	No Exp	555.49	3.237	0.00003	216.05	5.371	0.00061
hsa-miR-411	No Exp	16.876	0.913	0.00291	0.000	0.019	>0.9999
hsa-miR-422a		1.611	0.027	0.00194	1.742	0.026	0.00122

	HepG2	HepG2$^{OCLN+ siZO1}$			HepG2$^{shOCLN siZO1}$		
		Expression	SEM	P value	Expression	SEM	P value
hsa-miR-423-		1.674	0.030	0.00197	1.076	0.014	0.03229
hsa-miR-425-		1.558	0.032	0.00327	1.337	0.040	0.01379
hsa-miR-429		2.094	0.037	0.00114	0.830	0.054	0.08781
hsa-miR-433		1.102	0.200	0.00136	0.000	0.021	0.00044
hsa-miR-449	No Exp	4200.7	8.657	0.00000	5838.3	15.947	0.00000
hsa-miR-449b		0.000	0.000	-	0.000	0.000	-
hsa-miR-450b-	No Exp	379221.8	41.855		0.000	0.000	-
hsa-miR-452		0.757	0.063	0.06111	0.587	0.061	0.02112
hsa-miR-454		1.102	0.033	0.09066	0.832	0.024	0.01980
hsa-miR-455		1.151	0.037	0.05512	1.021	0.049	0.70997
hsa-miR-455-		0.962	0.031	0.34502	0.742	0.070	0.06636
hsa-miR-483-		1.343	0.059	0.02833	0.519	0.019	0.00155
hsa-miR-484		1.111	0.074	0.27239	1.163	0.039	0.05275
hsa-miR-485-		0.455	0.036	0.00404	2.691	0.045	0.00070
hsa-miR-486		18.198	1.148	0.00442	2.868	0.052	0.00077
hsa-miR-486-		10.854	0.066	0.00004	1.236	0.079	0.09616
hsa-miR-487a		0.835	0.032	0.03561	1.342	0.037	0.01150
hsa-miR-487b	No Exp	0.000	0.000	-	14.248	0.258	0.00470
hsa-miR-489		1.389	0.026	0.00443	0.542	0.036	0.00612
mmu-miR-491		1.046	0.060	0.52341	0.716	0.052	0.03192
hsa-miR-491-		0.001	0.000		0.001	0.000	-
hsa-miR-493	No Exp	0.000	0.000		0.000	0.000	0.00030
hsa-miR-494		1.628	0.024	0.00145	2.196	0.080	0.00444
mmu-miR-499	No Exp	1996.2	2.317	<0.00000	0.000	0.000	-
hsa-miR-500		0.834	0.009	0.00292	0.548	0.061	0.01773
hsa-miR-501		1.089	0.072	0.34189	1.100	0.056	0.21606
hsa-miR-501-		0.000	0.000	-	0.000	0.000	-
hsa-miR-502		0.721	0.011	0.00155	0.380	0.010	0.00162
hsa-miR-502-		1.301	0.043	0.01980	1.261	0.080	0.08249
hsa-miR-504	No Exp	21279.	15.349	<0.00000	842.88	4.537	0.00002
hsa-miR-505		0.000	0.000	-	1.453	0.037	0.00605
hsa-miR-507		0.002	0.000	-	0.002	0.000	-
hsa-miR-509-		0.088	0.012	0.00017	3.477	0.026	0.00011
hsa-miR-511	No Exp	368.85	4.567	0.00015	14.425	0.423	0.00259
hsa-miR-512-		14.073	0.178	0.00080	2.903	0.030	0.00024
hsa-miR-512-		0.002	0.000	-	0.002	0.000	-
hsa-miR-517a		5.351	0.040	0.00008	2.896	0.033	0.00030
hsa-miR-517c		34.281	2.154	0.00416	30.197	0.983	0.00113
hsa-miR-518a-	No Exp	18.422	0.930	0.00253	0.000	0.000	-
hsa-miR-518a-	No Exp	0.000	0.000	-	0.000	0.000	-
hsa-miR-518b		1.157	0.059	0.11696	1.688	0.042	0.00370
hsa-miR-518d		0.000	0.036	0.00129	1.158	0.051	0.09030
hsa-miR-518e		1.326	0.009	0.00076	1.507	0.009	0.00031

	HepG2	HepG2$^{OCLN+ siZO1}$			HepG2$^{shOCLN siZO1}$		
		Expression	SEM	P value	Expression	SEM	P value
hsa-miR-518f		0.095	0.017	0.00035	0.914	0.076	0.37523
hsa-miR-519a		49.201	1.750	0.00131	853.38	0.071	<0.0000
hsa-miR-519c	No Exp	543.43	5.329	0.00009	0.000	0.000	-
hsa-miR-519d		0.311	0.046	0.00442	3.351	0.047	0.00039
hsa-miR-519e	No Exp	49.201	2.648	0.00168	853.38	4.394	0.00002
hsa-miR-520e		0.266	0.020	0.00074	0.027	0.037	0.00420
hsa-miR-520f		0.430	0.032	0.00313	0.095	0.048	0.00455
hsa-miR-522	No Exp	0.000	0.000	-	443.09	5.640	0.00016
hsa-miR-523		6.305	0.325	0.001575	3.727	0.224	0.003594
hsa-miR-525		0.000	0.046	0.00210	0	0.042	0.00287
hsa-miR-532		1.033	0.052	0.59059	0.943	0.031	0.20733
hsa-miR-532-		1.151	0.023	0.02242	1.135	0.027	0.03775
hsa-miR-539		0.000	0.000	-	0.000	0.000	-
hsa-miR-542-	No Exp	0.000	0.000	-	7.167	0.33	0.00327
hsa-miR-545		2.152	0.050	0.00187	0.523	0.025	0.00434
hsa-miR-548b		1.134	0.028	0.04099	1.070	0.034	0.17572
hsa-miR-548b-		0.990	0.055	0.87248	0.505	0.029	0.00341
hsa-miR-548c-	No Exp	67.555	3.261	0.00232	29.547	0.912	0.00255
hsa-miR-548d		0.040	0.077	0.00023	0.436	0.038	0.00189
hsa-miR-548d-		0.932	0.078	0.47524	1.436	0.029	0.00439
hsa-miR-561		0.002	0.000	-	0.002	0.000	-
hsa-miR-570		2.827	0.039	0.00045	0.339	0.038	0.00423
hsa-miR-574-		0.730	0.037	0.01826	0.699	0.068	0.04743
hsa-miR-576-		2.088	0.057	0.00273	1.341	0.065	0.03446
hsa-miR-576-		0.001	0.000	-	0.001	0.000	-
hsa-miR-579		1.083	0.061	0.30667	1.135	0.036	0.06432
hsa-miR-582-		4.253	0.028	0.00007	2.675	0.063	0.00141
hsa-miR-582-		1.654	0.021	0.00102	0.179	0.024	0.00085
hsa-miR-589	No Exp	0.000	0.000	-	276.34	6.251	0.00051
hsa-miR-590-		0.938	0.049	0.33321	0.815	0.041	0.04577
hsa-miR-597		0.474	0.025	0.00175	0.451	0.021	0.00146
hsa-miR-616		14.093	0.226	0.00165	0.007	0.000	-
hsa-miR-618		2.675	0.079	0.00221	1.618	0.022	0.00126
hsa-miR-625		0.991	0.031	0.79890	0.530	0.071	0.02206
hsa-miR-627	No Exp	0.000	0.000	-	27.537	1.852	0.00449
hsa-miR-628-		0.291	0.018	0.00064	1.251	0.048	0.03468
hsa-miR-629		0.814	0.073	0.12565	0.159	0.04	0.00274
hsa-miR-636		1.123	0.018	0.02075	1.131	0.026	0.03720
hsa-miR-642	No Exp	548.70	0.987	0.00000	1149.2	4.389	0.00001
hsa-miR-651		1.185	0.050	0.06590	0.564	0.051	0.01340
hsa-miR-652		0.900	0.013	0.01648	1.258	0.030	0.01325
hsa-miR-655		0.016	0.056	0.00322	0.013	0.065	0.00430
hsa-miR-660		1.223	0.023	0.01047	1.158	0.058	0.11247

	HepG2	HepG2$^{OCLN+ siZO1}$			HepG2$^{shOCLN siZO1}$		
		Expression	SEM	P value	Expression	SEM	P value
hsa-miR-671-		1.253	0.026	0.01039	2.080	0.034	0.00099
hsa-miR-708		8.890	0.047	0.00003	6.964	0.061	0.00010
hsa-miR-744		1.028	0.030	0.44917	0.613	0.080	0.04017
hsa-miR-885-		0.904	0.056	0.22861	0.964	0.043	0.49057
hsa-miR-888	No Exp	20179.0	22.365	<0.00001	13885.1	7.968	<0.0001
hsa-miR-891a		0.002	0.000	<0.00001	0.002	0.000	-

The miRNA expression varies between HepG2^{Control} and the two experimental cell lines HepG2$^{OCLN+ siZO1}$ and HepG2$^{shOCLN siZO1}$. A total of 126 different miRNAs showed no expression between all three cell lines and were excluded from the results. Out of the remaining 258 miRNAs, 85 showed no significant difference and a further 37 miRNAs were only slightly significant and are between 0.65-1.45-fold. This left a remaining 136 miRNAs that showed a clear significant difference in at least one cell line.